

INTERACTIONS BETWEEN THE DIHYDROPYRIDINE
RECEPTOR BETA1A SUBUNIT AND THE RYANODINE
RECEPTOR FROM SKELETAL MUSCLE

by

Robyn Tricia Rebbeck

A thesis submitted for the degree of Doctor of Philosophy
of The Australian National University

January, 2014

The John Curtin School of Medical Research

The Australian National University

Canberra, Australia

INTERACTION BETWEEN THE DITHYRONE RECEPTOR
RECEPTOR FOR THE DATA SUBUNIT AND THE RYANODINE
RECEPTOR FROM SKELETAL MUSCLE

Robyn L. J. Kibick

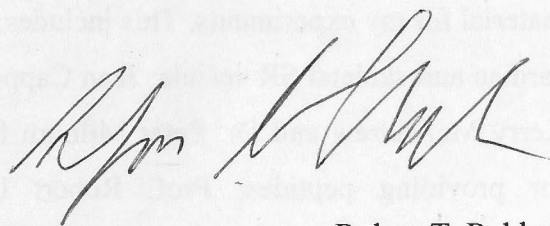
A thesis submitted to the Faculty of Science
of the Australian National University
in partial fulfillment of the requirements for the
degree of Doctor of Philosophy



Statement

In this thesis, I present the results of research undertaken in the Muscle Research Group, Department of Molecular Bioscience, John Curtin School of Medical Research at The Australian National University between February 2010 and January 2014. This study was supported by an Australian Postgraduate Award and an Australian National University Supplementary Scholarship.

All experiments and data analyses presented in this thesis are my own original work, accomplished under the supervision of Professor Angela F. Dulhunty, except where otherwise acknowledged.



Robyn T. Rebbeck

Muscle Research Group

Department of Molecular Bioscience

The John Curtin School of Medical Research

College of Medicine, Biology and Environment

The Australian National University

Acknowledgements

First and foremost, I would like to acknowledge my supervisor, Prof. Angela Dulhunty, for the extensive knowledge she brought to this project. I am extremely grateful for her guidance and patience over the course of this project and appreciate her generosity in funding my scholarship in the final stage of my study. I would also like to express my gratitude to her for editing this thesis.

I also wish to thank my advisory panel, Assoc. Prof. Nicole Beard and Assoc. Prof. Marco Casarotto, for experimental design advice, particularly in the first year. Also, I am very grateful to Assoc. Prof. Beard for her unreserved help in teaching me the fundamentals of many laboratory techniques that I used in undertaking this study.

I am grateful to those who helped teach and troubleshoot laboratory techniques. I thank Prof. Esther Gallant for extensive knowledge and help with lipid bilayer experiments. I thank Dr. Matthew Rosenberg for the crash course in using high performance liquid chromatography for peptide purification and Dr. Nicole Norris for helping me whenever the machine threatened to explode. I greatly appreciate Dr. Peter Milburn for instruction in mass spectrometry and for always having an open door when I needed to troubleshoot. I thank both Dr. Yamuna Karunasekara and Ms. Jean Cappello for instruction in protein expression and purification.

I am very thankful and would like to acknowledge the people who kindly provided material for my experiments. This includes: Mrs. Suzy Pace and Mrs. Joan Stivala for preparing cardiac and skeletal SR vesicle; Jean Cappello for synthesising β_{2a} and β_{1a} LLW/A mutant; Mr. Kerry McAndrew and Dr. Peter Milburn from the Biomolecular Resource Facility at JCSMR for providing peptides; Prof. Robert Dirksen and Dr. Linda Groom (Department of Pharmacology and Physiology, University of Rochester, New York, USA) for kindly providing WT and RyR1 RtoQ cDNA constructs; and, Prof. Martin Schneider and Dr. Erick Hernandez-Ochoa (Department of Biochemistry and Molecular Biology, University of Maryland School of Medicine, Maryland, USA) for providing the β_{1a} V490-A508 peptide and its scrambled form.

I am grateful to Prof. Dirksen and Prof. Schneider for allowing me to present results from their respective groups. I acknowledge that the experiments undertaken and figures generated in MF Schneider's laboratory were done by Prof. Schneider, Dr. Erick Hernandez-Ochoa and Dr. Rotimi Olojo. In addition, I acknowledge that the experiments undertaken and figures generated in RT Dirksen's laboratory were done by Dr. Linda Groom.

I am thankful to Ms. Courtney Segovis for undertaking the lipid bilayer experiments to examine the action of β_{2a} subunit. I also appreciate Dr. Karunasekara for providing lipid bilayer data for the hydrophobic surface mutant peptides.

I am, as always, grateful of my friends and family for their support, which was continuous during my PhD. A special thank you to Lora Jensen for editing my thesis and I

appreciate the time taken by Chris Thekkedam, Jennifer Rebbeck, Elize Wium, Deepthi Menon and Linwei Li for editing sections of my thesis.

Finally, I thank the Muscle Research Group and Molecular Genetics Group for their continuous help during my time at The John Curtin School of Medical Research. I have learnt so much invaluable information about research over the progression of this project, which is due to Prof. Dulhunty and the fellow researchers I worked with.

Abstract

Excitation-contraction (EC) coupling describes the process that links the excitatory action potential to muscle fibre contraction. Essential to this process is the release of Ca^{2+} from the sarcoplasmic reticulum (SR) via the ligand gated ryanodine receptor (RyR) in the SR membrane. In cardiac muscle fibres, RyR2 (cardiac isoform) activation is initiated by Ca^{2+} entry through the cardiac L-type voltage-gated dihydropyridine receptor (DHPR). In contrast, EC coupling in skeletal muscle fibres requires a physical interaction between skeletal DHPR and RyR1 (skeletal isoform), although the physical components of this interaction are unclear.

It had previously been shown that the C-terminus of the DHPR β_{1a} subunit strongly influences EC coupling in skeletal myotubes, since mutation of a heptad repeat motif (L478, V485 and V492) and C-terminal truncations > 29 residues reduce EC coupling. It has also been shown that the role of the C-terminal residues in EC coupling is likely via direct interaction with RyR1, because a polybasic K3495-R3502 motif in a RyR1 fragment (M3201-W3661) is important for β_{1a} association in pull-down assays and this region influences EC coupling in mouse myotubes. My previous work showed that a peptide (β_{1a} V490-M524) corresponding to the extreme 35 C-terminal residues directly increases RyR1 activity in planar lipid bilayers to the same level as β_{1a} subunit. One third of this peptide adopts an α -helix with a hydrophobic surface (residues L496, L500 and W503) on one side, which provides a putative RyR1 binding site. For this thesis I investigated the relative importance of the β_{1a} C-terminal heptad repeat and hydrophobic surface residues, and the RyR1 K3495-R3502 polybasic motif in the action of β_{1a} on RyR1 in lipid bilayers. I also compared the action of β_{1a} between RyR1 and RyR2, which was of particular interest given their systematic differences in receiving the EC coupling signal from DHPR.

Cytosolic exposure of β_{1a} A474-A508 peptide (containing both the heptad repeat and hydrophobic surface residues) to native RyR1 channels increased channel activity by 2-fold, which was similar to the action of β_{1a} V490-M524 peptide. Alanine substitution of heptad repeat residues did not alter the action of β_{1a} A474-A508 peptide on RyR1. In contrast, alanine substitution of hydrophobic surface residues abolished the action of β_{1a} V490-M524 on RyR1 and reduced pull-down of RyR1 by 85%. Curiously, individual substitution of the hydrophobic surface residues abolished the effect of the β_{1a} V490-M524 peptide at +40 mV, but not at -40 mV. Overall, the results show that the modulatory action of β_{1a} on RyR1 depends on all three β_{1a} hydrophobic surface residues, but not the heptad repeat.

The action of β_{1a} on RyR1 was abolished when the six basic residues in the RyR1 K3495-R3502 region were neutralised by mutation to glutamine residues. In addition and intriguingly, the β_{1a} subunit increased RyR2 activity in a similar manner as RyR1. This suggests

that β_{1a} may bind to a hydrophobic pocket conserved in RyR1 and RyR2 and that is influenced by the presence of the polybasic K3495-R3502 motif.

Publications

Papers:

Rebeck, R. T., Karunasekara, Y., Gallant, E. M., Board, P. G., Beard, N. A., Casarotto, M. G., and Dulhunty, A. F. (2011) The β_{1a} subunit of the skeletal DHPR binds to skeletal RyR1 and activates the channel via its 35-residue C-terminal tail. *Biophys J* 100:922-30.

Karunasekara, Y.¹, Rebeck, R. T.¹, Weaver, L. M., Board, P. G., Dulhunty A. F.² and Casarotto, M. G.² (2012) An α -helical C-terminal tail segment of the skeletal L-type Ca^{2+} channel β_{1a} subunit activates ryanodine receptor type 1 via a hydrophobic surface. *FASEB J* 26(12): 5049-59

¹equal first author contribution; ²equal senior author contribution.

Hernandez-Ochoa, E.O.^Δ, Olojo, R.O.^Δ, Rebeck, R.T.^Δ, Dulhunty, A.F. and Schneider, M. F. (2013) β_{1a} 490-508, a 19-residue peptide from C-terminal tail of Cav1.1 β_{1a} subunit potentiates voltage-dependent calcium release in adult skeletal muscle fibres. *Biophys J* (In Press)

^Δcontributed equally to this work

Rebeck, R. T., Karunasekara, Y., Board, P. G., Beard, N. A., Casarotto, G. and Dulhunty, A. F. (2013) Skeletal muscle excitation-contraction coupling: who are the dancing partners? *IJBCB* (In Press)

Conference attendance:

Gage Conference on Muscle, Canberra, Australia – 2010

Rebeck R. T., Gallant, E. M., Beard, N. A., Casarotto, M. G. and Dulhunty A. F. *In vitro* interactions between the 35 C-terminus residues of the β_{1a} subunit of DHPR and RyR1 from skeletal muscle. Poster presentation (co-recipient of Best Student Poster Prize)

Australian Physiological Society/Australian Society of Biophysics Meeting, Adelaide, Australia – 2010

Rebeck, R. T., Karunasekara, Y., Gallant, E. M., Beard, N. A., Casarotto M. G. and Dulhunty A. F. *In vitro* interactions between C-terminal residues of the β_{1a} subunit of DHPR and RyR1 from skeletal muscle. Poster presentation

Gage Conference on Ion Channels and Transporters, Canberra, Australia – 2011

Rebbeck, R. T., Karunasekara, Y., Gallant, E. M., Beard, N. A., Casarotto, M. G. and Dulhunty, A. F. *In vitro* interactions between C-terminal residues of the β_{1a} subunit of DHPR and RyR1 from skeletal muscle. Poster presentation

Gage Conference on Muscle, Canberra, Australia – 2012

Rebbeck, R. T., Karunasekara, Y., Board, P. G., Casarotto, M. G., Beard, N. A. and Dulhunty, A. F. *In vitro* interactions between C-terminal residues of the dihydropyridine receptor β_{1a} subunit and the type 1 ryanodine receptor. Poster presentation

Gordon Conference on Muscle: Excitation-Contraction Coupling, Les Diablerets, Switzerland – 2012

Rebbeck, R. T., Karunasekara, Y., Board, P.G., Casarotto, M.G., Beard, N. A. and Dulhunty, A. F. *In vitro* interactions between C-terminal residues of the DHPR β_{1a} subunit and the RyR1. Poster presentation

Biophysical Society 57th Annual Meeting Philadelphia, United States of America – 2013

Rebbeck, R. T., Willemse, H., Groom, L., Dirksen, R. T. and Dulhunty, A. F. Interactions between dihydropyridine β_{1a} subunit and ryanodine receptor isoforms. Poster presentation

Gage Conference on Ion Channels/Transporters, Canberra, Australia – 2013

Rebbeck, R. T., Willemse, H., Groom, L., Dirksen, R. T. and Dulhunty, A. F. Interactions between dihydropyridine β_{1a} subunit and ryanodine receptor isoforms. Poster presentation (Student Poster Prize “Runner Up”)

Abbreviations and Symbols

ADP	adenosine 5' diphosphate
AID	α -interaction domain
ANOVA	analysis of variance
APS	ammonium persulfate
ATP	adenosine 5' triphosphate
BAPTA	1,2-bis(2-aminophenoxy)ethane-N,N,N',N'-tetra-acetic acid
BCA	bicinchoninic acid
BID	β interacting domain
CaM	calmodulin
Cryo EM	cryo-electron microscopy
CSQ	calsequestrin
DHPR	dihydropyridine receptor
DTT	dithiothreitol
<i>E. coli</i>	Escherichia coli
EC coupling	excitation-contraction coupling
ECL	enhanced chemoluminescence
EDTA	ethylenediaminetetraacetic acid
EM	electron microscopy
ER	endoplasmic reticulum
FKBP	FK-506 binding protein
FRET	fluorescence resonance energy transfer
GK	guanylate kinase
HEK293	human embryonic kidney 293 cell line
HRP	horseradish peroxidase
I'	mean current
I'_F	fractional mean current
IPTG	isopropyl β -D-1-thiogalactopyranoside
JP	junctophilin

LB	lysogeny broth
Ni-NTA	nickel-nitrilotriacetic acid
NMR	nuclear magnetic resonance
PBS	phosphate buffered saline solution
P _i	orthophosphate
P _o	open probability
PVDF	polyvinylidene difluoride
RP-HPLC	reverse phase high performance liquid chromatography
RyR	ryanodine receptor
SDS	sodium dodecyl sulfate
SDS-PAGE	SDS-polyacrylamide gel electrophoresis
SEM	standard error of the mean
SH3	sarcoma (src) homology domain 3
SR	sarcoplasmic reticulum
STAC3	SH3 and cysteine rich domain 3
STIM1	stromal interaction molecule 1
TC	terminal cisternae
TEMED	tetramethylethylenediamine
TES	N-Tris[hydroxymethyl]methyl-2-aminoethansulfonic acid
Tris	tris(hydroxymethyl)aminomethane
T-tubule	transverse tubule
V	voltage
WT	wild type

Table of Figures

Figure 1. 1 Three types of muscle tissue.	2
Figure 1. 2 Structure of a mammalian skeletal muscle fibre.	3
Figure 1. 3 Structural components of a mammalian cardiac muscle cell.	5
Figure 1. 4 Mechanisms of myofibril shortening.	7
Figure 1. 5 Structure of the dihydropyridine receptor.	10
Figure 1. 6 Arrangement of DHPR in skeletal and cardiac fibres.	11
Figure 1. 7 Overall structure of RyR1.	30
Figure 1. 8 Models of the RyR1 pore-forming region.	31
Figure 1. 9 The potential interplay between proteins involved in EC coupling.	41
Figure 2. 1 Setup for peptide purification using RF-HPLP.	46
Figure 2. 2 A diagram illustrating the systematics of preparative gel electrophoresis and fraction collection using the BIO-RAD Prep-Cell system.	52
Figure 2. 3 The planar bilayer apparatus and setup.	57
Figure 3. 1 Single and multiple RyR1 openings within a bilayer.	65
Figure 3. 2 Single channel maximal current amplitude for +40 mV and -40 mV.	67
Figure 3. 3 Linear relationship of single channel I'_F and P_o in lipid bilayers at +40 and -40 mV	68
Figure 3. 4 Regulatory effect of <i>cis</i> [Ca^{2+}], ATP and ruthenium red on single channel activity in planar lipid bilayers.	70
Figure 4. 1 DHPR β C-terminal sequence alignment and similarity.	73
Figure 4. 2 The model structure of β_{1a} V490-M524 peptide.	74
Figure 4. 3 Sequences of the peptides corresponding to sections of the extreme 51 residues C-terminal region of mouse β_{1a} subunit.	75
Figure 4. 4 Similar modulatory action of β_{1a} V490-M524 and β_{1a} A474-A508 peptide on RyR1 activity in lipid bilayers.	79

Figure 4. 5 The effect of β_{1a} V490-M524 and β_{1a} A474-A508 peptides on single channel gating parameters in lipid bilayers.....	82
Figure 4. 6 The effect of β_{1a} V490-M524 and β_{1a} A474-A508 peptides on the open and closed dwell-times and on the probability of events occurring within each open and closed dwell-time constant components.....	84
Figure 4. 7 Similar modulatory action of β_{1a} A474-A508 and β_{1a} A474-A508 LVV/A peptides on RyR1 activity in lipid bilayers.....	86
Figure 4. 8 The similar modulatory effect of β_{1a} A474-A508 and β_{1a} A474-A508 LVV/A peptides on single channel gating parameters in lipid bilayers.....	88
Figure 4. 9 The similar modulatory effect of β_{1a} A474-A508 and β_{1a} A474-A508 LVV/A peptides on the open and closed dwell-times and on the probability of events occurring within each open and closed dwell-time constant components.....	89
Figure 4. 10 The similar the effect of β_{1a} A474-A508 and V490-A508 peptides on RyR1 activity in lipid bilayers.	91
Figure 4. 11 The similar modulatory effect of β_{1a} V490-A508 and β_{1a} A474-A508 peptides on single channel gating parameters in lipid bilayers.....	93
Figure 4. 12 The modulatory effect of β_{1a} V490-A508 peptides on the open and closed dwell-times and on the probability of events occurring within each open and closed dwell-time constant components.....	94
Figure 4. 13 Intracellular dialysis of β_{1a} V490-A508 peptide, not its scrambled form, increases voltage-induced SR Ca^{2+} release and membrane Ca^{2+} current through DHPR.....	97
Figure 4. 14 Binding of β_{1a} V490-M524 and β_{1a} V490-M524 LLW/A peptides to native RyR1.	99
Figure 4. 15 The effect of β_{1a} 490-524 hydrophobic surface mutants on RyR1 activity in lipid bilayers.....	101
Figure 4. 16 The effect of β_{1a} V490-M524 hydrophobic surface repeat peptides on single channel gating parameters in lipid bilayers.....	104
Figure 4. 17 The similar modulatory effect of mouse and zebrafish β_{1a} C-tail peptides on RyR1 activity in lipid bilayers.	106
Figure 4. 18 The effect of mouse and zebrafish β_{1a} C-tail peptides on single channel gating parameters in lipid bilayers.....	107

Figure 4. 19 The similar modulatory effects of mouse and zebrafish β_{1a} C-tail peptides on the open and closed dwell-times and on the probability of events occurring within each open and closed dwell-time constant components.	109
Figure 4. 20 The lack of modulatory effect of β_{1a} LLW/A, β_{2a} , and Trunc β_{1a} subunits on RyR1 activity in lipid bilayers.	111
Figure 4. 21 The lack of modulatory effect of β_{1a} LLW/A, β_{2a} , Trunc β_{1a} subunits on single channel gating parameters in lipid bilayers.	113
Figure 5. 1 The effect of β_{1a} subunit on RyR1 and RyR2 activity in lipid bilayers.....	126
Figure 5. 2 The similar modulatory effect of β_{1a} subunit on RyR1 and RyR2 single channel gating parameters in lipid bilayers.....	127
Figure 5. 3 The effect of β_{1a} subunit on the RyR1 or RyR2 open and closed dwell-times and on the probability of events occurring within each open and closed dwell-time constant components.....	129
Figure 5. 4 The voltage-induced maximal SR Ca^{2+} release and DHPR Ca^{2+} current in <i>dyspedic</i> myotubes expressing either WT RyR1 or RyR1 KtoQ mutant.	131
Figure 5. 5 The effect of β_{1a} subunit on WT RyR1 and RyR1 KtoQ mutant activity in lipid bilayers.	134
Figure 5. 6 The effect of β_{1a} subunit on WT RyR1 and RyR1 KtoQ single channel gating parameters in lipid bilayers.....	136
Figure 6. 1 The possible location of β_{1a} binding site on RyR1, as based on CaM binding site.	145
Figure 6. 2 The DHPR tetrad arrangement and possible β_{1a} subunit positioning in relation to RyR1.....	147
 Table of Tables	
Table 1. 1 Tissue distribution of β isoforms.	18
Table 2. 1 Corresponding sequence of peptides to the DHPR β_{1a} subunit.....	45
Table 2. 2 Reverse phase high performance liquid chromatography (RP-HPLC) elution gradient for peptides.	47

Table 4. 1 Mean control parameters for channels used in analysis of β_{1a} V490-M524 and β_{1a} A474-A508 peptides.....	80
Table 4. 2 Mean control parameters for channels used in analysis of β_{1a} A474A508 LVV/A peptide.....	87
Table 4. 3 Mean control parameters for channels used in analysis of β_{1a} V490-A508 and β_{1a} V490-A508 scm peptides.....	92
Table 4. 4a Mean control parameters for channels used in analysis of β_{1a} V490-M524 LLW/A, β_{1a} V490-M524 L496A, β_{1a} V490-M524 L500A and β_{1a} V490-M524 W503A peptides.....	102
Table 4. 5 Mean control parameters for channels used in analysis of β_{1a} V490-L520 zf peptide.	107
Table 4. 6 Mean control parameters for channels used in analysis of β_{1a} , β_{1a} LLW/A, β_{2a} and Trunc β_{1a} subunits.	112
Table 5. 1 Mean control parameters for channels used in analysis of β_{1a} subunit on RyR2.	127
Table 5. 2 Mean control parameters for channels used in analysis of β_{1a} on Wt RyR1 and RyR1 KtoQ.....	135

Table of Contents

1	Chapter One - Introduction	1
1.1	Muscle physiology	1
1.1.1	Skeletal muscle	1
1.1.2	Cardiac muscle.....	4
1.1.3	Smooth muscle.....	5
1.2	Excitation-Contraction (EC) Coupling	6
1.2.1	Skeletal EC coupling	8
1.2.2	Cardiac EC coupling.....	8
1.3	Dihydropyridine receptor (DHPR).....	9
1.3.1	The structure and function of the α_{1S} subunit	13
1.3.1.1	The function of α_{1S} subunit in EC coupling.....	14
1.3.2	The function and structure of the γ subunit	15
1.3.3	The structure and function of the $\alpha_{2\delta}$ subunit	16
1.3.4	The structure and function of the β subunit	17
1.3.4.1	Tissue distribution of β subunit	17
1.3.4.2	Constituents of β subunit and splicing variants	17
1.3.4.3	Function of β_{1a} subunit in skeletal muscle	19
1.3.5	Dihydropyridine receptor regulatory proteins during EC coupling	24
1.3.5.1	STIM1.....	24
1.3.5.2	STAC3	25
1.3.5.3	Junctophilin	25
1.3.5.4	JP-45	26
1.3.5.5	RyR1	27
1.4	Ryanodine receptor	28
1.4.1	RyR1 structure	29
1.4.2	Cytoplasmic regions of RyR1 involved in EC coupling.....	32
1.4.3	RyR1 regulation.....	34
1.4.3.1	Cytoplasmic Ca^{2+}	34
1.4.3.2	Cytoplasmic Mg^{2+}	35
1.4.3.3	ATP.....	35
1.4.3.4	Chemical modification.....	36
1.4.3.5	FKBPs.....	37
1.4.3.6	CaM and S100A1	37
1.4.3.7	Calsequestrin	38

1.4.3.8	Triadin	39
1.4.3.9	Junctin	40
1.5	Summary	40
1.6	Project Aims	42
1.7	This Thesis	42
2	Chapter Two – Materials and Methods	43
2.1	Materials	43
2.1.1	Reagents and chemicals	43
2.1.2	Peptides synthesised	44
2.1.3	Plasmid constructs	44
2.2	Methods	46
2.2.1	Purification of peptides	46
2.2.1.1	Reverse phase high performance liquid chromatography	46
2.2.1.2	Freeze drying the RF-HPLC eluate	47
2.2.1.3	Peptide identification	47
2.2.2	Isolation of skeletal SR vesicles	48
2.2.3	Expression and purification of recombinant proteins	49
2.2.3.1	Expression and purification of Usp2-cc	49
2.2.3.2	Expression and purification of β_{1a} subunit proteins	51
2.2.4	Laemmli SDS-PAGE for protein identification	53
2.2.5	Coomassie Brilliant Blue stain	54
2.2.6	Western blotting	54
2.2.6.1	Protein transfer	54
2.2.6.2	Immuno-detection	54
2.2.6.3	Visualisation (enhanced chemoluminescence, ECL)	55
2.2.6.4	Protein band density quantification	55
2.2.7	Protein quantification	55
2.2.7.1	Bicinchoninic acid (BCA) Protein Assay	55
2.2.7.2	Pierce 660nm Protein assay	56
2.2.7.3	Detergent compatible (DC) Protein Assay	56
2.2.8	[DNA] quantification using Nano-drop 1000	56
2.2.9	Planar lipid bilayers	56
2.2.9.1	Overview of lipid bilayer apparatus and setup	56
2.2.9.2	Agar bridges and silver chloride coated silver electrodes	58
2.2.9.3	Lipid bilayer formation and SR vesicle incorporation	58

2.2.9.4	Lipid bilayer experimental solutions	60
2.2.9.5	Channel recording.....	60
2.2.9.6	Data analysis.....	61
2.3	Statistics	62
3	Chapter Three – General properties of RyR1 in lipid bilayers	64
3.1	Introduction.....	64
3.1.1	Aim	64
3.2	Methods	64
3.3	Results.....	65
3.3.1	General observations.....	65
3.3.2	Characteristics of RyR1	66
3.3.3	Regulation of RyR1 activity during lipid bilayer experiments	69
3.3.3.1	Cytoplasmic [Ca ²⁺]	69
3.3.3.2	ATP.....	71
3.3.3.3	Ruthenium red	71
3.4	Conclusion	71
4	Chapter Four – Hydrophobic Beta1a subunit C-terminal residues that modulate RyR1 activity	72
4.1	Introduction.....	72
4.1.1	Aim	74
4.2	Materials and methods	75
4.2.1	Materials	75
4.2.1.1	Plasmid constructs	75
4.2.1.2	Synthesised peptides.....	76
4.2.2	Methods	76
4.2.2.1	Peptide synthesis, purification and identification	76
4.2.2.2	Expression and purification of β_{1a} , β_{1a} LLW/A and β_{2a} subunit	76
4.2.2.3	Preparation of SR vesicles	76
4.2.2.4	Planar bilayer recordings of RyR1	76
4.2.2.5	Affinity chromatography between β_{1a} peptides and RyR1	76
4.3	Results.....	78
4.3.1	Characterising the effect of the β_{1a} C-terminal residues A474-A508 on native RyR1 activity	78
4.3.2	The heptad repeat residues (L478, V485 and V492) do not impact the modulatory effect of A474-A508 on RyR1 activity.....	85

4.3.3	The overlapping region, V490-A508, is sufficient to replicate the effect of A474-A508 on RyR1 activity.....	90
4.3.4	The overlapping region, β_{1a} V490-A508, potentiates voltage-induced calcium release in adult skeletal myofibres	95
4.3.5	The hydrophobic surface residues (L496, L500 and W503) are important for the physical interaction between the β_{1a} C-terminal residues and RyR1.....	98
4.3.6	The hydrophobic surface residues are important for β_{1a} C-terminal modulation of RyR1 activity.....	100
4.3.7	The zebrafish β_{1a} C-terminal residues modulate RyR1 activity	105
4.3.8	The hydrophobic surface residues are important for β_{1a} subunit modulation of RyR1 activity.....	110
4.4	Discussion.....	114
4.4.1	Comparison between β_{1a} C-terminal regions: V490-M524 and A474-A508	114
4.4.1.1	Physiological implications	115
4.4.2	The irrelevance of heptad repeat residues in modulating RyR1 activity.....	115
4.4.2.1	Physiological implications	116
4.4.3	Importance of hydrophobic surface residue in modulating RyR1 activity.....	116
4.4.3.1	The action of the hydrophobic surface residues.....	116
4.4.3.2	The role of the individual proteins	117
4.4.3.3	Physiological implications	117
4.4.4	Comparison between the effectiveness of zebrafish and mouse β_{1a} C-tail residues in RyR1 modulation	118
4.4.4.1	Physiological implications	119
4.5	Conclusion.....	119

5 Chapter Five – Regions of the RyR responsible for the Beta1a subunit interaction 120

5.1	Introduction	120
5.1.1	Aim.....	120
5.2	Materials and Methods	121
5.2.1	Materials.....	121
5.2.1.1	Reagents and chemicals	121
5.2.1.2	Plasmid constructs.....	121
5.2.2	Methods.....	121
5.2.3	Expression and purification of β_{1a} subunit	121
5.2.4	Preparation of skeletal SR vesicles.....	121
5.2.5	Preparation of cardiac SR vesicles	121

5.2.6	Expression of recombinant WT RyR1 and RyR1 KtoQ mutant and isolation of micro vesicles	122
5.2.6.1	Expression of recombinant WT RyR1 and RyR1 KtoQ mutant.....	122
5.2.6.2	Isolation of micro vesicles	123
5.2.7	Planar bilayer recordings of RyR.....	123
5.3	Results.....	124
5.3.1	β_{1a} subunit modulates RyR2 activity.....	124
5.3.1.1	Characteristics of RyR2 in lipid bilayers.....	124
5.3.1.2	Response of RyR2 to cytosolic modulators.....	124
5.3.1.3	β_{1a} subunit increases RyR2 activity	125
5.3.2	The polybasic residues K3495-R3502 are important for β_{1a} subunit modulation of RyR1 activity	130
5.3.2.1	Polybasic RyR1 residues facilitate voltage-induced Ca^{2+} transients in transfected dyspedic myotubes.....	130
5.3.2.2	Characteristics of WT RyR1 and RyR1 KtoQ mutant in lipid bilayers.....	132
5.3.2.3	Response of WT RyR1 and KtoQ mutant to cytoplasmic regulators	133
5.3.2.4	The RyR1 polybasic K3495-R3502 motif residues are important for β_{1a} subunit modulation of RyR1 activity	135
5.4	Discussion.....	137
5.4.1	The action of β_{1a} subunit is conserved between RyR1 and RyR2	137
5.4.1.1	Physiological relevance and implications.....	137
5.4.2	Action of the β_{1a} subunit on WT RyR1.....	138
5.4.3	The importance of the RyR1 polybasic motif for interaction with β_{1a} subunit..	138
5.4.3.1	Physiological implications.....	139
5.5	Conclusion	140
6	Chapter six – General Discussion.....	141
6.1	Introduction.....	141
6.2	Possible mechanism of interaction between RyR1 and β_{1a}	143
6.3	Possible β_{1a} subunit binding sites on RyR1 and RyR2	144
6.4	Limitations	145
6.5	Proposed role of β_{1a} subunit and RyR1 interaction in skeletal EC coupling.....	146
6.6	Future work.....	148
6.7	Conclusion	149
7	References.....	150

CHAPTER ONE - INTRODUCTION

In this chapter, I provide a general background to muscle physiology and an extensive review of the mechanisms and proteins involved in skeletal excitation-contraction coupling. In particular, focusing on the components involved in the direct interaction between the dihydropyridine receptor and ryanodine receptor during skeletal muscle contraction. To provide context for the chimera studies that use heart specific isoforms, I also provide brief background to cardiac excitation-contraction coupling.

1.1 Muscle physiology

In mammals, there are three different classifications of muscle tissue, namely skeletal, cardiac and smooth. Each muscle type is composed of self-specific muscle fibres and cells (**Figure 1.1**), which are defined by physiological features catering for the specialised function of the muscle that they form. Unless cited otherwise, all general information in sections 1.1 and 1.2 is derived from text book sources (Kandel *et al.*, 2000, Hille, 2001, Marieb & Hoehn, 2010, Hill & Olson, 2012).

1.1.1 Skeletal muscle

Attached to the skeleton by tendons, skeletal muscle enables voluntary skeletal movement and helps maintain body posture. The primary requirements of skeletal muscle are to rapidly contract whilst maintaining a fine-tuned control over the strength of contraction. In brief, this is modulated by both the frequency of stimulations and percentage of fibres stimulated in a muscle, and is voluntarily controlled through the innervation of each muscle fibre by a motor neuron.

Structurally, skeletal muscle fibres are 10-100 μm in diameter and in humans, typically span the length of the muscle, which can be as long as 50 cm (Harris *et al.*, 2005). This exceptional fibre length is possible through the fusion of many embryonic progenitor cells, known as myoblasts, resulting in the multi-nucleated feature of skeletal muscle fibres (**Figure 1.1A**).

Each fibre is densely packed with bundles of longitudinally placed contractile components, known as myofibrils, which account for 80% of the cellular volume. The myofibrils are composed of overlapping thick and thin microfilaments constructed from myosin and actin molecules, respectively (Huxley & Niedergerke, 1954, Huxley & Hanson, 1954) (**Figure 1.2**). Each myofibril is segmented by contractile units, known as sarcomeres, which are individually boarded by Z discs and align with sarcomeres of neighbouring myofibrils. Consequently, alignment of the regions of thick microfilaments (A bands) and the non-overlapped thin microfilaments (I bands) appear as dark and light bands, respectively, under a light microscope; giving a striated appearance (**Figure 1.1A & Figure 1.2B**).

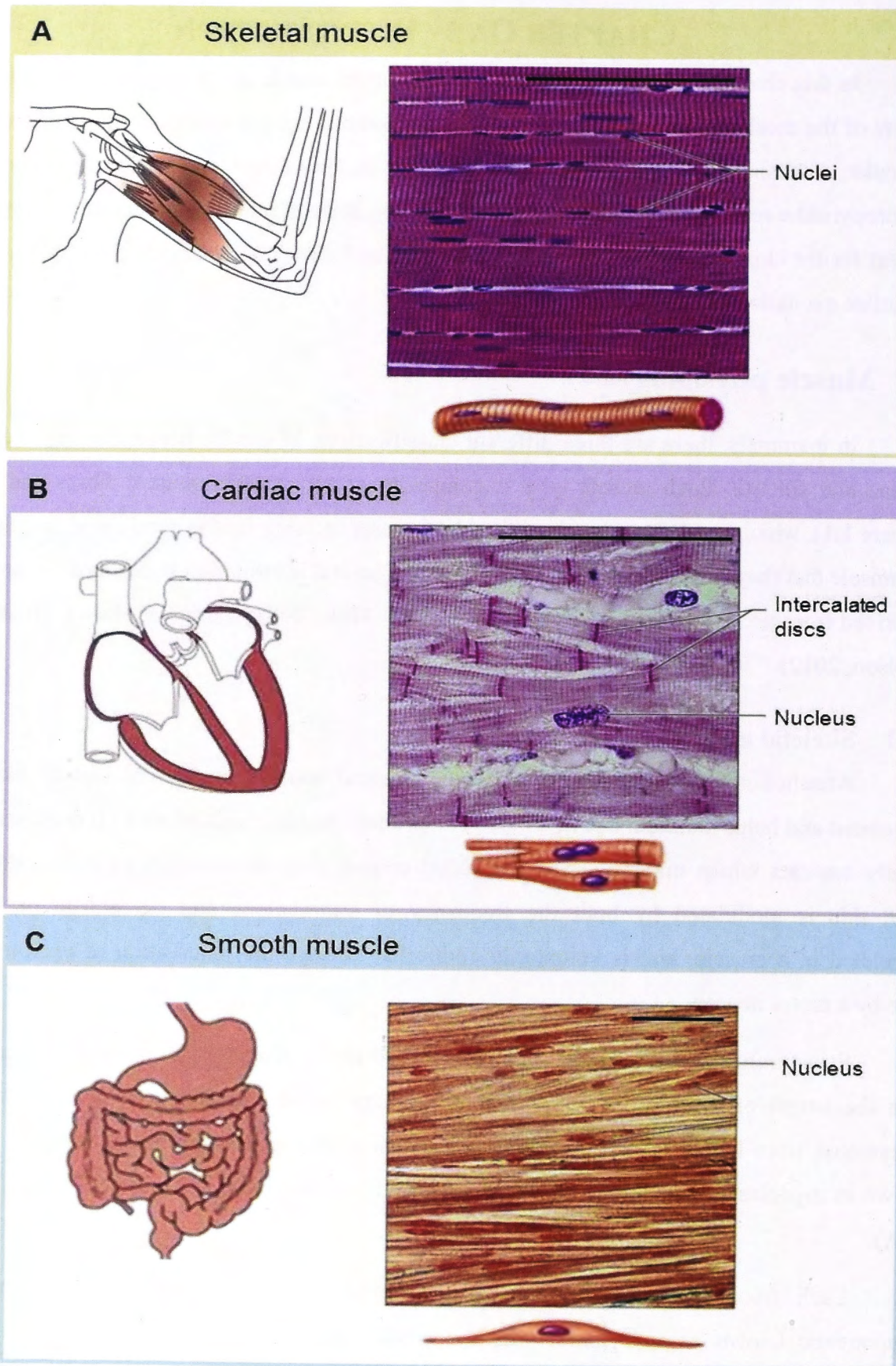


Figure 1. 1 Three types of muscle tissue.

The typical location (pink cartoon) and photomicrograph of Skeletal (**A**), Cardiac (**B**) and Smooth muscle (**C**). Scale bar (black) for each micrograph is $\sim 100 \mu\text{m}$. Skeletal and cardiac muscle fibres are characterised by striations, which are visible in the micrographs. **A**) Skeletal muscle tissue is connected to the skeleton via tendons. Each fibre typically extends the length of the tissue in humans and is multi-nucleated. **B**) Cardiac muscle tissue is exclusive to the heart, primarily lining the heart wall. Notably, small muscles extend from the wall into ventricular chamber to maintain valve closure. The fibres are mono- or di-nucleated, branched and connected at either end with intercalated discs. **C**) The smooth muscle lines the walls of hollow organs. Each cell is characterised by only one, centrally located nucleus. Images slightly adapted from Marieb and Hoehn (2010), Hill and Olson (2012).

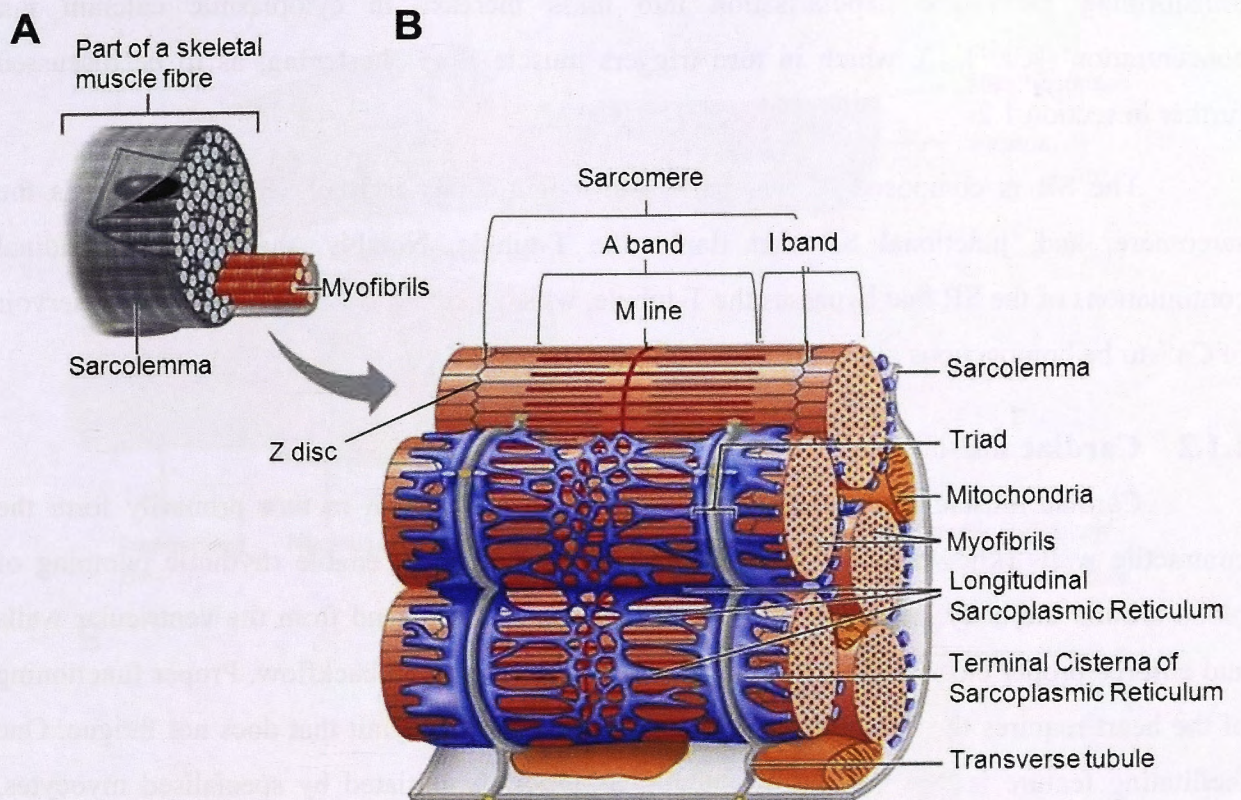


Figure 1.2 Structure of a mammalian skeletal muscle fibre.

A) The drawing shows a section of a skeletal muscle fibre, illustrating the parallel bundles of myofibrils that compose the bulk of a muscle fibre. **B)** A section of the fibre at higher magnification reveals each myofibril is composed of contracting units (individually known as sarcomeres) that are made up of partially overlapping thick and thin filaments. A prominent feature is the contrast between the regions consisting of thick filament (A-band) and the regions consisting of the non-overlapped thin filament (I-band) that provides the striated appearance. Each myofibril is surrounded by tubular networks of the sarcoplasmic reticulum. The transverse tubule invaginates from the surface to run along the A-I band junction and is flanked either side by the sarcoplasmic reticulum to form the triad. Image slightly adapted from Marieb and Hoehn (2010).

Muscle fibres have a specialised plasma membrane, known as the sarcolemma. As characteristic of excitable membranes, the sarcolemma contains voltage-gated ion channels that enable membrane depolarisation and hyperpolarisation for action potential propagation. The sarcolemma forms invaginations, known as transverse tubules (T-tubules) (Franzini-Armstrong & Porter, 1964). T-tubules penetrate deep into the fibre, running level with the A-I band junction, to permit action potential propagation throughout the fibre and local depolarisation near the contractile units (Huxley & Taylor, 1958). Each T-tubule is typically flanked on either side by the terminal cisternae (TC) of a modified endoplasmic reticulum tubular network, known as the sarcoplasmic reticulum (SR) (Franzini-Armstrong, 1972, Franzini-Armstrong, 1973). In skeletal muscle, the region where two TC associate with a T-tubule is known as the triad (**Figure 1.2B**), which was originally described as the flanking of endoplasmic reticulum on either side of an unclassified tubular network (Porter & Palade, 1957). This region is crucial for muscle contraction, as it enables close association between the components involved in

transforming membrane depolarisation into mass increase in cytoplasmic calcium ion concentration ($[Ca^{2+}]_{cyto}$), which in turn triggers muscle fibre shortening, as to be discussed further in section 1.2.

The SR is composed of two parts: the longitudinal, or free, SR that surrounds the sarcomere; and, junctional SR that flanks the T-tubule. Notably, there are longitudinal continuations of the SR that bypasses the T-tubule, which enables the large SR luminal reservoir of Ca^{2+} to be homogenous along the muscle fibre.

1.1.2 Cardiac muscle

Cardiac muscle fibres form cardiac muscle tissue, which in turn primarily form the contractile walls (known as the myocardium) of the heart that enable rhythmic pumping of blood around the body. In addition, small papillary muscles extend from the ventricular walls and enforce proper closure of valves in the heart to prevent blood backflow. Proper functioning of the heart requires the myocytes to contract as a co-operative unit that does not fatigue. One facilitating feature is that the action potential is regularly initiated by specialised myocytes, known as pacemaker cells in the sinoatrial node. Depolarisation is propagated from cell-to-cell across gap junctions at the intercalated discs bordering the end of each cell. Consequently, this provides uniform and paced contraction within sections of the heart. Another facilitating feature is that there is a high percentage of mitochondria, making up ~22-35% of the cytoplasm, which is thought to accommodate the high demand of adenosine 5' triphosphate (ATP) synthesis that is required for muscle contraction (section 1.2) and consequently preventing muscle fatigue. In contrast to skeletal muscle fibres, cardiac muscle cells are significantly smaller (average adult myocyte is 100-150 x 15-25 μm), interconnected through terminal intercalated discs and contain two nuclei at most (**Figure 1.3A**). However, several physiological features are very similar to those in skeletal muscle fibres. Firstly, the contractile units are similar and occupy ~50-60% of the cytoplasm, which gives cardiac muscle cells a striated appearance under a light microscope (**Figure 1.1B**). Secondly, the sarcolemma invaginates into the cell as T-tubules and is flanked in regions by the SR, which also encases each myofibril (**Figure 1.3B**). However, the T-tubule in cardiac muscle cells runs level with the Z disc and only interacts sparingly on one side of the T-tubule (**Figure 1.3B**). Hence the flanking region between the T-tubule and SR is known as a diad (**Figure 1.3B**), as opposed to a triad that are typical of skeletal myofibres (**Figure 1.2B**). Notably, the SR in cardiac muscle cells does not form TC and does not substantially expand at regions flanking T-tubule to form the TC observed in skeletal muscle fibres.

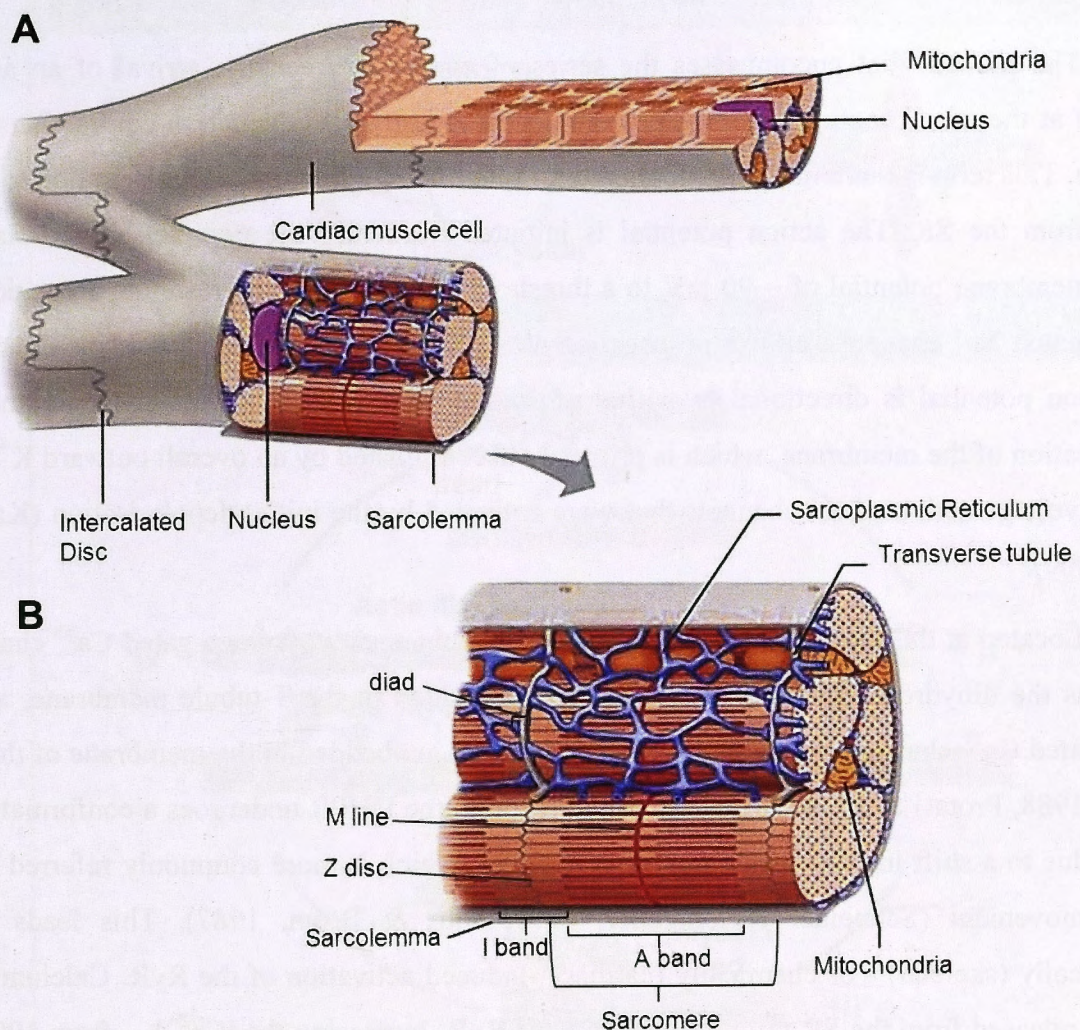


Figure 1.3 Structural components of a mammalian cardiac muscle cell.

A) The drawing shows a section of a cardiac muscle cell (cardiomyocyte), illustrating the parallel bundles of myofibrils and mitochondria that compose the bulk of the muscle fibre. Also, note the intercalated disks that connect the cells. **B)** A section of the fibre at higher magnification reveals each myofibril is composed of contracting units, individually known as sarcomere, that are mostly made up of partially overlapping thick and thin filaments. Each myofibril is sparsely surrounded by tubular networks of the sarcoplasmic reticulum and the transverse tubule that interact at the diad, which runs in line at the sarcomere border, called the Z disc. Note that it is the contrast between the region consisting of thick filament (A-band) and the region consisting of the non-overlapped thin filament (I-band) that provides a striated appearance of cardiomyocytes. An Image slightly adapted from Marieb and Hoehn (2010)

1.1.3 Smooth muscle

Smooth muscle fibres form smooth muscle tissue that line the walls of hollow organs such as arteries, veins and the gastrointestinal tract (**Figure 1.1C**), allowing involuntary contraction such as peristalsis in the gastrointestinal tract. As this study does not involve components that are specific to smooth muscle physiology or cellular contraction, it will not be discussed further.

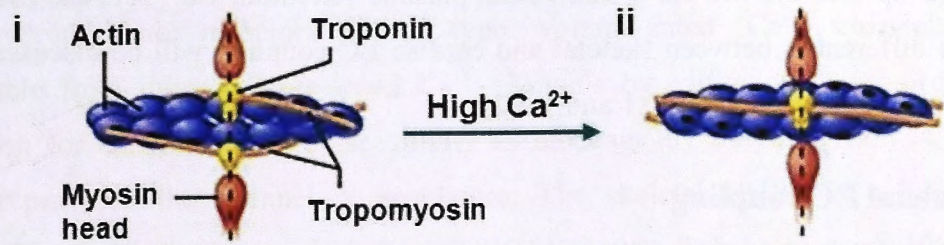
1.2 Excitation-Contraction (EC) Coupling

The process that encompasses the series of events between the arrival of an action potential at the triad junction and muscle contraction is known as excitation-contraction (EC) coupling. This term is more narrowly applied to events linking membrane depolarisation to Ca^{2+} release from the SR. The action potential is initiated by membrane depolarisation from the resting membrane potential of ~ 90 mV to a threshold of ~ 54 mV. The resultant activation of voltage-gated Na^+ channels, allows propagation along the sarcolemma and down the T-tubule. The action potential is directional by virtue of 1), fast inactivation of Na^+ channels and 2), repolarisation of the membrane, which is primarily accomplished by an overall outward K^+ flux through voltage-activated K^+ channels that were activated by the initial depolarisation (Kandel *et al.*, 2000).

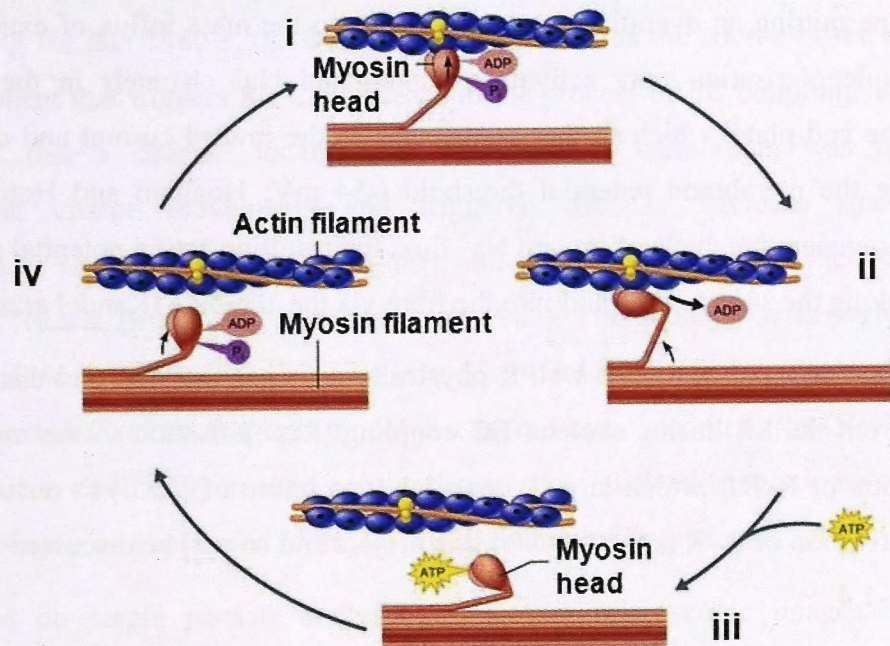
Located at the diad/triad are two types of Ca^{2+} channels: a voltage-gated Ca^{2+} channel, known as the dihydropyridine receptor (DHPR), embedded in the T-tubule membrane; and a ligand-gated Ca^{2+} channel, the ryanodine receptor (RyR), embedded in the membrane of the SR (Block, 1988, Protasi *et al.*, 1996). Upon depolarisation, the DHPR undergoes a conformational change due to a shift in intramembrane basic residues, which is more commonly referred to as charge movement (Schneider & Chandler, 1973, Rios & Brum, 1987). This leads to a mechanically (skeletal) - or chemically (cardiac) -induced activation of the RyR. Calcium ions are then released from the SR through the activated RyR, increasing the $[\text{Ca}^{2+}]_{\text{cyto}}$ from 100 nM to 1-10 μM and inducing myofibril shortening (Szent-Gyorgyi, 1975).

The molecular mechanism of myofibril shortening is known as cross bridge cycling (**Figure 1.4**). The term “cross bridge” refers to the interaction between myosin heads and actin. Under resting conditions, the myosin binding site on the actin filament is occluded by a complex with two other proteins, tropomyosin and troponin. As the $[\text{Ca}^{2+}]_{\text{cyto}}$ increases to the low μM range, Ca^{2+} binds to troponin, which weakens the troponin-actin interaction and results in tropomyosin no longer occluding the myosin binding site as it rotates around the actin filament (**Figure 1.4A**) (Narita *et al.*, 2001). Having access to its binding site and upon hydrolysis of ATP, myosin associates with actin and physically pulls the actin filaments longitudinally along the myosin filaments as the head rotates, levering a distance of ~ 7 nm (**Figure 1.4A**). This results in the release of the hydrolysis products (orthophosphate, P_i , and adenosine 5' diphosphate, ADP) and the site is quickly replaced by ATP, which rapidly dissociates actin and myosin (**Figure 1.4B**). The duration of each cycle is estimated to be < 5 ms and the distance of the cross bridge throw is ~ 10 nm. The continuation of this cycle leads to fibre shortening and ultimately muscle contraction (**Figure 1.4C**) (as reviewed by Gordon *et al.* (2000)).

A Rotation of tropomyosin to open myosin head binding site on actin filament



B A cross bridge cycle



C Muscle fibre shortening

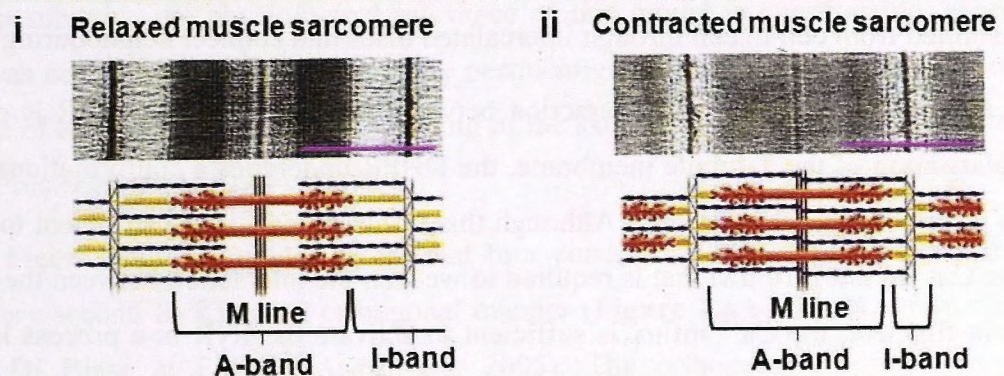


Figure 1. 4 Mechanisms of myofibril shortening.

A) Ca^{2+} induced rotation of tropomyosin from occluding the myosin head binding site on actin filament. **i)** Under resting conditions, the myosin head binding site on actin is occluded by tropomyosin, held in place by troponin. **ii)** Micromolar levels of Ca^{2+} bind to the troponin complex, resulting in a rotation of tropomyosin and consequently liberating the myosin binding site, which then permits **B)** the cross bridge cycling. **i)** With the myosin binding site free, this allows the actin to bind to the myosin head. The affinity of this interaction is strongly enhanced by the ATP hydrolysis components ($\text{ADP} + \text{P}_i$) attached to the myosin head. This leads onto **ii)** the myosin head rotating and pulling the myosin filament towards the M-line. ADP and P_i are released during the process, which leaves the site available for ATP. **iii)** Binding of ATP leads to dissociation of the actin filament. **iv)** Rapid ATP hydrolysis returns the orientation of the myosin head and allows high affinity binding at the actin binding site, returning to the position of **i)**. **C)** The micrographs and corresponding illustrations of a skeletal muscle fibre sarcomere in the relaxed (**i**) and contracting positions (**ii**). Scale bar (pink) for each micrograph is $\sim 1 \mu\text{m}$. Note, the actin filaments are pulled longitudinally into the M-line, resulting in shortening of the I-band, but not the A-band. Image adapted from Marieb and Hoehn (2010).

The contraction is arrested when the $[Ca^{2+}]_{cyto}$ returns to resting levels. Cytosolic Ca^{2+} is mainly taken up into the SR via a sarco/endo-plasmic reticulum Ca^{2+} ATPase (SERCA). The mechanistic differences between skeletal and cardiac EC coupling will be discussed further in the two following subsections (1.2.1 and 1.2.2).

1.2.1 Skeletal EC coupling

The skeletal action potential is initiated by neuronal presynaptic release of a transmitter, acetylcholine (ACh), that specifically activates nicotinic ACh receptors on the end-plate of the muscle fibre, permitting an overall inward current due to the mass influx of extracellular Na^+ . The resulting depolarisation may activate voltage-gated Na^+ channels in the sarcolemma, surrounding the end-plate, which further contributes to the inward current and depolarisation. Upon reaching the membrane potential threshold (-54 mV; Hodgkin and Horowitz (1960)) required for a regenerative cycle of inward Na^+ flux, the resulting action potential propagates bi-directionally along the sarcolemma and into the fibre via the T-tubule (Kandel *et al.*, 2000).

The depolarisation-activated DHPR physically activates the RyR and this permits mass Ca^{2+} release from the SR during skeletal EC coupling. Repolarisation of the membrane halts DHPR activation of RyR1, which largely contributes to return of $[Ca^{2+}]$ to resting levels. The mechanical activation of RyR is the focus of this project and so will be discussed in more detail in sections 1.3-1.4.

1.2.2 Cardiac EC coupling

As mentioned in section 1.1.2, pacemaker cells rhythmically initiate an action potential that is transmitted from cell to cell through intercalated discs that connect neighbouring cells.

In cardiac EC coupling, the interaction between the DHPR and the RyR is chemical. Upon depolarisation of the T-tubule membrane, the DHPR undergoes a conformational change that allows influx of extracellular Ca^{2+} . Although this influx of Ca^{2+} is not sufficient to increase cytoplasmic Ca^{2+} to the 1-10 μM that is required to weaken the interaction between the troponin and the actin filament, the Ca^{2+} influx is sufficient to activate the RyR in a process known as Ca^{2+} -induced Ca^{2+} release. The large SR luminal Ca^{2+} influx into the cytoplasm initiates the cardiac muscle fibre contraction (as reviewed by Dulhunty *et al.* (2002)).

Unlike skeletal EC coupling, the increase in cytoplasmic Ca^{2+} is substantially supplemented by extracellular Ca^{2+} . Thus, cellular relaxation requires cytoplasmic Ca^{2+} removal into both the SR luminal and extracellular environment at a ratio of $\sim 7:3$ in larger mammals, such as humans and rabbits. This Ca^{2+} removal primarily involves respective activity of SERCA2 and a Na^+/Ca^{2+} exchanger (NCX) (as reviewed by Bers (2002)).

Hereafter, the mechanisms described refer to mechanisms and predominant proteins found in skeletal muscle, unless otherwise indicated.

1.3 Dihydropyridine receptor (DHPR)

Dihydropyridine receptors are L-type voltage-gated Ca^{2+} channels that are distinguishable from other voltage-gated Ca^{2+} channels by virtue of 1) requiring a strong depolarisation for activation and 2) sensitivity to blockage by dihydropyridines, which is a feature that provided the channel nomenclature. The skeletal DHPR is a heteropentamer composed of the five subunits: α_1 , α_2 , β , δ , and γ (Curtis, 1984, Takahashi *et al.*, 1987), with the predicted assembly of a DHPR in the T-tubule membrane shown in **Figure 1.5A**.

During the late 1980's, the DHPR was recognised as the source of the intramembrane charge movement that triggers SR Ca^{2+} release in the process of EC coupling. The first studies demonstrated that a channel localised in the T-tubule membrane, was responsible for intramembrane charge movements and triggered SR Ca^{2+} release shared the same pharmacological response to dihydropyridines and structural identity as the DHPR (Lamb & Walsh, 1987, Rios & Brum, 1987, Tanabe *et al.*, 1987). This theory was strongly reinforced by a study published in the succeeding year that identified the DHPR α_{1S} subunit as the likely product mutated in a mouse *dysgenic* model that lacked muscle contraction (Beam *et al.*, 1986), particularly since electrically evoked contraction in these skeletal *dysgenic* myotubes could be restored by exogenous expression of the DHPR α_{1S} subunit (Tanabe *et al.*, 1988).

Based on single particle analysis of electron microscopic images, the current 3-dimensional reconstruction of the skeletal DHPR displays a main body of 17x11x8 nm (**Figure 1.5B**) (Szpyt *et al.*, 2012). Although this coincides with the predicted quaternary structure of the α_1 and β subunits, the physiological relevance of this model is questionable, especially since RyR1 was not present. This is particularly pertinent given as other studies have shown that the presence of RyR1 influences the positioning of the skeletal α_1 cytoplasmic loops (Paolini *et al.*, 2004a, Polster *et al.*, 2012).

Freeze fracture replicas reveal that four clustered DHPRs form a tetrad that interacts with every second RyR1 in an orthogonal manner (**Figure 1.6A**) (Block, 1988, Paolini *et al.*, 2004b, Di Biase & Franzini-Armstrong, 2005). The orthogonal manner refers to DHPR alignment with every second RyR1 in two orthogonal directions. This arrangement appears to be specific to skeletal muscle. When compared to the DHPR arrangement in cardiac myocytes, although DHPR are clustered in junctional regions, they do not form tetrads and are not disposed in any detectable ordered arrangement in regions of the sarcolemma that junction the SR membrane, as shown in **Figure 1.6B** (Franzini-Armstrong *et al.*, 1998).

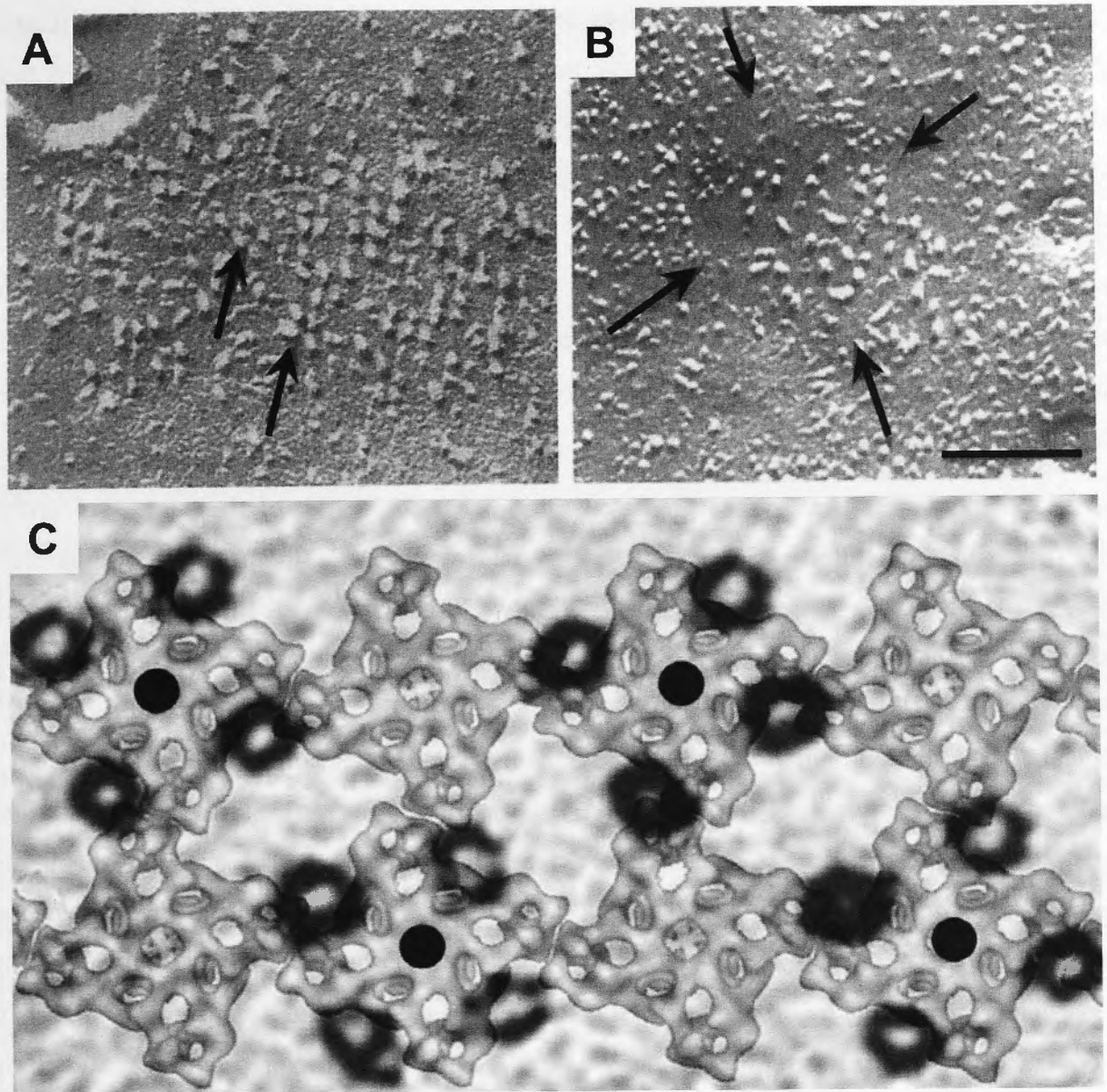


Figure 1. 6 Arrangement of DHPR in skeletal and cardiac fibres.

A and **B**) DHPR clustering in freeze fracture EM images of the surface membrane of a mouse skeletal myotube (**A**), and a chick ventricular myocyte (**B**). Individual DHPR can be seen as the primary membrane embedded particle. Note that although both surfaces are densely occupied by DHPR, only the skeletal membrane displays a regular tetrad arrangement, as highlighted by arrows directly (**A**) or within the region indicated (**B**). Scale bar (black) is $\sim 0.1 \mu\text{m}$. Image from Franzini-Armstrong *et al.* (1998). **C**) A scaled superimposition of the DHPR tetrads above the juxtaposed RyR1 (3-dimensional reconstruction) in skeletal muscle. Note, each tetrad is predicted to interact with every second RyR1 with orthogonal arrangement. Image from Paolini *et al.* (2004b).

A physical interaction between the DHPR and RyR1 during resting and contracting states is highly likely. During contraction, this is especially likely given that skeletal EC coupling does not depend on extracellular Ca^{2+} (Armstrong *et al.*, 1972, Miledi *et al.*, 1984) and no other chemical transmitter has been discovered as of yet. Furthermore, chelation of cytoplasmic Ca^{2+} in skinned toad skeletal muscle fibres does not halt SR Ca^{2+} release following T-tubule depolarisation (Lamb & Stephenson, 1990). In conditions that replicate the resting state, modulation of RyR1 activity alters the conformation of the DHPR in tetrads (Paolini *et al.*, 2004a). Moreover, addition of pharmaceutical agents that alter RyR1 gating indirectly alter

DHPR Ca^{2+} current (Balog & Gallant, 1999, Bannister & Beam, 2009) and vice versa (Lee *et al.*, 2004, Robin & Allard, 2012).

DHPR location is not restricted to the triad. Immunohistochemistry has also identified DHPR in discrete foci in the sarcolemma (Jorgensen *et al.*, 1989, Pietri-Rouxel *et al.*, 2010). The functional role of DHPR that are both sarcolemmal-localised and RyR1-uncoupled is unclear. However, recent research suggests that sarcolemmal DHPR may facilitate gene expression in skeletal muscle fibres (Pietri-Rouxel *et al.*, 2010). This function may extend to cardiac myocytes as well, but this has not been experimentally established yet.

The Ca^{2+} current and charge movement properties of functional DHPRs have been well defined. Charge movement is measured as the non-linear component of the capacitive current, that reflects intramembrane movement of the basic residues within the α_{1S} transmembrane segment, following membrane depolarisation (Hille, 2001). The charge movement density can be used to quantify the relative density of functional DHPR proteins in the plasmalemma (e.g. Beurg *et al.* (1997), Beurg *et al.* (1999a), Beurg *et al.* (1999b), Cheng *et al.* (2005)). This is a logical connection, particularly since charge movement is deficient in α_{1S} -null myotubes and is restored with α_{1S} expression (Adams *et al.*, 1990). Furthermore, the level of skeletal fibre contraction closely reflects the level of charge movement in response to membrane depolarisation (Dulhunty & Gage, 1983). However, it is notable that the level of charge movement does not necessarily reflect the levels of DHPR expressed in the plasmalemma. This is particularly indicated by the fact that the presence of skeletal β_1 and RyR isoforms appears to modulate the ratio of charge movement to DHPR membrane expression, which will be discussed further in sections 1.3.4.3.3 and 1.3.5.5.

Currently, the DHPR appears to have three primary functions in skeletal muscle fibres. Firstly, the DHPR located in the triadic regions of the T-tubule is essential for physical activation of RyR1 during EC coupling, a process termed “orthograde” coupling. Secondly, several studies suggest that during resting conditions, the DHPR maintains the closed conformation of RyR, preventing “leak” (Lee *et al.*, 2004, Eltit *et al.*, 2011, Robin & Allard, 2012). The term “leak” refers to excess Ca^{2+} release above healthy levels through RyR1 in its open conformation when the fibre is in the resting state. Indeed, an uncoupling of DHPR and RyR1, attributed to mutations associated with malignant hyperthermia, has been suggested to enhance RyR1 leak and consequently lead to abnormally high $[\text{Ca}^{2+}]_{\text{cyto}}$ and low SR luminal $[\text{Ca}^{2+}]$ ($[\text{Ca}^{2+}]_{\text{lumen}}$) (Yang *et al.*, 2007, Eltit *et al.*, 2012). The authors suggest that the increased $[\text{Ca}^{2+}]_{\text{cyto}}$ may contribute to the pathology of malignant hyperthermia promoting hypersensitivity of RyR1 to volatile halogenated anaesthetics, which is a trigger of a malignant hyperthermia episode. Finally, the DHPR is thought to also be involved in maintaining gene expression, in a signalling process known as excitation-transcription coupling. However, the direct role that the

DHPR has in this process is unclear and perhaps includes more than one pathway. Pietri-Rouxel and colleagues (2010) suggest that the small sub-population of DHPRs in the sarcolemma is responsible for preventing cellular atrophy (Pietri-Rouxel *et al.*, 2010). Interestingly, other studies demonstrate that the DHPR modulates the transcription pathways that govern skeletal muscle fibre type (Araya *et al.*, 2003, Jorquera *et al.*, 2013), although whether this is restricted to a specifically located subpopulation of DHPRs is unknown.

A recurring observation in the literature is that effective DHPR tetrad formation and charge movement is necessary for functional EC coupling, but this does not necessarily infer functional EC coupling. EC coupling function is typically assessed as membrane depolarisation-induced force production and/or SR Ca^{2+} release (Ca^{2+} transients), presumably via RyR1. The latter is measured using Ca^{2+} sensitive fluorescent dyes in the cytoplasm. The role of individual DHPR subunits in EC coupling will be explored in sections 1.3.1 – 1.3.4, particularly focusing on the potential roles in tetrad formation, charge movement and direct interaction with the RyR1.

1.3.1 The structure and function of the α_{1S} subunit

The skeletal α_1 subunit ($\text{Ca}_v1.1$; 175 kDa) contains the Ca^{2+} channel pore and the binding site for dihydropyridines (Takahashi *et al.*, 1987). The α_1 subunit is composed of four trans-membrane domains that surround the pore of the DHPR ion channel, with loops linking the four domains exposed to the cytoplasm (Tanabe *et al.*, 1987)(**Figure 1.5**). Each domain contains six trans-membrane segments (S1-S6), with S4 forming the voltage sensor of the channel (**Figure 1.5A**) and S5 and S6 composing the pore forming region. The voltage sensing properties depend on the regularly spaced basic residues that reside in S4, which translocate in the membrane in response to membrane depolarisation, effectively moving the whole S4 segment and constituting the DHPR charge movement (Tanabe *et al.*, 1987).

Although there are ten different genes encoding the α_1 subunits that form the basis of all voltage-gated Ca^{2+} channels in mammals, α_{1S} is the predominant form in skeletal muscle (as reviewed by Ertel *et al.* (2000)). Two studies report the presence of the predominant cardiac isoform (α_{1C} ; $\text{Ca}_v1.2$) in certain types of skeletal muscle (Pereon *et al.*, 1998, Froemming *et al.*, 2000). However, absence of detectable muscle contraction in the α_{1S} -null (*dysgenic*) mouse model suggests that any α_{1C} does not functionally contribute to skeletal EC coupling (Tanabe *et al.*, 1988). Notably, α_{1C} is thought to be responsible for the small voltage-induced DHPR current observed in *dysgenic* myotubes. This is particularly since the voltage-induced DHPR current in *dyspedic* myotubes displays kinetic- and pharmacological-properties that are more similar to those observed in *dysgenic* myotubes that express α_{1C} rather than α_{1S} (Adams & Beam, 1989, Tanabe *et al.*, 1990b, Adams & Beam, 1991).

Functionally, the α_{1S} forms the core of the protein, the ion channel and its gating properties, targeting the other subunits to the triad and enabling EC coupling. However, each of these functions is influenced to various degrees by interactions with one or more of the additional subunits, which will be discussed in sections 1.3.2-1.3.4, particularly focusing on the potential roles in tetrad formation, charge movement and direct interaction with the RyR1.

1.3.1.1 The function of α_{1S} subunit in EC coupling

The presence of α_{1S} is essential for skeletal EC coupling. Indeed, restoration of EC coupling in *dysgenic* models appears to be restricted to transfection with the skeletal isoform, α_{1S} subunit. It is exclusively the II-III loop region in α_{1S} , not α_{1C} , that enables tetrad formation and depolarisation-induced SR Ca^{2+} transients. This has primarily been observed in chimera studies through the ability of exogenously expressed chimera constructs, with α_{1S} loops and termini in an α_{1C} background, to restore tetrad formation and EC coupling (Tanabe *et al.*, 1990a, Carbonneau *et al.*, 2005). Notably, tetrad formation does not appear to confer functional EC coupling, as a chimera with the house fly (*Musca domestica*) α_1 isoform (α_{1M}) II-III loop in an α_{1S} background restored tetrad formation, but not EC coupling, in myotubes from a cultured *dysgenic* cell line GLT (Takekura *et al.*, 2004). The α_{1S} sequence that supports both tetrad formation and EC coupling is in the II-III loop residues L720-764/5, and this is generally referred to as the “critical” region (Nakai *et al.*, 1998b, Wilkens *et al.*, 2001, Takekura *et al.*, 2004). Critical residues have been further narrowed down to the α_{1S} specific residues of A739, F741, P742 and D744 which differ in the α_{1C} isoform (Kugler *et al.*, 2004).

Another region of the α_{1S} II-III loop that was implicated in EC coupling is the “A domain” between α_{1S} residues 671-690, which is upstream of the critical region. *In vitro* studies have shown that a peptide corresponding to the A domain increases RyR1 activity by interacting with the second of three SPRY (SPRY2; so named due to identification in *Dityostelium discoideum* splA kinase and mammalian RyR) domains on RyR1. The first of these *in vitro* studies was undertaken by El-Hayek and colleagues (1995), who found a peptide corresponding to 671-690 increased RyR1 activity and SR Ca^{2+} release in native SR preparations (El-Hayek *et al.*, 1995). Curiously, the increase was reduced by addition of a peptide corresponding largely to the critical domain, known as the “C domain” peptide (E724-P760). This group further isolated the functional region of the A domain to residues 681-690 (El-Hayek & Ikemoto, 1998). More recent *in vitro* studies demonstrate that the II-III loop is able to bind to the second of three SPRY domains (SPRY2 domain; rabbit S1085-V1208) on RyR1 and increase single channel activity. In agreement with El-Hayek and colleagues’ studies, these studies also demonstrate that the A domain peptide and the C domain peptide bind with micromolar affinity to SPRY2 domain (Cui *et al.*, 2009, Tae *et al.*, 2009, Tae *et al.*, 2011).

Despite the importance of the A domain for *in vitro* interaction with RyR1, several *in vivo* studies show that this region has no functional relevance in EC coupling. This was particularly evident given that expression of an α_{1S} construct with the scrambled 681-690 residues fully restored EC coupling in *dysgenic* myotubes (Proenza *et al.*, 2000) and complete deletion of 671-690 of α_{1S} did not alter EC coupling restoration (Ahern *et al.*, 2001a, Flucher *et al.*, 2002). Furthermore, attaching fluorescent probes to physically obstruct the A domain did not alter EC coupling (Lorenzon *et al.*, 2004, Papadopoulos *et al.*, 2004, Lorenzon & Beam, 2007, Bannister *et al.*, 2009). Notably, deletion of the critical region 720-765 abolished restoration of voltage-induced SR Ca^{2+} transients and DHPR Ca^{2+} current in *dysgenic* myotubes (Ahern *et al.*, 2001a). Therefore, it is likely that the α_{1S} II-III loop is essential for EC coupling through the critical region, but not the A domain.

Although the α_{1S} region responsible for directly participating in EC coupling likely resides within the II-III loop critical region, several studies suggest that the critical residues are not the only potential α_{1S} sites for direct contribution to EC coupling. Expression of the α_{1S} II-III loop critical residues in a α_{1H} (low voltage activated α_1 subunit) background does not restore Ca^{2+} transients in *dysgenic* myotubes (Wilkins & Beam, 2003), whereas expression in a α_{1C} background does (Tanabe *et al.*, 1990a). Consequently, Wilkins and Beam (2003) suggest that a region additional to the II-III loop residues and conserved between α_{1C}/α_{1S} sequences likely contributes to EC coupling. Indeed, lysine mutation of E736 in α_{1C}/α_{1S} II-III was found to greatly reduce restoration of Ca^{2+} transients (Carbonneau *et al.*, 2005) and, although deletion of the critical residues in α_{1S} abolishes restoration of Ca^{2+} transients in *dysgenic* myotubes, additional deletion of II-III loop residues 671-690 partially restored Ca^{2+} transients (Ahern *et al.*, 2001a). Overall, multiple α_{1S} regions likely contribute to EC coupling.

Another α_{1S} region thought to directly facilitate EC coupling is the III-IV loop. This loop has been shown to bind to a RyR1 fragment (922-1112) *in vitro* (Leong & MacLennan, 1998). Tested *in vivo*, Bannister and colleagues (2008) found expression of α_{1A} III-IV loop in α_{1S} background greatly reduces restoration of maximal SR Ca^{2+} transients in *dysgenic* myotubes, which suggests that this region is important for EC coupling (Bannister *et al.*, 2008). However, the authors attribute the disruption of Ca^{2+} to the similarly reduced intramembrane charge movements, rather than direct association with RyR1 (Bannister *et al.*, 2008).

1.3.2 The function and structure of the γ subunit

The skeletal γ subunit has a molecular weight of 30 kDa and consists primarily of hydrophobic domains that contribute to four putative membrane spanning domains with the N- and C-termini exposed to the cytoplasmic solution, as shown in **Figure 1.5A** (Takahashi *et al.*, 1987). Humans have eight γ genes with γ_1 as the predominant isoform expressed in the skeletal

muscle tissue (Burgess *et al.*, 2001), interacting exclusively with the α_1 subunit of the DHPR (Arikkath *et al.*, 2003).

The functional influence of γ on DHPR gating and EC coupling has mostly been examined in *in vivo* knockout studies. Freise and colleagues (2000) found that γ -null myotubes from neonatal mice display increased DHPR Ca^{2+} current and prolonged voltage-dependent inactivation at higher voltages without altered single channel conductance, suggesting that the γ enhances the voltage sensitivity of DHPR inactivation (Freise *et al.*, 2000). However, myotubes derived from adult muscle, do not display the same degree of increased voltage-induced DHPR Ca^{2+} current and a voltage sensitivity of DHPR activation was not evident. Additionally, the voltage-induced SR Ca^{2+} release and muscle contraction did not significantly differ from control myofibres (Ursu *et al.*, 2001). A similar γ -null study using myotubes from mouse embryos also demonstrated diminished DHPR inactivation, but no alteration in EC coupling function as described by Freise *et al.* (2000) and Ursu *et al.* (2001), respectively (Ahern *et al.*, 2001b). Overall, the γ subunit does not appear to be directly involved in skeletal EC coupling, but does alter embryonic DHPR inactivation.

1.3.3 The structure and function of the $\alpha_2\delta$ subunit

The skeletal α_2 subunit is a 143 kDa glycoprotein that is linked through a disulfide bond to the δ_1 subunit, which is 24-27 kDa (Takahashi *et al.*, 1987). Both subunits are derived from the same gene and are post-translationally cleaved. There are four $\alpha_2\delta$ genes, of which $\alpha_2\delta$ -1 is the predominant isoform in skeletal muscle. Of five splice α_2 variants, α_{2A} is the predominant isoform in adult skeletal muscle (Angelotti & Hofmann, 1996, Nabhani *et al.*, 2005).

Similar to the γ subunit, the $\alpha_2\delta_1$ complex is deemed non-essential for EC coupling, rather it has a role in determining the functional properties of the α_1 subunit. Knockdown of $\alpha_2\delta_1$ in cultured myotubes from the mouse GLT cell line, increased the rate of DHPR activation without altering voltage sensitivity or maximal voltage-induced DHPR Ca^{2+} current, indicating that the $\alpha_2\delta_1$ complex has a significant role in modulating the activation kinetics of the DHPR Ca^{2+} current (Obermair *et al.*, 2005). Importantly, EC coupling was not altered (Obermair *et al.*, 2005), which is consistent with the findings from another study where the $\alpha_2\delta_1$ complex was completely knocked out in mice (Gach *et al.*, 2008). However, the voltage-induced SR Ca^{2+} transients abnormally decreased over time when a continuous train of action potentials was applied to the $\alpha_2\delta_1$ -null myotubes, but tetrad formation was not altered (Gach *et al.*, 2008). Thus, Gach and colleagues (2008) suggest that $\alpha_2\delta_1$ is physiologically important for sustaining functional EC coupling following prolonged depolarisation or a high frequency of stimuli.

1.3.4 The structure and function of the β subunit

The β subunit is a 54-68 kDa cytosolic protein that is well known for trafficking high voltage activated α_1 subunits to the plasma membrane. Historically, the first β subunit gene to be cloned and partially sequenced was taken from skeletal muscle (Ruth *et al.*, 1989). This gene and the expressed protein were given the nomenclature *CACNB1* and β_1 , respectively. In rapid progression, three other β subunit (β_2 , β_3 and β_4) genes (*CACNB2*, *CACNB3* and *CACNB4*, respectively) were cloned from cardiac muscle and brain tissue, and identified on the basis of partial amino acid sequence complementation with β_1 (Hullin *et al.*, 1992, Perez-Reyes *et al.*, 1992, Castellano *et al.*, 1993a, Castellano *et al.*, 1993b). Each β subunit has isoform variants that are attributed to either splicing variations of β_1 , β_2 and β_4 or truncation of β_3 (Buraei & Yang, 2010).

1.3.4.1 Tissue distribution of β subunit

Brain and heart tissue contain a range of β isoforms, as shown in **Table 1.1**. In contrast, skeletal muscle tissue almost exclusively expresses one β isoform, which is β_{1a} . Notably, some studies have determined β isoform expression in tissues by measuring only mRNA levels, as also indicated in **Table 1.1**.

1.3.4.2 Constituents of β subunit and splicing variants

Structurally, the β subunit is divided into 5 domains (**Figure 1.5A**), of which only domains 2 and 4 share a high sequence homology (68-92%) between the different isoforms (De Waard *et al.*, 1994, Hanlon *et al.*, 1999, Opatowsky *et al.*, 2003). Domain 2 retains a Src Homology-3 (SH3)-like sequence and domain 4 retains a Guanylate Kinase like (GK) motif as determined by homology modelling and X-ray crystallographic studies (Hanlon *et al.*, 1999, Chen *et al.*, 2004, Opatowsky *et al.*, 2004b, Van Petegem *et al.*, 2004). Although the β subunit GK domain lacks the ATP binding site necessary for kinase function (Kistner *et al.*, 1995, Hanlon *et al.*, 1999), it has an important role in trafficking the α_1 subunit of the DHPR (discussed in section 1.3.4.3.1). Domains 1 and 5 are highly divergent between the β isoforms and are located at the N- and C-termini, respectively (De Waard *et al.*, 1994). The other non-homologous region, domain 3, is classified as the “linker” or “hook” region and is located between the main body of the SH3 (De Waard *et al.*, 1994).

Both, β_1 and β_2 have splicing variants of the hook region and splicing variants in the C- and N-terminal region, respectively. Similar to β_2 , β_4 variants primarily involve alternate splicing of exons encoding the N-terminus (review Buraei and Yang (2010)).

Although the crystal structure of β_{1a} is currently unknown, bimolecular fluorescence complementation assays and fluorescence resonance energy transfer (FRET) both demonstrate that the N- and C- termini are closely positioned, perhaps even as close as ≤ 5 nm (Leuranguer

et al., 2006, Sheridan *et al.*, 2012). Additionally, as both techniques did not detect evidence of interaction between termini from adjacent β_{1a} subunits in the tetrad, the N- and C- termini are thought to be positioned away from the tetrad centre.

Table 1. 1 Tissue distribution of β isoforms.

β isoform	Tissue distribution	References
β_1	Brain, skeletal muscle, retina, heart, T cells and spleen (mRNA)	Powers <i>et al.</i> (1992), Tanaka <i>et al.</i> (1995), Volsen <i>et al.</i> (1997), Stokes <i>et al.</i> (2004), Ball <i>et al.</i> (2011)
β_{1a}	Skeletal muscle and heart	Ruth <i>et al.</i> (1989), Powers <i>et al.</i> (1992), Witcher <i>et al.</i> (1995), Pichler <i>et al.</i> (1997), Chu <i>et al.</i> (2004), Foell <i>et al.</i> (2004)
β_{1b}	Brain	Powers <i>et al.</i> (1992), Witcher <i>et al.</i> (1995), Scott <i>et al.</i> (1996), Vance <i>et al.</i> (1998), Foell <i>et al.</i> (2004)
β_{1c}	Brain	Powers <i>et al.</i> (1992)
β_{1d}	Heart	Cohen <i>et al.</i> (2005)
β_2	Heart, brain, retina and osteoblasts	Perez-Reyes <i>et al.</i> (1992), Tanaka <i>et al.</i> (1995), Witcher <i>et al.</i> (1995), Ludwig <i>et al.</i> (1997), Pichler <i>et al.</i> (1997), Volsen <i>et al.</i> (1997), Foell <i>et al.</i> (2004), Shao <i>et al.</i> (2009), Ball <i>et al.</i> (2011)
β_{2a}	Heart, brain (mRNA) and aorta (mRNA)	Hullin <i>et al.</i> (1992), Herzig <i>et al.</i> (2007)
β_{2b}	Heart, brain (mRNA) and aorta (mRNA)	Hullin <i>et al.</i> (1992), Herzig <i>et al.</i> (2007)
β_{2c}	Heart	Herzig <i>et al.</i> (2007)
β_{2d}	Heart	Herzig <i>et al.</i> (2007)
β_{2e}	Heart	Herzig <i>et al.</i> (2007)
β_3	Brain, retina, heart, spleen, aorta (mRNA), trachea (mRNA), lung (mRNA) and skeletal muscle (mRNA)	Hullin <i>et al.</i> (1992), Castellano <i>et al.</i> (1993b), Tanaka <i>et al.</i> (1995), Witcher <i>et al.</i> (1995), Haase <i>et al.</i> (1996), Scott <i>et al.</i> (1996), Ludwig <i>et al.</i> (1997), Pichler <i>et al.</i> (1997), Volsen <i>et al.</i> (1997), Hullin <i>et al.</i> (2003), Chu <i>et al.</i> (2004), Foell <i>et al.</i> (2004), Stokes <i>et al.</i> (2004), Vendel <i>et al.</i> (2006), Ball <i>et al.</i> (2011)
β_{3trunc}	Heart (mRNA)	Hullin <i>et al.</i> (2003)
β_4	Brain and retina	Castellano <i>et al.</i> (1993a), Tanaka <i>et al.</i> (1995), Witcher <i>et al.</i> (1995), Ludwig <i>et al.</i> (1997), Pichler <i>et al.</i> (1997), Volsen <i>et al.</i> (1997), Vance <i>et al.</i> (1998), Foell <i>et al.</i> (2004), Ball <i>et al.</i> (2011)
β_{4a}	Brain	Helton <i>et al.</i> (2002), Vendel <i>et al.</i> (2006)
β_{4b}	Brain	Helton <i>et al.</i> (2002), Vendel <i>et al.</i> (2006)
β_{4c}	Brain	Xu <i>et al.</i> (2011)

1.3.4.3 Function of β_{1a} subunit in skeletal muscle

The importance of the β_{1a} subunit in skeletal muscle contraction was first demonstrated in 1996 by Gregg and colleagues, essentially by establishing that complete β_1 subunit knockout in mice resulted in death at birth due to asphyxia (Gregg *et al.*, 1996). Curiously, this was in contrast to the heterozygous mutant mice that were phenotypically indistinguishable from WT mice. The skeletal myotubes extracted from 18-day-old β_1 -null murine foetuses did not contract in response to electrical stimulation. Although action potential generation and caffeine (RyR1 agonist; section 1.4.4) induced SR Ca^{2+} release was similar to control (normalised with muscle mass), depolarisation-induced SR Ca^{2+} transients were abolished. Additionally, the voltage-induced DHPR Ca^{2+} peak was shifted 10 mV to more positive potentials and peak amplitude was reduced 10-fold, which suggests that both voltage-dependent DHPR activation and Ca^{2+} current were reduced. Indeed, the DHPR Ca^{2+} current density was decreased 16-fold compared to control myotubes, which was attributed to severe reduction (seen in 50% of myotubes) or complete lack of detectable α_{1S} (seen in 50% of myotubes), as determined by immunofluorescence (Gregg *et al.*, 1996, Strube *et al.*, 1998). Further examination demonstrated that the charge movement was 2.8-fold lower in β_1 -null myotubes (Strube *et al.*, 1996). The functional role of the β_{1a} subunit has also been investigated using a β_{1a} -null zebrafish model, known as *relaxed* (Schredelseker *et al.*, 2005, Schredelseker *et al.*, 2009, Dayal *et al.*, 2010, Dayal *et al.*, 2013). Similar to the β_1 -null murine myotubes, electrical field stimulation-induced contraction and SR Ca^{2+} transients were absent in *relaxed* myotubes, although action potential generation and caffeine-induced SR Ca^{2+} release were normal (Ono *et al.*, 2001, Schredelseker *et al.*, 2005, Zhou *et al.*, 2006). The levels of α_{1S} targeted to the triad were reduced by ~50% as determined by immunofluorescence and by the fraction of particles attributed to DHPR embedded in plasmalemmal membrane in freeze fracture replicas. In disproportion to the 50% reduction in the DHPR, charge movement was reduced by 7.4-fold and tetrad formations were not visible in freeze fracture replicas (Schredelseker *et al.*, 2005). As a result of subsequent research (Neuhuber *et al.*, 1998a, Neuhuber *et al.*, 1998b, Beurg *et al.*, 1999a, Garcia *et al.*, 2002, Ahern *et al.*, 2003, Sheridan *et al.*, 2003, Sheridan *et al.*, 2004, Cheng *et al.*, 2005, Garcia *et al.*, 2005, Schredelseker *et al.*, 2009, Rebbeck *et al.*, 2011, Dayal *et al.*, 2013), the decreased DHPR channel current, fewer plasmalemmal α_{1S} and abolished EC coupling were attributed to five different roles β_{1a} subunits. These include: 1) enhancing membrane expression of the α_{1S} subunit, 2) modulation of depolarisation-induced DHPR Ca^{2+} current, 3) modulation of depolarisation-induced DHPR charge movement, 4) tetrad formation at the triad and, 5) regulation of Ca^{2+} release from the SR during EC coupling, possibly through direct interaction with RyR1.

1.3.4.3.1 β_{1a} subunit's role in enhancing α_{1S} subunit membrane expression

Both the β_1 -null mouse and zebrafish models display significantly reduced membrane expression of α_{1S} subunit, suggesting the β_{1a} subunit has an important role in this process (above in section 1.3.4.3). Notably, this regulatory role is not restricted to skeletal isoforms, as regulation of the membrane expression of high-voltage-activated α_1 subunits is a common feature of all β isoforms. However, the particular mechanisms involved are effectively unknown due to the complexity of the system (reviews Buraei and Yang (2010), Simms and Zamponi (2012)). Some suggested mechanisms include: β - α_1 binding rearranges the intracellular α_1 domains such that the export signal dominates the retention signals, which then permits trafficking from the ER to the plasma membrane (Fang & Colecraft, 2011); or, β prevents α_1 ubiquitination and/or proteasomal degradation (Altier *et al.*, 2011, Waithe *et al.*, 2011). In support of the first mechanism, exogenous expression of the β_{1a} subunit is necessary for trafficking exogenously expressed α_{1S} subunit from the ER to the plasma membrane in a transformed human kidney cell line, tsA201 (Neuhuber *et al.*, 1998b). However, the relative reduction in α_{1S} membrane expression equates to reduced whole cell α_{1S} levels in myotubes from *relaxed* zebrafish (Schredelseker *et al.*, 2005), suggesting that there is no additional ER or SR retention of the α_{1S} subunit without β_{1a} subunit expression. Although these results do not directly support the second mechanism, they do suggest alternative possibilities.

The α_{1S} - β_{1a} interaction is sufficiently stable such that the rate of fluorescence recovery of GFP-labelled α_{1S} and β_{1a} subunits locating to the triad in *dysgenic* myotubes following photo-bleaching is the same, suggesting the same turnover rate at the plasmalemma (Campiglio *et al.*, 2013). Nevertheless, the necessity of a stable interaction is questionable. Reduction in interaction stability due to α_{1S} mutation, destroys β_{1a} subunit, but not α_{1S} subunit, targeting to the triad in myotubes (Neuhuber *et al.*, 1998a). Therefore, α_{1S} trafficking to the plasmalemma does not require a stable α_{1S} - β_{1a} interaction, but β_{1a} targeting to the triad does.

Localisation of the β_{1a} and α_{1S} subunits to the triad requires the α -interaction domain (AID) located on the I-II loop on the α_{1S} subunit (Neuhuber *et al.*, 1998a, Bichet *et al.*, 2000) and both the SH3 domain and the GK domain of the β_{1a} subunit (Maltez *et al.*, 2005, Sheridan *et al.*, 2012). Notably, association with the I-II loop with nanomolar affinity *in vitro* is a constant feature of β isoforms (Pragnell *et al.*, 1994, De Waard *et al.*, 1995, Witcher *et al.*, 1995, Opatowsky *et al.*, 2003). The β interacting domain (BID) on the β GK domain was first thought to be the binding site for AID (De Waard *et al.*, 1994), particularly as truncated forms of β_{1b} , encompassing the BID, were sufficient to restore α_1 current in *Xenopus* oocytes and mutations in the BID disrupted this restoration (De Waard *et al.*, 1994). However, resolution of crystal structure of the β_3 and β_{2a} core (containing SH3 and GK domains) with the AID region bound reveals that BID is not involved in the interaction (Chen *et al.*, 2004, Van Petegem *et al.*, 2004). Instead, this region was found to be crucial for SH3 and GK structural integrity and

intermolecular interaction between the domains (Chen *et al.*, 2009). As an alternative binding site, Van Petegem (2004) and Chen (2004) both suggested an AID binding site composed of a hydrophobic cleft, named the α binding pocket, on the GK domain. Markedly, the α binding pocket sequence is conserved in β isoforms, with mutant studies revealing β_{2a} M245 is a hotspot for β_1 -AID interaction (Van Petegem *et al.*, 2008).

1.3.4.3.2 β_{1a} subunit's role in modulation of DHPR activity

A common feature of β isoforms is the ability to modulate the voltage sensitivity of high-voltage-activated α_1 subunits, specifically altering both voltage-dependent activation and inactivation (reviews Buraei and Yang (2010), Buraei and Yang (2013)). The shift in maximal voltage-induced DHPR Ca^{2+} current to more positive potentials in β_{1a} -null murine myotubes reflects the lack of β_{1a} mediated increase in DHPR activation (Gregg *et al.*, 1996). Beurg *et al.* (1997) and Ahern *et al.* (2003) have commented that modulation of inactivation could not be monitored in myotubes due to the characteristically slow inactivation rate that exceeded experimental parameters. Exogenous expression of both β_{1a} and α_{1S} constructs in a mammalian fibroblast-like cell line, COS-7, increases Ca^{2+} current by ~ 2 -fold relative to the expression of α_{1S} alone (Garcia *et al.*, 2002). The benefit of this model is that α_{1S} membrane expression and charge movement do not appear to be influenced by β_{1a} subunit expression, suggesting that β_{1a} specifically increases Ca^{2+} current. In contrast to myotube studies, β_{1a} expression did not alter activation or inactivation of the α_{1S} Ca^{2+} current (Garcia *et al.*, 2002). However, this may be attributed to a lack of RyR1, which appears to be essential for the complete restoration of DHPR peak current and voltage-dependent activation in RyR1-null (*dyspedic*) myotubes (Ahern *et al.*, 2003).

X-ray crystallography and circular dichroism studies demonstrate that binding with the α binding pocket promotes α helical formation of the AID region (Chen *et al.*, 2004, Opatowsky *et al.*, 2004a, Van Petegem *et al.*, 2004, Almagor *et al.*, 2012). This is suggested to extend to the helical propensity of the region between the S6 segment of the first α_1 transmembrane domain (indicated as "I" in **Figure 1.5A**) and AID (Arias *et al.*, 2005), particularly as mutations that reduce propensity for α helical formation reduce the functional effects of the β subunit on α_1 voltage-inactivation characteristics (Arias *et al.*, 2005, Findeisen & Minor, 2009, Almagor *et al.*, 2012). As α_1 S6 is thought to influence both activation and inactivation, the general consensus is that the domain I S6 region is altered upon binding with β subunit, consequently altering activation and inactivation gating characteristics.

1.3.4.3.3 β_{1a} subunit's role in modulating charge movement in α_{1S}

In *relaxed* zebrafish, the reduction of charge movement exceeds the 50% reduction in the plasmalemmal α_{1S} subunit present that was observed in both freeze fracture electron microscopy and immunocytochemistry (Schredelseker *et al.*, 2009). This signifies that the β_{1a}

subunit likely increases charge movement directly, as opposed to by virtue of increasing α_1 membrane expression (Schredelseker *et al.*, 2009). Using chimera studies with β_{1a} domains in a β_3 background, Dayal and colleagues (2013) demonstrated that co-operative presence of SH3 and C-terminal β_{1a} domains is necessary for functional charge movement and EC coupling. The β_3 isoform is ideal for chimera studies to analyse restoration of charge movement as exogenous expression of β_3 in *relaxed* zebrafish larvae only slightly restores charge movement, though α_{1S} membrane expression and tetrad formation are fully restored (Dayal *et al.*, 2013). Specifically, expression of a β_{1a} construct containing a single proline mutation at the C-terminal PXXP motif (P467) significantly reduced charge movement to similar levels as myotubes expressing β_3 . The authors suggest this is of interest as the PXXP motif has a putative binding site in the SH3 domain; they propose that the C-terminal-SH3 interaction may be important for modulation of α_{1S} charge movement (Dayal *et al.*, 2013).

1.3.4.3.4 β_{1a} subunit's role in DHPR tetrad formation

The role of the β_{1a} subunit in tetrad formation has mostly been investigated in *relaxed* zebrafish. For all the β isoforms investigated, exogenous expression in *relaxed* zebrafish has restored α_{1S} membrane expression, given slight overexpression, as measured with immunocytochemistry. However, only expression of β_{1a} and β_3 in *relaxed* zebrafish can impart normal tetrad formation with particles mostly in orthogonal arrays. Expression of rat β_{2a} and a housefly β_M prevented restoration of ~60% of tetrad structures, with either no or 50% less orthogonal arrangement, respectively (Schredelseker *et al.*, 2009, Dayal *et al.*, 2013).

1.3.4.3.5 β_{1a} subunit's role in Ca^{2+} transients during EC coupling

As of yet, it is difficult to define the direct role that β_{1a} subunits have in EC coupling. There is *in vitro* evidence that β_{1a} directly interacts with the RyR1 and mutation of these regions in myotubes produces a range of effects on EC coupling. Simultaneously, the quantifiable contribution to EC coupling from DHPR tetrad formation, α_{1S} membrane expression and charge movement is unknown.

Regions of β_{1a} that are involved in EC coupling have been mostly assessed by expressing chimeras and truncations of β in mouse and zebrafish β_{1a} -null models. Expression of the skeletal and cardiac β subunit isoforms, β_{1a} and β_{2a} respectively, in β_{1a} -null mouse myotubes revealed that expression of the β_{1a} subunit alone could completely restore SR Ca^{2+} transients (Beurg *et al.*, 1999b). Similarly, expression of rabbit β_{1a} or zebrafish β_{1a} subunit isoforms fully restored motility in *relaxed* zebrafish (Schredelseker *et al.*, 2009), whereas zebrafish β_{2a} subunit expression only restored motility by 26%. This result suggested that a non-conserved region between β_{1a} and β_{2a} is a likely contributing factor to β_{1a} subunit's role in EC coupling. The ability of the non-conserved domains (linker and N- and C-termini) to recover DHPR Ca^{2+} current and charge movement, and EC coupling in β_{1a} -null mice myotubes has been examined

by exogenous expression of constructs with these regions either removed or exchanged with the corresponding β_{2a} sequence (Beurg *et al.*, 1999a). Although removal or chimeric replacement of the N-terminus and “linker” region did not greatly influence restoration of EC coupling, β_{1a} C-terminus did influence the restoration (Beurg *et al.*, 1999a, Sheridan *et al.*, 2004). In agreement, truncations of the 29, 35 and 60 residue tail on the C-terminal produced a 5-fold reduction in restoration of voltage-induced SR Ca^{2+} transients in β_{1a} -null myotubes compared to β_{1a} -null myotubes expressing the complete β_{1a} subunit (Sheridan *et al.*, 2003). This is in contrast to the finding that truncation of 7 or 21 residues in the C-tail did not prevent full restoration of EC coupling (Sheridan *et al.*, 2003). Deletion of the 35 residue C-tail did not prevent full restoration of charge movement density, or α_{1S} membrane expression, though EC coupling was reduced β_{1a} -null myotubes (Beurg *et al.*, 1999a). This indicates that the reduction of EC coupling could not be attributed to an alteration β_{1a} 's roles in DHPR charge movement and membrane expression. Notably, deletions of ≥ 29 final C-terminal residues also resulted in a 50% reduction in DHPR Ca^{2+} current. Though this is more likely attributed to reduced RyR1 activity rather than DHPR Ca^{2+} current altering EC coupling (section 1.3.5.5). In identification of the C-terminal residues responsible for EC coupling, Sheridan and colleagues (2004) found that expression of a mutant β_{1a} construct (L478A, V485A and V492A; hydrophobic heptad repeat mutant) decreased the maximal SR Ca^{2+} transients by 80% relative to WT β_{1a} (Sheridan *et al.*, 2004). This implies that one, or all, of these hydrophobic residues on the β_{1a} subunit are important for functional EC coupling. In contrast, expression of heptad repeat mutant in *relaxed* zebrafish almost fully restored EC coupling (Dayal *et al.*, 2010). This is despite similar β_{1a} subunit isoform selectivity for restoration of EC coupling in β_{1a} -null myotubes, as mentioned above. Moreover, truncation of the C-terminus and the last 10 residues of GK of the β_{1a} subunit in zebrafish myotubes resulted in paralysis (Zhou *et al.*, 2006), which agrees with the findings from β_{1a} C-terminus truncation studies in mouse myotubes (Sheridan *et al.*, 2003).

In addition to chimera and truncation studies, further suggestion of β_{1a} subunits direct role in EC coupling is given by the fact that pressure injection of β_{1a} subunit into mouse muscle fibres significantly increased voltage-induced SR Ca^{2+} transients (Garcia *et al.*, 2005). Notably, pressure injection of a truncated form (missing 40 residues of the C-terminal tail) did not alter SR Ca^{2+} transients (Garcia *et al.*, 2005). In accord with chimera and truncation studies, the DHPR Ca^{2+} currents were also increased though charge movements were not altered (Garcia *et al.*, 2005). Together, these results suggest that the C-terminus of the β_{1a} subunit plays a crucial role in EC coupling that is at least more than the β_{1a} subunit's contribution to DHPR charge movements and membrane expression.

The question arises as to whether the β_{1a} subunit facilitates EC coupling by virtue of a direct interaction with RyR1 or by an indirect interaction via positioning the α_{1S} subunit so that it can interact with RyR1. *In vitro* experiments suggest the former may be possible. The β_{1a}

subunit has been shown to associate with RyR1 fragments in affinity chromatography, with the residues within a polybasic K³⁴⁹⁵KKRR__R³⁵⁰² motif centrally located in RyR1 identified as being important, because RyR1 fragments had little affinity for the β_{1a} subunit *in vitro* when this region was removed or neutralised (Cheng *et al.*, 2005). The authors also demonstrated that expression of RyR1 with the polybasic region either removed or mutated in RyR1-null (*dyspedic*) myotubes significantly decreased maximal SR Ca²⁺ transients by 50% when compared with myotubes expressing WT RyR1 (Cheng *et al.*, 2005). This was attributed to a hindered interaction between the β_{1a} subunit and the RyR1. In agreement with Cheng (2005) and Beurgs' (1999a) studies, we have found a 35 residue peptide corresponding to the β_{1a} subunit C-tail that can bind to full-length RyR1 using pull down assays (Rebbeck *et al.*, 2011). Functionally, this peptide and the full-length β_{1a} subunit increase RyR1 activity with an AC₅₀ of 450-600 pM (Rebbeck *et al.*, 2011). Thus, this provides further evidence that the β_{1a} subunit C-terminus increases EC coupling by virtue of directly activating of RyR1.

Conversely, other work has led to the conclusion that β_{1a} is unlikely to interact with RyR1 during EC coupling. Firstly, two studies demonstrated that fluorescently labelled β_{1a} does not locate to the membrane without α_{1S} expression (Neuhuber *et al.*, 1998a, Leuranguer *et al.*, 2006). Arguably, this could also suggest that the α_{1S} subunit is necessary for physical β_{1a} -RyR1 interaction *in vivo*. Secondly, the use of size-interfering streptavidin tags attached to the C-terminus did not hinder EC coupling (Lorenzon & Beam, 2007). A counter argument is that the RyR1 binding site on β_{1a} may be sufficiently upstream that streptavidin attachment does not interfere with the interaction between β_{1a} and RyR1. Furthermore, the mouse β_{1a} C-terminus has two putative glycine hinges at places 12-13 and 20-21 residues upstream of the extreme C-tail that could provide a large degree of flexibility with streptavidin bound to the extreme C-terminus. This is assuming that the β_{1a} C-terminal residues involved in the RyR1- β_{1a} interaction are > 21 residues upstream of the C-tail, as suggested by truncation studies discussed above (Sheridan *et al.*, 2003).

1.3.5 Dihydropyridine receptor regulatory proteins during EC coupling

Functional EC coupling appears to be reliant on DHPR association with several proteins, including stromal interaction molecule 1 (STIM1), SH3 and cysteine rich domain 3 (STAC3), junctophilin (JP) and JP-45. Additionally, RyR1 is known to modulate DHPR activity during EC coupling, but the degree of importance of this “retrograde” function for EC coupling is difficult to define.

1.3.5.1 STIM1

STIM1 is located in the SR/ER membrane and is typically associated with the process of store operated Ca²⁺ entry. In brief, this is a common process in mammalian cells that sequentially involves detection of low SR/ER Ca²⁺, recruitment of ORAI and facilitation of

extracellular Ca^{2+} influx into the cytoplasm via ORAI1 (as reviewed by Muik *et al.* (2012)). However, a recent study has shown that STIM1 negatively regulates SR Ca^{2+} transients during skeletal EC coupling. In mouse myotubes, over expression or knockdown of STIM1 results in a reduction or increase, respectively, in the amplitude of SR Ca^{2+} transients without altering caffeine-induced SR Ca^{2+} release, suggesting that SR Ca^{2+} load and RyR1 function was not compromised. Co-immunoprecipitation demonstrates that STIM1 can precipitate the DHPR α_{1S} subunit, but not RyR1, suggesting that STIM1 alters EC coupling by virtue of interaction with DHPR α_{1S} (Lee *et al.*, 2013). Similar to a previous study that identified a direct interaction between STIM1 and the DHPR α_{1C} subunit, the interaction appeared to be independent of STIM1's functions in store operated Ca^{2+} entry, including: the ability to interact with ORAI1 and the properties of the SR Ca^{2+} sensor for store operated Ca^{2+} entry (Wang *et al.*, 2010, Lee *et al.*, 2013).

1.3.5.2 STAC3

Similar to STIM1, another protein recently shown to influence EC coupling via interaction with DHPR α_{1S} subunit is STAC3. However, unlike STIM1, STAC3 has been shown to also co-immunoprecipitate RyR1 (Horstick *et al.*, 2013, Lee *et al.*, 2013). In both mouse and zebrafish STAC3-null models, depolarisation-induced muscle contraction and SR Ca^{2+} transients are abolished (Horstick *et al.*, 2013, Nelson *et al.*, 2013). Studies published a few months prior to these studies demonstrate that STAC3-null mouse and zebrafish models lack proper myoblast differentiation, which was suggested to have contributed to the lack of muscle contraction (Bower *et al.*, 2012, Reinholt *et al.*, 2013). However, Nelson *et al.* (2013) suggested that the aberrant myogenesis in the mouse STAC3-null model may be a by-product of EC coupling disruption. This was suggested because similar phenotypic attributes were also observed in null models of other proteins crucial for EC coupling, such as DHPR α_{1S} subunit, DHPR β_{1a} subunit and RyR1 (Powell *et al.*, 1984, Takeshima *et al.*, 1994, Gregg *et al.*, 1996, Chen *et al.*, 2011). More importantly, 4-chloro-m-cresol induced activation of RyR1 resulted in normal muscle contraction (normalised to muscle weight) and myocyte SR Ca^{2+} release (Nelson *et al.*, 2013). This suggests that the muscle was still functional, and that STAC3 may be directly involved in the interaction between DHPR and RyR1 during EC coupling (Nelson *et al.*, 2013). Curiously, STAC3 contains a few well-known protein-binding motifs that make it a feasible binding partner to RyR1 and/or DHPR. Thus, perhaps STAC3 should be taken into account in future models of EC coupling.

1.3.5.3 Junctophilin

Junctophilin (JP) isoforms 1 and 2 are localised to the junctional membranes and are involved in anchoring the SR to the sarcolemma or T-tubule in skeletal muscle (Nishi *et al.*, 2000). With the hydrophobic C-terminus embedded in the SR membrane, the large cytoplasmic

domain is likely attached to the T-tubule by virtue of a MORN motif (Takeshima *et al.*, 2000). JP1 co-immunoprecipitates with both DHPR and RyR1, suggesting that JP also bridges the junctional membranes by forming a complex with DHPR and RyR1 (Golini *et al.*, 2011). In cultured myotubes from the C2C12 cell line, JP knockdown contributed to reduced DHPR charge movements and DHPR Ca^{2+} currents, although voltage-induced SR Ca^{2+} transients were not altered (Golini *et al.*, 2011). The authors suggest that EC coupling may not be altered due to the compensatory action of perhaps Ca^{2+} -induced Ca^{2+} release. Interestingly, a very recent study demonstrated that depolarisation-induced contractions in skeletal muscle fibres can be abolished upon Ca^{2+} dependent cleavage of JP1, which is attributed to uncoupling of DHPR and RyR1 (Murphy *et al.*, 2013). Therefore, JP1 is likely to be necessary for EC coupling in adult fibres, not cultured myotubes, by facilitating coupling between DHPR and RyR1.

1.3.5.4 JP-45

JP-45 was identified as a 45 kDa protein in a biochemical screen of the junctional SR proteins (Zorzato *et al.*, 2000) and is currently thought to indirectly regulate EC coupling. Embedded in the SR membrane with one predicted transmembrane segment, the N-terminus (125 residues in mouse JP-45) and C-terminus (183 residues) face the cytoplasm and SR lumen, respectively (Anderson *et al.*, 2003). Co-immunoprecipitation shows that JP-45 interacts with the α_{1S} subunit and with calsequestrin (CSQ) (Anderson *et al.*, 2003), the main SR Ca^{2+} binding protein and a SR luminal RyR1 regulator (section 1.4.3.7; Beard *et al.* (2002)). In terms of interactions with DHPR, Anderson and colleagues (2006) describe the interaction between JP-45 N-terminus (residues 1-80) with the α_{1S} subunit I-II loop and C-terminus, as well as the β_{1a} subunit. Interestingly, the presence of β_{1a} subunit was found to drastically reduce the ability of JP-45 N-terminus to pull down or precipitate α_{1S} I-II loop during pull down and co-immunoprecipitation assays (Anderson *et al.*, 2006). Therefore, the authors suggested that β_{1a} and JP-45 compete for the same AID site on the I-II loop. Interestingly, overexpression or knockdown of JP-45 in C2C12 myotubes reduces DHPR charge movement, although α_{1S} expression levels were reduced only in JP-45 KO myotubes (Anderson *et al.*, 2006). The proposed model suggests that JP-45 competes with the interaction between β_{1a} subunit and α_{1S} subunit at the triad and hence overexpression reduces the β_{1a} subunit modulation of DHPR charge movement. The model also proposes that knockout of JP-45 contributes to reduced DHPR membrane expression because there is no JP-45 to locate the DHPR to the triad via interaction between JP-45 and α_{1S} C-terminus (Anderson *et al.*, 2006). Interestingly, another study has shown that 4-chloro-m-cresol induced fibre contraction was identical in JP-45 knockout and WT mouse muscle fibres, which suggests that RyR1 activity and SR Ca^{2+} store load was not affected in the JP-45 knockout muscle fibres (Delbono *et al.*, 2007). Thus, the slightly reduced contraction force observed in JP-45 null muscle fibres is likely attributed to reduced DHPR charge movement (Delbono *et al.*, 2007).

1.3.5.5 RyR1

As alluded to earlier, several studies have demonstrated that the DHPR physically induces RyR1 activation. However, the interaction is bidirectional, in that the physical coupling alters DHPR gating properties in an interaction termed “retrograde” coupling (Nakai *et al.*, 1996, Nakai *et al.*, 1998a, Avila & Dirksen, 2000, Ahern *et al.*, 2001a, Avila *et al.*, 2001). This was first demonstrated in RyR1-null (*dyspedic*) myotubes that displayed a 30-fold reduction in depolarisation-induced DHPR Ca^{2+} current density (Nakai *et al.*, 1996) and a lack of tetrad formation in freeze fracture replicas, although, notably, the number of DHPR particles in freeze fracture replicas was unchanged (Protasi *et al.*, 2002). Avila and Dirksen (2000, 2001) demonstrated that myotubes derived from *dyspedic* mice display a ~40% reduction in maximal charge movement and a 5-fold reduction in DHPR Ca^{2+} current to charge movement ratio relative to cultured myotubes from phenotypically normal littermates (Avila & Dirksen, 2000). The exogenous expression of WT RyR1 or RyR1 mutant (deficient in depolarisation-induced SR Ca^{2+} transients) in *dyspedic* myotubes, restores the depolarisation-induced DHPR Ca^{2+} current to charge movement ratio. As a consequence, the authors suggest that it is the presence of RyR1 rather than RyR1 function that governs restoration of DHPR Ca^{2+} current. Given that Avila and Dirksen found charge movement was restored by expression of WT RyR1, but not RyR1 mutant, the authors suggested that RyR1 activity likely influences a signalling pathway that promotes expression of DHPR (Avila *et al.*, 2001). However, this is questionable as Protasi and colleagues (1998) note that skeletal DHPRs cluster to the same level in the plasmalemmal regions that overlay the SR membrane in freeze fracture replicas of 1B5 *dyspedic* myotubes, regardless of whether RyR1 is exogenously expressed. Thus, membrane expression does not appear to always be influenced by RyR1 presence. It is important to note that DHPR tetrad formation was only observed in freeze fracture replicas when RyR1 was exogenously expressed (Protasi *et al.*, 1998).

That EC coupling is dependent on DHPR charge movement and tetrad formation, but independent of DHPR Ca^{2+} current, has been demonstrated by several studies. Firstly, depolarisation-induced Ca^{2+} transients in frog muscle fibres are independent of extracellular Ca^{2+} (Armstrong *et al.*, 1972, Miledi *et al.*, 1984). This also apparent in zebrafish, as zebrafish α_{1S} isoforms do not conduct detectible Ca^{2+} current (Schredelseker *et al.*, 2009, Schredelseker *et al.*, 2010). Secondly, expression of α_{1S} mutants, R174W and E111K, in *dysgenic* myotubes abolishes the DHPR Ca^{2+} current, but not charge movements or depolarisation-induced SR Ca^{2+} transients (Dirksen & Beam, 1999, Eltit *et al.*, 2012). Thirdly, although the absence of the DHPR γ subunit significantly increases DHPR Ca^{2+} current, the strength of EC coupling is not affected (Ahern *et al.*, 2001b, Ursu *et al.*, 2001).

1.4 Ryanodine receptor

The RyR ion channel contributes to Ca^{2+} signalling in striated muscle and is essential for EC coupling. Named due to its specific and high affinity interaction with the plant alkaloid ryanodine, this channel is composed of four monomers (homotetramer; >2000kDa). Each monomer consists of ~5000 amino acid with a large (~80%) portion composing a cytoplasmic region. The C-terminal region contains the transmembrane component that forms the channel pore when the four monomers associate in the SR membrane (Takeshima *et al.*, 1989).

Historically, RyR1 was identified as the primary SR Ca^{2+} release channel in skeletal EC coupling during the mid- to late-1980s. Thin section electron microscopy of amphibian skeletal muscle revealed large “feet” (singular “foot”) erupting from the SR membrane, almost completely extending the ~12 nm distance between the SR and T-tubule membranes (Franzini-Armstrong, 1972, Franzini-Armstrong, 1973). Studies in 1985-6 found that Ca^{2+} release from junctional SR preparations was influenced by ryanodine (Fleischer *et al.*, 1985, Meissner, 1986) and therefore the Ca^{2+} release channel was termed the ryanodine receptor. This was closely followed by a study that demonstrated that purified RyR, reconstituted into planar phospholipid bilayer, responded to ryanodine, ruthenium red, ATP and $[\text{Ca}^{2+}]$ (section 1.4.4) in a similar manner as the primary Ca^{2+} release channel in junctional SR preparations (Imagawa *et al.*, 1987). In the following years, the RyR1 was firmly identified as the “foot” structure that stretched the triad junction (Lai *et al.*, 1988) and the primary structure was predicted from the cloned and sequenced RyR1 cDNA (Takeshima *et al.*, 1989).

Currently, three RyR genes (*RYR1-3*) have been identified in mammals. These isoforms share ~65% homology. The greatest sequence variance is in three regions, known as the “divergent regions” that encompass RyR1 residues 4254-4631 (D1), 1342-1403 (D2) and 1872-1923 (D3).

Originally, each isoform was first identified in specific tissues, skeletal muscle (RyR1), cardiac muscle (RyR2) and brain (RyR3) (Takeshima *et al.*, 1989, Nakai *et al.*, 1990, Otsu *et al.*, 1990, Zorzato *et al.*, 1990, Hakamata *et al.*, 1992). However it soon became clear that each isoform is expressed in a range of tissues (review Lanner *et al.* (2010)). Never-the-less, RyR1 and RyR2 are still the primary isoforms expressed in skeletal and cardiac muscle, respectively. Although RyR3 is endogenously expressed in cultured myotubes from neonatal mice, it does not compensate for RyR1 in its role in EC coupling in myotubes from *dyspedic* mice (Yamazawa *et al.*, 1997). RyR3 is generally expressed in adult mammalian diaphragm (Jeyakumar *et al.*, 1998) and, in smaller amounts, soleus muscle (Conti *et al.*, 1996, Bertocchini *et al.*, 1997).

The use of planar bilayer techniques was important for RyR1 identification, and for characterising RyR1 ion conductance and selectivity. The technique involves incorporation of

the isolated RyR1 or native SR preparations into a planar phospholipid bilayer that transects two aqueous compartments. The ionic current through single channels is then monitored under voltage clamp conditions. In the exciting era of RyR1 discovery, Smith and colleagues (1988) used this technique to demonstrate that RyR1 is permeable to a range of organic monovalent cations and inorganic divalent and monovalent cations. Monovalent conductance follows the sequence $Cs^+ > Na^+ > K^+ > Li^+ \gg choline^+ \geq Tris^+$. Notably, inorganic monovalent cation conductance is typically greater than inorganic divalent cations, for example conductance with 250:50 mM gradient across bilayer for K^+ is ~ 1 nS and for Ca^{2+} is ~ 170 pS (Smith *et al.*, 1988). However, RyR1 in lipid bilayers display a slight selectivity preference for divalent over monovalent cations, for example the estimated ratio for K^+ to Ca^{2+} ions is $\sim 1:6$, as determined by a 50:50 mM gradient of K^+ (*cis*) to Ca^{2+} (*trans*) (Smith *et al.*, 1988). The Ca^{2+} conductance and selectivity is very similar between RyR from adult rabbit skeletal and canine cardiac SR preparations, suggesting similar selectivity and conductance between RyR1 and RyR2 isoforms (as reviewed by Williams (1992)).

It is of interest to note that Ca^{2+} signalling via RyR1 is not exclusively associated with EC coupling in skeletal muscle. Voltage-induced Ca^{2+} release via RyR1 is also observed in neurons at the nerve terminal (De Crescenzo *et al.*, 2012). The authors hypothesise that the resulting small burst of Ca^{2+} into the nerve terminal ‘microdomain’ suppresses exocytosis in hypothalamic magnocellular neurons, which inhibits their function in secreting neuropeptides. RyR1 has been associated with Ca^{2+} signalling in a variety of other neurons (Sawada *et al.*, 2008, Kakizawa *et al.*, 2012, Kakizawa *et al.*, 2013, Ohashi *et al.*, 2014). Indeed, Ca^{2+} signalling via RyR1 also is important in a range of non-excitabile tissues, for example it plays a role modifying the speed of immune system response to antigenic stimulation (Vukčević *et al.*, 2013).

1.4.1 RyR1 structure

The crystal structure of RyR1 has yet to be resolved. However, modelling based on single particle analysis of cryo-EM images has provided a low resolution (~ 10 Å) map of the RyR1 domains (**Figure 1.7**) (Ludtke *et al.*, 2005, Samsó *et al.*, 2005, Serysheva *et al.*, 2005, Samsó *et al.*, 2009). The overall dimensions of the cytoplasmic and transmembrane region are $275 \times 275 \times 100$ Å and $115 \times 115 \times 60$ Å, respectively (Samsó *et al.*, 2005). The RyR1 structure has prominent regions that are classed as the “clamps”, “handle”, “central rim” and “column”, each of which contain numerically assigned globular domains. The RyR1 map has been further resolved using a combination of modelling based on structural similarities to other channels whose crystal structures have been resolved (e.g. KCsA), X-ray crystallographic images of isolated RyR1 regions, single particle analysis of site specific immunofluorescently labelled RyR1 in cryo-EM images and, relative locations of intra- and inter-molecular interactions

measured by FRET (Fruen *et al.*, 2005, Cornea *et al.*, 2009, Cornea *et al.*, 2010, Peralvarez-Marín *et al.*, 2011, Fessenden & Mahalingam, 2013, Girgenrath *et al.*, 2013, Kimlicka *et al.*, 2013, Ramachandran *et al.*, 2013, Zhu *et al.*, 2013).

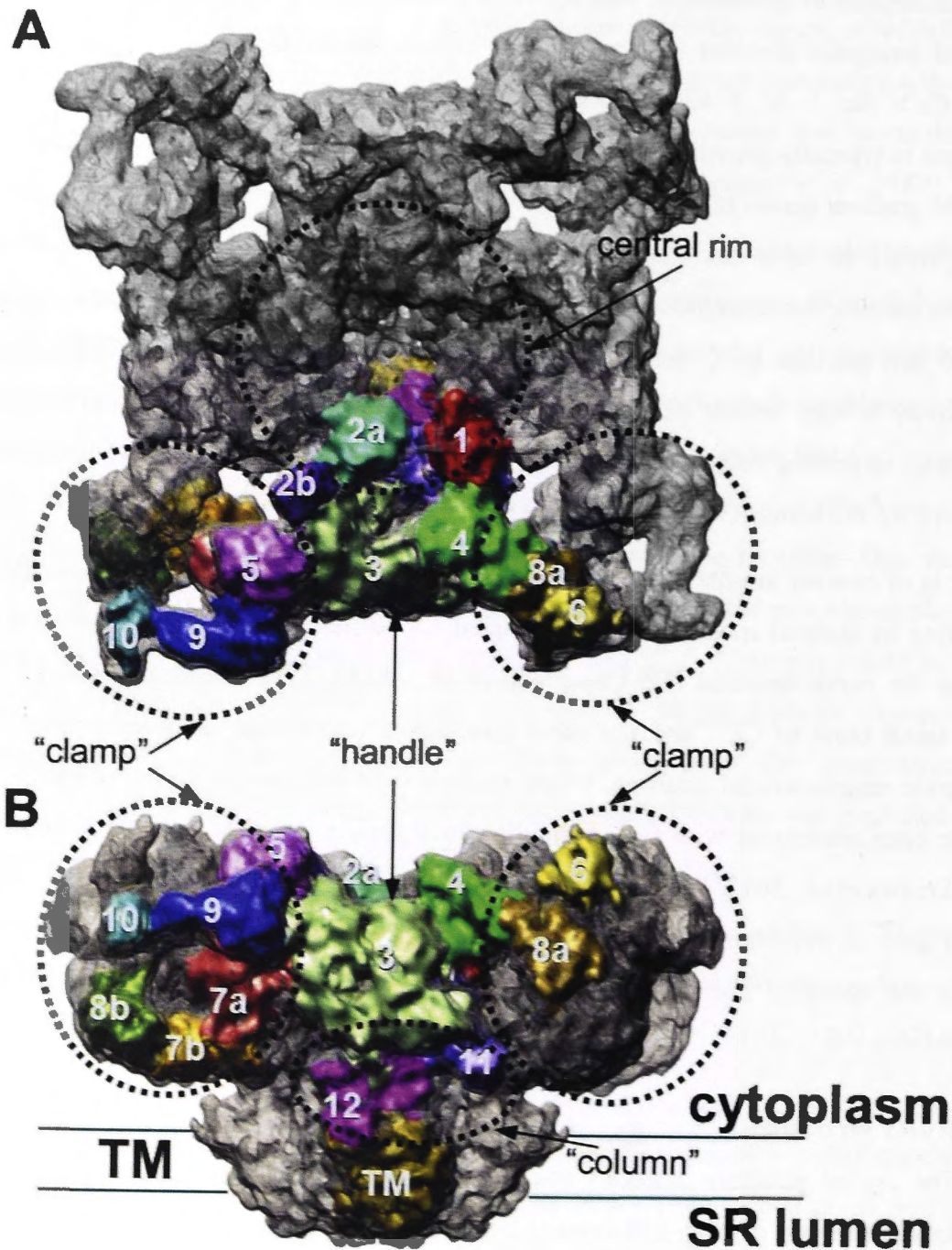


Figure 1.7 Overall structure of RyR1.

A 9.6 Å reconstruction of closed RyR1 from single particle analysis of cryo-EM images (Ludtke *et al.*, 2005). Slightly adapted by Serysheva *et al.* (2008) to include highlighted globular domains of one monomer and circled RyR1 regions. Viewpoints are from the cytoplasm (A) and the side (B) to include the approximated transmembrane (TM) spanning region and small SR luminal domain (Serysheva *et al.*, 2008).

Currently, there are two 2-dimensional models for the pore-forming region of RyR1. Both models propose six putative transmembrane segments per monomer, but the models vary slightly in the RyR1 sequences that form each of these transmembrane segments (Figure 1.8). In 2007, Zissimopoulos and Lai proposed a model (Figure 1.8A) based on the original 10

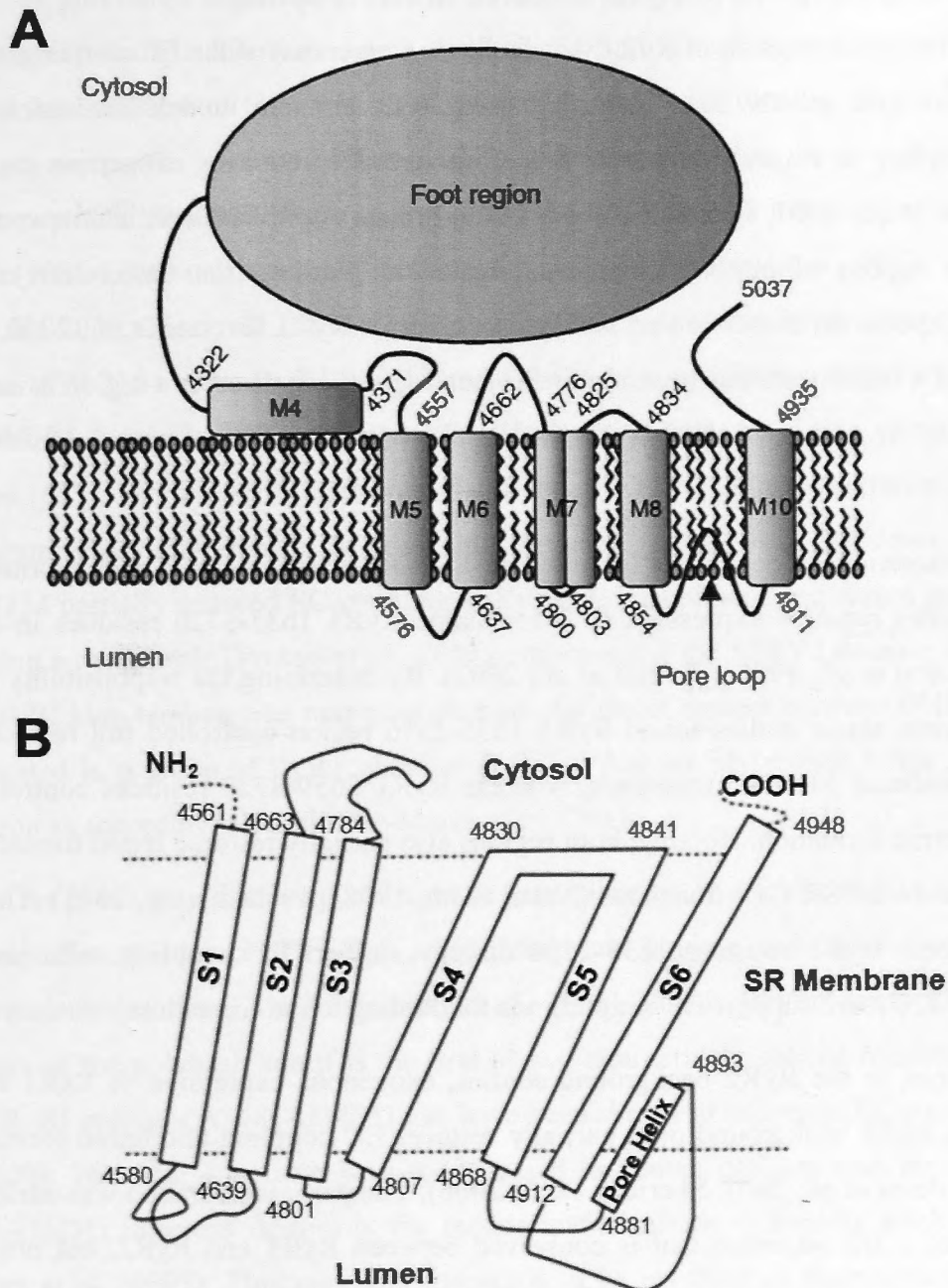


Figure 1.8 Models of the RyR1 pore-forming region.

A) A model of the RyR1 pore-forming region with six transmembrane segments (M), as proposed by Zissimopoulos and Lai (2007). The transmembrane segments named in accord with a 10 transmembrane segment model proposed by Zorzato *et al.* (1990). **B)** A model of the six transmembrane segments (S), as proposed by Ramachandran *et al.* (2013). This model is based on collation of transmembrane and secondary structure prediction results, in addition to experimental results by Du *et al.* (2002), Du *et al.* (2004). Image slightly adapted from (Ramachandran *et al.*, 2013).

putative transmembrane segment model proposed by Zorzato *et al.* (1990) that was adjusted to incorporate experimental evidence from later years (Du *et al.*, 2002, Du *et al.*, 2004, Ludtke *et al.*, 2005). This model proposed that RyR1 transects the SR membrane with transmembrane segments correspond to M5, M6, M7, M8 and M10 of the Zorzato *et al.* (1990) model. Recently, a slightly altered version of this model was presented by Ramachandran *et al.* (2013). The new model (**Figure 1.8B**) adjusts the sequences of the six transmembrane segments and is based on the overlay of transmembrane prediction and secondary structure prediction, and incorporates with experimental data provided by Du *et al.*, (2002, 2004).

1.4.2 Cytoplasmic regions of RyR1 involved in EC coupling

The cytoplasmic regions of RyR1 that facilitate conversion of the EC coupling signal to RyR1 activation have mostly been identified using RyR chimera models, as restoration of skeletal EC coupling in *dyspedic* myotubes is isoform specific, requiring exogenous expression of RyR1 (Nakai *et al.*, 1997, Fessenden *et al.*, 2000, Protasi *et al.*, 2000). It is noteworthy that identifying the regions of importance is complicated by findings that restoration of tetrad formation in *dyspedic* myotubes is also isoform specific for RyR1 (Protasi *et al.*, 2000, Protasi *et al.*, 2002). As a result, care has been required when identifying whether a region is important for EC coupling by virtue of directly facilitating EC coupling or promoting DHPR tetrad formation.

Full restoration of depolarisation-induced SR Ca^{2+} transients and tetrad formation in *dyspedic* myotubes requires expression of cytoplasmic RyR1 1635-3720 residues in a RyR2 background (Nakai *et al.*, 1998a, Protasi *et al.*, 2002). By examining the responsibility of each half of this region, these studies found RyR1 1635-2556 region controlled full restoration of depolarisation-induced SR Ca^{2+} transients, whereas RyR1 2659-3720 residues controlled full restoration of tetrad formation. Notably, both regions also partially restored tetrad formation and depolarisation-induced SR Ca^{2+} transients (Nakai *et al.*, 1998a, Protasi *et al.*, 2002). Thus, in a RyR2 background, RyR1 residues 1635-2556 directly support EC coupling, whereas RyR1 residues 2659-3720 more support EC coupling via facilitating tetrad formation.

In contrast to the RyR2 background studies, exogenous expression of RyR1 residues 1635-3720 in a RyR3 background only partially restores EC coupling and tetrad formation in IB5 myotubes (Perez *et al.*, 2003, Sheridan *et al.*, 2006). The partial restoration was attributed to the likelihood of a D2 sequence that is conserved between RyR1 and RyR2, but not RyR3, because Yamazawa and colleagues (1997) had demonstrated that expression of RyR2 D2 residues in a RyR1 background fully restored EC coupling (Yamazawa *et al.*, 1997). This is despite only 35% sequence similarity between the D2 regions of RyR1 and RyR2, but the RyR3 D2 region has greater sequence deviation with a substantial section of this region being absent. Certainly, expression of RyR3 D2 residues 1271-1349 in a RyR1 background does not restore any SR Ca^{2+} transients in IB5 myotubes (Perez *et al.*, 2003). It is noteworthy that the RyR1/RyR2 D2 region is insufficient alone for EC coupling restoration in a RyR3 background, particularly since expression of the RyR1 D2 residues 1272-1455 does not restore EC coupling (Perez *et al.*, 2003). Overall, Sheridan and colleagues (2006) found that expression of both RyR1 regions 1285-1448 and 1682-3769 in RyR3 background is necessary for near complete restoration of depolarisation-induced SR Ca^{2+} transients and tetrad formation (Sheridan *et al.*, 2006).

As previously mentioned, the DHPR α_{1S} II-III loop critical region and β_{1a} C-terminus are important for EC coupling, which is likely through physical coupling with RyR1 being required for initiation of Ca^{2+} transients. However, the direct binding sites on RyR1 are still effectively unknown. In terms of the α_{1S} II-III loop critical region, *in vitro* assays demonstrate that the peptides corresponding to this region (724-765) may be binding to the RyR1 SPRY2 domain (1085-1208) or upstream at residues 1827-2168 (Proenza *et al.*, 2002, Cui *et al.*, 2009, Tae *et al.*, 2009, Tae *et al.*, 2011). However, when investigated *in vivo*, expression of RyR1 residues 1837-2154 in the RyR2 background did not restore voltage-induced SR Ca^{2+} transients in myotubes from *dyspedic* neonatal mice. Indeed, expression of the corresponding RyR2 residues 1637-2118 in a RyR1 background did not alter EC coupling restoration, suggesting that this region is not important in EC coupling (Proenza *et al.*, 2002). However, RyR1 residues 1837-2154 partially restored EC coupling in RyR1/RyR2 chimeras expressed in 1B5 myotubes, indicating a partial role (Protasi *et al.*, 2002). Structurally, the SPRY2 domain, but not in terms of the II-III loop binding site, may provide a site for direct contact between DHPR and RyR1 as it is located in a group of RyR1 globular domains that are juxtaposed to the DHPR in tetrad formation as according to Peralvarez-Marín *et al.* (2011).

As previously discussed, deletion or neutralisation of a RyR1 polybasic K3495-R3502 motif significantly reduces DHPR β_{1a} -RyR1 fragment binding and depolarisation-induced SR Ca^{2+} transients (section 1.3.4.3.5) (Cheng *et al.*, 2005). This is very interesting, as nine residues upstream of the polybasic motif is the first of two alternatively spliced regions (ASI: “-” lacks rabbit RyR1 residues A3481-Q3485) that have been shown to influence EC coupling (Kimura *et al.*, 2009). The ASI(-) isoform is over-expressed in human patients with myotonic dystrophy type 1 (MD1), whereas ASI(+) is the predominant isoform in healthy adult skeletal muscle (Kimura *et al.*, 2005). This region is suspected to be involved in inter-domain inhibition and removal of the ASI residues relieves this inhibition. This was concluded from the effect of peptides corresponding to the region that included and surrounded the ASI domain on RyR1 activity. Interestingly, part of this surrounding region includes the first five basic residues in the polybasic motif, which if neutralised abolishes the effect of the peptide (Kimura *et al.*, 2007, Kimura *et al.*, 2009). In addition, expression of RyR1 ASI(-) in *dyspedic* myotubes increases the maximal voltage-induced Ca^{2+} release by 60% relative to RyR1 ASI(+), without alteration of SR Ca^{2+} store level (Kimura *et al.*, 2009). Although, the polybasic region is important for interaction between the β_{1a} subunit and RyR1, the research thus far has not determined whether these residues form the β_{1a} binding site, or simply influences the ability of β_{1a} to bind to a separate site.

Another region thought to be potentially involved in EC coupling through direct interaction with RyR1 was the α_{1S} III-IV loop (section 1.3.1.1). *In vitro* binding studies demonstrate that the RyR1 residues 922-1112, not the corresponding RyR2 residues, bind to the

α_{1S} III-IV loop (Leong & MacLennan, 1998). However, RyR1/2 chimera studies show that EC coupling does not depend on this region being isoform specific (Nakai *et al.*, 1998a, Protasi *et al.*, 2002), suggesting that III-IV binding does not influence EC coupling through direct interaction with RyR1.

1.4.3 RyR1 regulation

RyR1 is regulated by a myriad of proteins in order to maintain tight control of cellular Ca^{2+} homeostasis and EC coupling. In addition, small molecules and post-translational modifications influence RyR1 gating and dynamic interactions with regulatory proteins. The principal small molecules involved in EC coupling are Ca^{2+} , Mg^{2+} and ATP. Post translational modifications include S-oxidation, S-glutathionylation and S-nitrosylation. Another chemical modification that alters RyR1 activity is phosphorylation.

Aside from the DHPR (section 1.3), other established cytosolic RyR1 regulatory proteins include FK506 binding proteins (FKBPs), calmodulin (CaM) and S100A1. Structurally, the DHPR is aligned with globular domains 4 and 6 of RyR1 (Paolini *et al.*, 2004b) and a combination of Cryo-EM and FRET studies has localised the FKBP binding site to a region on globular domain 9 that borders domains 3 and 5 on the “handle” domain (Samsó *et al.*, 2006, Cornea *et al.*, 2010). Neighbouring this region, CaM binding has been localised to a cleft between domains 3 and 8 with slight adjustment between nano- and micro-molar $[\text{Ca}^{2+}]_{\text{cyto}}$ (Wagenknecht *et al.*, 1997, Samsó & Wagenknecht, 2002, Cornea *et al.*, 2009).

In the classical model, RyR1 forms a quaternary complex through luminal interaction with SR membrane attached triadin and junctin proteins, which scaffold calsequestrin (CSQ) to the RyR1 (Guo & Campbell, 1995, Jones *et al.*, 1995, Caswell *et al.*, 1999, Shin *et al.*, 2000, Glover *et al.*, 2001). These proteins are known to influence EC coupling by modulating RyR1 activity directly and/or by determining the amount of Ca^{2+} stored within the SR.

1.4.3.1 Cytoplasmic Ca^{2+}

Cytoplasmic Ca^{2+} is both a RyR1 agonist and antagonist. Analysis of RyR1 channel activity in planar bilayer experiments and $[^3\text{H}]$ ryanodine binding demonstrate that $[\text{Ca}^{2+}]_{\text{cyto}}$ has a biphasic effect on RyR1 activity. That is, increasing $[\text{Ca}^{2+}]_{\text{cyto}}$ from 100 nM to as much as 200 μM increases channel activity from zero in a non-linear fashion, higher $[\text{Ca}^{2+}]_{\text{cyto}}$ decreases channel activity (Meissner, 1986, Ma *et al.*, 1988, Laver, 2001).

It is notable that the ability of RyR1 to respond to $[\text{Ca}^{2+}]$ has been found to strongly influence EC coupling. O'Brien and colleagues (2002) expressed a RyR1 (E4032A) mutant, known to greatly reduce Ca^{2+} -dependent RyR1 activation, in *dyspedic* myotubes and found that maximal SR Ca^{2+} transients were reduced by $\sim 80\%$ relative to expression of WT RyR1. Markedly, the Ca^{2+} transients were identical between WT RyR1 and RyR1 E4032A mutant

when normalised to relative maximal Ca^{2+} release. As a result, although RyR1 sensitivity to cytoplasmic Ca^{2+} influences EC coupling, the authors suggested that Ca^{2+} activation of RyR1 was not necessary for initiation of Ca^{2+} release during EC coupling (O'Brien *et al.*, 2002).

The general consensus is that the cytosolic domain of RyR1 contains multiple Ca^{2+} binding sites. This likely includes at least two high affinity Ca^{2+} binding sites that enable RyR1 activation and one low affinity binding sites that enable RyR1 inactivation once occupied by Ca^{2+} (Balog *et al.*, 2001, Laver *et al.*, 2004, Laver *et al.*, 2007). The two high affinity Ca^{2+} binding sites are distinguishable through separate competitive antagonism by Mg^{+} (section 1.4.3.2) (Laver *et al.*, 1997a, Laver *et al.*, 2004) and neomycin, an aminoglycoside antibiotic that inhibits RyR1 activity (Laver *et al.*, 2007). Notably, the cytoplasmic RyR2 domain contains a high affinity Ca^{2+} binding site that once occupied inhibits RyR2 activity (Laver, 2007), which may also be present on RyR1, but this has not been experimentally demonstrated. Currently, the exact residues for Ca^{2+} binding are unknown. However, the activation sites have been localised to the pore-forming region, as a protein comprising the 1377 amino acid region of the RyR1 C-tail, that composes the pore-forming region, displays typical Ca^{2+} -dependent activation in lipid bilayers (Bhat *et al.*, 1997). Markedly, this RyR1 region did not display evidence of Ca^{2+} -dependent inactivation, which suggests that the inactivation site(s) is not localised to the pore-forming region (Bhat *et al.*, 1997).

1.4.3.2 Cytoplasmic Mg^{2+}

Cytoplasmic Mg^{2+} is a key endogenous inhibitor of RyR activity and prevents RyR1 opening under healthy fibre resting conditions (Lamb & Stephenson, 1991, Lamb & Stephenson, 1994). This is particularly evident as Lamb and Stephenson (1991) found that lowering the free cytoplasmic $[\text{Mg}^{2+}]$ ($[\text{Mg}^{2+}]_{\text{cyto}}$) from 1 to 0.05 mM resulted in a large SR Ca^{2+} release in skinned rat skeletal muscle fibres. This finding has contributed to the formulation of the currently accepted model known as the Mg^{2+} de-repression hypothesis that was proposed in 1992 by Lamb and Stephenson. This model states that the interaction between DHPR and RyR1 during EC coupling reduces the sensitivity of $[\text{Mg}^{2+}]_{\text{cyto}}$ inhibition of RyR1 by more than 10-fold (Lamb & Stephenson, 1992). This reduced inhibition, enables RyR1 activation by physiological [ATP], which is enhanced when the $[\text{Ca}^{2+}]_{\text{cyto}}$ reaches 1 μM in a positive feedback loop created by Ca^{2+} binding to the A sites on neighbouring RyR1 (Laver, 2006). Currently, the reduced Mg^{2+} binding affinity of RyR1 during EC coupling by DHPR is theoretical, as no experimental data has demonstrated this to be the case.

1.4.3.3 ATP

Cytoplasmic ATP is an endogenous agonist of RyR1 (Meissner, 1984, Smith *et al.*, 1986). There are two mechanisms by which ATP increases RyR1 activity, as primarily demonstrated in planar lipid bilayer experiments. Firstly, ATP can immediately and reversibly

activate RyR1 by binding to a specific adenosine nucleotide binding site located on the cytoplasmic domain of RyR1 (Smith *et al.*, 1986, Laver *et al.*, 2001). Secondly, ATP can progressively (within 5- to 8-min) and irreversibly activate RyR1 activity by providing a substrate for phosphorylation via an endogenous calcium calmodulin kinase II (CaMKII) (Wang & Best, 1992, Herrmann *et al.*, 1993, Hain *et al.*, 1994, Sonnleitner *et al.*, 1997, Dulhunty *et al.*, 2001). Popova and colleagues (2012) recently localised the ATP binding site on RyR1 to a binding pocket that is close to the clamp region and consisting of primarily N-terminal sequences (Popova *et al.*, 2012).

1.4.3.4 Chemical modification

Cysteine residues contain thiol groups that are sensitive to redox modification. Each RyR1 monomer has ~100 cysteines, of which ~21 are susceptible to S-oxidation when stimulated by physiologically high versus low partial O₂ pressure (pO₂) (Sun *et al.*, 2013). In C2C12 myotubes, the increase in S-oxidation of RyR1 has been shown to significantly increase the maximal depolarisation-induced SR Ca²⁺ transients and contraction (Sun *et al.*, 2011).

Although not definitively proven, S-glutathionylation and S-nitrosylation may also impact EC coupling. This is particularly given as S-glutathionylation has been shown to reduce the inhibitory effect of Mg²⁺ and S-nitrosylation has been shown to enhance Ca²⁺ dependent activation of junctional SR Ca²⁺ release kinetics (Aracena *et al.*, 2003). Follow on studies by Aracena and colleagues demonstrated that S-glutathionylation and S-nitrosylation alter binding kinetics of two endogenous RyR1 antagonists, FKBP12 and CaM, and suggest that this could be the pathway that these oxidative modifications alter RyR1 activity. Specifically, S-nitrosylation decreased FKBP12 binding affinity, whereas both S-nitrosylation and S-glutathionylation decreased CaM binding (Aracena *et al.*, 2005).

Another chemical modification that regulates RyR activity is phosphorylation of certain serines. Phosphorylation of mouse RyR1 S2844 by protein kinase A (PKA) is involved in the enhancement of muscle contraction by neuro-endocrine stimulation via activation of muscle β -adrenergic receptors. That is, preventing PKA phosphorylation of S2844 through alanine mutation (S2844A) leads to ablation of β -adrenergic-mediated increase in voltage-induced SR Ca²⁺ transients and muscle force (Andersson *et al.*, 2012). Markedly, phosphorylation did not appear to contribute to FKBP12 dissociation from RyR1 as β -adrenergic receptor stimulation of the WT fibres did not alter the immunofluorescently labelled FKBP12 retained by RyR1 (Andersson *et al.*, 2012). This is intriguing as PKA phosphorylation of RyR1 has previously been shown to promote FKBP12 dissociation from RyR1 (Reiken *et al.*, 2003). Indeed, this has been associated with the pathology of skeletal muscle weakness in a heart failure model (Reiken *et al.*, 2003, Ward *et al.*, 2003, Rullman *et al.*, 2013). Andersson and colleagues (2012) suggest that this discrepancy may be due to the duration of pathological stress, as Andersson

investigated an acute model relative the chronic models (e.g. skeletal muscle weakness in a heart failure model) examined in other studies.

1.4.3.5 FKBPs

The FKBP

s are binding proteins for a potent immunosuppressant drug, FK-506 (Siekierka *et al.*, 1989), and are classed by molecular mass (kDa). There are eight isoforms of the FKBP in mammals, of which skeletal muscle exclusively express isoform FKBP12 (Collins, 1991, Jayaraman *et al.*, 1992), whereas cardiac muscle expresses isoforms FKBP12 and 12.6 (Timerman *et al.*, 1996, Jeyakumar *et al.*, 2001). FKBP12 has been shown to modulate RyR1 activity independent of its *cis-trans* peptidyl-prolyl isomerase activity that is characteristic of several FKBPs (Timerman *et al.*, 1995). FK-506-mediated dissociation of FKBP12 from RyR1 has been shown to increase single RyR1 channel activity (Ahern *et al.*, 1994) and promote SR Ca^{2+} leak (Timerman *et al.*, 1993). Similarly, rapamycin-mediated dissociation of FKBP12 from RyR1 in planar bilayers promotes sub-maximal conductance (sub-state) openings (Ahern *et al.*, 1997). Thus the current model is that FKBPs are important for setting RyR1 gating properties by stabilising the closed conformation and promoting channel opening to maximal conductance (Timerman *et al.*, 1993, Ahern *et al.*, 1994, Brillantes *et al.*, 1994, Timerman *et al.*, 1995, Ahern *et al.*, 1997).

The function of FKBP12 on single channel RyR1 activity does not translate well to its influence on skeletal EC coupling. Myotubes from FKBP12-null mice displayed increased maximal voltage-induced DHPR Ca^{2+} current without alteration in DHPR expression level, but reduced SR Ca^{2+} transients relative to myotubes taken from healthy mice (Tang *et al.*, 2004). Furthermore, maximal caffeine-induced SR Ca^{2+} release and resting $[\text{Ca}^{2+}]_{\text{cyto}}$ did not differ between FKBP12-null myotubes and WT myotubes, suggesting similar SR Ca^{2+} loads and no additional RyR1 leak (Tang *et al.*, 2004). These observations are very similar to an earlier study that examined the influence of expressing RyR1 V246I, mutation that abolishes RyR1-FKBP12 binding, relative to WT RyR1 in myotubes from *dyspedic* mice, with the exception that DHPR Ca^{2+} current was not altered (Avila *et al.*, 2003). Overall, Tang and colleagues (2004) suggest that disparity between *in vivo* and *in vitro* studies could be due to the muscle environment that could either prevent FKBP dissociated RyR1 leak or counteract RyR1 leak in resting conditions.

1.4.3.6 CaM and S100A1

Calmodulin and S100A1 have several similar features. Both are small proteins (~17 and ~22 kDa, respectively) that contain classic Ca^{2+} binding motifs, EF hands, which have Ca^{2+} occupancy at contracting $[\text{Ca}^{2+}]$ but not at resting $[\text{Ca}^{2+}]$. Additionally, both proteins undergo conformational changes in the Ca^{2+} bound form compared to the Ca^{2+} unbound form (Apo), which is critical for exposure of a putative binding site in the form of a hydrophobic pocket (Maier & Bers, 2002, Wright *et al.*, 2005). Functionally, CaM has been shown to activate single

RyR1 channel activity when $[Ca^{2+}]$ is ≤ 200 nM and inhibit when the $[Ca^{2+}]$ is increased to micromolar and above $[Ca^{2+}]$ (Tripathy *et al.*, 1995). In resting $[Ca^{2+}]_{cyto}$ conditions, S100A1 has also been shown to increase caffeine-induced SR Ca^{2+} release in skinned muscle fibres and single channel RyR1 activity (Treves *et al.*, 1997, Most *et al.*, 2003). Interestingly, although the apo and Ca^{2+} bound states of S100A1 have both been shown to pull-down RyR1, only the apo state appears to directly alter RyR1 activity (Treves *et al.*, 1997). Markedly, myotubes from S100A1-null mice display reduced maximal voltage-induced SR Ca^{2+} transients relative to myotubes from WT mice without alteration of resting $[Ca^{2+}]_{cyto}$ levels (Prosser *et al.*, 2008). This fits well into a model where CaM and S100A1 compete for the same binding site on RyR1, as suggested by competition between CaM and S100A1 for binding to SR vesicles (Prosser *et al.*, 2008, Wright *et al.*, 2008). Binding to the same site is supported by studies that demonstrated that CaM and S100A1 binding to RyR1 and the functional effect of these proteins on RyR1 activity is abolished by mutation of a single RyR1 residue (L3625D) (Yamaguchi *et al.*, 2001, Yamaguchi *et al.*, 2011). In myotubes, the consequence of S100A1 binding to RyR1 is that it reduces the antagonistic effect of CaM on RyR1 activity at excitatory $[Ca^{2+}]_{cyto}$ levels. However, the consequence of expressing RyR1 L3625D mutant is a reduction in overall voltage-induced SR Ca^{2+} release. The authors suggested that this may have been due to a lack of agonistic S100A1 and CaM action on RyR1 at lower $[Ca^{2+}]_{cyto}$ (Yamaguchi *et al.*, 2011). Although RyR1 L3625D mice are phenotypically normal, the study does provide evidence that CaM and S100A1 play a role in fine tuning SR Ca^{2+} release during EC coupling (Yamaguchi *et al.*, 2011).

1.4.3.7 Calsequestrin

Calsequestrin (CSQ) is a low-medium affinity, high capacity Ca^{2+} binding protein localised to the SR lumen. The predominant skeletal CSQ isoform (CSQ1) is the most abundant Ca^{2+} binding protein in the sarcoplasmic reticulum (Damiani *et al.*, 1990). Inherently, CSQ1 lowers the levels of free Ca^{2+} in the SR lumen ($[Ca^{2+}]_{lumen}$), which is thought to facilitate SR Ca^{2+} uptake, particularly since lower $[Ca^{2+}]_{lumen}$ has been shown to enhance SERCA activity (Inesi & de Meis, 1989, Tripathy & Meissner, 1996). Notably, planar bilayer results reveal that CSQ1 has additional functions in increasing isolated RyR1 activity by direct binding or indirectly decreasing native RyR1 activity through binding to junctin in a Ca^{2+} dependent manner (Szegedi *et al.*, 1999, Beard *et al.*, 2002, Wei *et al.*, 2009). The physiological role of direct binding is not clear, as junctin is normally present.

The importance of CSQ1 in EC coupling has so far been primarily investigated in skeletal myofibres and myotubes from CSQ1-null mice. In conjunction with visible structural deformities at the triad, the SR Ca^{2+} load is lower in CSQ1-null myofibres relative to WT myofibres (Paolini *et al.*, 2007, Canato *et al.*, 2010, Royer *et al.*, 2010). Interestingly, the

voltage-induced maximal SR Ca^{2+} transient is 84% greater in CSQ1-null myotubes, although the skeletal muscle contraction force is only slightly greater in tissue taken from CSQ1-null mice (Paolini *et al.*, 2007, Dainese *et al.*, 2009). The increased maximal Ca^{2+} transients and muscle contraction has been attributed to the inability of SR re-uptake due to defective SERCA activity and loss of CSQ1-mediated inhibition of RyR1 (Protasi *et al.*, 2011).

1.4.3.8 Triadin

There are four triadin isoforms expressed in skeletal muscle, including triadin skeletal (Trisk) 32, 49, 51 and 95 (Knudson *et al.*, 1993, Marty *et al.*, 2000, Vassilopoulos *et al.*, 2005). However, the only Trisk 95 is localised to junctional SR and involved in EC coupling (Knudson *et al.*, 1993, Rezgui *et al.*, 2005, Vassilopoulos *et al.*, 2005). With a small 47 residue cytoplasmic domain and a single SR membrane spanning region, Trisk 95 is largely (638 of 706 residues) exposed to the SR lumen (Knudson *et al.*, 1993, Marty *et al.*, 1995). Functionally, peptides corresponding to cytoplasmic residues 18-46 and luminal residues 200-232 can directly decrease and increase RyR1 activity, respectively (Groh *et al.*, 1999, Wium *et al.*, 2012). This is in agreement with other planar lipid bilayer experiments that find isolated RyR1 activity decreases upon exposure of full-length triadin to the cytoplasmic side of RyR1 and increases upon exposure to the luminal surface (Ohkura *et al.*, 1998, Wei *et al.*, 2009).

The role of triadin in EC coupling is unclear. Myotubes from triadin-null mice display reduced maximal depolarisation-induced SR Ca^{2+} transients (Shen *et al.*, 2007). However, this change was insignificant when the SR Ca^{2+} release was normalised with the reduced caffeine-induced SR Ca^{2+} release, which was attributed to the 15% reduction in SR Ca^{2+} load in triadin-null myotubes (Shen *et al.*, 2007). In addition, the resting $[\text{Ca}^{2+}]_{\text{cyto}}$ was ~63% greater in triadin-null myotubes. Shen and colleagues (2007) found that the increased resting $[\text{Ca}^{2+}]_{\text{cyto}}$ and reduced SR Ca^{2+} load was not attributed to alteration of RyR1 sensitivity to Ca^{2+} , Mg^{2+} and caffeine. Instead, the studies suggested that the aberrant resting Ca^{2+} homeostasis in triadin-null myotubes may be attributed to a reduction in FKBP12-RyR1 binding and abnormal triadic arrangement due to reduced CSQ anchorage to junctional SR (Shen *et al.*, 2007, Eltit *et al.*, 2010, Boncompagni *et al.*, 2012). In other myotube studies, the lack of sufficient triadin-RyR1 association, via knockdown of triadin or mutation of the luminal triadin binding site on RyR1 (D4878A/D4907A/E4908A), also displays a decrease in voltage-induced SR Ca^{2+} transients (Goonasekera *et al.*, 2007, Wang *et al.*, 2009). Curiously, both studies demonstrate that SR Ca^{2+} load was not altered. Combined, the studies demonstrate that triadin likely modulates depolarisation-induced SR Ca^{2+} release, and that a lack of triadin in long-term *in vivo* systems contributes to alteration in resting Ca^{2+} homeostasis and suggests that compensatory mechanisms may reduce the modulatory effect of triadin on EC coupling.

1.4.3.9 Junctin

Very similar to trisk95, junctin is a SR membrane protein with a small cytoplasmic domain (22 residues), a single transmembrane domain and a larger luminal domain that interacts with both CSQ1 and RyR1 (Jones *et al.*, 1995, Glover *et al.*, 2001). Furthermore, luminal exposure of isolated RyR1 to junctin in lipid bilayer experiments also increases channel activity (Wei *et al.*, 2009). However, Wei and colleagues found subsequent addition of CSQ1 decreased RyR1 activity with junctin, but not with triadin, present. Additionally, this was restricted to luminal Ca^{2+} concentrations that reflected physiological resting levels rather than contracting levels. Thus, the authors concluded that junctin facilitated CSQ1 inhibition of RyR1 at rest (Wei *et al.*, 2009).

Knockdown of junctin in C2C12 myotubes reduces depolarisation-induced SR Ca^{2+} transients and this has been attributed to the similarly reduced SR Ca^{2+} load (Wang *et al.*, 2009). Indeed, myotubes from junctin-null mice display no alteration of depolarisation-induced SR Ca^{2+} transients or SR Ca^{2+} load (Boncompagni *et al.*, 2012). Varying results between studies could be due to intrinsic differences between models, particularly as Wang and colleagues found a decrease in CSQ protein level, while Boncompagni and colleagues found no alteration in CSQ levels. Interestingly, Boncompagni and colleagues found the $[\text{Ca}^{2+}]_{\text{cyto}}$ level was slightly increased in myotubes from junctin-null mice. Never-the-less, the myotube studies both suggest that junctin is not directly involved in EC coupling, but rather important for maintaining SR Ca^{2+} content (Wang *et al.*, 2009, Boncompagni *et al.*, 2012).

1.5 Summary

Contraction of cardiac myocytes and skeletal muscle fibres requires depolarisation-induced mass SR Ca^{2+} release into the cytoplasm that enables interaction and sliding of the microfilaments. The series of events involved in this process is known as EC coupling. The translation of an action potential to SR Ca^{2+} release involves interplay between a myriad of proteins, particularly the DHPR and RyR, situated on juxtaposed regions of T-tubule and SR membranes, respectively (**Figure 1.9**). Skeletal EC coupling relies on physical RyR1 activation by depolarisation-activated DHPR. However, the components involved in this interaction are unclear. Deletion and chimera studies highlight the α_{1S} II-III loop critical region and the β_{1a} C-terminus of the DHPR as likely candidates involved in the interaction. Similar studies highlight RyR1 regions as important for EC coupling, including: RyR1 and RyR2 D2 region, ASI region, polybasic K3495-R3502 region and, RyR1 1635-2556 region.

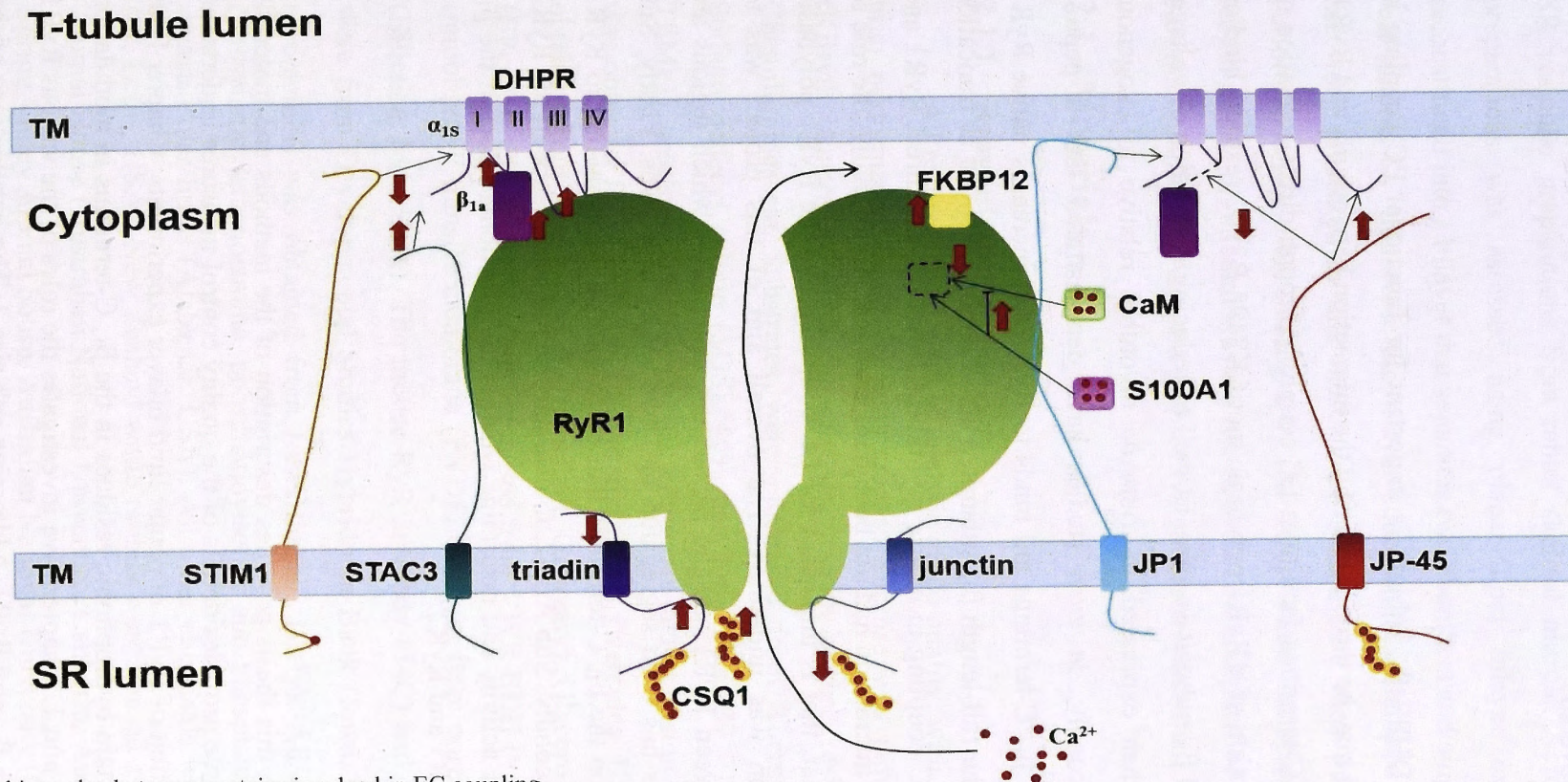


Figure 1.9 The potential interplay between proteins involved in EC coupling.

At the junctions between T-tubule and SR, EC coupling involves an interplay of proteins that are primarily located around two Ca^{2+} channels: DHPR (purple) and RyR1 (green) located in the T-tubule membrane and SR membrane, respectively. The red arrows demonstrate the theoretical influence of the proteins or interactions on skeletal EC coupling, as discussed in this chapter, Chapter One. The DHPR α_{1S} (light purple) and β_{1a} (dark pink) subunits are both crucial for EC coupling, but whether this is through direct interaction and/or indirectly facilitating interaction of the alternate subunit, with RyR1 is not clear (sections 1.3.1.1, 1.3.4 and 1.4.2). STIM1 (orange) is thought to reduce EC coupling through interaction with α_{1S} (1.3.5.1). Equally, JP-45 (red) is thought to minimise EC coupling by disrupting the α_{1S} - β_{1a} interaction, though also facilitating EC coupling by virtue of targeting the α_{1S} subunit to the triad (1.3.5.4). Similarly, JP1 (light blue) is thought to minimise EC coupling by disrupting the α_{1S} - β_{1a} interaction, though also facilitating EC coupling by virtue of targeting the α_{1S} subunit to the triad (1.3.5.3). STAC3 (dark teal) is crucial for the interaction between DHPR and RyR1 during EC coupling (1.3.5.2). Although CSQ1 (light orange) can directly interact with RyR1 to increase activity, CSQ1's interaction through junctin (dark blue) provides an overall negative effect on EC coupling (1.4.3.7). Even though cytoplasmic interaction of triadin (dark purple) with RyR1 provides a negative effect on RyR1 activity, luminal interaction is thought to promote EC coupling (1.4.3.8). FKBP12 (yellow) is thought to increase EC coupling through interaction with RyR1 (1.4.3.5). CaM (light green) decreases EC coupling through inhibition of RyR1 activity, although S100A1 (light pink) competes for the same binding site on RyR1 and consequently increases EC coupling (1.4.3.6).

Never-the-less, whether these residues play a direct role by forming a binding site or act indirectly through intra- or inter-molecular interactions is effectively unknown for most of these regions. Notably, an array of associated proteins appears to be involved, including: triadin, CaM, S100A1, CSQ1, JP-45, STAC3 and STIM1. However, the exact involvement of most of these proteins remains to be discovered.

1.6 Project Aims

The C-terminus of the DHPR β_{1a} subunit is important for functional EC coupling in skeletal myotubes. Although this may be through altering the interaction between α_{1S} and RyR1, two studies suggest that the β_{1a} C-terminus facilitates EC coupling through direct activation of RyR1. Firstly, deletion and mutation of a RyR1 polybasic motif K3495-R3502 restricts binding between the RyR1 fragment and β_{1a} subunit *in vitro*, as well as reducing restoration of voltage-induced SR Ca^{2+} transients when expressed in *dyspedic* myotubes relative to exogenous expression of WT RyR1. Secondly, *in vitro* studies have demonstrated that a peptide corresponding to the 35-residue β_{1a} C-terminus tail binds to RyR1 and increases native RyR1 activity in a similar fashion as the full-length β_{1a} subunit. This is important given as truncation of this region greatly reduces EC coupling in mouse myotubes. However, the direct RyR1 and β_{1a} binding sites involved in this interaction had not been demonstrated. Additionally, the role of the β_{1a} heptad hydrophobic repeat, that is important for EC coupling, and the RyR1 polybasic region in this direct interaction was undefined. The overall aim of this project was to characterise the interaction between RyR1 and the β_{1a} subunit in terms of which regions are involved in the interaction. This has been segregated into two major objectives. Firstly, Sub Aim 1, to identify the residues on the β_{1a} C-terminus that are responsible for binding to RyR1 and increasing RyR1 activity. Secondly, Sub Aim 2, to characterise the importance of the RyR1 polybasic motif in terms of RyR1 activity and determine whether the functional effect of the β_{1a} subunit is conserved between RyR1 and RyR2.

1.7 This Thesis

The following chapter in this thesis provides description of the methods and materials used (Chapter Two). Chapter Three provides details of the quality control measures undertaken establish the identity and orientation of RyR1 in planar lipid bilayer experiments. Chapter Four examines the involvement of certain hydrophobic residues in the β_{1a} C-terminus in modulation of RyR1 activity, addressing sub aim 1. Chapter Five investigates the roles of the various RyR1 regions in the interaction between β_{1a} and RyR1, addressing sub aim 2. The implications of the results presented in Chapters Four and Five will be discussed in detail in the final chapter (Chapter Six).

CHAPTER TWO – MATERIALS AND METHODS

This chapter provides general details of the material and methods for experimental protocols that recur throughout the result chapters. This includes the techniques used to obtain proteins/peptides and assess RyR activity. The source of native RyR1 was isolated junctional SR vesicular preparations from rabbit skeletal muscle. Activity of RyR1 from SR vesicle preparations was assessed using planar lipid bilayer experiments, whereby RyR1 is reconstituted into a bilayer that separates two chambers and single channel gating is measured in real time as Cs^+ transverse the bilayer under voltage clamped conditions. All peptides used in the work presented in this thesis were synthesised, then purified using reverse phase high performance liquid chromatography (RP-HPLC) and identified using mass spectrometry. Full-length mouse β_{1a} subunit was expressed in *E. coli* and purified using immobilised metal affinity chromatography (IMAC) and preparative gel electrophoresis.

2.1 Materials

2.1.1 Reagents and chemicals

All reagents used were of analytic grade quality, with exception of acetonitrile used for high performance liquid chromatography. Sucrose was purchased from MERCK Pty. Ltd. (Kilsyth, Australia). High capacity streptavidin-agarose resin and Super Signal West Pico Chemiluminescent Substrates were purchased from Thermo Scientific (Rockford, USA). Sodium dodecyl sulfate (SDS), 40% acrylamide-bis (37.5:1), ammonium persulfate (APS), TEMED, precision StrepTactin-HPR conjugate and Precision Plus Protein Dual Color standard was obtained from BIO-RAD Laboratories Inc. (Hercules, USA). Ethanol and methanol were obtained from Merck Group (Darmstadt, Germany). Glycerol and Acetonitrile Super gradient HiPerSolv Chromanorm were purchased from VWR BDH Prolabo (Murarrie, QLD, Australia). Immobilon-P transfer membrane (PVDF, 0.45 μm from pore size) was from Merck Millipore (Billerica, MA, USA). The mouse RyR antibody (34C) and DHP β_{1a} antibody (VD₂(1)B12) were from Developmental Studies Hybridoma Bank (Iowa, USA). Peptide calibration Mix 4 (Proteomix) was obtained from LaserBioLabs (Italy). All stock solutions of phospholipids (phosphatidylethanolamine, phosphatidylserine and phosphatidylcholine) were purchased from Avanti Polar lipids (Alabaster, USA). All other chemicals were obtained from Sigma-Aldrich (St. Louis, USA). New Zealand white rabbits were housed at the Research School of Biology Animal House (Australian National University, Canberra, Australia). Sheep were housed at the Spring Valley Animal house, Australian National University (Canberra, Australia).

Unless otherwise mentioned, all solutions and chemicals were dissolved or diluted in deionised water, obtained from a Milli-Q Plus Ultra-Pure Water System (Millipore, MA, USA). The pH of solutions was measured using a TPS digital pH meter (Bacto Laboratories; Lane

Cove, Australia). The $[Ca^{2+}]$ of solutions was determined using a Radiometre Analytical ISE25Ca Ca^{2+} electrode (Villeurbanne Cedex; France), where appropriate. Where indicated, peptide concentrations were determined using either: NanoDrop ND-100 spectrophotometer (BioLab: Scoresby, Australia), Pierce™ bicinchoninic acid (BCA) Protein Assay Kit from Thermo Fisher Scientific (Scoresby, Australia), Pierce™ 660nm Protein Assay Kit from Thermo Fisher Scientific (Scoresby, Australia), or DC Protein Assay from BIO-RAD Laboratories Inc (Hercules, USA). The EL800 – Universal microplate reader (BIO-TEK Instruments, INC: Vermont, United States) was used to measure sample fluorescence from the protein assay kits.

2.1.2 Peptides synthesised

Most peptides were synthesised by the JCSMR Biomolecular Resource Facility using a CEM Liberty Microwave Peptide Synthesiser. Two other peptides, β_{1a} V490-A508 and β_{1a} V490-A508 scrambled, were obtained from Prof. Martin F. Schneider. These peptides were synthesised at the Biopolymer/Genomic Core Facility at the University of Maryland School of Medicine, and were purified by the facility to $\geq 96\%$ by high performance liquid chromatography and mass spectrometry. The synthesised peptides corresponded to regions of the mouse (*Mus musculus*) DHPR β_{1a} subunit (U.S. National Center for Biotechnology Information (NCBI) reference sequence NP_112450.1) and zebrafish (*Danio rerio*) DHPR β_{1a} subunit (GenBank AAY29573.1). The N-terminal regions of β_{1a} V490-M524 and β_{1a} V490-M508 LLW/A peptides were biotinylated and four residues corresponding to S486-Q489 were added to the N-termini of the biotinylated peptides as a linker between the sequence and the biotin. Sequences for the peptides are shown in **Table 2.1**.

2.1.3 Plasmid constructs

The β_{1a} cDNA (GenBank accession number NM_031173) in a poly histidine tagged ubiquitin expression vector (pHUE vector: *BamHI* at the 5' end and *HindIII* at the 3') was obtained from Dr. Yamuna A. Karunasekara (Muscle Research Group, John Curtin School of Medical Research, Canberra, Australia). The benefit of this plasmid construct is that the β_{1a} cDNA is inserted in-frame and upstream of the poly-histidine and ubiquitin sequence. Attached to the β_{1a} N-terminus, the histidine tag can be used for purification and then cleaved using a deubiquitylating enzyme, or domain, such as the catalytic core of Usp2-45 (Usp2-cc) – as was used in the experimental protocol for β_{1a} purification (section 2.5.2). The Usp2-cc cDNA in a Novagen pET-15b vector (plasmid GenBank accession number AY751540.1) was obtained from Prof. Philip G. Board (Molecular Genetics Group, John Curtin School of Medical Research, Canberra, Australia) (Catanzariti *et al.*, 2004). It is noteworthy that the pHUE vector was constructed using Novagen pET-15b as a backbone construct (Catanzariti *et al.*, 2004). As a result, both vectors have a T7 promoter and a coding region for ampicillin resistance.

Table 2. 1 Corresponding sequence of peptides to the DHPR β_{1a} subunit.

Peptide name	Species	Region	mutation	Sequence
β_{1a} V490-M524	Mouse	V490-M524	None	VQVLTSLRRNLSFWGGLEASPRGGDAVAQPQEHAM
Biotinylated β_{1a} V490-M524	Mouse	S486-M524	None	Biotin-SNLQ- VQVLTSLRRNLSFWGGLEASPRGGDAVAQPQEHAM
β_{1a} A474-A508	Mouse	A474-A508	None	ATAALAASPAPVSNLQVQVLTSAARRNASFAGGLEA
β_{1a} A474-A508 LVV/A	Mouse	A474-A508	L478A/V485A/V492A	ATAAAAASPAPASNLQVQALTSARRNASFAGGLEA
β_{1a} V490-M524 LLW/A	Mouse	V490-M524	L496A/L500A/W503A	VQVLTSAARRNASFAGGLEASPRGGDAVAQPQEHAM
Biotinylated β_{1a} LLW/A peptide	Mouse	S486-M524	L496A/L500A/W503A	Biotin-SNLQ- VQVLTSAARRNASFAGGLEASPRGGDAVAQPQEHAM
β_{1a} V490-M524 L496A	Mouse	V490-M524	L496A	VQVLTSAARRNLSFWGGLEASPRGGDAVAQPQEHAM
β_{1a} V490-M524 L500A	Mouse	V490-M524	L500A	VQVLTSLRRNASFWGGLEASPRGGDAVAQPQEHAM
β_{1a} V490-M524 W503A	Mouse	V490-M524	W503	VQVLTSLRRNLSFAGGLEASPRGGDAVAQPQEHAM
β_{1a} V490-A508	Mouse	V490-A508	None	VQVLTSLRRNLSFWGGLEA
β_{1a} V490-A508 scrambled	Mouse	V490-A508	Scrambled	RVFRGELSQLNLGLTASVW
β_{1a} V490-L520 zf	Zebrafish	V490-L520	None	VQVLTSLRRNMELLDGSPAVMQGQQEDEHAL

2.2 Methods

2.2.1 Purification of peptides

Each peptide was purified using reverse phase high performance liquid chromatography (RP-HPLC) and identified using matrix-assisted laser desorption/ionization time-of-flight (MALDI-TOF) mass spectroscopy as described in Karunasekara *et al.* (2012).

2.2.1.1 Reverse phase high performance liquid chromatography

As shown in **Figure 2.1**, RP-HPLC was set up with a flow of combined buffer *A* (0.1% trifluoroacetic acid (TFA)) and buffer *B* (0.1% TFA in degassed acetonitrile) into a Jupiter 10 μm C4 300 Å column 250 x 10 mm (Phenomenex: Torrance, CA, USA) and out to a Waters 2487 dual λ absorbance detector (Waters Corporation: Milford, MA, USA). Both buffers were individually pumped into the mixing chamber via Waters 515 HPLC pumps (Waters Corporation: Milford, MA, USA). From the mixing chamber, the combined solution flowed through tubes to the column. The ratio of buffers pumped into the mixing chamber, the flow rate and the wavelengths detected were remotely controlled by Empower software (Waters Corporation: Milford, MA, USA). This software also collated the absorbance measured every 6 s for dual wavelengths.

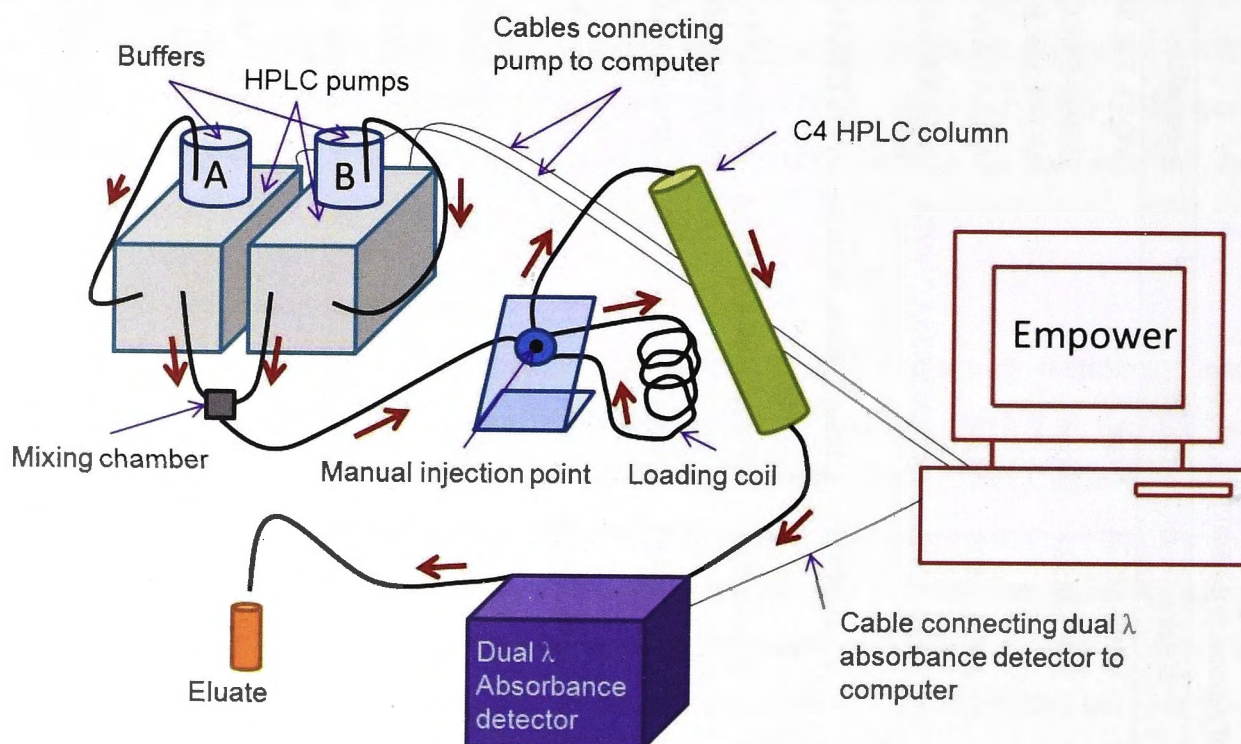


Figure 2. 1 Setup for peptide purification using RF-HPLP.

Buffer *A* and buffer *B* are combined and pumped through an injection coil, a Jupiter 300 C4 column and dual absorbance detector before being collected as eluate. Peptides in solution can be loaded on the column by manual injection into the loading coil that flows onto the column under a constant flow of buffers from the pumps. Notably the pumps and UV absorbance detector are remotely controlled by Empower software, which also collates the absorbance measurements from dual λ absorbance detector.

Three to ten mg of synthesised peptide was added to a 5 ml solution of 10% buffer *B* / 90% buffer *A* and gently vortexed until visibly dissolved. The mixture was manually injected into a 5 ml equivalent coil via a manual sample injector (Rhenodyne: Cotati, CA, USA) that preceded the column. A combination of 10% buffer *B* / 90% buffer *A* was run through injection coil and into the column – allowing loading the peptide onto the column via hydrophobic interaction with immobilized 4-alkyl (C4) ligands attached to the column. The peptide of interest was eluted using an increasing linear gradient of buffer *B* at a gradient rate of 0.5-0.8% per min and flow rate of 3 ml/s, as specified in **Table 2.2**. Eluates corresponding to individual peaks on the UV absorbance spectrum were manually collected in separate tubes.

Table 2.2 Reverse phase high performance liquid chromatography (RP-HPLC) elution gradient for peptides.

Linear gradient of buffer <i>B</i>	Gradient rate (%/min)	Peptide	Elution peak gradient (% buffer <i>B</i>)*
25-45%	0.5	β_{1a} V490-M524	28.9-29.4
		Biotinylated β_{1a} V490-M524	36.8-38
		β_{1a} A474-A508	39.6-41
		β_{1a} A474-A508 LVV/A	35-36.4
		Biotinylated β_{1a} LLW/A peptide	32-33.7
10-40%	0.8	β_{1a} V490-M524 LLW/A	22.7-23.7
		β_{1a} V490-M524 L496A	33.1-34.1
		β_{1a} V490-M524 L500A	34-34.8
		β_{1a} V490-M524 W503A	35.4-35.9
20-50%	0.5	β_{1a} V490-L520 zf	29.2-30.2

*This value may vary slightly between experiments

2.2.1.2 Freeze drying the RF-HPLC eluate

The RF-HPLC eluates corresponding to individual peaks were frozen in dry ice and lyophilised using a Dura-Dry microprocessor control freeze dryer (FTS systems, SP Industries: Warminster, PA, USA) over 3-5 days to ensure maximal buffer evaporation.

2.2.1.3 Peptide identification

An Opti-TOFTM 384 well insert (123x8 mm) plate was prepared by spotting 0.5 μ l of α -cyano-hydroxy-cinnamic acid (α matrix) solution (8 mg/ml in 70% acetonitrile and 0.1% TFA) and then left for solvent evaporation. Then, 0.5 μ l of RP-HPLC eluate (corresponding to the UV absorbance-identified peak that provided the largest lyophilised mass) was spotted above the dried α matrix and again the plate was left until the solvent had visibly evaporated. An additional spot was occupied by 0.5 μ l of Peptide Calibration Mix 4 dissolved in α matrix

solution. Notably, the cocktail masses ranged from 500 to 3500 Da, containing bradykinin [1-5] (572.7 Da), angiotensin II (1046.2 Da), neurotensin (1672.9 Da), adrenocorticotrophic hormone [18-39] (2465.7 Da) and bovine Insulin chain B (3495.9 Da). The plate was then loaded into an AB MDS Sciex 4800 MALDI TOF-TOF Mass Analyzer (AB SCIEX: Framingham, MA, USA), which was remotely controlled with 4000 Series Explorer software. The reflector positive mode and linear low mass mode were internally calibrated with a minimum 3-point calibration using the calibration spot. Data acquisition was generated from the average of 50 shots in 10 non-overlapping sites within the spot. The sample MS spectra were acquired in the range of 500 – 4500 mass (m/z). The intensity of the peptide signal provided an indication of approximate purity, particularly since most of the potential contaminants were theoretically similar synthesised peptides. The proteins were deemed sufficiently pure when the peptide of interest was the “base” or “mother” peak (largest peak) and the half peak was the second or third highest peak. The half peak refers to a peptide signal that was half the expected mass, which is the result of two protons being attached to the peptide during ionisation.

2.2.2 Isolation of skeletal SR vesicles

The experimental process of SR vesicle preparation was undertaken by Mrs. Suzy Pace and Mrs. Joan Stivala (Muscle Research Group, John Curtin School of Medical Research, Australian National University, Canberra, Australia). All buffers used in preparation include a cocktail of protease inhibitors (1 mM benzamidine, 1mg/L of Leupeptin, 0.05 mM 4-(2-aminoethyl) benzenesulfonyl fluoride hydrochloride, 1 mM Pepstatin, anti-calpain I and anti-calpain II).

SR vesicles were prepared from back and leg muscles (fast twitch skeletal muscle) from New Zealand white rabbits in accord to Saito *et al.* (1984), with adjustments described in Ahern *et al.*, (1994, 1997). Skeletal muscle was immediately rinsed in phosphate buffered saline (PBS), containing: 137 mM NaCl; 7 mM Na₂HPO₄; 2.5 mM NaH₂PO₄.H₂O; and, 2 mM ethylene glycol tetraacetic acid, pH 7.4. Sequentially, excess fat was removed, the muscle was diced, and aliquots of 50 g were snap-frozen in liquid nitrogen and stored at -70 °C. To prepare SR vesicles, 100 g of frozen skeletal muscle was homogenised four times in 15 s bursts at high speed using a Waring blender (Waring Products Division; Connecticut, USA) in *homogenising* buffer, containing: 20 mM imidazole and 300 mM sucrose, pH adjusted to 7.4 with 6 M HCl. The homogenate was centrifuged at 11 000 x g for 20 min at 4 °C using a Sorvall SLA-1500 rotor in a Sorvall RC-5B high-speed centrifuge (Dupont; Norwalk, USA). Supernatant was removed and the pellets were sequentially suspended in 170 ml of *homogenising* buffer, re-homogenised and centrifuged as before. The resulting supernatant was filtered through four layers of cotton gauze and centrifuged at 110 000 x g using a Ti-45 rotor in a Beckman L8-70 centrifuge (Beckman Instruments; Gladesville, Australia) for 1-2 h. The pellet obtained was resuspended in *homogenising* buffer to a total volume of 42 ml and homogenised in a Dounce

teflon homogenizer (Edwards Instrument Company, Narellan, Australia). Eight ml of homogenised sample was added to the top of a discontinuous sucrose density gradient, containing in order from the bottom: 4 ml of 45%, 7 ml of 38%, 7 ml of 34%, 7 ml of 32% and 4 ml of 27 % sucrose (w/w) in *SR diluting* buffer consisting of: 20 mM imidazole, pH adjusted to 7.4 with 6 M HCl. The sucrose gradient was centrifuged at 70 000 x g in a Beckman SW-28 rotor for 16 h at 4°C. The fractions found at the 34/38% (band 3) and the 38/45% interface were collected, diluted with equal volume of 20 mM imidazole and centrifuged at 125 000 x g in a Beckman SW-28 rotor for 1 h at 4 °C. Following resuspension in 1 ml *homogenising* buffer, 15 µl aliquots were snap frozen in liquid nitrogen and stored at -70 °C. This preparation consists of skeletal SR vesicles that contain “native” RyR1 and associated proteins (section 1.4.3 for description of RyR1 interaction and regulation). Associated proteins at least included junctin, triadin, FKBP12.0 and calsequestrin. The presence of these proteins was routinely checked using SDS-PAGE (section 2.2.4) and then western blot (section 2.2.6). It is notable that no β_{1a} subunit levels were detected during western blotting, indicating that the skeletal SR vesicle preparation did not contain β_{1a} subunit.

2.2.3 Expression and purification of recombinant proteins

Procuring isolated β_{1a} subunit was achieved by first employing an *E. coli* based expression system to produce β_{1a} subunit (N-terminally fused to poly-histidine tagged ubiquitin). The β_{1a} subunit was partially isolated by immobilised metal affinity chromatography (IMAC) of the His tag to the nickel-nitrilotriacetic acid (Ni-NTA) resin. The tag was then cleaved using the catalytic core of a deubiquitin enzyme, Usp2 (Usp2-cc). As the Usp2-cc was also fused to a poly-histidine (His) tag, this protein was obtained and partially purified using a similar method of *E. coli* expression and IMAC as described in Catanzariti *et al.* (2004). Notably, expression was undertaken in BL21 DE5 because this *E. coli* strain expresses T7 RNA polymerase and the experimental protocol for Usp2-cc expression has been previously established using this strain (Catanzariti *et al.*, 2004).

Although the protocols are similar for protein expression and purification between Usp2-cc and β_{1a} subunit, the protocol for β_{1a} subunit purification extends to His-tag cleavage and an additional purification step using SDS-PAGE in a BIO-RAD Prep cell system.

2.2.3.1 Expression and purification of Usp2-cc

2.2.3.1.1 *E. coli* expression system

Firstly, 25 µl of competent BL21 DE5 were transformed with ~50 ng of Usp2-cc pET-15b using heat shock. This involved: incubation at 4 °C for 30 min, addition of 125 µl of lysogeny broth (alternatively known as “Luria broth”; LB: 25 g/L of LB-medium), incubation at 42 °C for 30 s, incubation at 4 °C for 2 min, addition of 125 µl of LB and final incubation at 37 °C for 1 h. Then 100 µl of the cell sample was used to inoculate the surface of a LB/Amp agar

(125 µg/ml ampicillin and 1.5% Bacto-agar in LB) plate, which were incubated at 37 °C for 8 h. One cell colony was inoculated into 30 ml of LB/Amp solution (125 µg/ml ampicillin in LB) and incubated 12-16 h at 37 °C with rotation. Twenty ml of this starter culture was divided between four flasks of 400 ml of LB/Amp solution, which was incubated at 37 °C for ~3 h until culture $A_{600\text{nm}}$ reached ~0.7, as measured using Cary 100 Conc UV-Vis spectrophotometer (Varian, inc.: Palo Alto, CA, USA). Protein expression was then induced through addition of 0.1 mM isopropyl β-D-1-thiogalactopyranoside (IPTG) and incubated for a further 3 h. The cells were then spun down at 4225.1 x g using a Sorval SLA 3000 Super lite rotor in a Sorvall RC-5B high speed centrifuge (Dupont: Norwalk, USA) for 20 min at 4 °C. The resulting supernatant was removed and the cell pellets were combined and stored at -20 °C for up to 1 week.

2.2.3.1.2 Partial purification using IMAC

The cell pellets were resuspended in 30 ml of resuspension buffer (20 mM imidazole, 10% glycerol, 50 mM Na₃PO₄ and 300 mM NaCl, pH 8) and lysed by sonication using a Branson Ultrasonics Sonifier 250 (Danbury, CT) five times in 30 s bursts. After centrifugation at 26 891.8 x g for 30 min at 4 °C using a Sorval SS-34 rotor in a Sorval RC-5B centrifuge (Dupont: Norwalk, USA), the cell lysate was incubated for 1 h at 4 °C with 2 ml of nickel-nitrilotriacetic acid (Ni-NTA) resin, which was produced in-house in accordance with Hochuli *et al.* (1987). The His-tagged proteins were retained with the resin following centrifugation at 297.8 x g using a Himac CT6E (Hitachi Koki, Co., Ltd: Tokyo, Japan) for 5 min at 4 °C and non His-tagged proteins were removed in the supernatant. The proteins were washed three times using a process of adding 50 ml of resuspension buffer, centrifugation at 297.8 x g using a Himac CT6E for 5 min at 4 °C and removal of the supernatant. The resin was then transferred into a chromatography column using an additional 20 ml of resuspension buffer that was then flown through the column. The His-Usp2-cc was then eluted using 10 ml each of 50, 100 and 250 mM imidazole *elution* buffer (50, 100 or 250 mM imidazole respectively, 20 mM β-mercaptoethanol, 30% glycerol, 50 mM Na₃PO₄ and 300 mM NaCl, pH 8).

2.2.3.1.3 Dialysis – removal of imidazole

The partially purified Usp2-cc solution was concentrated to 8 ml using an Amicon Ultra-15 10K concentrator (Merck Millipore: Billerica, MA, USA) and dialysed with 3 L of *dialysis* buffer (20 mM β-mercaptoethanol, 30% glycerol, 50 mM Na₃PO₄ and 300 mM NaCl, pH 8), so as to remove high concentrations of imidazole. The dialysed solution was subsequently concentrated to ~3 ml and stored at -70 °C. Partial purity was visualised by Coomassie blue staining of dialysed sample on a 5-17% gradient denaturing gel (sections 2.2.4 and 2.2.5). Protein concentration was determined using the NanoDrop ND-100 spectrophotometer (BioLab: Scoresby, Australia).

2.2.3.2 Expression and purification of β_{1a} subunit proteins

The procedure of β_{1a} subunit expression and purification was very similar to that used in preparation of Usp2-cc and was undertaken in accordance with (Rebbeck *et al.*, 2011).

2.2.3.2.1 *E. coli* expression system

The His-Ub- β_{1a} subunit was expressed in BL21(DE5) cells using the same process described for expression of Usp2-cc, with the exceptions that the starter culture was 40 ml, six flasks of 400 ml of LB/Amp were inoculated and protein expression in BL21(DE5) was induced for 2 h at 37 °C following addition of 0.1 mM IPTG.

2.2.3.2.2 Purification using IMAC

The cell pellets were resuspended in 40 ml of *resuspension* buffer consisting of 8 M urea, 5 mM imidazole, 12 mM β -mercaptoethanol, 10% glycerol, 50 mM Na_3PO_4 and 300 mM NaCl, pH 8. The cells were then sonicated using a Branson Ultrasonics Sonifier 250 five times in 30 s bursts. The soluble protein was isolated using centrifugation at 26 891.8 x g in a Sorvall SS-34 rotor using a Sorvall RC-5B centrifuge (Dupont: Norwalk, USA) for 30 min at 4 °C. The resulting cell lysate was added to 3 ml of Ni-NTA resin and incubated for 1 h at 4 °C. Following incubation, the resin was spun down at 297.8 x g using a Himac CT6E (Hitachi Koki, Co., Ltd: Tokyo, Japan) for 5 min and the supernatant was removed. Then the resin was washed, which involved subsequent addition of 50 ml of *resuspension* buffer, centrifugation at 297.8 x g using a Himac CT6E for 5 min and removal of the supernatant for three washes. The resin was then transferred to a chromatography column and the His-Ub- β_{1a} protein was eluted in fifteen 1 ml aliquots following addition of *elution* buffer (8 M urea, 500 mM imidazole, 12 mM β -mercaptoethanol, 10% glycerol, 50 mM Na_3PO_4 and 300 mM NaCl, pH 8). The protein content in each fraction was determined by Coomassie staining the resolved proteins in a 5-17% gradient denatured gel (sections 2.2.4 and 2.2.5). The fractions that contained a band reflecting His-Ub- β_{1a} were collated.

2.2.3.2.3 Cleavage of His-Ub fusion tag

The combined fractions were diluted with *phosphate* buffer (50 mM Na_3PO_4 and 300 mM NaCl, pH 8), to reduce the urea concentration to 2.6 M, which enables enzymatic activity of the Usp2-cc that was added (1: 150 v/v: ~ 0.25 mg) in combination with 1 mM dithiothreitol. This mixture was incubated for 16 h at 37 °C to enable full cleavage of the His-Ub tag from β_{1a} subunit and then concentrated to ~2 ml using an Amicon Ultra-15 10K concentrator (Merck Millipore: Billerica, MA, USA) with 1191 x g in a Himac CT6E (Hitachi Koki, Co., Ltd: Tokyo, Japan).

2.2.3.2.4 Purification using preparative gel electrophoresis

Purification of the β_{1a} subunit was achieved using the Prep-Cell system, which involves the process of preparative electrophoresis through a cylindrical gel and fractionation of the

resulting eluates. At 4 °C, the BIO-RAD Prep-Cell system (BIO-RAD Laboratories, Inc.: Hercules, CA, USA) was set up following manufacture recommendations, as shown in **Figure 2.2**. Within a 28 mm gel tube cast, the model 491 Prep-Cell was setup with a 10 cm 7% acrylamide Tris-glycine *resolving* gel (0.375 mM tris[hydroxymethyl]aminomethane (TRIS), 7% acrylamide/bis 37.5:1 mixture, 1 mM ammonium persulfate (APS) and 1.7 mM tetramethylethylenediamine (TEMED)) and 2 cm of 6% acrylamide Tris-glycine *stacking* gel (0.375 mM TRIS, 6% acrylamide/bis 37.5:1 mixture, 2 mM APS and 6.8 mM TEMED) that surrounded a cooling core. A Variable Speed Pump (BIO-RAD Laboratories, Inc) maintained circulation of the electrophoresis solution (25 mM TRIS, 191 mM glycine, 3.52 mM SDS) through the cooling core to minimise temperature gradients across the gel. The top and bottom of the gel was immersed in electrophoresis solution to enable electrophoresis driven by a constant voltage that was controlled with a BIO-RAD PowerPac Universal Power Supply. Retained by a dialysis membrane at the base of the gel, the preparative gel eluates of proteins > 6 kDa were continuously pumped (1 ml/min) through the middle of the cooling core and to a BioFrac Fraction Collector using a Model EP-1 Econo Pump.

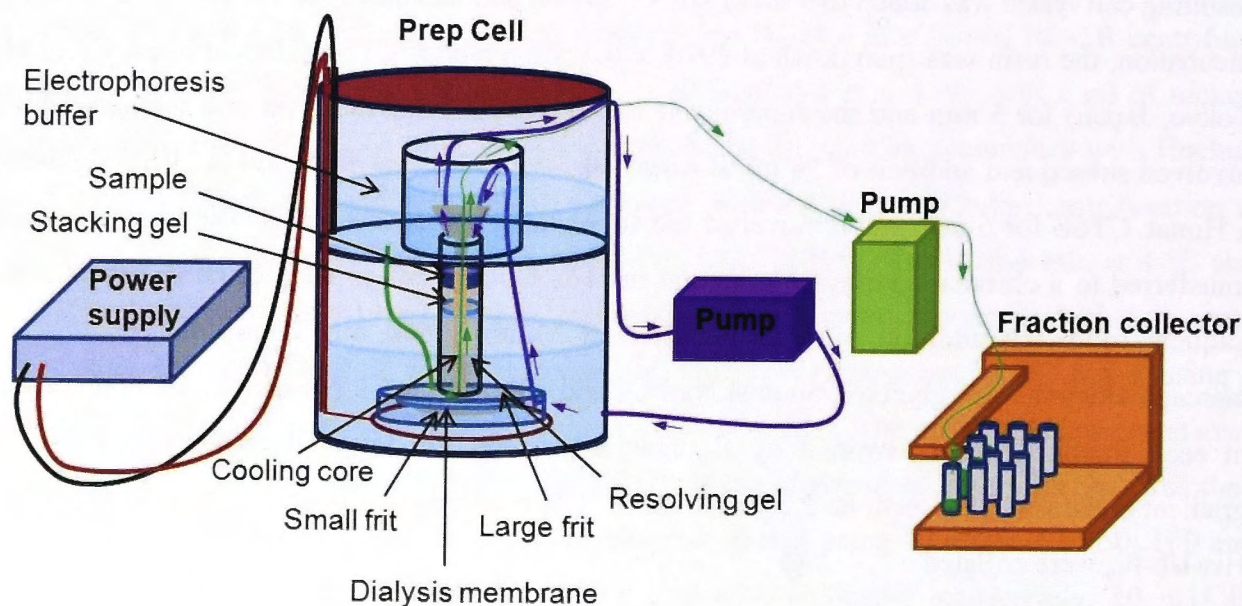


Figure 2. 2 A diagram illustrating the systematics of preparative gel electrophoresis and fraction collection using the BIO-RAD Prep-Cell system.

The system is used to resolve proteins via SDS-PAGE, then fractionate the eluates pumped from the base of the gel through the cooling core using a Model EP-1 Econo Pump (green) and BioFrac Fraction Collector (orange), as represented by green tubing. The dialysis membrane that is situated between frits at the base of the gel, retains proteins > 6 kDa from diffusing with the electrophoresis buffer. To maintain equal temperature across the gel, the gel is cast around a cooling core unit that has electrophoresis buffer continuously circulating through the core using a Variable Speed pump, as reflected by purple tubing. The protein migration is driven by constant 40 V, which is delivered using a PowerPac Universal Power Supply.

The concentrated β_{1a} sample was prepared for gel electrophoresis by addition of 1 ml of *denaturing sample loading dye* (100 mM TRIS-HCl, 4% sodium dodecyl sulfate, 25 μ M EDTA, 20% Glycerol, 0.294 M β -mercaptoethanol and 0.04% bromethyl blue stain, pH 6.8) and heated

for 10 min at 60 °C in a Julabo U3 water bath (JULABO USA, Inc.: Allentown, PA, USA). The concentrated sample was then loaded above the stacking gel and the cell was run constantly at 40 V. The eluted sample was discarded until the dye front reached the bottom of the gel after ~ 5 h, then the eluate was connected for fraction collection with 4 ml per tube. Fractions that contained exclusively β_{1a} subunit, as determined by Coomassie blue staining of resolved samples on a 5-17% gradient SDS gel (sections 2.2.4 and 2.2.5), were collated.

2.2.3.2.5 Acetone precipitation

The collated fractions were diluted 1:4 with acetone and incubated at -20 °C for 16 h. Then, the precipitated protein was spun down at 2117.8 x g using a Himac CT6E (Hitachi Koki, Co., Ltd: Tokyo, Japan) for 30 min at 4 °C. The acetone was decanted and replaced with fresh acetone, then spun down at 2117.8 x g using a Himac CT6E for 30 min at 4°C. This step was repeated once more. Then the precipitate was dried under vacuum for 5-15 min.

2.2.3.2.6 Refolding and dialysis

The protein collected in section 2.2.3.2.5 was re-dissolved in ~6 ml of *denaturing* buffer consisting of 6 mM guanidine HCl, 50 mM Na₃PO₄ and 300 mM NaCl, pH 8. To promote refolding by slowly removing guanidine HCl, the sample was dialysed with 4 L of *phosphate* buffer (50 mM Na₃PO₄ and 300 mM NaCl, pH 8) over 16 h at 4 °C. The dialysed solution was subsequently concentrated using an Amicon Ultra-15 10K concentrator (Merck Millipore: Billerica, MA, USA) to ~2 ml and stored at -70 °C. Purity was visualised by Coomassie blue stain of dialysed sample on a 5-17% gradient gel and β_{1a} subunit was identified using western blotting (sections 2.2.4-2.2.6). Protein concentration was determined using the NanoDrop ND-100 spectrophotometer (BioLab: Scoresby, Australia) and Pierce BCA kit.

2.2.4 Laemmli SDS-PAGE for protein identification

Laemmli mini polyacrylamide gel electrophoresis (PAGE) of denatured protein samples was performed using the BIO-RAD Mini-Protean Tetra cell system (BIO-RAD Laboratories, Inc.: Hercules, CA, USA). Depending on the size of the proteins, the resolving gel consisted of a range of 7.5%, 10% and 5-17% acrylamide/bis (37.5:1 solution) in 375 mM TRIS-HCl (pH 8.8), 0.1% SDS, 0.05% APS and 0.2% TEMED. The 7 cm resolving gel was set 1 cm below the stacking gel composed of 4% acrylamide/bis 37.5:1 mixture in 1.25 TRIS-HCl (pH 6.8), 0.1% SDS, 0.1% APS and 0.2% TEMED. Denatured loading samples were prepared by addition of the *denaturing sample loading* dye (50 mM TRIS-HCl, 2% SDS, 12.5 mM EDTA, 10% glycerol, 0.02% bromophenyl blue and 0.147 M β -mercaptoethanol) and incubated for 10 min at 60 °C in a Julabo U3 water bath (JULABO USA, Inc.: Allentown, PA, USA). Samples were run into the stacking gel under constant voltage of 100 V that was delivered by a BIO-RAD PowerPac 300 (BIO-RAD Laboratories, Inc.: Hercules, CA, USA). Then, the voltage was increased to 175 V until the dye front had reached 1 cm from the bottom of the gel. The gel was

then used in one of two experimental procedures for protein visualisation: Coomassie blue staining (section 2.2.5) or western blotting (section 2.2.6).

2.2.5 Coomassie Brilliant Blue stain

The Coomassie Brilliant Blue R-250 dye is utilised for its affinity to basic residues, permitting visualisation of a large range of proteins (Tal *et al.*, 1985). Immediately following electrophoresis, the gel was bathed in 100 ml of Coomassie Brilliant Blue R-250 stain solution, consisting of 0.1% (w/v) Coomassie Brilliant Blue R-250, 10% acetic acid and 40% of ethanol, for 1 h at ~21 °C. Then the gel was transferred to a de-stain solution, of 10% acetic acid and 40% ethanol, until the background was clear.

2.2.6 Western blotting

The protocols for protein transfer and immuno-detection were similar to those described in Kimura *et al.* (2005).

2.2.6.1 Protein transfer

Following SDS PAGE, proteins were transferred from a gel (section 2.2.4) to Immobilon-P polyvinylidene difluoride (PVDF) membrane using a BIO-RAD Mini PROTEAN Tetra Cell with Mini Trans-Blot module (BIO-RAD Laboratories, Inc.: Hercules, CA, USA). Each PVDF membrane was prepared by sequentially soaking in methanol for 20 s, floating on Milli-Q water for 5 min and soaking in *transfer* buffer, composed of 37 mM TRIS, 140 mM glycine and 20% methanol, for 15 min. The proteins were then transferred onto the prepared membrane in *transfer* buffer at 100 V for 1.5 h, then 150 V for 1 h using a BIO-RAD Power Pac 200 (BIO-RAD Laboratories, Inc.: Hercules, CA, USA). Notably, any variation in the composition of *transfer* buffer and transfer protocol will be specified in individual results chapters.

2.2.6.2 Immuno-detection

Following protein transfer, the membrane was blocked to minimise non-specific protein binding by immersing the membrane in *blocking* buffer (5% [w/v] low-fat milk dissolved in PBS) for 1 h at room temperature as according to Kimura *et al.* (2005). Then, the membrane was washed by immersion in 10 ml of PBS for 5 min with slow rotation using a Navigator rotation wheel (BioComp Instruments, Inc.: Fredericton, NB, Canada).

Identification of RyR: The membrane was immersed in 1:5 000 dilution of mouse RyR antibody concentrate (34C) in TPBS (0.05% Tween in PBS) for 16 h with slow rotation at 4 °C. Then the membrane was then washed six times with 10 ml of TPBS for 5 min with slow rotation. The mouse primary RyR antibody was probed using a 1:6 000 dilution of horseradish peroxidase (HRP) conjugate of goat anti-mouse antibody in TPBS for 2 h at ~21 °C with slow

rotation. Then, the wash procedure was repeated with the exception of the last wash being in PBS rather than TPBS.

Identification of β_{1a} subunit: the membrane was exposed to 1:200 dilution of mouse DHPR β_{1a} antibody concentrate (VD₂(1)B12) for 16 h with slow rotation at 4 °C. This was followed with the same wash, incubation with secondary antibody and re-wash protocol as described for identification of RyR (above).

Identification of biotinylated β_{1a} peptides: the membrane was exposed to 1:6 000 dilution of BIO-RAD Precision Protein StrepTactin-HRP conjugate for 2 h with slow rotation at ~21 °C. The membrane was then washed five times with 10 ml of TPBS for 5 min each with slow rotation. This was followed by another 5 min wash in 10 ml of PBS.

2.2.6.3 Visualisation (enhanced chemoluminescence, ECL)

The membranes were lightly covered with SuperSignal West Pico Chemiluminescent Substrate (ECL solution) over 2 min. In a darkroom, the membrane was exposed to Super RX Fuji medical X-ray film (Fujifilm Corporation: Tokyo, Japan) within a Kodak Biomax cassette (Eastman Kodak Company: Rochester, NY, USA) for 5 s to 5 min. Then the film was developed by sequentially submerging in Kodak Readymatic dental Developer (Carestream Health; Rochester, USA) for 1 min, shaken, submerging in Kodak Readymatic dental Fixer for 1 min, shaken, and finally washed in water for 1 min.

2.2.6.4 Protein band density quantification

The film was scanned and band density (intensity/area) was obtained using BIO-RAD Quantity One 1-D Analysis software (BIO-RAD Laboratories Inc.: Hercules, CA, USA). The background was removed by subtracting the density of a section directly underneath the protein band from the density of the protein band.

2.2.7 Protein quantification

2.2.7.1 Bicinchoninic acid (BCA) Protein Assay

The Pierce BCA Protein Assay kit was used in accordance with the enhanced microplate protocol recommended by the manufacture (Thermo Scientific: Rockford, IL, USA) to determine the final concentration of purified β_{1a} protein and peptide samples. This assay relies on colour development from the copper/BCA interaction with either certain amino acid (tryptophan and tyrosine) side chains or the peptide bond (Wiechelman *et al.*, 1988). All BCA assay incubations were at 60 °C, promoting optimal association of BCA with the peptide bond, which enabled quantification of peptides that lacked tryptophan residues. The absorbance was measured at 562 nm using an EL800 – Universal microplate reader (BIO-TEK Instruments, INC: Vermont, United States) and the protein concentrations were determined by reference to an absorbance response curve for 0.125 – 2 mg/ml bovine serum albumin.

2.2.7.2 Pierce 660nm Protein assay

The Pierce 660nm Protein Assay was used in accordance with the microplate procedure recommended by the manufacture (Thermo Scientific: Rockford, IL, USA) to determine the concentration of proteins in HEK293 derived microsomal vesicle preparations. The sample concentration was determined by reference to the bovine serum albumin standard curve.

2.2.7.3 Detergent compatible (DC) Protein Assay

The BIO-RAD DC Protein Assay was used in accordance with the microplate assay protocol recommended by the manufacture (BIO-RAD Laboratories Inc.: Hercules, CA, USA) to determine the protein concentration of the SR vesicle preparations from rabbit skeletal muscle.

2.2.8 [DNA] quantification using Nano-drop 1000

The Nano-drop spectrophotometer (ND 1000: Thermo Fisher Scientific, Wilmington, DE, USA) was used in conjunction with ND1000 v3.8.1 software for [DNA] determination in accordance with the manufacturer's recommendations (Thermo Fisher Scientific, Wilmington, DE, USA). Upon loading 2 μ l of DNA sample the spectrophotometer measured the samples absorbance at 230 nm and 260 and 280 nm with a 1 mm pathlength. The software calculated the concentration using a modified form of the Beer-Lambert equation (Equation 2.1) from the 260 nm reading and purity was assessed from the 260/280 nm and 260/230 nm reading.

$$C = A / (b * e) \quad \text{[Equation 2.1]}$$

Where **C** is the nucleic acid concentration in $\text{ng} \cdot \mu\text{l}^{-1}$, **A** is the absorbance at 260 nm, **e** is the wavelength dependent extinction coefficient in $\mu\text{l} \cdot \text{ng}^{-1} \cdot \text{cm}^{-1}$ and **b** is the path length in cm.

2.2.9 Planar lipid bilayers

The planar lipid bilayer experiments were undertaken as described in Karunasekara *et al.* (2012).

2.2.9.1 Overview of lipid bilayer apparatus and setup

The planar lipid bilayer equipment was setup as described in Laver *et al.* (1995). The planar lipid bilayer is a two chamber setup consisting of a Delrin cup (Caillac Plastics; Seaford, Australia) that fits snugly into a two compartment Teflon mould (**Figure 2.3A**) with each chamber containing specific solutions. The Delrin cup has a 150-200 μm aperture, across which a lipid bilayer film was painted. The aperture was visualised at 40 x magnification using a light microscope (Olympus; Tokyo, Japan) and illuminated by two 5 mm round High-Brightness white light emitting diodes (Cree Inc.: Durham, NC, USA). Silver chloride coated silver electrodes, within in each chamber, provide an electrical connection between the solutions and

an Axopatch 200B Capacitor Feedback Patch Clamp amplifier (Axon Instruments, USA) through a CV 203BV head stage (Axon instruments, USA) (**Figure 2.3A**).

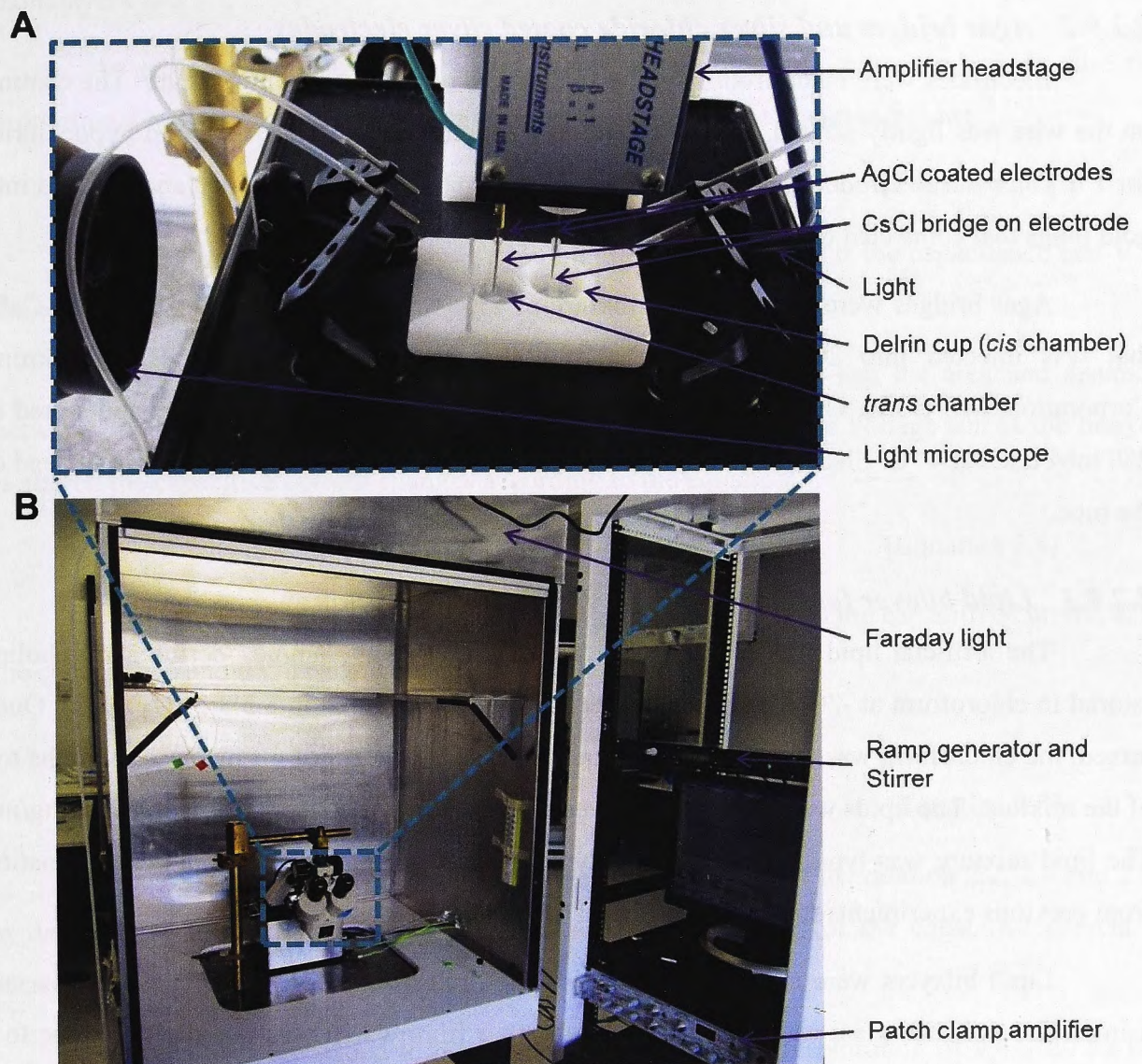


Figure 2. 3 The planar bilayer apparatus and setup

A) A photograph taken of chamber setup. The 1 cm Delrin cup fits in a two chamber Teflon base. Electrodes encased in agar bridges are submerged in *cis* and *trans* solutions. Through the amplifier headstage, one electrode is held at ground and the other is voltage clamped. **B)** A photograph taken of the overall setup of the apparatus. The chambers and head stage are within a Faraday cage to reduce electrical noise.

This setup enables current between the chambers to be monitored under voltage clamp conditions. Each electrode is immersed in a salt agar bridge that reduces the junction potential between the solution and the electrode (Williams, 1995).

SR vesicles were added to the stock solution in the Delrin cup. This compartment, known as the *cis* chamber, was voltage clamped at +40 or -40 mV. The opposing chamber, known as the *trans* chamber, was grounded. The potentials were expressed in accordance with standard physiological convention of $V_{cis} - V_{trans}$. The current was filtered at 1 kHz with a lowpass 8-pole Bessel filter integrated in the Axopatch 200B and displayed using the in-house analog/digital conversion program BLM2, and recorded at a bandwidth of 5 kHz. Both

chambers and headstage were surrounded by a grounded Faraday cage with a closable front that reduced electrical noise (**Figure 2.3B**).

2.2.9.2 Agar bridges and silver chloride coated silver electrodes

Electrodes were made from silver wire that was cut to the required length. The coating on the wire was lightly sanded and the electrode was immersed in 12.5% sodium hypochlorite for 1 h. Once the electrode was coated with black silver chloride, it was wiped and inserted into gold plugs that connected to the CV 203BV head stage.

Agar bridges were made from a mixture of 2% (w/v) agar powder and 250 mM CsCl that was injected into 20-30 cm lengths of 1.47 mm laboratory tubing (Dow Corning Corporation; MI, USA). Once set, the tubing was cut into 15 – 20 mm segments and stored in 250 mM CsCl at 4 °C. Electrodes were inserted into the agar bridges until 5 mm from the end of the tube.

2.2.9.3 Lipid bilayer formation and SR vesicle incorporation

The artificial lipid was composed of phosphatidyl-ethanolamine, -serine and -choline (stored in chloroform at -20 °C) (Borchman et al., 1982), combined in a 5:3:2 (v/v) ratio. Once mixed, the chloroform was evaporated by dispersing a small stream of nitrogen gas over the top of the mixture. The lipids were then re-dissolved in n-decane at a concentration of 45-50 mg/ml. The lipid mixture was typically prepared daily so as to avoid potential channel contamination from previous experiments that used a different SR vesicle preparation.

Lipid bilayers were created by spreading the lipid over the aperture in the Delrin cup using a fire polished glass rod. The lipid spread into a film, which was initially thick due to a large amount of n-decane between each monolayer of the bilayer (Laver et al., 2001). Sometimes gentle pressure was required to induce the n-decane to seep out of the bilayer, resulting in the optimally thin bilayer desired for SR vesicle incorporation. The thickness of the bilayer was monitored by observing the changes in the bilayer capacitive current amplitude after applying a one second 10 V/s triangular ramp via a ramp generator (JCSMR workshop, ANU, Canberra, Australia). A thinning bilayer could be seen as an increase in bilayer capacitive current amplitude. This is explained by the equations below:

The lipid bilayer has the ability to separate ions between solutions, and as such has capacitive properties (Blaustein, 2004). The capacitance of the lipid bilayer is described in the equation below:

$$C = \epsilon * (A / d) \quad \text{[Equation 2.2]}$$

Where C is the capacitance, ϵ is the dielectric constant of the n-decane between the lipid monolayers, A is the area of the lipid bilayer, and d is the distance between the lipid monolayers.

As a capacitor, the lipid bilayer stores an amount of charge, which is directly proportional to the voltage across the bilayer, as described in the equation below:

$$Q = C * V \quad \text{[Equation 2.3]}$$

Where Q is the charge stored on the lipid bilayer, C is the capacitance and V is the voltage.

Given that the capacitance of a lipid bilayer is constant when the area and distance between the lipid monolayers remains constant (Equation 2.2), if the voltage across the bilayer is altered the capacitive current changes according to the equation:

$$(dQ/dt) = I_c = C * (dV/dt) \quad \text{[Equation 2.4]}$$

Where dQ/dt is the change in charge over time, I_c is the capacitive current, C is the capacitance and dV/dt is the change in voltage over time.

Combination of equation 2.2 and 2.4 provides the equation:

$$I_c = \epsilon * (A / d) * (dV/dt) \quad \text{[Equation 2.5]}$$

Thus, if the thickness of the lipid bilayer (represented as d in equation 2.2, 2.4 and 2.5) is decreased when a triangular ramp is applied, then the height of the capacitive current is increased.

SR vesicles were added to the *cis* chamber to a final concentration of 9.4 – 20 $\mu\text{g/ml}$. SR vesicles were encouraged to incorporate into the bilayer by 1) an osmotic gradient created by a 5:1 ratio of cesium ions (Cs^+) in the *cis* to *trans* chambers (Laver *et al.*, 1995), 2) stirring the *cis* chamber, and 3) a high $[\text{Ca}^{2+}]$ of 1 mM in the *cis* chamber (Miller & Racker, 1976). Typically, SR vesicles added to the *cis* chamber incorporated into the bilayer with the cytosolic side of the SR channel exposed to the *cis* chamber, while the SR luminal side of the channel was exposed to the *trans* chamber. Correct orientation of SR vesicles is routinely observed by the Muscle Research Group Laboratory (John Curtin School of Medical Research, Australian National University, Canberra, Australia) and has been reported in $\geq 99\%$ of cases in many different laboratories (e.g. Miller and Racker (1976), Ashley and Williams (1990), Sitsapesan and Williams (1994)). In the present study, an observable increase in channel activity upon *cis* addition of ATP (an endogenous agonist of the RyR that activates the channel only via its cytosolic domain; section 1.4.3.3) and *cis* addition of BATPA (a Ca^{2+} chelator that was used to reduce free Ca^{2+} from 1 mM to 10 μM , section 1.4.3.1) was used to indicate correct orientation. Confirmation that the SR channel recorded was a RyR channel was further supported by

channel inactivation upon addition of ruthenium red, an exogenous RyR antagonist (Ma, 1993). Channel experiments were typically carried out at $21 \pm 2^\circ\text{C}$.

2.2.9.4 Lipid bilayer experimental solutions

Each solution used was adjusted to a pH of 7.4 with 4 M CsOH using a digital pH meter (TPS Pty. Ltd, Brisbane, Australia). All solutions were made using MilliQ water, including β_{1a} peptide stock solutions. All solutions used in the lipid bilayer experiments were stored at -20°C , with exception of the *cis* and *trans* solutions and ruthenium red, which were stored at 4°C .

The chamber solutions consisted of: *cis*: 20 mM CsCl, 230 mM CsCH₃O₃S, 10 mM N-Tris[hydroxymethyl]methyl-2-aminoethansulfonic acid (TES) and 1 mM CaCl₂; and *trans*: 20 mM CsCl, 30 mM CsCH₃O₃S, 10 mM TES and 1 mM CaCl₂.

For multiple reasons, Cs⁺ was used as the current carrier as opposed to Ca²⁺. Firstly, the conductance of 100-200 mM Ca²⁺ through open RyR1 is much lower than that of 100-200 mM Cs⁺, leading to a 5-fold reduction in signal (channel open current) to noise ratio (Sitsapesan and Williams, 1994). Secondly, high [Cs⁺] has a negligible regulatory effect on RyR (Laver et al., 2001), unlike high [Ca²⁺] that is a known modulator of channel activity (section 1.4.3.1). Thirdly, Cs⁺ effectively blocks SR K⁺ channels, as Cs⁺ through SR K⁺ channels has a low-conductance but dominantly competes with any other permeant-cation that enters the K⁺ channel (Cukierman et al., 1985). Methanesulfonate, CH₃O₃S⁻, was used as the major anion due to low permeability through SR Cl⁻ channels (Laver et al., 1995). BAPTA was used to chelate Ca²⁺ and to adjust [Ca²⁺]. The amount of BAPTA required to adjust the [Ca²⁺] to a desirable concentration was calculated using the in-house program Bound And Determined, and the purity of BAPTA was accessed using a Ca²⁺ electrode.

2.2.9.5 Channel recording

As soon as a channel(s) incorporated into the lipid bilayer, recording commenced using the acquisition program BLM2. Then 200 mM CsCH₃O₃S was added to the *trans* chamber, to achieve symmetrical solutions with respect to [Cs⁺], [Cl⁻] and [CH₃O₃S]. Following the addition of solutions or compounds, solutions in the desired chamber were stirred for 10 – 15 s. The control condition was achieved by reducing the [Ca²⁺]_{cis} to 10 μM with the addition of 1 mM BAPTA and then addition of 2 mM ATP (additionally containing the pH buffer, 0.1 mM TES, pH 7.4) to the *cis* chamber. Control activity was recorded for a minimum of 10 min under each condition: alternating between +40 and -40 mV every 30 s. Zero, 10 or 100 nM of β_{1a} peptide/subunit were achieved by adding appropriate amounts of peptide stock solution to the *cis* chamber. Channel activity was recorded for a minimum of 10 min: with the bilayer potential alternated between +40 and -40 mV every 30 s. Only one or two concentrations of peptide were used in each experiment to examine possible time dependent effects of the peptide on channel activity. To further confirm that the channel was RyR, 40 μM of ruthenium red was added to the

cis chamber and channel activity recorded for 4 min. To ensure that the solution of the peptide/subunit was dissolved/dialysed in did not affect channel gating properties, additional lipid bilayer experiments were undertaken with deionised water or dialysis buffer (section 2.2.3.2.6) added to the *cis* chamber, in place of the peptide/subunit solution. The channel activity was monitored for 10-20 min following addition. The volumes of control solution added were the same as the volumes of experimental peptide.

2.2.9.6 Data analysis

Single and multiple channel parameters were obtained from the in-house program, Channel 2 (developed by P.W. Gage and M. Smith, John Curtin School of Medical Research, Canberra, Australia). The channel parameters (see below) were measured from 90 s of channel activity at each potential, before and after the addition of the β_{1a} subunit/peptide. Prior to analysis, each experiment record was further filtered at 500 Hz using a Gaussian filter.

Mean open channel time (T_o), mean closed channel time (T_c), total time recorded (T_{time}), total time channel open (T_{open}), total time channel closed (T_{closed}), number of channel openings (n), mean current (I') and maximal current (I_{max}) were measured. RyR1 activity was quantified by calculating either: the probability that the channel would be open at any one time, i.e. open probability (P_o), or the average current as a function of the maximum current, known as the fractional mean current (I'_F). Equations shown below:

$$\text{Open probability } (P_o) = \frac{T_{open}}{T_{time}} \quad [\text{Equation 2.6}]$$

$$\text{Fractional mean current } (I'_F) = I' / I_{max} \quad [\text{Equation 2.7}]$$

Where T_{open} is the total channel open time, T_{time} is the total time of analysed record, I' is mean current that is an average of all data points obtained during a recording period, and I_{max} is maximum current amplitude of the analysed record.

I'_F is approximately equal to P_o and it has been shown that P_o and I'_F values obtained from a single channel record that contained a predominately active channel are very similar (section 3.3.2; Beard *et al.* (2008)). P_o most accurately quantifies RyR1 channel activity when only one channel is active in a bilayer. In contrast, I'_F is the most accurate measure of RyR1 activity when more than one channel is active. These features will be discussed further in section 3.3.2. Since I'_F is approximately equal to P_o , all channel activity (measured as I'_F or P_o) is expressed as P_o in this thesis. To measure P_o , an open channel threshold discriminator was placed at 15-20% of the I_{max} and the closed threshold was placed above baseline noise, as described by Goonasekera *et al.* (2007). As all analyses of channel properties required a constant baseline, any significant baseline variation from zero was corrected using the in-house program Baseline (developed by Dr. D. R. Laver).

Beside P_o , five additional parameters were measured from single channel records: T_o , T_c , open frequency (F_o), mean open time constant (τ_o) and mean closed timeconstant (τ_c). The first three are defined by the following equations:

$$\text{Open frequency } (F_o; \text{s}^{-1}) = n / T_{\text{time}} \quad [\text{Equation 2.8}]$$

$$\text{Mean open time } (T_o; \text{ms}) = T_{\text{open}} / n \quad [\text{Equation 2.9}]$$

$$\text{Mean closed time } (T_c; \text{ms}) = T_{\text{closed}} / n \quad [\text{Equation 2.10}]$$

Where T_{open} is the total channel open time, T_{closed} is the total channel closed time, n is the total number of channel openings, and T_{time} is the total time analysed.

The mean time constants were calculated as described in Laver and van Helden (2011), which involves use of a log-bin method that was formulated by Sigworth and Sine (1987). The open and closed time histograms for each channel record were constructed with the square root of the event frequency (probability) per bin versus equally spaced bins on the logarithmic scale for open or closed durations (seven bins per decade). In accord with Sigworth and Sine (1987), the time constants were equated from the frequency peaks. A manual fit to the dwell-time histogram was used to determine the area under each frequency peak, which equated to the fraction of single channel open or closure events falling into each time constant.

All single channel parameters were measured from 30 – 90 s of channel activity at each potential during the control period and after the addition of the β_{1a} subunit/peptide. Notably, channel activity (I'_F or P_o) was measured from 80-90 s of channel record.

In addition, the maximal conductance of a channel was calculated from the voltage across the bilayer and the maximal current through the channel, using the equation below:

$$G = I / V \quad [\text{Equation 2.11}]$$

Where G is the maximal conductance, I is the maximal current and V is the voltage across the lipid bilayer. Please note that the maximal conductance is contingent on the ion charge equilibrium across the lipid bilayer.

2.3 Statistics

Average data was presented as mean \pm standard error of the mean (SEM). Correlation between P_o and I'_F values was determined using a Pearson correlation test. Significance between control and the test condition was determined using either a paired or unpaired two-tailed Student's t-test or analysis of variance (ANOVA) when appropriate. The number of observations (n) for each data set is given in corresponding figure legends or tables. To reduce the effects of variability in control parameters in planar bilayer experiments, all (P_o , T_o , T_c , F_o) values were expressed as their logarithmic (\log_{10}) value. The effect of β_{1a} peptide/subunit

addition was evaluated by subtraction of the control values ($\text{Log}_{10}P_{oC}$, $\text{Log}_{10}T_{oC}$, $\text{Log}_{10}T_{cC}$) from the post β_{1a} addition values ($\text{Log}_{10}P_{oB}$, $\text{Log}_{10}T_{oB}$, $\text{Log}_{10}T_{cB}$) for each channel, e.g. $\text{Log}_{10}P_{oB} - \text{Log}_{10}P_{oC}$. The variance between $\text{Log}_{10}P_{oC}$ and $\text{Log}_{10}P_{oB}$ was assessed using a paired, two-tailed Student's t-test and variance between the effect of β_{1a} subunit/peptide in different conditions (i.e. voltage, concentration and peptide) was assessed using a Fisher's least significant difference test of ANOVA. A p value < 0.05 was considered to be significant.

CHAPTER THREE – GENERAL PROPERTIES OF RYR1 IN LIPID BILAYERS

3.1 Introduction

Electrophysiological techniques, such as the patch clamp technique, are commonly used to investigate ion channel gating properties. Given that RyR1 is embedded in an intracellular membrane that is not accessible for cellular patch clamping technique, reconstitution of RyR1 in a planar biomolecular lipid membrane (lipid bilayer) is an alternative method for employing electrophysiological techniques to assess RyR1 activity over time. This setup enables ionic currents across RyR to be monitored over time while the composition of solutions surrounding the cytoplasmic and luminal domains of the RyR1 in the *cis* and *trans* chamber, respectively, are controlled. The gating characteristics of RyR1 and their response to a range of modulators are well established and consequently provide markers indicative of channel identity and orientation within the lipid bilayer. Commonly used markers include response of RyR1 to endogenous modulators, such as ATP, Ca^{2+} and Mg^{2+} , and exogenous inhibitors, such as ruthenium red and ryanodine (e.g. Ahern *et al.* (1994), Laver *et al.* (1995), Ahern *et al.* (1997), Copello *et al.* (1997), Laver *et al.* (2000)). Additionally, single channel conductance for a range of ions has been well established, as described in section 1.4. Indeed, the ions used as the current carrier in this technique include Ca^{2+} , Ba^{2+} , Cs^+ , K^+ and Na^+ (e.g. Smith *et al.* (1986), Lai *et al.* (1992), Seok *et al.* (1992), Laver *et al.* (1995), Copello *et al.* (1997)). Notably, Cs^+ was chosen as the current carrier for reasons mentioned in section 2.2.9.4.

3.1.1 Aim

The objective in this chapter was to establish the identity and orientation of single channels from skeletal SR vesicles in lipid bilayer experiments. To achieve this, the single channel gating characteristics and response of single channels to *cis* [Ca^{2+}], ATP and ruthenium red were compared with the well-established response and gating characteristics of RyR1.

3.2 Methods

The skeletal SR vesicles were prepared as described in section 2.2.2. These skeletal SR vesicles were incorporated into lipid bilayers and the experiments were carried out as described in section 2.2.9. Following channel incorporation the initial *cis* and *trans* chamber solutions were identical, consisting of 20 mM CsCl, 230 mM $\text{CsCH}_3\text{O}_3\text{S}$, 10 mM TES and 1 mM CaCl_2 , pH 7.4.

3.3 Results

3.3.1 General observations

SR vesicles typically incorporated into the artificial lipid bilayer within 5 min following their addition to the *cis* chamber. If channel incorporation did not occur within 30 min of painting the lipid bilayer, the chambers were washed, the solutions were replaced and a new bilayer painted. Addition of $\text{CsCH}_3\text{O}_3\text{S}$ to equilibrate the $[\text{Cs}^+]$ between the chambers was found to halt further incorporation. This was confirmed multiple times when lipid bilayers were painted whilst the $[\text{Cs}^+]$ was symmetrical. In these cases, the lipid bilayer was monitored for up to 25 minutes and no SR channel incorporation was observed.

During this study, more than one channel frequently incorporated into the bilayer. Multiple channels could be seen as additional step increments in current above the maximal open current for a single channel opening (**Figure 3.1**). A notable feature of native RyR1 was that most openings of periods ≥ 6 ms were full single channel openings rather than a fraction (sub-state) of the full channel opening. Similarly, Copello *et al.* (1997) reported that the frequency of substate openings relative to full openings was $< 1\%$ during recordings of native RyR1 activity.

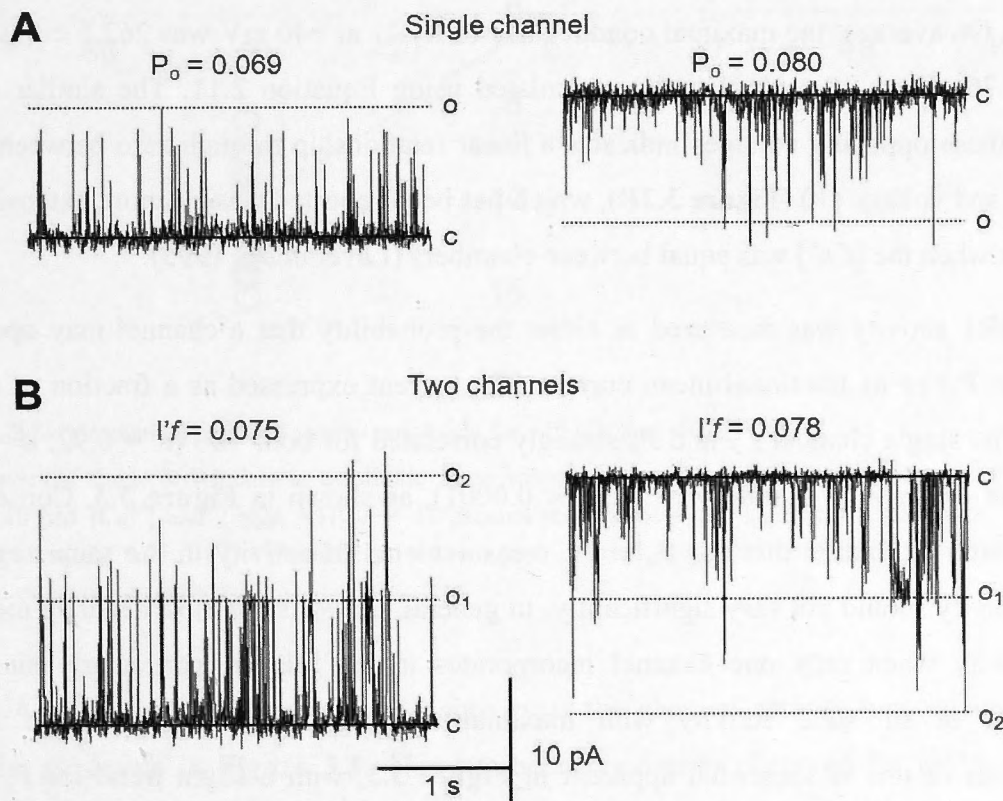


Figure 3. 1 Single and multiple RyR1 openings within a bilayer.

A and **B**) Three second recordings from a typical single channel (**A**) and a multiple channel (**B**) recording, voltage clamped at +40 mV (left panel) and -40 mV (right panel). Channel openings are upward (left panel) or downward (right panel) inflections from zero current (c, continuous) to maximum conductance (o, broken line). **B**) Conductance additional to the maximal conductance (o_1) is due to conductance from a second channel. Maximal conductance of a second channel is indicated as o_2 .

The time frame for a complete channel recording was limited by the integrity of the lipid bilayer. Typically, 45-60 min after incorporation, the lipid bilayer would become unstable. This was visible as either jagged inflections in the current due to non-specific leak from bilayer breakdown that was easily distinguishable from channel openings, or bilayer thickening. Thickening of the bilayer was observed as a decrease in capacitance across the membrane (section 2.2.9.3), which was typically accompanied by a visible reduction in the amplitude of channel maximal openings. Recording of channel activity was halted when reduction in membrane capacitance was observed.

On rare occasions, a channel record would inactivate within seconds of shifting the voltage from -40 mV to +40 mV. This phenomenon of voltage-dependent inactivation at +40 mV has previously been reported by Laver and Lamb (1998). Due to concern that 90 s measurement of the activity of these channels would provide an inaccurate measurement of true channel modulation by peptides/subunits, channel records that displayed obvious voltage-dependent inactivation were not analysed.

3.3.2 Characteristics of RyR1

In this study, the maximal current of a single RyR1 was very similar when channels were recorded at +40 and -40 mV (with 10 μM *cis* [Ca^{2+}] and 2 mM *cis* [ATP]; **Figure 3.2A**, $r^2 = 0.957$). On average, the maximal conductance of RyR1 at +40 mV was 262.5 ± 9.24 pS and 262.9 ± 7.76 pS at -40 mV ($n = 44$), calculated using Equation 2.11. The similar maximal current at these opposing voltages indicates a linear relationship through zero between channel current (I) and voltage (V) (**Figure 3.2B**), which has been reported using a more extensive range of voltages when the [Cs^+] was equal between chambers (Laver *et al.*, 1995).

RyR1 activity was measured as either the probability that a channel may open (open probability: P_o) or as fractional mean current (I'_F ; current expressed as a fraction of maximal current). The single channel I'_F and P_o strongly correlated for both +40 ($r^2 = 0.92$, $n = 53$, $p < 0.0001$) and -40 mV ($r^2 = 0.86$, $n = 42$, $p < 0.0001$), as shown in **Figure 3.3**. Consequently, there is a high likelihood that the P_o or I'_F measurements of activity in the same segment of channel activity should not vary significantly. In general, the P_o is the most accurate measure of RyR1 activity when only one channel incorporates in the bilayer, particularly since P_o is independent of sub-state activity with maximal openings at ≥ 2 pA, unlike I'_F . The consequences of this is somewhat apparent in **Figure 3.3**, with a slight trend for $P_o > I'_F$ at higher channel activity values. Unfortunately, P_o cannot be unambiguously used to measure activity when bilayers contain more than one channel as it becomes a measure of nP_o where n is the number of channels. To avoid multiple assumptions that would be required to deconvolute individual P_o , I'_F was used to measure RyR1 activity when multiple channels are open.

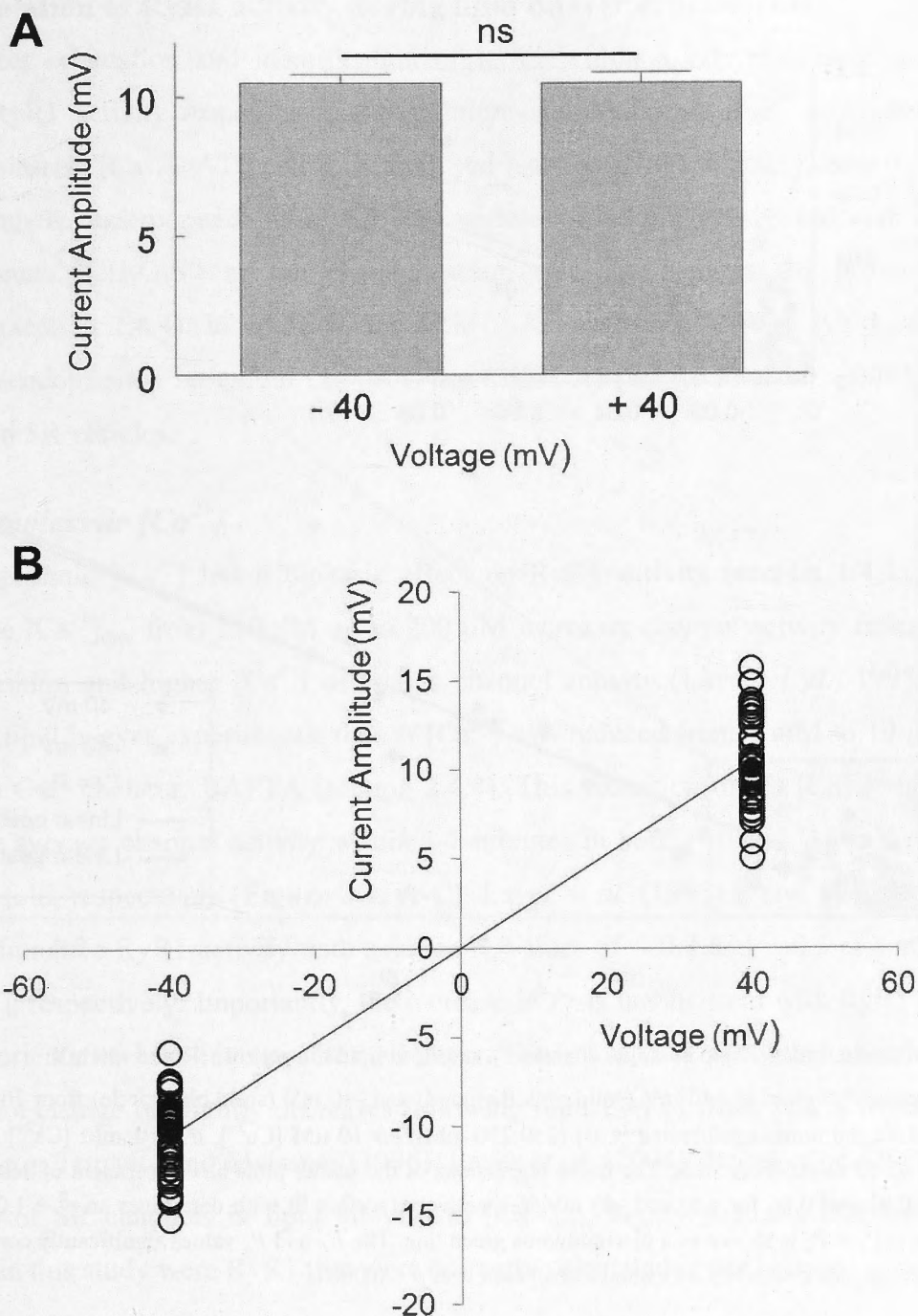


Figure 3. 2 Single channel maximal current amplitude for +40 mV and -40 mV.

A) The average single RyR1 current amplitude when voltage clamped at either +40 or -40 mV. The *cis* solution contains 10 μM $[\text{Ca}^{2+}]$ and 2 mM ATP. $n = 44$ channel records, ns – “no significant” difference, determined by Student’s t-test, $p > 0.05$. **B)** The linear fit (continuous line) is based on the scatter of single current amplitude (open circles) at each voltage analysed.

A consistent attribute of RyR1 activity is the channel activity heterogeneity between channels, as shown in **Figure 3.3**. This has been previously observed for rabbit skeletal SR vesicles in lipid bilayers (Ma, 1995, Copello *et al.*, 1997, Laver *et al.*, 2001). Copello and colleagues (1997) noted that although most channels displayed the typical biphasic response to *cis* $[\text{Ca}^{2+}]$, the peak of open probability at 10-200 μM varied greatly between channels. Both, Ma (1995) and Laver *et al.* (2001) demonstrate a large distribution in the maximal P_o values following *cis* addition of ATP.

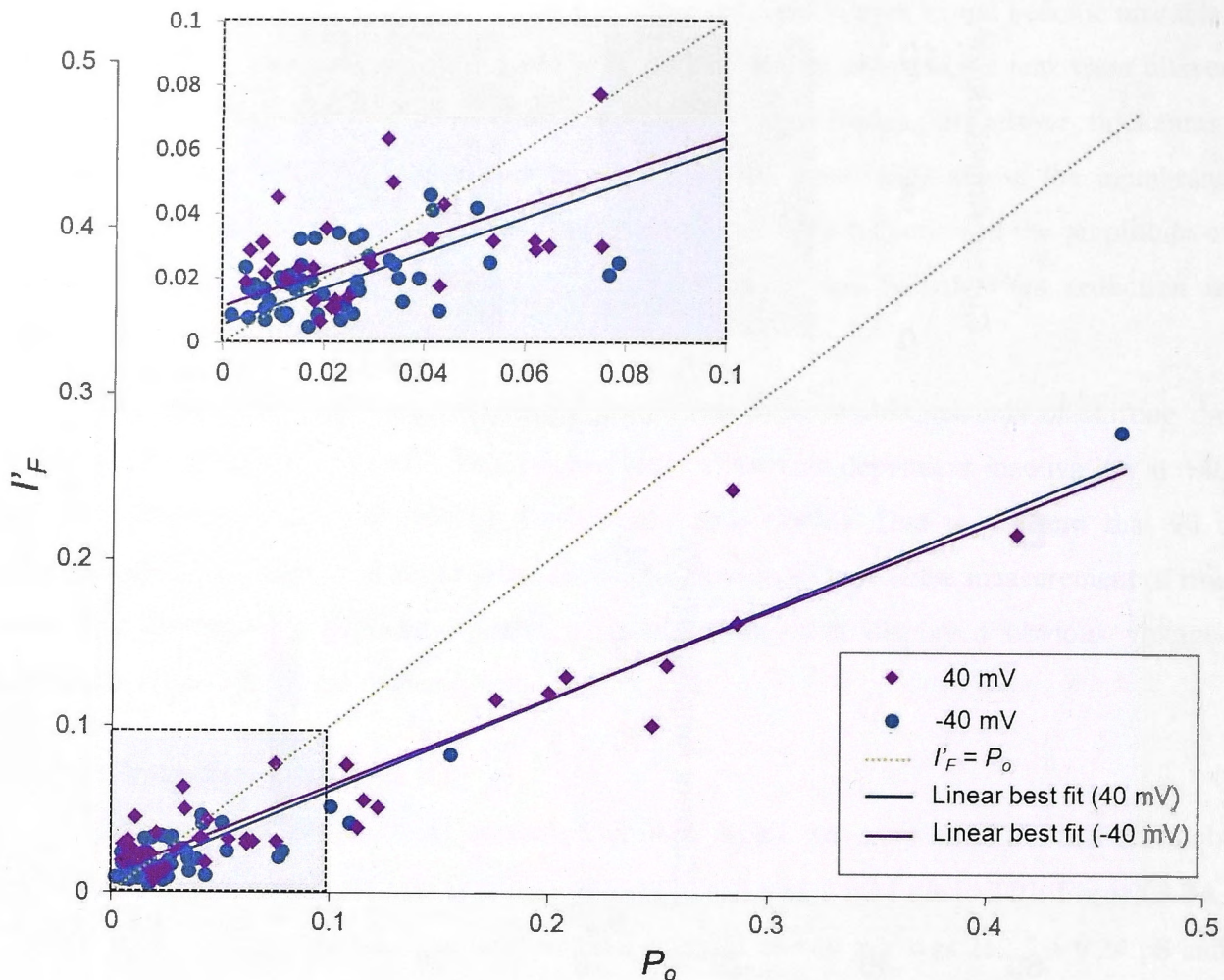


Figure 3. 3 Linear relationship of single channel I_F and P_o in lipid bilayers at +40 and -40 mV

The I_F versus P_o values at +40 mV (solid pink diamond) and -40 mV (solid blue circle) from 70-90 s traces of RyR1 under conditions: equilibrated $[Cs^+]$ (250:250 mM), *cis* 10 μM $[Ca^{2+}]$, *trans* 1 mM $[Ca^{2+}]$ and *cis* 2 mM ATP. $n = 42-53$ channels records. The linear regressions of the scatter plots has co-efficient of determination (r^2) values of 0.92 and 0.86 for +40 and -40 mV, respectively (perfect fit with data gives an $r^2 = 1.00$). The linear regression if $I_F = P_o$ is shown as a discontinuous green line. The I_F and P_o values significantly correlate for each channel record, determined by a Pearson Correlation test, $p < 0.0001$.

The heterogeneity between channels could be due to many factors. As previously discussed, the chemical modification state of RyR1 and the levels of FKBP12.0 and CaM bound to RyR1 influences RyR1 activity (sections 1.4.3.4-6). Indeed, the response of native RyR1 activity in lipid bilayers to Mg^{2+} varies within rabbit skeletal SR vesicle preparations in accordance with the phosphorylation state of individual RyR1 (Hain *et al.*, 1994). Overall, Hain *et al.* (1994) suggested that only 40% of RyR1 in the SR vesicle preparation were phosphorylated. Given that phosphorylation modulates RyR1 activity (section 1.4.3.4), this could account, at least partially, for the heterogeneity of channel activity observed in this thesis.

3.3.3 Regulation of RyR1 activity during lipid bilayer experiments

Correct orientation and identification of RyR1 within a bilayer was established by monitoring RyR1 activity responses to the addition of cytoplasmic RyR1 regulators, which include cytoplasmic $[Ca^{2+}]$, ATP and ruthenium red (section 2.4.4). Notably, activity from Cl⁻ and K⁺ channels incorporated with the SR vesicles was effectively blocked by using methanesulfonate (CH₃O₃S⁻) as the primary anion and Cs⁺ ions as the primary cation, respectively (section 2.4.4). In addition, the lack of K⁺ ions and the high $[Cs^{+}]$ inhibits the sarcoplasmic/endoplasmic reticulum Ca²⁺ ATPase (SERCA) (Kargacin *et al.*, 2005), which is also present in SR vesicles.

3.3.3.1 Cytoplasmic $[Ca^{2+}]$

Cytoplasmic $[Ca^{2+}]$ has a biphasic effect on RyR1 activity (section 1.4.2), whereby increasing the $[Ca^{2+}]_{cyto}$ from 100 nM up to 200 μ M increases channel activity from zero in a non-linear fashion and higher $[Ca^{2+}]$ decreases channel activity (Laver *et al.*, 1995) (section 1.4.2). In all lipid bilayer experiments, the *cis* $[Ca^{2+}]$ was reduced from 1 mM to 10 μ M by the addition of a Ca²⁺ chelator, BAPTA (section 2.4.4). This reduction of *cis* $[Ca^{2+}]$ significantly increased the average channel activity within 1-2 minutes in both +40 and -40 mV records by 1.6- and 2.2-fold, respectively (**Figure 3.4, A-C**). Laver *et al.* (1995) found a similar increase (~ 2.5-fold) in native RyR1 activity with average P_o values of ~ 0.2 and ~ 0.5 at 1 mM and 10 μ M *cis* $[Ca^{2+}]$, respectively. Importantly, the increase in P_o is inconsistent with RyR1 activity if the channel orientation was reversed in the bilayer. Several studies show that channel activity either does not change or slightly decreases following reduction of *trans* $[Ca^{2+}]$ from 1 mM to 10-100 μ M (e.g. Tripathy and Meissner (1996), Laver *et al.* (2004), Beard *et al.* (2008)). Thus, the response of SR channels in lipid bilayers to $[Ca^{2+}]_{cyto}$ highly suggests that the channels investigated in this study were RyR1 that were correctly orientated in the bilayer.

A very small portion (< 5%) of RyR in bovine diaphragm muscle is RyR3, which are capable of incorporating into lipid bilayers (Jeyakumar *et al.*, 1998). Despite a report that rabbit skeletal muscle does not contain amounts of RyR3 detectable by immuno-blotting, the possibility that RyR3 may have incorporated into a bilayer during the experiments undertaken for this project could not be excluded. Although RyR3 display similar conductance properties to RyR1 in lipid bilayers, activity of RyR3 does not appreciably vary between *cis* 10 μ M and 1 mM Ca²⁺ (Jeyakumar *et al.*, 1998). Consequently, the response of channels used in this study to *cis* $[Ca^{2+}]$ would highly suggest that these channels are not RyR3.

The average P_o values found by Laver *et al.* (1995) are greater (~10-fold) than the values found in this study. This deviation is unlikely to be due to the chamber solutions used. The solutions used by Laver *et al.* (1995) were similar to those used in this study, with

exception that Laver *et al.* (1995) used disproportionate levels of CsCl (250 mM *cis* / 50 mM *trans*). Another study noted that this solution difference does not change the concentration dependent effect of *cis* $[Ca^{2+}]$ and $[Mg^{2+}]$ on RyR1 activity (Laver *et al.*, 1997b), suggesting that the solution difference does not change channel P_o . An alternative hypothesis for the P_o variance is channel heterogeneity (3.3.1) between the SR vesicle preparations used in this study and those used by Laver *et al.* (1995).

3.3.3.2 ATP

ATP is a strong activator of RyR1 (section 1.4.2). Addition of 2 mM ATP increased channel activity at both +40 and -40 mV by 2- to 3-fold on average within 1-2 min of addition (**Figure 3.4**). This increase in RyR1 activity agrees with a previously reported ~2.2-fold increase in channel activity upon *cis* addition of 2 mM ATP to RyR1 in lipid bilayers (Dulhunty *et al.*, 2001).

Channel activity typically remained increased for up to 30 min (**Figure 3.4**, $n=3$ channels), although activity varied over time, which agrees with previous reports of native RyR1 activity in lipid bilayers (Copello *et al.*, 1997, Laver *et al.*, 1997a). Activation upon addition of 2 mM ATP was consistent for all skeletal SR channels analysed and verified the identity of channels as RyRs.

3.3.3.3 Ruthenium red

Ruthenium red greatly reduces or abolishes channel activity (Ma, 1993). Concentrations of 15 to 80 μ M have been used by this laboratory (Laver *et al.*, 1995, Ahern *et al.*, 1997) and the typical response is highly diminished channel activity. The response of channel activity to *cis* addition of ruthenium red was either greatly reduced or abolished within 1-3 minutes of its addition in all channels recorded with ruthenium red, (**Figure 3.4A-B**) at both +40 and -40 mV. This suggests that the SR channels recorded were RyR1 channels. Unfortunately, some channel experiments were halted prior to ruthenium red addition, due to lipid bilayer instability and/or breakage. In these cases, the level of maximal channel conductance, response to *cis* $[Ca^{2+}]$ and 2 mM ATP were used as markers to confirm RyR1 identity.

3.4 Conclusion

Native RyR1 activity was assessed in this study by fusion of skeletal SR vesicles in planar lipid bilayers. The channel records that were analysed displayed the single channel gating characteristics and responses to known RyR1 modulators that were typical of RyR1, suggesting that the channels were indeed native RyR1 that were correctly orientated in the bilayer. The single channel experiments in which RyRs did not respond typically to changes in *cis* $[Ca^{2+}]$ or ATP were discontinued. Furthermore, any channels that did not respond typically to the addition of 40 μ M ruthenium red at the end of the experiment were not analysed.

CHAPTER FOUR – HYDROPHOBIC BETA1A SUBUNIT C-TERMINAL RESIDUES THAT MODULATE RYR1 ACTIVITY

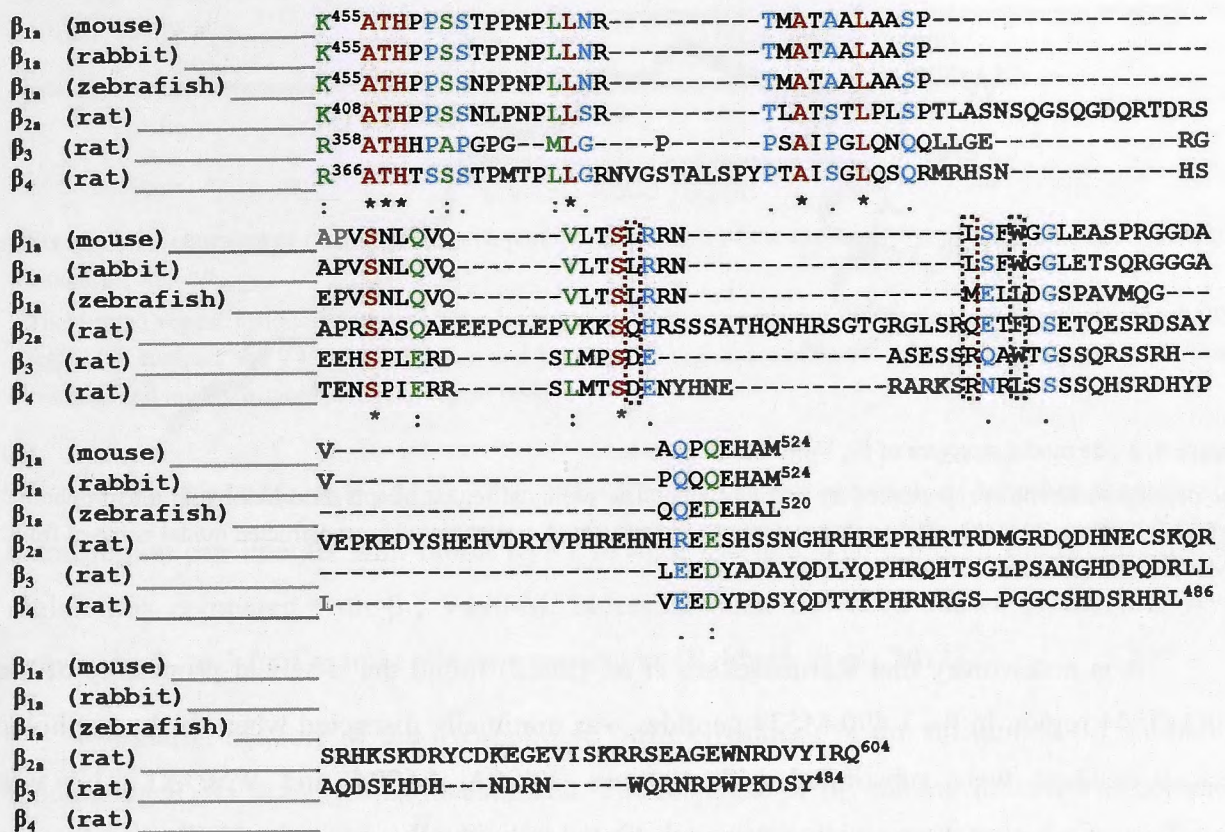
4.1 Introduction

The DHPR β_{1a} subunit is essential for skeletal EC coupling (Gregg *et al.*, 1996, Strube *et al.*, 1996, Strube *et al.*, 1998), which is thought to be due to a combination of β_{1a} 's role in DHPR tetrad formation, α_{1S} membrane expression and α_{1S} charge movements (sections 1.3.4.3.1, 1.3.4.3.3 and 1.3.4.3.4). However, there are several lines of evidence which suggest that the β_{1a} subunit also facilitates EC coupling by directly increasing RyR1 activity during excitation (section 1.3.4.3.5). In particular, a peptide (β_{1a} V490-M524) corresponding to the β_{1a} C-terminal (35 C-tail) residues, that are important for restoration of voltage-induced SR Ca^{2+} transients in β_{1a} -null myotubes (Beurg *et al.*, 1999a, Sheridan *et al.*, 2003), can bind and increase RyR1 activity in *in vitro* studies (Rebbeck *et al.*, 2011). Interestingly, the β_{1a} V490-M524 peptide contains one of three hydrophobic residues that compose the hydrophobic heptad repeat (abbreviated to heptad repeat in this chapter) that strongly influences EC coupling in mouse myotubes (Sheridan *et al.*, 2004). However, it could be argued that this region is not important, particularly given as the β_{1a} V490-M524 peptide modulates RyR1 activity with the same concentration dependence as the full length β_{1a} subunit (Rebbeck *et al.*, 2011). Additionally, mutation of these residues in a zebrafish model does not alter EC coupling, suggesting that these residues are not important in the zebrafish system (Dayal *et al.*, 2010). These points bring into question 1) the role of the heptad repeat region of the C-terminus in terms of modulating RyR1 activity and 2) whether the zebrafish β_{1a} C-terminus is able to increase RyR1 activity. Indeed, it is likely that the zebrafish C-tail also increases RyR1 activity given that the mammalian β_{1a} subunit isoforms are able to fully replace zebrafish β_{1a} subunit function in zebrafish muscle contraction (Dayal *et al.*, 2010).

Interestingly, mouse and zebrafish β_{1a} isoforms restore EC coupling in mouse and zebrafish β_{1a} -null myotubes, respectively (Beurg *et al.*, 1997, Schredelseker *et al.*, 2009), and have similar C-terminal sequences (**Figure 4.1**). Indeed, a large variation in this sequence in β_{2a} , β_3 and β_4 subunits is correlated with the inability of these β subunits to restore skeletal EC coupling when expressed in the mouse and zebrafish β_{1a} -null models (Beurg *et al.*, 1999a, Beurg *et al.*, 1999b, Sheridan *et al.*, 2003, Sheridan *et al.*, 2004, Schredelseker *et al.*, 2009, Dayal *et al.*, 2013), as discussed in section 1.3.4.3. Whether these variations in sequence and EC coupling are due to a direct interaction with RyR1, α_{1S} or intramolecular β_1 interactions is not definitively known. However, this correlation highlights the residues that may be important for such an interaction by virtue of conservation between β_{1a} isoforms and disparity with β_{2a} , β_3 and β_4 subunit sequences. These facts underpinned the experiments described in this chapter to

explore whether the β_{1a} C-terminal regions that are important for EC coupling are also important for functional interaction with RyR1 in lipid bilayer experiments.

A



B

	β_{1a} (zebrafish)	β_{1a} (rabbit)	β_{2a} (rat)	β_3 (rat)	β_4 (rat)
β_{1a} (mouse)	83%	97%	28%	34%	47%
β_{1a} (zebrafish)		84%	27%	37%	45%

Figure 4. 1 DHPR β C-terminal sequence alignment and similarity.

A) C-terminal sequence alignment of β sequences corresponding to mouse β_{1a} (residues 455-524; NCBI reference sequence NP_112450.1), rabbit β_{1a} (455-524; NCBI reference sequence NP_001075748.1), zebrafish β_{1a} (455-520; GenBank AAY29573.1), rat β_{2a} (408-604; GenBank AAK14821.1), rat β_3 (358-484; GenBank AAA18486.1) and rat β_4 (366-486; NCBI NP_001099203.1). The aligned residues are either identical (red, *), similar (green, :), weakly similar (blue, .) or dissimilar (black). The corresponding hydrophobic surface residues (red discontinuous box) vary between β isoforms. **B)** Similarity of these sequences to mouse and zebrafish β_{1a} C-terminal sequences. The similarity was calculated as the combined percentages for sequence identity and similarity (inclusive of strong and weak). Alignment and similarity was determined using a CLUSTALW multiple alignment (Combet *et al.*, 2000).

The nuclear magnetic resonance (NMR) determined secondary structure of the β_{1a} V490-M524 peptide shown in **Figure 4.2** reveals a hydrophobic surface region in the nascent α -helical region between residues L493-G504, which provides a putative RyR1 binding site (Karunasekara *et al.*, 2012). This α -helical region is situated in a β_{1a} C-terminal region that has previously been shown to be important for EC coupling by truncation studies of a β_{1a}/β_{2a} chimera (1-287 $\beta_{2a}/325$ -524 β_{1a}) expressed in mouse β_{1a} -null myotubes. Interestingly, truncation of residues downstream of W503 did not alter restoration of EC coupling by the chimera, but

truncation of residues downstream of V495 reduced EC coupling restoration by ~70% (Sheridan *et al.*, 2003).

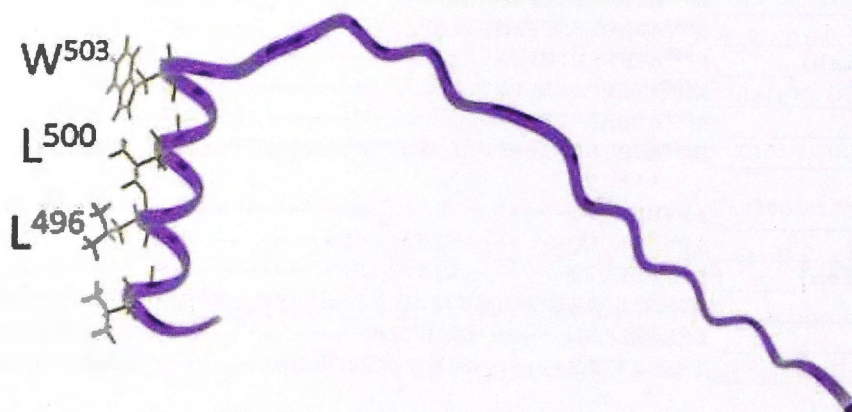


Figure 4. 2 The model structure of β_{1a} V490-M524 peptide.

The peptide backbone is represented by purple ribbon. The proximal region adopts an α -helix with a hydrophobic surface, as reflected by chemical stick structure of the amino acid side chains. The constructed model is based from NMR analysis (Karunasekara *et al.*, 2012).

It is noteworthy that Karunasekara *et al.* (2012) found the α -helical propensity of the L493-G504 region in β_{1a} V490-M524 peptides was minimally disrupted when the hydrophobic surface residues were substituted with alanines (L496A, L500A and W503A). This was regardless of whether these residues were substituted individually or together, indicating that the hydrophobic surface residues are not important for the structural integrity of the β_{1a} V490-M524 peptide.

Sequence comparison between β isoforms also supports the potential importance of the hydrophobic surface residues, given that they are similar in β_{1a} isoforms that support EC coupling and dissimilar in isoforms that do not support EC coupling. The hydrophobic surface residues are identical in mouse and rabbit β_{1a} sequences and very similar with the comparable residues (L496, M500 and L503) in the zebrafish β_{1a} sequence. Furthermore, secondary structure prediction studies suggest that the zebrafish β_{1a} sequence adopts a similar α -helical region that also encourages the hydrophobic surface residues to align on one side (Karunasekara *et al.*, 2012). It is interesting to note that there are no comparable hydrophobic residues within the β_{2a} , β_3 and β_4 sequences (**Figure 4.1A**, red box surrounds residues aligned with mouse β_{1a} hydrophobic surface residues).

4.1.1 Aim

The overall objective in this chapter was to determine the β_{1a} C-terminal residues responsible for functional modulation of RyR1 activity. This aim was addressed in four parts. Firstly, via an investigation of the role of the heptad repeat residues and the hydrophobic surface residues on RyR1 activity in lipid bilayer experiments using peptides corresponding to the C-terminal regions, as shown in **Figure 4.3**. Secondly, the influence of the hydrophobic surface

for physical interaction between β_{1a} V490-M524 peptide and RyR1 was investigated using a biotin-streptavidin based affinity chromatography assay.

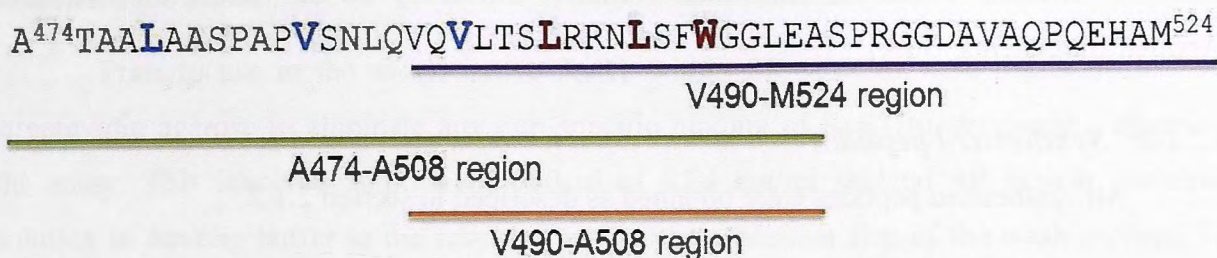


Figure 4. 3 Sequences of the peptides corresponding to sections of the extreme 51 residues C-terminal region of mouse β_{1a} subunit.

The heptad repeat residues (blue) and the hydrophobic surface residues (red) are encased by the A474-A508 region. In contrast, the V490-M524 region and V490-A508 region are inclusive of only the hydrophobic surface residues and one hydrophobic heptad repeat residue

The third objective addressed in this chapter was the question of whether the zebrafish C-tail region can interact with rabbit RyR1 in lipid bilayers. The effect of the zebrafish C-tail region was compared with β_{1a} V490-M524 peptide that has been shown to increase RyR1 activity by 2- to 3-fold in lipid bilayer experiments (Rebbeck *et al.*, 2011).

Finally, the role of the hydrophobic surface residues in the full-length β_{1a} subunit on modulating RyR1 activity was investigated. The response of β_{1a} subunit mutant was compared with the effect of the truncated form of the β_{1a} subunit (missing C-terminal residues A456-M524) and the rabbit β_{2a} subunit on RyR1 activity in lipid bilayers.

4.2 Materials and methods

4.2.1 Materials

4.2.1.1 Plasmid constructs

The β_{1a} subunit was obtained as described in section 2.1.3. The β_{1a} LLW/A cDNA and Trunc β_{1a} (M1-K455) cDNA in the pHUE vector (*Bam*HI at the 5' end and *Hind*III at the 3') were obtained from Dr Yamuna A. Karunasekara (Muscle Research Group, John Curtin School of Medical Research, Canberra, Australia). Both constructs were modified from the mouse β_{1a} subunit construct. The β_{1a} LLW/A cDNA was made using site directed mutagenesis that was adapted from Kupzig *et al.* (2006). The process of creating a Trunc β_{1a} cDNA construct involved specifically amplifying the coding sequence for β_{1a} (1M-K455) in accord with the Phusion High Fidelity PCR kit (New England BioLabs Inc, Ipswich, MA, USA) and cloning the amplified product into the pHUE vector (*Bam*HI at the 5' end and *Hind*III at the 3').

The rabbit β_{2a} subunit cDNA sequence (NCBI Reference Sequence: NM_001082396.1) was synthesised by DNA2.0 Inc. (Menlo Park, CA, USA) and cloned into a pHUE vector (*Sac*II at the 5' end and *Eco*RI at the 3' end) by Dr. Yamuna A. Karunasekara.

To ensure the sequences completely aligned with the reference sequences, all β subunit cDNA constructs were sequenced by the ACRF Biomolecular Resource Facility at John Curtin School of Medical Research, Australian National University on an ABI 3730 Sequencer (Applied Biosystems, USA).

4.2.1.2 Synthesised peptides

All synthesised peptides were obtained as described in section 2.1.2.

4.2.2 Methods

4.2.2.1 Peptide synthesis, purification and identification

The β_{1a} peptides synthesised in this chapter were synthesised and purified as described in section 2.2.1.

4.2.2.2 Expression and purification of β_{1a} , β_{1a} LLW/A and β_{2a} subunit

Both β_{1a} LLW/A subunit and β_{1a} subunit were expressed and purified by Ms. Jean Cappello (Molecular Genetics Group, John Curtin School of Medical Research, Australian National University, Canberra, Australia). β_{1a} subunit, β_{1a} LLW/A subunit and β_{2a} subunit were purified using the same procedure as described in section 2.2.3, with the exception that β_{1a} LLW/A was dialysed in buffer containing with 10% glycerol, which was added as a pre-emptive measure to reduce potential protein stability issues.

4.2.2.3 Preparation of SR vesicles

Skeletal SR vesicles were obtained as described in section 2.2.2.

4.2.2.4 Planar bilayer recordings of RyR1

Bilayer experiments were carried out and analysed as described in section 2.2.9. Prior to addition of peptide/subunit the *cis* and *trans* chambers consisted of: *cis* solution (20 mM CsCl, 230 mM CsCH₃O₃S, 10 mM TES, 2 mM ATP and 10 μ M free Ca²⁺) and *trans* solution (20 mM CsCl, 230 mM CsCH₃O₃S, 10 mM TES, 2 mM ATP and 1 mM CaCl).

4.2.2.5 Affinity chromatography between β_{1a} peptides and RyR1

Affinity chromatography assays were undertaken as described in Karunasekara *et al.* (2012). Notably, this method was used only for results described in this chapter and was not addressed in the general methods in Chapter Two.

4.2.2.5.1 Pre-incubation of skeletal SR vesicles with streptavidin agarose

Streptavidin-agarose was washed by sequentially sedimenting 100 μ l of resin at 500 x g for 5 mins (SIGMA 1-14 Microfuge: Osterode am Harz, Germany), removing supernatant and resuspending in 1 ml of *binding* buffer (150 mM NaCl, 20 mM 3-[*N*-morpholino]propane-

sulfonic acid, 1 mM BAPTA and ~1 mM CaCl₂ was added in amounts determined using a Ca²⁺ electrode to obtain 10 μM free Ca²⁺, pH adjusted to 7.4 using 6 M HCl) This wash step was repeated three times.

Prior to use in the assay, native RyR1 within SR vesicles were pre-incubated with streptavidin agarose to eliminate any non-specific binding of RyR1 to streptavidin agarose in the assay. This involved addition of 650 μl of 0.24 mg/ml skeletal SR vesicle containing solution in *binding* buffer to the resin in the final resuspension step of the wash process. The mixture was incubated with rotation for 16 h at 4 °C. The resin was spun down at 500 x g for 5 min at 4 °C and the supernatant was retained as pre-cleared SR vesicles for use in the subsequent affinity chromatography assay.

4.2.2.5.2 Affinity chromatography

One hundred μl of washed resin (section 4.2.2.5.1) was resuspended in 300 μl of either 1 mg/ml biotinylated β_{1a} V490-M524 peptide solution, 1 mg/ml biotinylated β_{1a} V490-M524 peptide solution or deionised water. The agarose-peptide mix was incubated with rotation for 3 h at room temperature. The resin was washed by centrifugation (SIGMA 1-14 Microfuge) at 500 x g for 5 min, the supernatant was removed and the pellet was resuspended in 1 ml of *binding* buffer. This wash step was repeated four times so as to fully remove any unbound peptide. The resin was sedimented by centrifugation at 500 x g for 5 min, and the supernatant was replaced with 200 μl of pre-cleared skeletal SR vesicles. The mixture was incubated with rotation at 4 °C for 48–72 h. Unbound protein was removed by five repeats of the wash step. The washed pellet (streptavidin agarose complex) was added to sample buffer (20 mM TRIS-HCl, 40% glycerol, 8% sodium dodecyl sulfate (SDS), 0.05 M EDTA, 0.588 M mercaptoethanol, and 0.08% bromophenyl blue, pH 6.8), and incubated at 60 °C for 10 min. The supernatant was run on an 8.5% acrylamide/bis SDS-PAGE (section 2.2.4). The proteins were transferred to a PVDF membrane in a *transfer* buffer (37 mM TRIS, 140 mM glycine and 27% methanol) at 100 V for 5 h and 150 V at 1 h. The membrane was cut in half to allow separate detection of RyR1 with anti-RyR antibody (34C) and biotinylated peptide with Precision Protein™ StrepTactin-HRP conjugate proteins, as described in section 2.2.6.2. The protein bands were visualised using ECL (section 2.2.6.3) and density was quantified using the Quantity One 1-D Analysis Software (BIO-RAD, Hercules, CA, USA).

4.3 Results

4.3.1 Characterising the effect of the β_{1a} C-terminal residues A474-A508 on native RyR1 activity

To assess the effect of the heptad repeat motif on the modulation of RyR1 activity by the β_{1a} C-terminus, a peptide corresponding to C-terminal residues A474-A508 (β_{1a} A474-A508 peptide, encasing both the heptad repeat and α -helical region) was tested in lipid bilayer experiments. The cytoplasmic side of RyR1 was exposed to the peptide by its addition to the *cis* chamber in the presence of 10 μM Ca^{2+} (*cis*), 2 mM ATP (*cis*) and 1 mM Ca^{2+} (*trans*). These conditions were chosen as they enable determination of channel identity and orientation in the bilayer, as described in Chapter Three. Furthermore, an earlier report indicated that β_{1a} V490-M524 peptide is only functionally effective in *cis* Ca^{2+} concentrations that reflect cytoplasmic levels in a muscle fibre undergoing EC coupling. Hence, this includes *cis* 1 and 10 μM [Ca^{2+}], but not 100 nM [Ca^{2+}] (Rebbeck *et al.*, 2011). It is worth noting that with *cis* 1 or 10 μM , the functional effects of β_{1a} V490-M524 peptide and β_{1a} subunit on native RyR1 in lipid bilayer experiments are the same in the presence and absence of 2 mM ATP (Rebbeck *et al.*, 2011).

Channel activity was recorded for 15 to 20 min following addition of either 10 or 100 nM peptide. These experiments were repeated with equivalent volumes of deionised water rather than peptide solution, so as to test the functional influence of the solution that the peptide was dissolved in. The peptide concentrations were chosen on the basis of 1) 10 nM is the minimal concentration for maximal effect of β_{1a} subunit and β_{1a} V490-M524 peptide on RyR1 activity in lipid bilayer experiments (Rebbeck *et al.*, 2011) and, 2) 100 nM was used to assess any changes in concentration dependence between 10 nM and 100 nM. Depending on bilayer stability over time, channel activity was recorded with either one addition of peptide or sequential addition of peptide (e.g. addition of 10 nM peptide that was increased to 100 nM after 15-20 min). Notably, the functional effect of β_{1a} subunit or V490-M524 peptide was identical between 10 and 100 nM [β_{1a}] when tested with individual, rather than sequential, addition of subunit/peptide to a channel experiment (Rebbeck *et al.*, 2011). This reflects the observed outcome with sequential addition (shown here).

The records of single channel activity at +40 mV (**Figure 4.4A**) and -40 mV (**Figure 4.4B**) show typical channel gating before (control) and after addition of 100 nM β_{1a} A474-A508 peptide. These records clearly demonstrate that 100 nM β_{1a} A474-A508 peptide increased channel activity at both +40 and -40 mV by similar amounts.

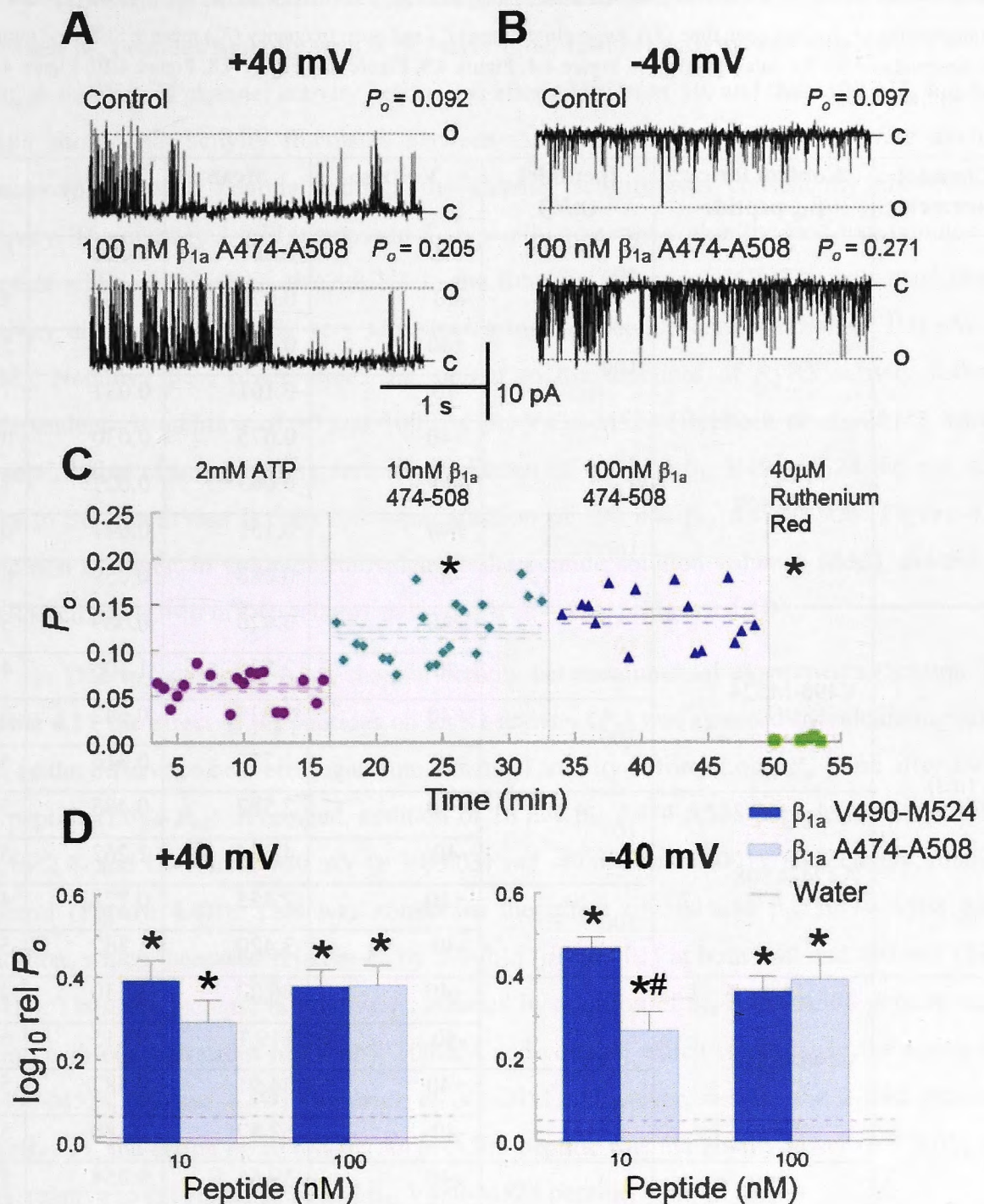


Figure 4. Similar modulatory action of β_{1a} V490-M524 and β_{1a} A474-A508 peptide on RyR1 activity in lipid bilayers.

A and B) Three second records of single channel activity at +40 mV (left) or -40 mV (right) that are representative channel traces before (top traces: control, *cis* 10 μ M [Ca²⁺] and 2 mM ATP) and after *cis* addition 100 nM β_{1a} A474-A508 peptide (bottom traces). Open probability (P_o) is shown in the right top corner. Channel openings are upward (A) or downward (B) current inflections from zero current (c, continuous line) to maximal conductance (o, discontinuous line). **C)** A timeline of channel activity following sequential *cis* addition of 2 mM ATP (pink circle), 10 nM β_{1a} A474-A508 (green diamonds), 100 nM β_{1a} A474-A508 (blue triangles) and 40 μ M ruthenium red (light green square). The channel activity over 10 s was taken from ~30 s intervals of activity at +40 and -40 mV. For each condition, there is a mean (continuous line) \pm SEM (discontinuous line) of the scatter plot. *Significantly different from prior condition, determined by Student's t-test, $p < 0.05$. **D)** Average relative P_o ($\log_{10} \text{rel } P_o$) is the average of the differences between the logarithm of P_o value measured after ($\log_{10} P_{oP}$) and before (control: $\log_{10} P_{oC}$) peptide addition for each channel recording. Error bars indicate \pm SEM. P_o was measured from ~90 s traces of RyR1 activity, $n = 5-7$ channel traces. Control P_o values in Table 4.1. The mean \pm SEM $\log_{10} \text{rel } P_o$ values for deionised water additions are shown as continuous pink line and discontinuous pink line, respectively. *Significantly different from control activity set at zero, determined by paired Student's t-test, $p < 0.05$. #Significantly different from 10 nM β_{1a} V490-M524 peptide, determined by ANOVA, $p < 0.05$.

Table 4. 1 Mean control parameters for channels used in analysis of β_{1a} V490-M524 and β_{1a} A474-A508 peptides.

Open probability (P_o), mean open time (T_o), mean closed time (T_c) and open frequency (F_o) mean \pm SEM and number (n) of observations for the data presented in Figure 4.4, Figure 4.5, Figure 4.7, Figure 4.8, Figure 4.10, Figure 4.11, Figure 4.15 and Figure 4.16.

Channel parameter	Control for <i>cis</i> β_{1a} peptide	[peptide] (nM)	Voltage (mV)	Mean parameter	\pm SEM	n	
P_o	V490-M524	10	+40	0.027	0.008	6	
			-40	0.070	0.035	5	
		100	+40	0.109	0.014	5	
			-40	0.101	0.031	7	
	A474-A508	10	+40	0.075	0.030	6	
			-40	0.063	0.027	7	
		100	+40	0.151	0.047	6	
			-40	0.088	0.059	6	
	T_o (ms)	V490-M524	10	+40	0.920	0.089	3
				-40	2.730	1.506	4
			100	+40	2.735	0.642	3
				-40	1.772	0.316	5
A474-A508		10	+40	2.582	0.485	5	
			-40	4.034	1.262	5	
		100	+40	2.155	0.728	4	
			-40	3.420	1.362	5	
T_c (ms)		V490-M524	10	+40	96.23	37.30	4
				-40	119.1	97.15	6
			100	+40	34.91	9.587	5
				-40	52.87	22.88	5
	A474-A508	10	+40	39.66	9.854	5	
			-40	97.79	45.70	5	
		100	+40	25.99	10.35	5	
			-40	58.31	31.51	4	
	F_o (s ⁻¹)	V490-M524	10	+40	7.960	3.643	3
				-40	36.99	6.989	5
			100	+40	38.04	15.59	3
				-40	33.11	11.81	5
A474-A508		10	+40	29.78	7.162	5	
			-40	30.36	13.42	5	
		100	+40	54.15	15.46	5	
			-40	11.22	6.244	3	

To examine potential time dependent effects and gauge the stability of the interaction between β_{1a} peptides/subunits with RyR1 over time, channel activity was monitored for 15-20 min. A timeline of channel activity before and after addition of 10, and then 100 nM, β_{1a} A474-A508 shows that activity fluctuates between the 30-60 s time points that were analysed. However, following peptide addition the channel activity was consistently above control activity. The average 2-fold increase in P_o typically occurred within the first two minutes after peptide addition, which is also visible in the timeline (**Figure 4.4C**). The enhanced channel activity did not significantly vary after increasing the peptide concentration to 100 nM ($p = 0.12$). Notably, these observations are similar to the timelines of RyR1 activity following independent *cis* addition of 10 and 100 nM β_{1a} V490-M524 (Rebbeck *et al.*, 2011), with the exception that channel activity following addition of 100 nM β_{1a} V490-M524 did not visibly vary to the extent that it does following addition of 100 nM β_{1a} A474-A508 (**Figure 4.4C**). Addition of water, in volumes equivalent to the peptide solution volumes added, did not alter RyR1 activity at +40 mV ($p = 0.96$) and -40 mV ($p = 0.24$) (**Figure 4.4D**).

Due to heterogeneity of channel activity between channel experiments (Section 3.3.2; **Table 4.1**), the effect of β_{1a} peptides on RyR1 activity (P_o) was assessed by calculating relative P_o , as the difference between logarithmic channel activity before ($\text{Log}_{10} P_{oC}$) and after addition of peptide ($\text{Log}_{10} P_{oB}$). Averaged, addition of 10 nM β_{1a} A474-A508 peptide increased relative P_o by 2.0- and 1.9-fold at +40 mV ($p = 0.003$) and -40 mV ($p = 0.001$), respectively, relative to control (**Figure 4.4D**). This was similar to the effect of 100 nM β_{1a} A474-A508 peptide addition, which increased relative P_o by 2.4-fold ($p < 0.001$) at both +40 and -40 mV (**Figure 4.4D**). Thus, the increase in relative P_o induced by addition of β_{1a} A474-A508 peptide was the same with concentrations of 10 nM, 100 nM and voltage, which is similar to the action of β_{1a} V490-M524 (**Figure 4.4D**) (Rebbeck *et al.*, 2011). However, despite the 2-fold increase in relative P_o , the action of 10 nM β_{1a} A474-A508 peptide was marginally lower ($p = 0.01$) at -40 mV relative to the action of 10 nM β_{1a} V490-M524 peptide.

The effect of β_{1a} peptides on RyR1 gating was assessed by measuring single channel mean open times (T_o), mean closed times (T_c) and open frequency (F_o). The values for these parameters varied between channel records, which has been reported by other studies using skeletal SR vesicles (e.g. Laver *et al.* (1995), Copello *et al.* (1997), Laver *et al.* (2001)). Consequently, the effects of the β_{1a} peptide/subunit on single channel gating parameters were measured relative to control for each channel record, as with P_o . Addition of β_{1a} A474-A508 did not significantly ($p = 0.69-0.92$) alter the average relative T_o of single channels (**Figure 4.5A**). Whereas, average relative T_c values were decreased ($p = 0.001-0.015$) by 2.2- to 2.5-fold (**Figure 4.5B**) and average relative F_o values were increased ($p = 0.002-0.023$) by 2- to 2.1-fold (**Figure 4.5C**) with both 10 and 100 nM peptide additions and at +40 and -40 mV.

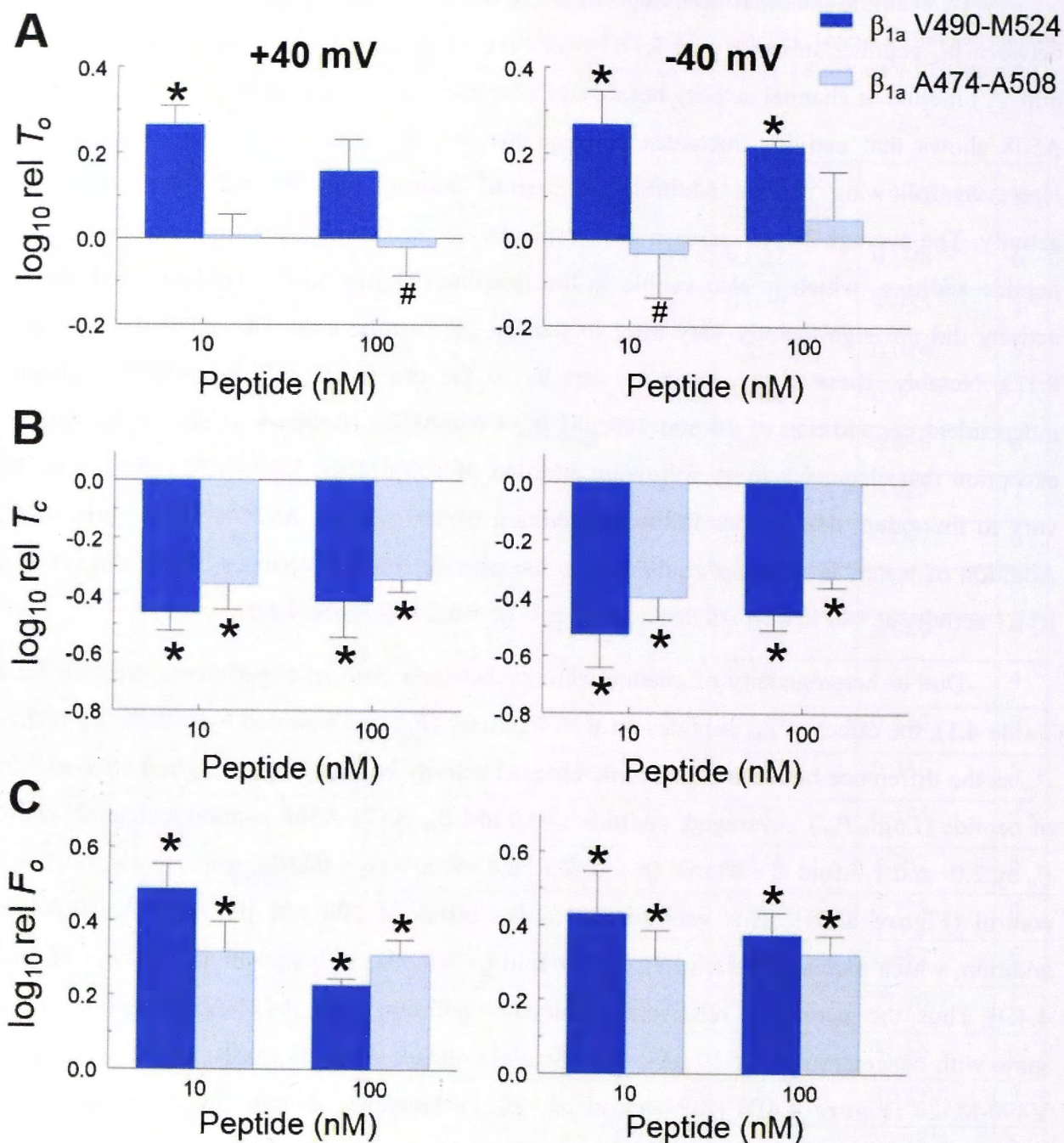


Figure 4. 5 The effect of β_{1a} V490-M524 and β_{1a} A474-A508 peptides on single channel gating parameters in lipid bilayers.

The average mean open time ($\log_{10} \text{ rel } T_o$; **A**), mean closed time ($\log_{10} \text{ rel } T_c$; **B**) and open frequency ($\log_{10} \text{ rel } F_o$; **C**) was calculated in the same way as the $\log_{10} \text{ rel } P_o$ (Figure 4.4) from ~ 90 s of single channel activity at either +40 mV (left) or -40 mV (right). Error bars indicate + or - SEM. Control values shown in Table 4.1, $n = 3-6$ channel traces. *Significantly different from control activity set at zero, determined using a paired Student's t-test, $p < 0.05$. #Significant difference between β_{1a} V490-M524 and β_{1a} A474-A508 peptide, determined by ANOVA, $p < 0.05$.

Collectively, these single channel parameter changes suggest that β_{1a} A474-A508 peptide alters relative P_o by decreasing closed times between channel openings and, increasing the frequency of single channel openings, but not the average channel open duration. In contrast, 10 and 100 nM β_{1a} V490-M524 peptide (**Figure 4.5**; Rebbeck *et al.* (2011)) and β_{1a} subunit increased relative T_o in conjunction with decreasing relative T_c and increasing relative F_o (section 4.3.7; Rebbeck *et al.* (2011)). Indeed, the effect of 10 nM β_{1a} V490-M524 on single channel mean open time at -40 mV was significantly greater ($p = 0.027$) than 10 nM β_{1a} A474-A508. This may

account for the reduced action of 10 nM β_{1a} A474-A508 on relative P_o in comparison to the action of 10 nM β_{1a} V490-M524 peptide.

The single channel mean open and closed times were further dissected by measuring the distribution of open and closed dwell-times to yield open (τ_o) and closed (τ_c) time constants. Earlier reports have shown that the time constants and the fraction of events falling into each constant can also vary between channel records of the same condition (e.g. Laver *et al.* (1995), Copello *et al.* (1997)). To reduce the potential variability, the dwell-time distributions were calculated from channel records with similar control activity (typically P_o values between 0.04-0.15). From these channels, the open and closed times were collected into logged bins and the square root of the frequency of events was plotted against the logarithmic values of the open and closed times. The square root of the frequency of open events primarily fell into three different dwell-time components (time constants): ~ 1 ms (τ_{o1}), ~ 10 ms (τ_{o2}) and ~ 100 ms (τ_{o3}). The closed events also fell into similar three time constants: ~ 1 ms (τ_{c1}), ~ 10 ms (τ_{c2}) and ~ 100 ms (τ_{c3}). The average fraction of events (probability) was plotted as a function of the average time constant before (control) or after addition of 10 or 100 nM peptide. Neither the time constants nor the probability of events in each time constant varied significantly ($p = 0.12-0.99$) between +40 and -40 mV values, the combined +40 and -40 mV values for each condition were presented.

Addition of either 10 or 100 nM β_{1a} A474-A508 significantly shifted a fraction of events from the τ_{o1} to the τ_{o2} by $13.0 \pm 5.4\%$ ($p = 0.049$) or $18.6 \pm 7.2\%$ ($p = 0.011$) (**Figure 4.6A**) respectively, relative to control. There was no significant change in the values of the time constants. Combined, these changes in distribution between time constants would result in an increase in relative T_o , as seen for β_{1a} V490-M524 peptide (**Figure 4.5B**). However, though there is a change in the probability of events falling into τ_{o1} and τ_{o2} with the β_{1a} A474-A508 peptide, the relative T_o was not altered, as mentioned above. Note that addition of β_{1a} V490-M524 peptide, not β_{1a} A474-A508 peptide, significantly increased the τ_{o1} value, indicating an increase in the duration of the briefest channel openings. This likely explains the significant change in relative T_o by β_{1a} V490-M524 peptide, not β_{1a} A474-A508 peptide.

Both, 10 and 100 nM β_{1a} A474-A508 significantly shifted a fraction of closed time events from the τ_{c3} value to the τ_{c1} value by $24.0 \pm 7.3\%$ ($p = 0.023$) and $29.4 \pm 8.5\%$ ($p = 0.005$), respectively, relative to control (**Figure 4.6B**). Moreover, addition of 10 or 100 nM β_{1a} A474-A508 peptide also significantly decreased the τ_{c3} value from control of ~ 160 ms to ~ 102 ms ($p < 0.001$) or ~ 111 ms ($p = 0.009$), respectively (**Figure 4.6B**). Combined, the increased fraction of brief closure events and reduced average duration of long closure events (τ_{c3}) is responsible for the reduced relative T_c following addition of β_{1a} A474-A508 peptide (**Figure 4.5**). The action of β_{1a} A474-A508 peptide on the distribution of closed time constants was similar to the effect of β_{1a} V490-M524 peptide, but for one minor difference. That is, addition of

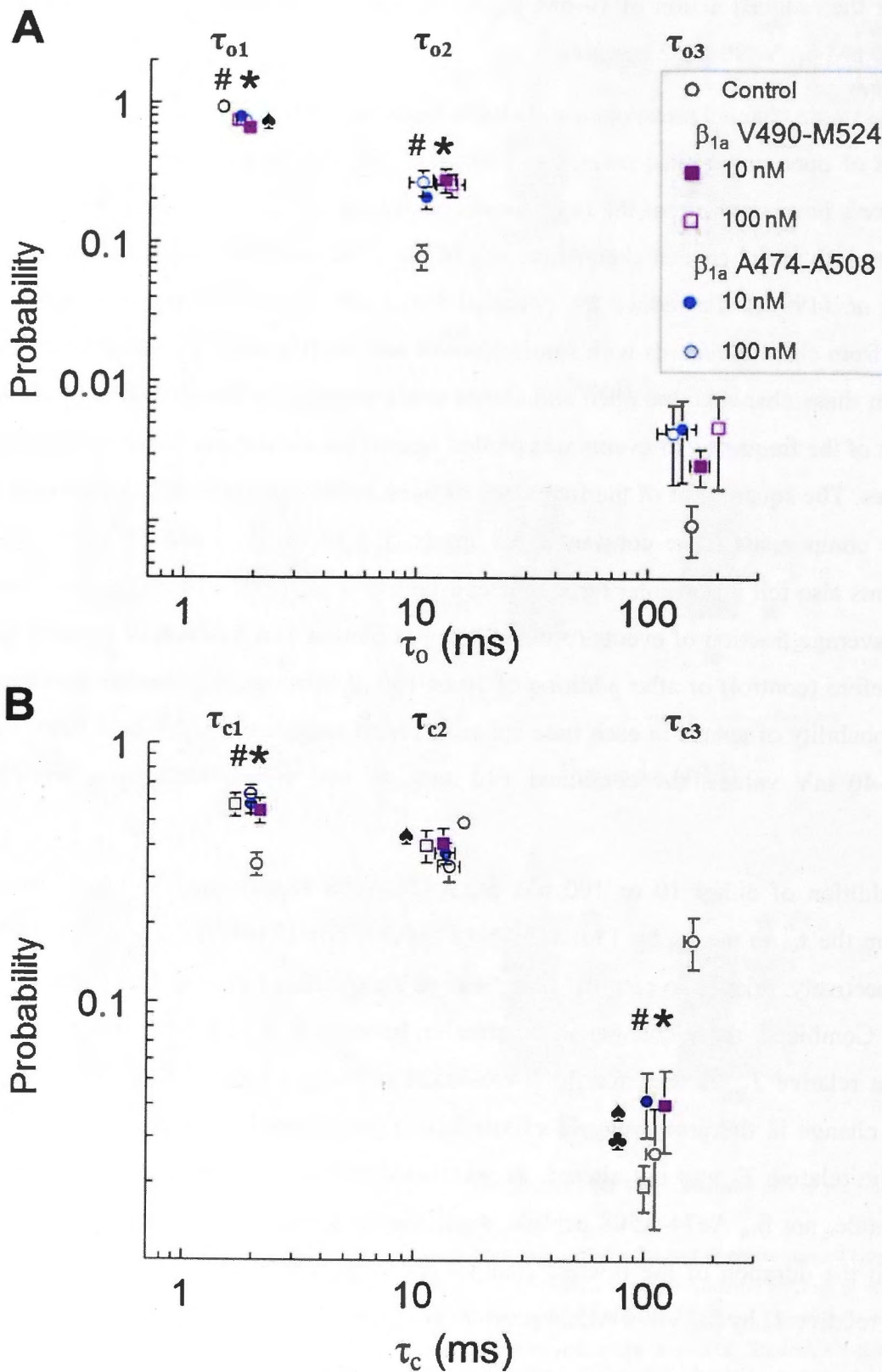


Figure 4. 6 The effect of β_{1a} V490-M524 and β_{1a} A474-A508 peptides on the open and closed dwell-times and on the probability of events occurring within each open and closed dwell-time constant components.

The open (τ_o , **A**) and closed (τ_c , **B**) time constants and the probability of events in each time constant component were calculated from ~ 90 s of single channel activity, $n = 6-9$ channel traces. The individual open time constants (τ_{o1} , τ_{o2} and τ_{o3}) and individual closed time constants (τ_{c1} , τ_{c2} and τ_{c3}) are indicated on the graphs in **A** and **B**, respectively. Error bars indicate \pm SEM. *Significant difference between the probability of events in each time constant in control with 10 or 100 nM β_{1a} A474-A508. #Significant difference between the probability of events in each time constant in control with 10 or 100 nM β_{1a} V490-M524 peptide. *Significant difference between dwell time constant with 10 and 100 nM β_{1a} A474-A508. *Significant difference between dwell time constant in control with 10 or 100 nM β_{1a} V490-M524. *** Significance determined by ANOVA, $p < 0.05$.

10 and 100 nM β_{1a} V490-M524 peptide also decreased the duration of the τ_{c2} events ($p = 0.036$ and 0.0002 , respectively) (**Figure 4.6B**). It is noteworthy that this difference was insufficient to contribute to the average relative T_c value, as the overall average effect of β_{1a} A474-A508 and β_{1a} V490-M524 on relative T_c did not differ (described above; **Figure 4.5B**).

Typically, the dwell-time data reflects the mean open and closed times (Laver, 2001). However, this appears to apply more to the closed dwell-time distributions than open dwell-time distribution in the effect of β_{1a} A474-A508 (**Figure 4.6**). The discrepancy between the β_{1a} A474-A508 peptides effects on relative T_o and open dwell-time distribution may be due to the large fraction of events falling into the briefest time constant (control probability of ~ 0.9 for $\tau_{o1} = \sim 1.5$ ms; **Figure 4.6A**), which are within the realm of data inaccuracy caused by data filtering of 1000 Hz and 500 Hz for data recording and analysis, respectively. The result of this filtering is that channel openings are truncated if they are less than 2 ms and consequently the open times are artificially reduced.

Overall, the results suggest that the β_{1a} A474-A508 peptide has similar effects on RyR1 gating properties to the β_{1a} V490-M524 peptide. This similarity is marginally reduced by the lack of action of β_{1a} A474-A508 peptide on single channel mean open times. Regardless, these results highlight that an overlapping region (V490-A508) between the tested peptides likely contains residues responsible for the modulatory action of the C-terminal residues on RyR1 activity in lipid bilayers. As a consequence, two of the three heptad repeat residues (namely L478 and V485) are unlikely to contribute to the interaction between β_{1a} and RyR1.

4.3.2 The heptad repeat residues (L478, V485 and V492) do not impact the modulatory effect of A474-A508 on RyR1 activity

The role of the heptad repeat residues (**Figure 4.3**, *blue* residues) in modulating RyR1 activity was assessed by substituting the residues with alanines (L478A, V485A, V492A) in the β_{1a} A474-A508 peptide. The effect of this heptad repeat mutant peptide (β_{1a} A474-A508 LVV/A) on RyR1 activity was assessed using the same experimental design used to assess the modulatory effect of β_{1a} A474-A508 peptide. As shown in **Figure 4.7, A and B**, addition of 100 nM β_{1a} A474-A508 LVV/A peptide to the *cis* chamber increased single channel activity. Similar to β_{1a} A474-A508 (**Figure 4.4C**), 10 nM β_{1a} A474-A508 LVV/A peptide increased channel activity and this was not altered by increasing β_{1a} A474-A508 LVV/A peptide to 100 nM. Despite fluctuations in intrinsic channel activity over time, addition of 10 nM β_{1a} A474-A508 LVV/A peptide increased activity (**Figure 4.7C**), which did not vary following further addition of β_{1a} A474-A508 LVV/A peptide to 100 nM. On average, both 10 and 100 nM β_{1a} A474-A508 LVV/A increased relative P_o at +40 and -40 mV 2-fold ($p = 0.001-0.02$), similar to the effect of β_{1a} A474-A508 peptide (**Figure 4.7D**). This strongly suggests that the heptad repeat residues have no impact on the overall action of β_{1a} A474-A508 peptide on RyR1 activity.

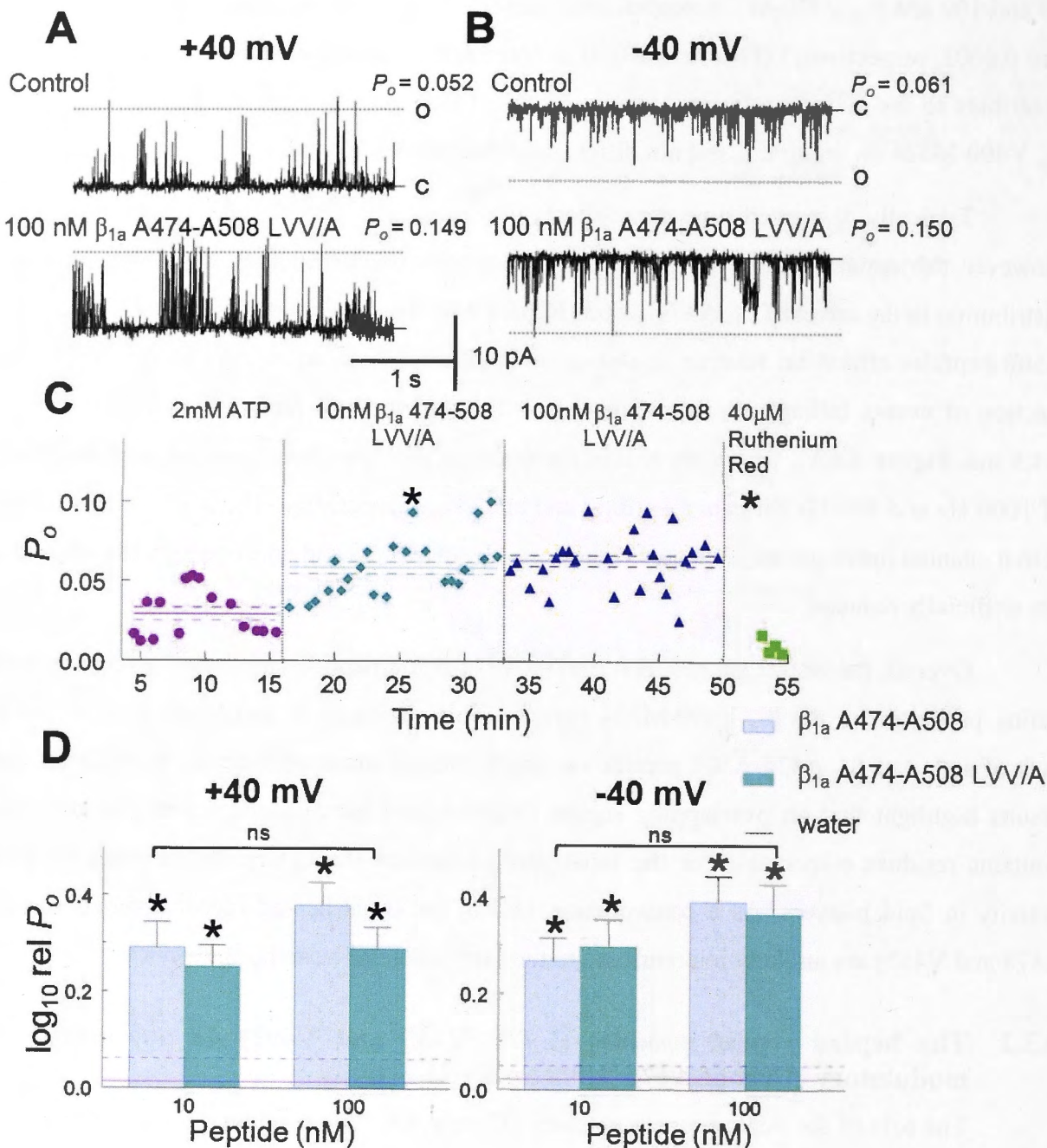


Figure 4.7 Similar modulatory action of β_{1a} A474-A508 and β_{1a} A474-A508 LVV/A peptides on RyR1 activity in lipid bilayers.

A and **B**) Three second records of single channel activity at +40 mV (left) or -40 mV (right) that are representative channel traces before (top traces: control, *cis* 10 μ M $[Ca^{2+}]$ and 2 mM ATP) and after *cis* addition of 100 nM β_{1a} A474-A508 LVV/A peptide (bottom traces). Channel openings are upward (**A**) or downward (**B**) current inflections from zero current (c, continuous line) to maximal conductance (o, discontinuous line). Open probability (P_o) is shown in the right top corner. **C**) A timeline of channel activity following sequential *cis* addition of 2 mM ATP (pink circle), 10 nM β_{1a} A474-A508 LVV/A (green diamonds), 100 nM β_{1a} A474-A508 LVV/A (blue triangles) and 40 μ M ruthenium red (light green square). The channel activity over 10 s was taken from \sim 30 s intervals of activity at +40 and -40 mV. For each condition, there is a mean (continuous line) \pm SEM (discontinuous line) of the scatter plot. * Significantly different from prior condition, $p < 0.05$. **D**) Average relative P_o (\log_{10} rel P_o) was calculated in the same way as in Figure 4.4. Error bars indicate +SEM. P_o was measured from \sim 90 s traces of RyR1 activity, $n = 3-11$ channel traces. Control P_o values in Tables 4.1 and 4.2. The mean \pm SEM \log_{10} rel P_o values for peptide buffer (water) additions are shown as continuous pink line and discontinuous pink line, respectively. The data for A474-A508 peptide is a re-plot of the data shown in Fig. 4.4D. *Significantly different from control activity set at zero, determined using a paired Student's t-test, $p < 0.05$. No significant (ns) difference, determined by ANOVA, $p > 0.05$.

Table 4. 2 Mean control parameters for channels used in analysis of β_{1a} A474A508 LVV/A peptide.

Open probability (P_o), mean open time (T_o), mean closed time (T_c) and open frequency (F_o) mean \pm SEM and number (n) of observations for the data presented in Figure 4.7 and Figure 4.8.

Channel parameter	[peptide] (nM)	Voltage (mV)	Mean parameter	\pm SEM	n
P_o	10	+40	0.032	0.008	7
		-40	0.018	0.010	11
	100	+40	0.072	0.017	3
		-40	0.076	0.029	6
T_o (ms)	10	+40	1.757	0.415	3
		-40	3.320	1.374	5
	100	+40	1.494	0.232	3
		-40	1.315	0.194	4
T_c (ms)	10	+40	102.6	78.29	5
		-40	169.1	70.91	5
	100	+40	75.46	35.34	3
		-40	67.99	48.79	4
F_o (s^{-1})	10	+40	42.71	30.02	3
		-40	22.30	6.212	5
	100	+40	34.74	23.09	4
		-40	46.33	21.89	4

Analysis of the single channel gating parameters demonstrate that the β_{1a} A474-A508 LVV/A reduced relative T_c and increased relative F_o to similar levels as β_{1a} A474-A508 at +40 and -40 mV (**Figure 4.8**). Additionally, neither 10 nor 100 nM β_{1a} A474-A508 LVV/A peptide significantly ($p = 0.499$ and 0.871 , respectively) altered the average relative T_o (**Figure 4.8A**) at +40 mV. In contrast, at -40 mV, 10 and 100 nM β_{1a} A474-A508 LVV/A peptide significantly increased average relative T_o by 43% ($p = 0.024$) and 37% ($p = 0.010$), respectively (**Figure 4.8A**). This increase is similar to the 85% (10 nM, $p = 0.040$) and 65% (100 nM, $p < 0.001$) increases in relative T_o observed by addition of β_{1a} V490-M524 peptide, rather than the lack of a significant ($p = 0.768$ and 0.690 , respective to 10 and 100 nM) alteration that was observed by the wild type β_{1a} A474-A508 peptide (**Figures, 4.5A and 4.8A**).

The open and closed dwell-time distributions did not significantly differ between +40 and -40 mV for each condition ($p = 0.474$ - 0.912), and were combined for the same conditions. The 10 and 100 nM β_{1a} A474-A508 LVV/A peptide shifted a fraction of events from the τ_{o1} to the τ_{o2} by $16.1 \pm 3.5\%$ ($p = 0.001$) and $17.4 \pm 6.5\%$ ($p = 0.016$), respectively (**Figure 4.9A**). This increase in the fraction of single channel openings falling into the longer open time constant (τ_{o2}) likely explains the increase in average relative T_o at -40 mV following addition of β_{1a} A474-A508 LVV/A peptide, but does not explain the lack of effect on relative T_o at +40 mV

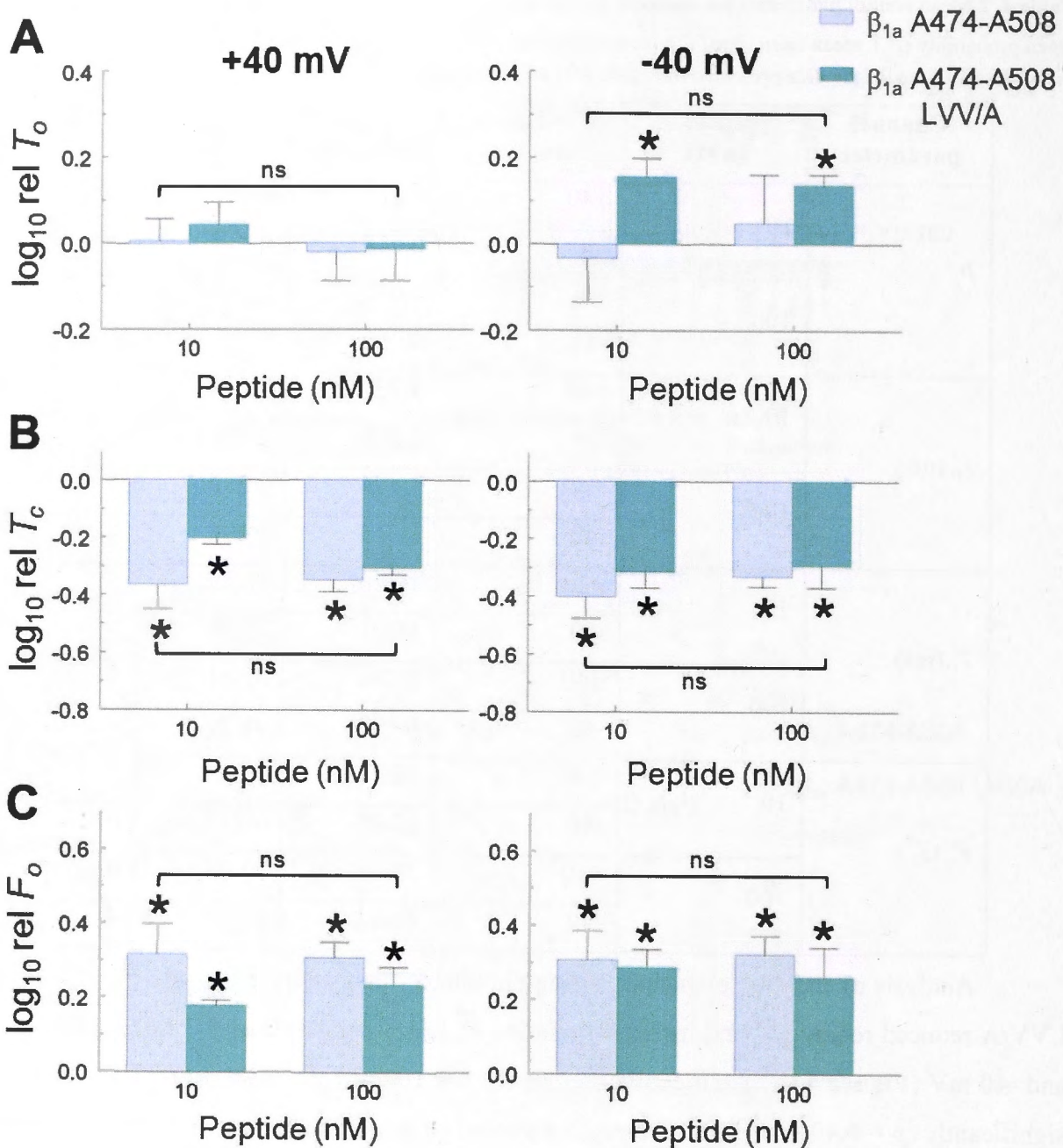


Figure 4.8 The similar modulatory effect of β_{1a} A474-A508 and β_{1a} A474-A508 LVV/A peptides on single channel gating parameters in lipid bilayers.

The average mean open time (\log_{10} rel T_o ; **A**), mean closed time (\log_{10} rel T_c ; **B**) and open frequency (\log_{10} rel F_o ; **C**) were calculated in the same way as the \log_{10} rel P_o (Figure 4.4) from ~ 90 s of single channel activity at either +40 mV (left) or -40 mV (right). Error bars indicate + or - SEM. Control values are given in Table 4.1 and 4.2, $n = 3-5$ channel traces. The data for A474-A508 peptide is a re-plot of the data shown in Fig. 4.5. *Significantly different from control activity set at zero, determined using a paired Student's t-test. No significant (ns) difference, determined by ANOVA, $p < 0.05$.

(**Figure 4.8A**). Interestingly, the influence of β_{1a} A474-A508 LVV/A peptide on open dwell-time distributions was very similar to the effects of β_{1a} A474-A508 peptide (**Figure 4.9A**), with a similar redistribution of a fraction of the open events from the τ_{o1} to the τ_{o2} , as mentioned in section 4.3.1. The discrepancies between the influence of the peptides on open dwell-time distributions and relative T_o may again be due to data filtering, as mentioned previously (section 4.3.1).

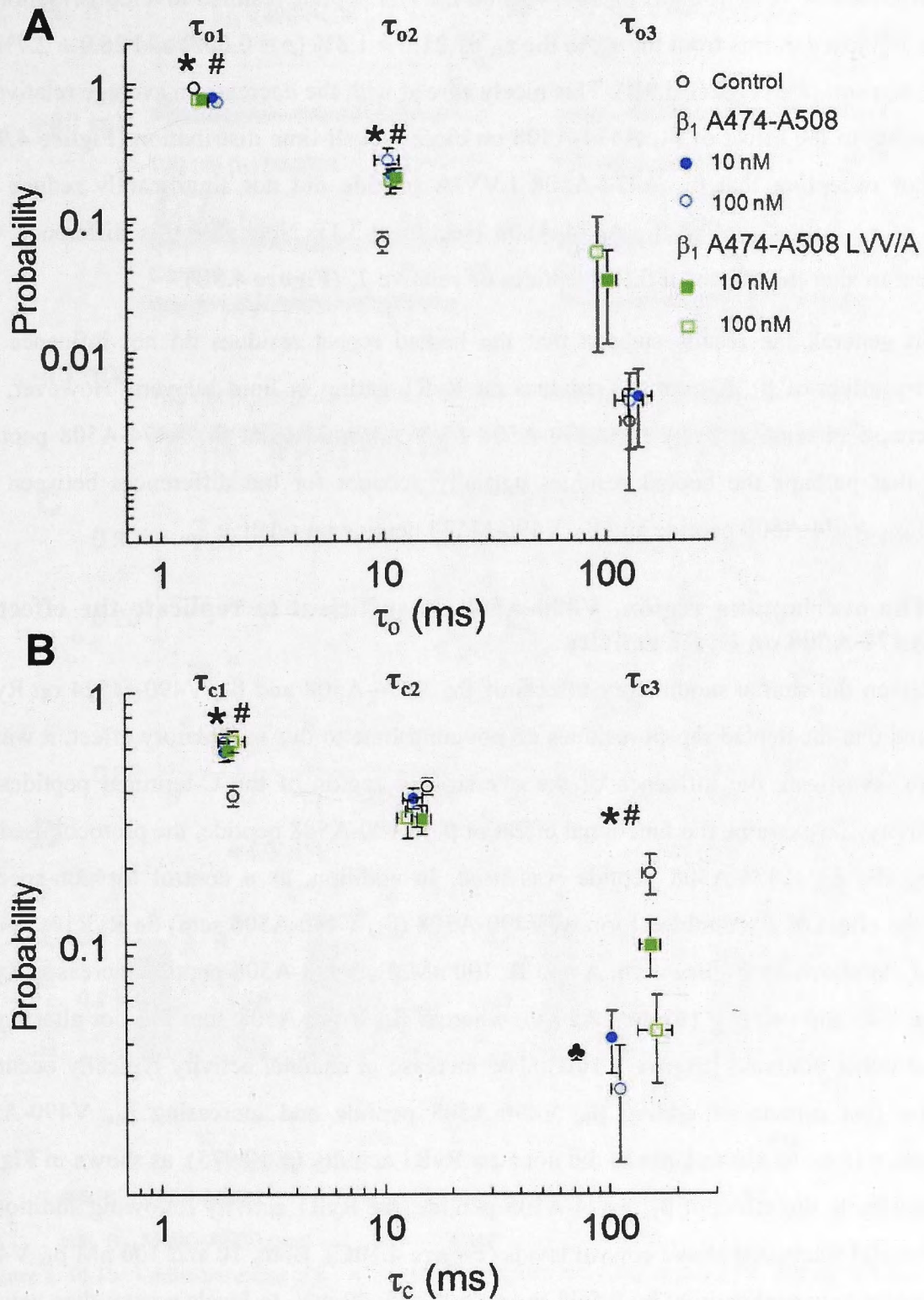


Figure 4. 9 The similar modulatory effect of β_{1a} A474-A508 and β_{1a} A474-A508 LVV/A peptides on the open and closed dwell-times and on the probability of events occurring within each open and closed dwell-time constant components:

The open (τ_o , **A**) and closed (τ_c , **B**) time constants and the probability of events in each time constant component were calculated from ~ 90 s of single channel activity. $n = 6-9$ channel traces. The individual open time constants (τ_{o1} , τ_{o2} and τ_{o3}) and individual closed time constants (τ_{c1} , τ_{c2} and τ_{c3}) are indicated on the graphs in **A** and **B**, respectively. Error bars indicate \pm SEM. The data for A474-A508 peptide is a re-plot of the data shown in Fig. 4.6. *Significant difference between the probability of events in each time constant in control with 10 or 100 nM β_{1a} A474-A508. #Significant difference between the probability of events in each time constant in control with 10 and 100 nM β_{1a} A474-A508 LVV/A. *Significant difference between dwell time constant with 10 and 100 nM β_{1a} A474-A508. *** Significance determined by ANOVA, $p < 0.05$.

Addition of 10 or 100 nM β_{1a} A474-A508 LVV/A peptide resulted in a redistribution of a fraction of closed events from the τ_{c3} to the τ_{c1} by $21.0 \pm 1.8\%$ ($p = 0.002$) and $26.0 \pm 2.7\%$ ($p = 0.003$), respectively (**Figure 4.9B**). This nicely agreed with the decrease in average relative T_c and is similar to the effect of β_{1a} A474-A508 on closed dwell-time distribution (**Figure 4.9B**), with minor exception that β_{1a} A474-A508 LVV/A peptide did not significantly reduce the duration of τ_{c3} values, unlike β_{1a} A474-A508 (section 4.3.1). Note that this difference was insufficient to alter the effects of these peptides on relative T_c (**Figure 4.8B**).

In general, the results suggest that the heptad repeat residues do not influence the modulatory effect of β_{1a} C-terminal residues on RyR1 gating in lipid bilayers. However, the slight increase in relative T_o by β_{1a} A474-A508 LVV/A peptide, not β_{1a} A474-A508 peptide, suggests that perhaps the heptad residues partially account for the differences between the effects of β_{1a} A474-A508 peptide and β_{1a} V490-M524 peptide on relative T_o .

4.3.3 The overlapping region, V490-A508, is sufficient to replicate the effect of A474-A508 on RyR1 activity

Given the similar modulatory effects of β_{1a} A474-A508 and β_{1a} V490-M524 on RyR1 activity and that the heptad repeat residues do not contribute to this modulatory effect, it was of interest to investigate the influence of the overlapping region of the C-terminal peptides on RyR1 activity. To examine the functional effect of β_{1a} V490-A508 peptide, the protocol used for examining the β_{1a} A474-A508 peptide was used. In addition, as a control for non-specific binding, the effect of a scrambled form of V490-A508 (β_{1a} V490-A508 scm) on RyR1 was also examined. As shown in **Figure 4.10, A and B**, 100 nM β_{1a} V490-A508 peptide increased RyR1 activity at +40 and -40 mV (**Figure 4.10A**), whereas β_{1a} V490-A508 scm did not alter RyR1 activity at either potential (**Figure 4.10B**). The increase in channel activity typically occurred within the first minute of adding β_{1a} V490-A508 peptide and increasing β_{1a} V490-A508 concentration from 10 nM to 100 nM did not alter RyR1 activity ($p = 0.975$), as shown in **Figure 4.10C**. Similar to the effect of β_{1a} A474-A508 peptide, the RyR1 activity following addition of β_{1a} V490-A508 fluctuated above control levels (**Figure 4.10C**). Both, 10 and 100 nM β_{1a} V490-A508 increased channel activity by 2-fold at +40 mV and -40 mV, to levels greater than activity before peptide addition (control; $p \leq 0.001$), or after addition of β_{1a} V490-A508 scm ($p \leq 0.001$) (**Figure 4.10D**). Importantly, the β_{1a} V490-A508 scm peptide did not significantly ($p = 0.184-0.745$) alter RyR1 activity, suggesting that the effect of β_{1a} V490-A508 was sequence specific. The effect of β_{1a} V490-A508 peptide on RyR1 activity more closely resembled the effect of β_{1a} A474-A508 peptide rather than β_{1a} V490-M524 peptide. This was particularly evident at -40 mV, whereby the modulatory effect of 10 nM β_{1a} V490-M524 peptide was significantly greater ($p = 0.016$ and 0.004) than 10 nM β_{1a} V490-A508 peptide and 10 nM β_{1a} A474-A508 peptide (**Figure 4.10D**).

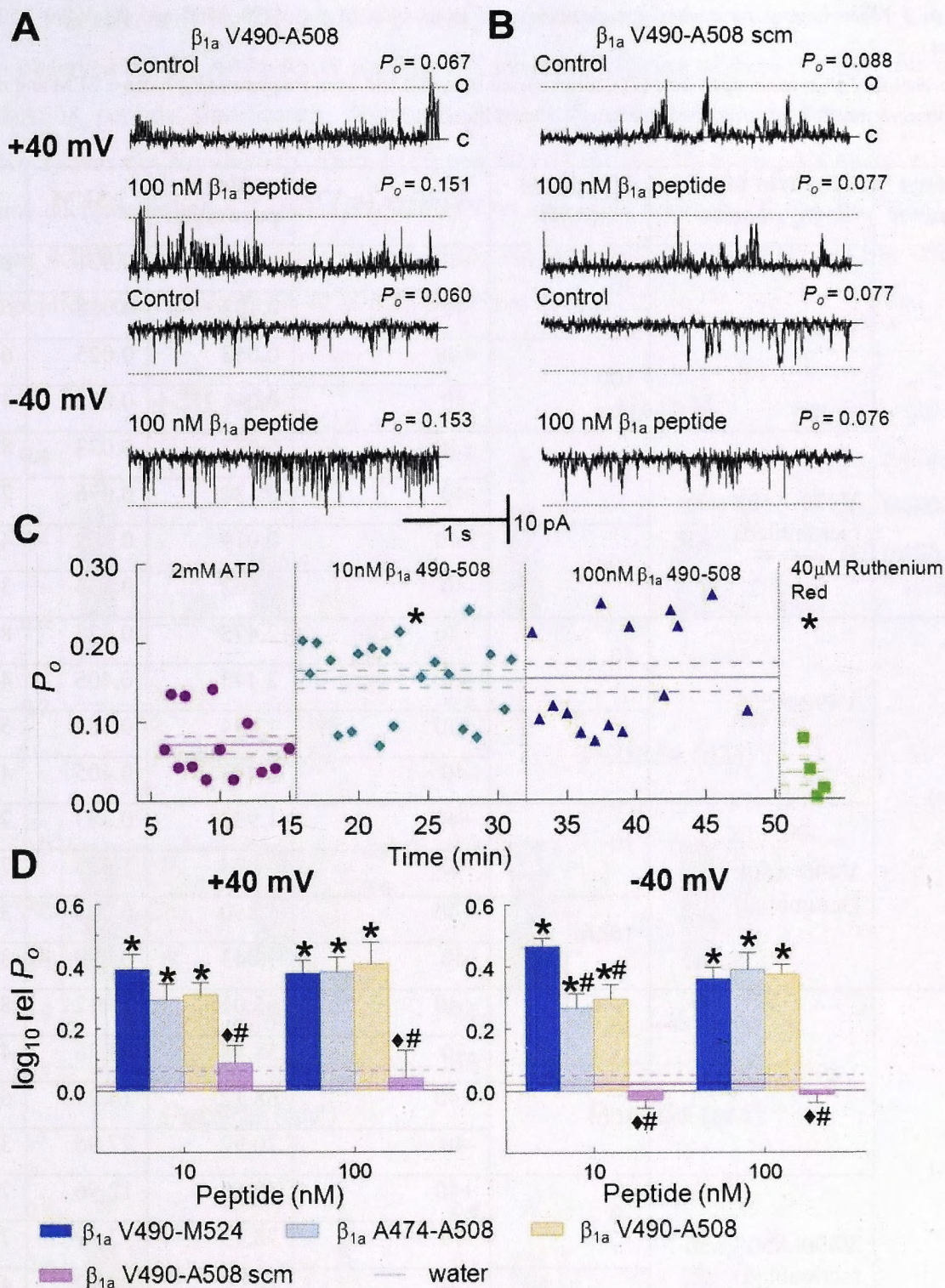


Figure 4. The similar effect of β_{1a} A474-A508 and V490-A508 peptides on RyR1 activity in lipid bilayers. **A** and **B**) Three second records of single channel activity at +40 (top) or -40 mV (bottom) that display representative channel activity before (upper traces: control) and after *cis* addition of 100 nM β_{1a} V490-A508 (lower traces) peptide (**A**) and β_{1a} V490-A508 scrambled peptide (**B**). Open probability (P_o) is shown in the right top corner. **C**) A timeline of channel activity following sequential *cis* addition of 2 mM ATP (pink circle), 10 nM β_{1a} V490-A508 (green diamonds), 100 nM β_{1a} V490-A508 (blue triangles) and 40 μ M ruthenium red (light green square). The channel activity over 10 s was taken from \sim 30 s intervals of activity at +40 and -40 mV. For each condition, there is a mean (continuous line) \pm SEM (discontinuous line) of the scatter plot. *Significantly different from prior condition, determined by unpaired Student's t-test, $p > 0.05$. **D**) Average relative P_o (\log_{10} rel P_o) was calculated in the same way as above (Figure 4.4). Error bars indicate + or - SEM. P_o was measured from \sim 90 s traces of RyR1 activity, $n = 3-8$ channel traces. Control P_o values in Tables 4.1 and 4.3. The mean \pm SEM \log_{10} rel P_o values for peptide buffer (water) additions are shown as continuous pink line and discontinuous pink line, respectively. The data for A474-A508 and V490-M524 peptides are a re-plot of the data shown in Figure 4.4D. *Significantly different from control activity set at zero, determined using a paired Student's t-test, $p < 0.05$. #Significantly different from β_{1a} V490-M524 peptide. *Significantly different β_{1a} V490-A508 scm from β_{1a} V490-A508. **Significance determined by ANOVA, $p < 0.05$.

Table 4. 3 Mean control parameters for channels used in analysis of β_{1a} V490-A508 and β_{1a} V490-A508 scm peptides.

Open probability (P_o), mean open time (T_o), mean closed time (T_c) and open frequency (F_o) mean \pm SEM and number (n) of observations for data presented in Figure 4.10 and Figure 4.11.

Channel parameter	Control for <i>cis</i> β_{1a} peptide	[peptide] (nM)	Voltage (mV)	Mean parameter	\pm SEM	n		
P_o	V490-A508	10	+40	0.056	0.021	8		
			-40	0.103	0.038	6		
		100	+40	0.053	0.025	6		
			-40	0.061	0.022	4		
	V490-A508 scm (scrambled)	10	+40	0.077	0.033	8		
			-40	0.130	0.076	7		
		100	+40	0.019	0.003	4		
			-40	0.162	0.113	3		
		T_o (ms)	V490-A508	10	+40	2.475	0.623	8
					-40	2.443	0.405	4
100	+40			1.944	0.382	5		
	-40			2.443	0.405	4		
V490-A508 scm (scrambled)	10		+40	1.933	0.353	7		
			-40	3.024	1.495	7		
	100		+40	1.450	0.308	3		
			-40	1.043	0.099	3		
	T_c (ms)		V490-A508	10	+40	65.01	13.12	8
					-40	58.44	23.38	4
100		+40		68.12	14.27	6		
		-40		70.92	27.96	3		
V490-A508 scm (scrambled)		10	+40	49.62	12.96	7		
			-40	78.13	17.69	7		
		100	+40	168.9	84.92	4		
			-40	105.9	34.49	3		
		F_o (s^{-1})	V490-A508	10	+40	21.08	5.844	8
					-40	25.29	8.365	4
100	+40			16.67	2.950	6		
	-40			19.58	8.648	3		
V490-A508 scm (scrambled)	10		+40	31.75	10.29	7		
			-40	15.03	2.476	7		
	100		+40	12.09	1.531	3		
			-40	11.51	3.604	3		

The effects of β_{1a} V490-A508 peptide on gating parameters were also very similar to those observed by β_{1a} A474-A508 peptide. On average, addition of both 10 and 100 nM β_{1a} V490-A508 peptide significantly decreased relative T_c and increased relative F_o , whereas relative T_o was not significantly altered (**Figure 4.11B**). At 10 nM, the β_{1a} V490-A508 peptide did not decrease relative T_c values at -40 mV to the same level as 10 nM β_{1a} V490-M524 (**Figure 4.11B**), which likely contributed to the significant differences between the effects of these peptides on relative P_o at -40 mV, as discussed above.

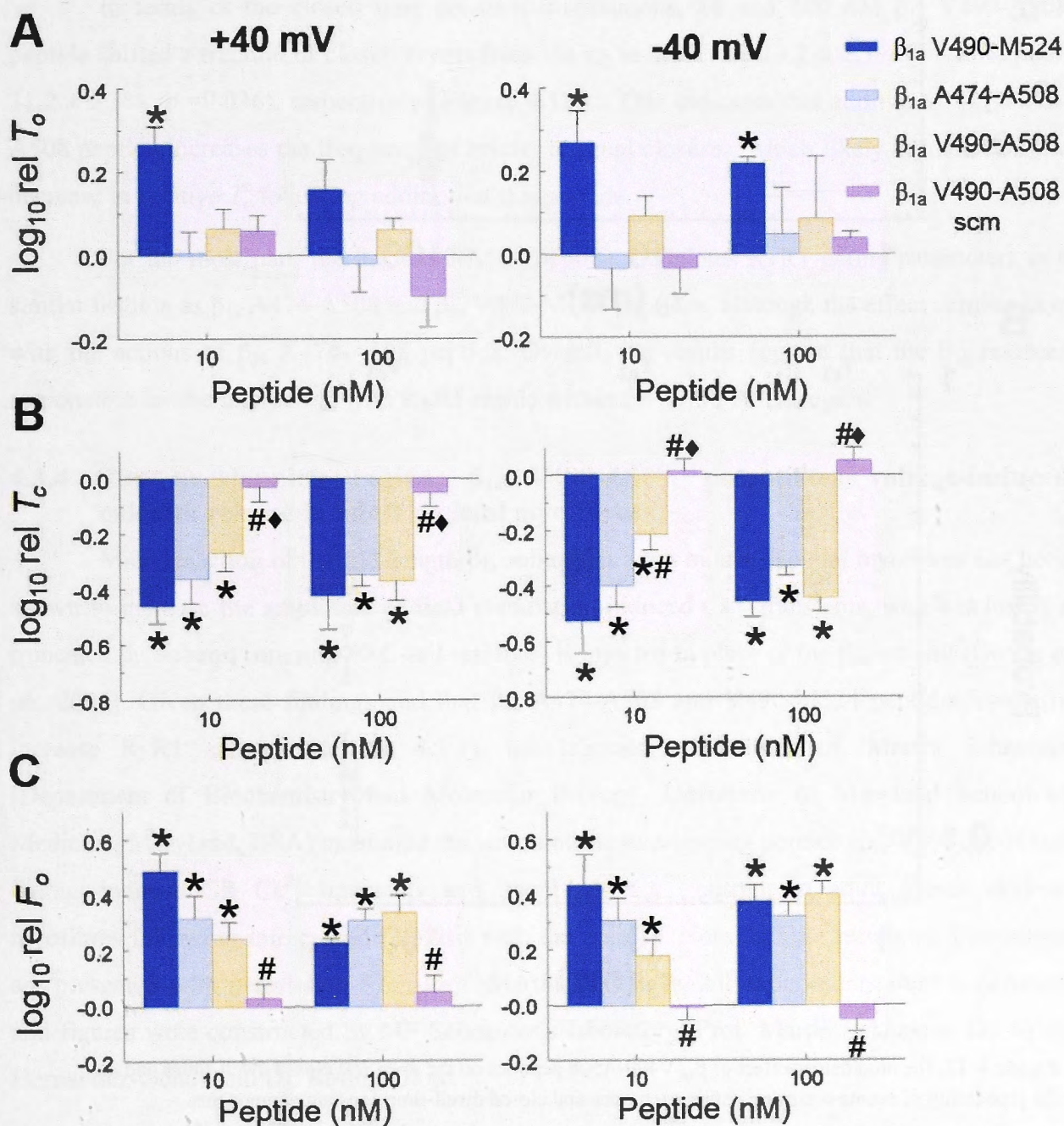


Figure 4. 11 The similar modulatory effect of β_{1a} V490-A508 and β_{1a} A474-A508 peptides on single channel gating parameters in lipid bilayers.

The average mean open time (\log_{10} rel T_o ; **A**), mean closed time (\log_{10} rel T_c ; **B**) and open frequency (\log_{10} rel F_o ; **C**) was calculated in the same way as the \log_{10} rel P_o (Figure 4.4) from ~90 s of single channel activity at either +40 mV (left) or -40 mV (right). Error bars indicate + or - SEM. Control values shown in Table 4.1 and Table 4.3 $n = 3-8$ channel traces. The data for A474-A508 and V490-M524 peptides are a re-plot of the data shown in Figure. 4.5. *Significantly different from control activity set at zero, determined using a paired Student t-test, $p < 0.05$. # Significantly different from β_{1a} V490-M524 peptide, determined by ANOVA, $p < 0.05$.

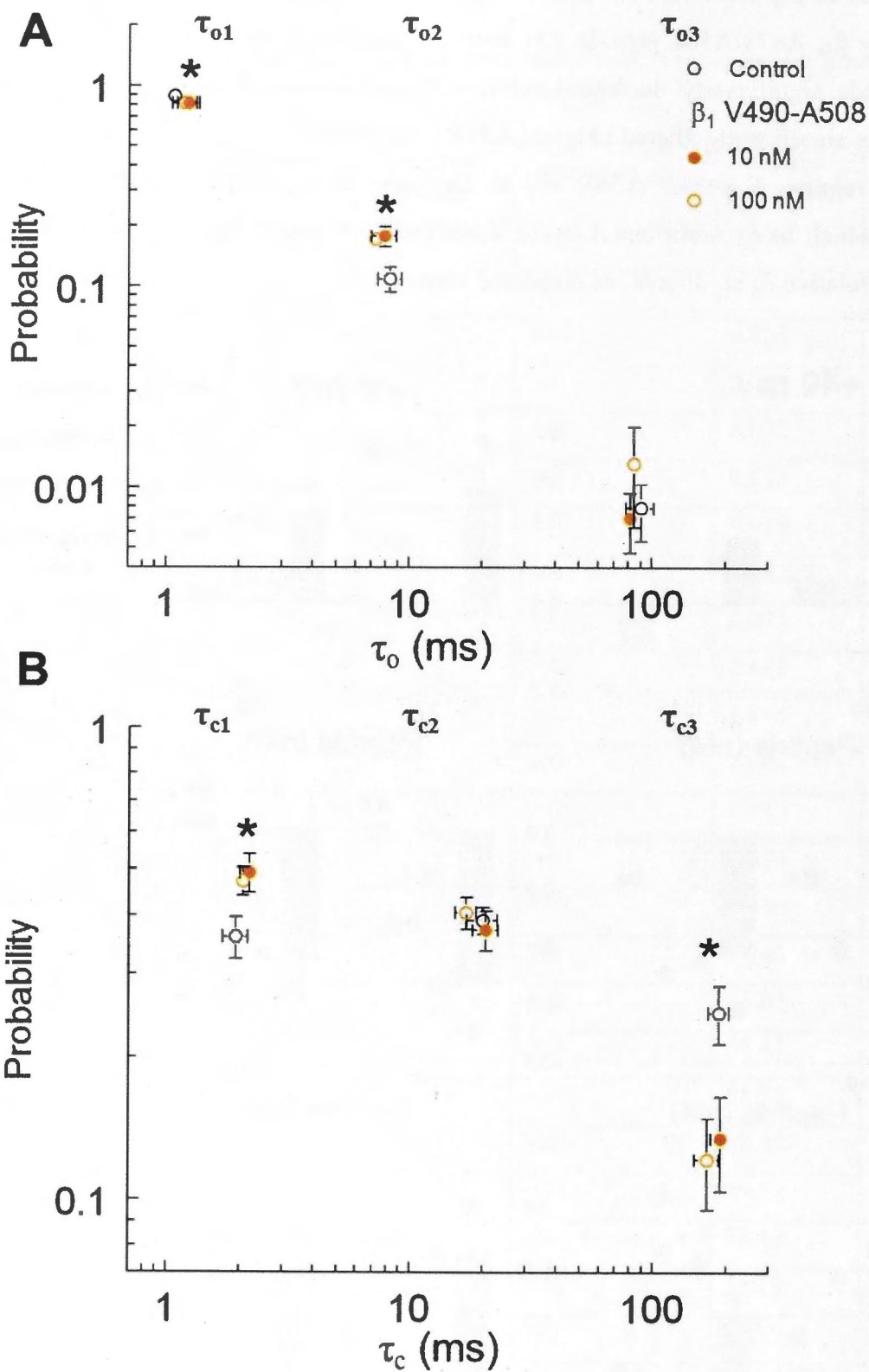


Figure 4.12 The modulatory effect of β_{1a} V490-A508 peptides on the open and closed dwell-times and on the probability of events occurring within each open and closed dwell-time constant components.

The open (τ_o , **A**) and closed (τ_c , **B**) time constants and the probability of events in each time constant component were calculated from ~ 90 s of single channel activity. $n = 8-12$ channel traces. The individual open time constants (τ_{o1} , τ_{o2} and τ_{o3}) and individual closed time constants (τ_{c1} , τ_{c2} and τ_{c3}) are indicated on the graphs in **A** and **B**, respectively. Error bars indicate \pm SEM. *Significant difference between the probability of events in each time constant in control with 10 and 100 nM β_{1a} A474-A508, determined by ANOVA, $p < 0.05$

The dwell-time distributions for +40 and -40 mV were not significantly different ($p = 0.267-0.930$) and as a result, the data was combined. As shown in **Figure 4.12A**, 10 and 100 nM β_{1a} V490-A508 peptide shifted a fraction of events from the τ_{o1} to the τ_{o2} by $7.0 \pm 3.6\%$ ($p = 0.013$) and $6.3 \pm 2.4\%$ ($p = 0.026$), respectively. The increase in the fraction of channel openings falling into the τ_{o2} group did not appear to be sufficient to alter the relative T_o values for this peptide (**Figure 4.11B**). Again this could also be attributed to the data filtering, as discussed in section 4.3.1.

In terms of the closed time constant distributions, 10 and 100 nM β_{1a} V490-A508 peptide shifted a fraction of closed events from the τ_{c3} to the τ_{c1} by $13.2 \pm 2.3\%$ ($p = 0.012$) and $11.2 \pm 5.3\%$ ($p = 0.036$), respectively (**Figure 4.12B**). This indicates that addition of β_{1a} V490-A508 peptide increases the frequency of briefer channel closures, which likely accounts for the decrease in relative T_c following addition of this peptide.

For the most part, the β_{1a} V490-A508 peptide modulates RyR1 gating parameters in a similar fashion as β_{1a} A474-A508 and β_{1a} V490-M524 peptides, although the effect is more akin with the actions of β_{1a} A474-A508 peptide. Overall, the results suggest that the β_{1a} residues responsible for the interaction with RyR1 reside within the V490-A508 region.

4.3.4 The overlapping region, β_{1a} V490-A508, potentiates voltage-induced calcium release in adult skeletal myofibres

Microinjection of the full-length β_{1a} subunit in adult mouse skeletal myofibres has been shown to increase the amplitude of field stimulation-induced Ca^{2+} transients, which is lost if a truncated β_{1a} subunit (missing 40 C-tail residues) is injected in place of the β_{1a} subunit (Garcia *et al.*, 2005). Given these findings and that β_{1a} A474-A508 and V490-M524 peptides similarly increase RyR1 activity (section 4.3.1), the laboratory led by Prof. Martin Schneider (Department of Biochemistry and Molecular Biology, University of Maryland School of Medicine, Maryland, USA) examined the action of the overlapping peptide (β_{1a} V490-A508) on voltage-induced SR Ca^{2+} transients and membrane Ca^{2+} current in adult mouse skeletal myofibres following intracellular dialysis with the peptide. Note that the results in this section are presented with permission from Prof. Martin Schneider. All experiments were undertaken and figures were constructed by MF Schneider's laboratory: Prof. Martin Schneider, Dr. Erick Hernandez-Ochoa and Dr. Rotimi Olojo.

Skeletal muscle fibres were from *flexor digitorum brevis* muscles of six- to seven-week-old mice in accord with (Liu *et al.*, 1997, Olojo *et al.*, 2011). The fibres were dialysed via pipette with the fluo-4 and either β_{1a} V490-A508 peptide, β_{1a} scrambled (V490-A508 sequence scrambled) peptide or no peptide (control). Following the 20 minute dialysis, these fibres were subjected to simultaneous high-speed fluo-4 confocal measurements and voltage-clamp

experiments to measure the voltage-induced Ca^{2+} release flux and DHPR Ca^{2+} current (Prosser *et al.*, 2009, Olojo *et al.*, 2011).

The effect of dialysing fibres with 25 nM β_{1a} V490-A508 peptide or 25 nM β_{1a} scrambled peptide on voltage-induced SR Ca^{2+} release was assessed from high-speed fluo-4 confocal measurements by plotting the peak Ca^{2+} rate as a function of voltage. MF Schneider's laboratory found that intracellular dialysis with 25 nM β_{1a} V490-A508 peptide enhanced the amplitude of the peak Ca^{2+} release at 20 mV, as shown in **Figure 4.13A**. With the data fit by a Boltzmann equation, the maximum release rate (R_{max}) was significantly increased 49% ($p < 0.05$) in fibres dialysed with 25 nM β_{1a} V490-A508 peptide relative to the control fibre R_{max} value (**Figure 4.13Ci**). The accompanied Boltzmann-derived parameters, V_{half} (potential when $R = \text{half } R_{\text{max}}$) and k (inverse measure of R-V slope), were not altered by fibre dialysis with 25 nM β_{1a} V490-A508 peptide (**Figure 4.13Ci**). This indicates that the voltage-dependence of SR Ca^{2+} release initiation was not affected. It is important to note that dialysis with β_{1a} scrambled peptide did not significantly ($p > 0.05$) alter R_{max} in fibres. Furthermore, neither V_{half} nor k values were altered ($p > 0.05$) in fibres dialysed with β_{1a} scrambled peptide (**Figure 4.13Ci**).

Upon examining the influence of the β_{1a} V490-A508 peptides on voltage-induced membrane Ca^{2+} currents through DHPR, the β_{1a} V490-A508, not its scrambled form, potentiated maximal voltage-induced DHPR Ca^{2+} currents, when DHPR current was plotted as a function of voltage (**Figure 4.13B**). The least squares fits of data to a modified Boltzmann-Ohm equation (as described in Olojo *et al.* (2011)), indicated that the maximum conductance (G_{max}) was enhanced by 24% ($p < 0.05$) when compared to fibres that were dialysed with β_{1a} scrambled peptide. This enhancement was found to be voltage independent as the other Boltzmann parameters, V_{half} and k , remained unaltered following dialysis with β_{1a} V490-A508 peptide (**Figure 4.13Cii**) compared to control fibres.

Overall, the β_{1a} V490-A508 peptide, not its scrambled form, increased voltage-induced RyR1 Ca^{2+} release and DHPR Ca^{2+} current in adult skeletal myofibres. Importantly, the effect of β_{1a} V490-A508 peptide on skeletal EC coupling replicates the effects observed by microinjecting full-length β_{1a} subunit into adult skeletal myofibres, as found by Garcia *et al.* (2005).

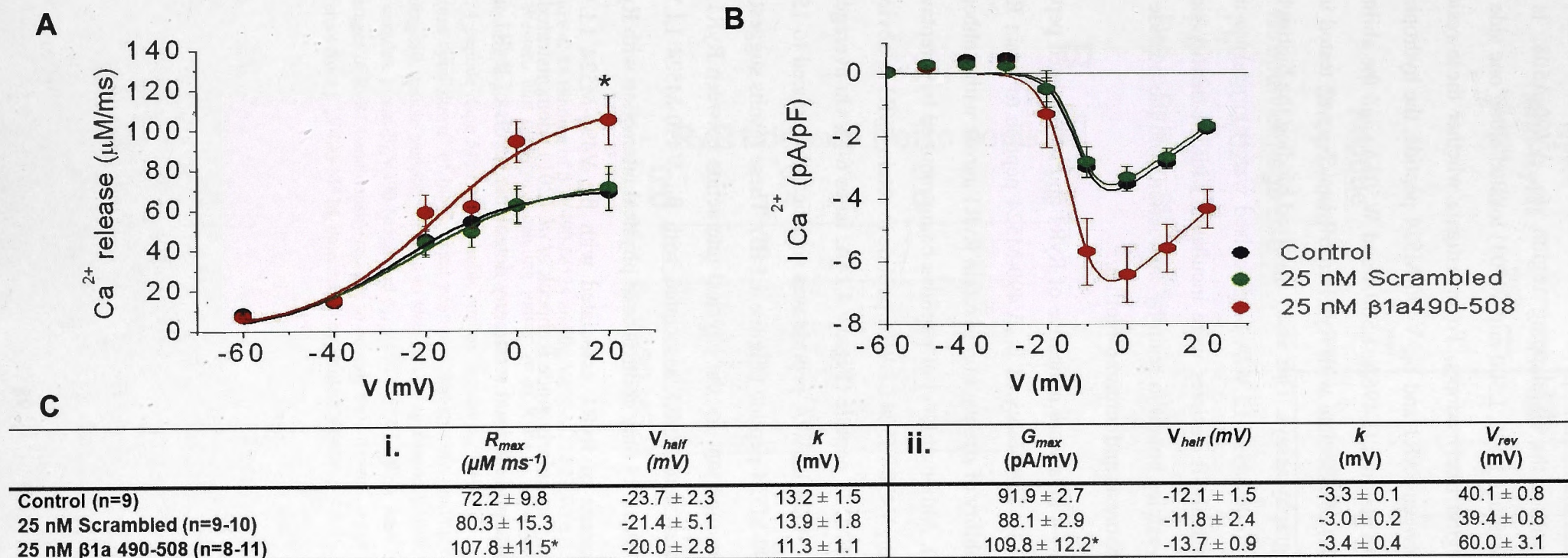


Figure 4.13 Intracellular dialysis of β_{1a} V490-A508 peptide, not its scrambled form, increases voltage-induced SR Ca^{2+} release and membrane Ca^{2+} current through DHPR.

Flexor digitorum brevis fibres were dialysed with either β_{1a} 490-508 peptide, β_{1a} scrambled (V490-508 sequence scrambled) or no peptide (control). **A**) Average fibre peak Ca^{2+} release (R) data plotted as a function of voltage. The data was fit (continuous line) with a Boltzmann function. Error bars indicate \pm SEM. * Significantly different from Ca^{2+} release in fibres dialysed with β_{1a} scrambled peptide, determined by Student's t-test, $p < 0.05$. **B**) Average data of membrane Ca^{2+} current in fibres as a function of voltage. The continuous line between data points represents the least squares fit of the data with a modified Boltzmann-Ohm equation (Olojo *et al.*, 2011). **C**) The parameters from fitting the i), R-V data to a single Boltzmann function, and ii), I-V data to a modified Boltzmann-Ohm function. i) The mean \pm SEM for the Boltzmann parameters, including: maximum release rate (R_{max}), the potential when $R=0.5 R_{max}$ (V_{half}) and slope factor (k). ii) the mean \pm SEM for the modified Boltzmann-Ohm parameters, including: maximum conductance (G_{max}), V_{half} , k and reversal potential (V_{rev}). * Significant difference from the control parameter, determined by Student's t-test, $p < 0.05$. All experiments undertaken by Drs. E.O. Hernandez-Ochoa and R.O. Olojo (MF Schneider's Laboratory, Department of Biochemistry and Molecular Biology, University of Maryland School of Medicine, Maryland, US) and the figures were kindly provided by Prof. M. F. Schneider.

4.3.5 The hydrophobic surface residues (L496, L500 and W503) are important for the physical interaction between the β_{1a} C-terminal residues and RyR1

An obvious binding site within the overlapping region, β_{1a} V490-A508, is the hydrophobic surface (composed of residues L496, L500 and W503) located along one side of a nascent α -helix that most of this region likely adopts. To investigate whether these residues influence the physical interaction between RyR1 and β_{1a} V490-M524 peptide, the hydrophobic surface residues were substituted with alanines (L496A, L500A and W503A) and the ability of this peptide (β_{1a} V490-M524 LLW/A) to associate with RyR1 in SR vesicles was tested using biotin-streptavidin affinity chromatography assays. This assay involved binding the biotinylated peptide (either β_{1a} V490-M524, β_{1a} V490-M524 LLW/A or deionised water) to agarose using streptavidin covered resin. Then skeletal SR vesicles were incubated with the peptide-bound resin and the level of RyR1 in SR vesicles bound to resin by interaction with the peptide was assessed using analytical gel electrophoresis and immuno-blotting.

The bands at ~ 560 kDa and ~ 4 kDa were indicative of RyR1 and biotinylated peptide, respectively (**Figure 4.14A**, lanes 1-3). The ability of β_{1a} V490-M524 peptide to retain RyR1 from skeletal SR vesicles and the inability of streptavidin to retain RyR1 agrees with Rebbeck *et al.* (2011) (**Figure 4.14A**, lanes 4-5). Although level of peptides being retained by streptavidin agarose is similar, the ability of the β_{1a} V490-M524 LLW/A peptide to retain RyR1 is obviously lower than that retained by β_{1a} V490-M524 peptide (**Figure 4.14A**, lanes 6-7). On average, the level of RyR1 retained by β_{1a} V490-M524 LLW/A peptide was significantly reduced to $15.2 \pm 7.1\%$ ($p = 0.026$) relative to β_{1a} V490-M524 peptide (**Figure 4.14B**). These results suggest that the hydrophobic surface residues are important for the physical interaction between RyR1 and β_{1a} V490-M524. However, given that some RyR1 associated with β_{1a} V490-M524 LLW/A peptide, other residues in the β_{1a} V490-M524 may contribute to physical interaction with RyR1. It is noteworthy that this small amount of RyR1 associated with β_{1a} V490-M524 LLW/A peptide is unlikely to be non-specific, particularly since Rebbeck *et al.* (2011) demonstrated that a scrambled form of β_{1a} V490-M524 peptide did not retain any detectable levels of RyR1 using this assay.

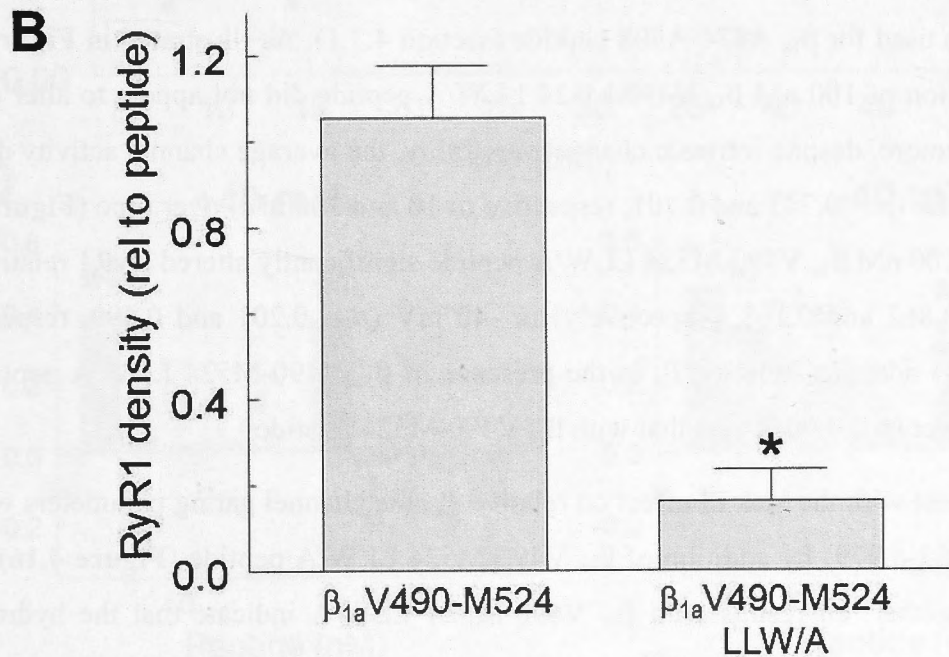
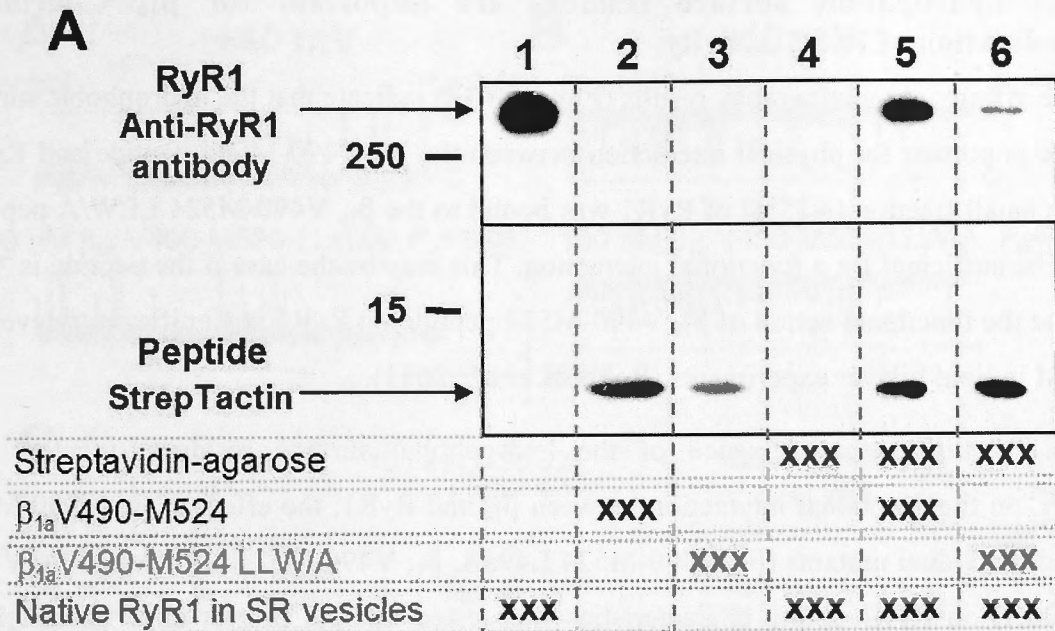


Figure 4. 14 Binding of β_{1a} V490-M524 and β_{1a} V490-M524 LLW/A peptides to native RyR1.

A) Western blot displaying banding indicative of RyR1 (~560 kDa) and biotinylated peptide (~4 kDa), as detected using 34C and StrepTactin, respectively. Association between RyR1 with either wild type β_{1a} V490-M524 peptide (lane 5) or hydrophobic surface mutant β_{1a} V490-M524 LLW/A (lane 6) by virtue of streptavidin agarose “pull down” of biotinylated peptides. Non-specific binding of Streptavidin agarose was controlled by loading SR vesicle samples retained to streptavidin agarose in lane 4. As positive controls for immuno-blotting: SR vesicles, biotin- β_{1a} V490-M524 and β_{1a} V490-M524 LLW/A were loaded in lanes 1, 2 and 3, respectively. **B)** Averages of RyR1 band density relative to peptide band density, $n = 4$. Error bars indicate + SEM. *Significantly different from β_{1a} V490-M524, determined by Student’s t-test, $p < 0.05$

4.3.6 The hydrophobic surface residues are important for β_{1a} C-terminal modulation of RyR1 activity

The affinity chromatography results (**Figure 4.14**) indicate that the hydrophobic surface residues are important for physical interaction between the β_{1a} V490-M524 peptide and RyR1. However, a small fraction (~15%) of RyR1 was bound to the β_{1a} V490-M524 LLW/A peptide, which may be sufficient for a functional interaction. This may be the case if the peptide is ≥ 6.6 nM, because the functional action of β_{1a} V490-M524 peptide on RyR1 is significant to levels as low as 1 nM in lipid bilayer experiments (Rebbeck *et al.*, 2011).

To investigate the influence of the hydrophobic surface residues, together and individually, on the functional interaction between β_{1a} and RyR1, the effect of β_{1a} V490-M524 LLW/A and individual mutants (β_{1a} V490-M524 L496A, β_{1a} V490-M524 L500A and β_{1a} V490-M524 W503A) on RyR1 gating characteristics was tested in lipid bilayer experiments. Each peptide was added to the *cis* chamber and channel activity was recorded for 15-20 min using the same conditions used for β_{1a} A474-A508 peptide (section 4.3.1). As illustrated in **Figure 15, A and B**, *cis* addition of 100 nM β_{1a} V490-M524 LLW/A peptide did not appear to alter channel activity. Furthermore, despite intrinsic channel variability, the average channel activity does not significantly differ ($p = 0.743$ and 0.701 , respective to 10 and 100 nM) over time (**Figure 15C**). Neither 10 nor 100 nM β_{1a} V490-M524 LLW/A peptide significantly altered RyR1 relative P_o at +40 mV ($p = 0.862$ and 0.168 , respectively) or -40 mV ($p = 0.201$ and 0.699 , respectively) (**Figure 15D**). In addition, relative P_o in the presence of β_{1a} V490-M524 LLW/A peptide was significantly lower ($p \leq 0.004$) than that with β_{1a} V490-M524 peptide.

Consistent with the lack of effect on relative P_o , the channel gating parameters were not altered ($p = 0.063$ - 0.979) by addition of β_{1a} V490-M524 LLW/A peptide (**Figure 4.16**) at +40 or -40 mV. Together, all results with β_{1a} V490-M524 LLW/A indicate that the hydrophobic surface residues are essential for the functional interaction between β_{1a} V490-M524 peptide and RyR1 in lipid bilayers. Intriguingly, the effects of the individual mutant peptides on RyR1 activity and gating parameters depend on the membrane potential. At +40 mV, neither 10 nor 100 nM of the individual mutants altered ($p = 0.205$ - 0.978) relative P_o or gating parameters, which paralleled the effect of β_{1a} V490-M524 LLW/A peptide (**Figure, 4.15D and 4.16**). Indeed, the only difference at +40 mV was the effect of 10 nM β_{1a} V490-M524 W503A on relative T_c , which was significantly ($p = 0.048$) greater than β_{1a} V490-M524 LLW/A peptide, but notably not significantly ($p = 0.567$) different from control and significantly lower than β_{1a} V490-M524 peptide ($p = 0.013$) (**Figure 4.16A**). At -40 mV, both 10 and 100 nM of the individual mutants increased relative P_o values significantly ($p = 0.002$ - 0.022) by 1.8-2.3-fold, which was also significantly ($p = 0.005$ - 0.044) greater than relative P_o in the presence of β_{1a} V490-M524 LLW/A peptide (**Figure 4.15D**). Consistently, the individual mutants also significantly ($p = 0.006$ - 0.029) increased relative T_o by 1.3- to 1.9- fold (**Figure 4.16A**).

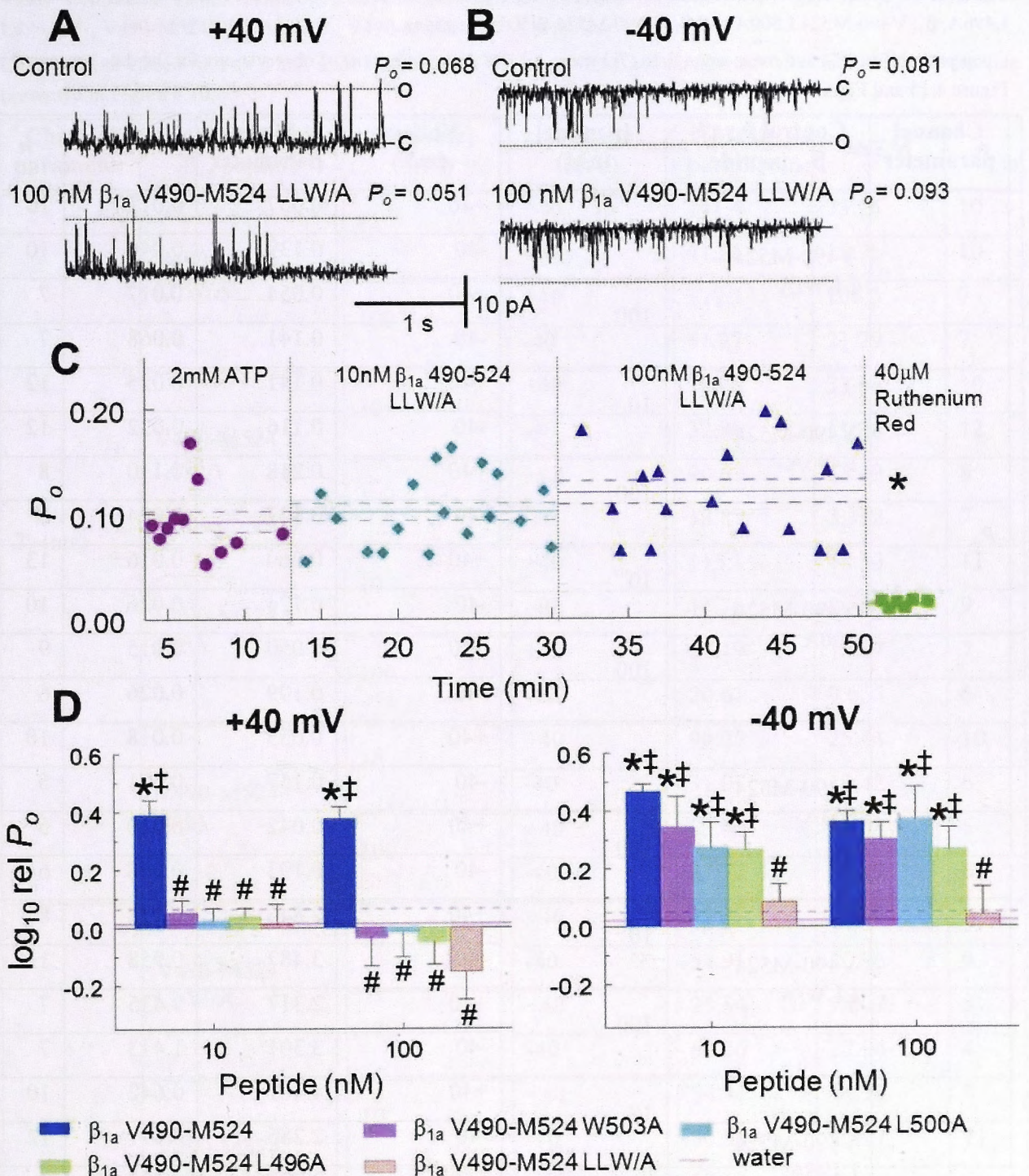


Figure 4.15 The effect of β_{1a} 490-524 hydrophobic surface mutants on RyR1 activity in lipid bilayers.

A and **B**) Three second records of single channel activity at +40 mV (**A**) or -40 mV (**B**) that display representative channel activity before (top traces: control) and after (bottom traces) *cis* addition of 100 nM β_{1a} V490-M524 LLW/A peptide. Open probability (P_o) is shown in the right top corner. **C**) A timeline of channel activity following sequential *cis* addition of 2 mM ATP (pink circle), 10 nM β_{1a} V490-M524 LLW/A (green diamonds), 100 nM β_{1a} V490-M524 LLW/A (blue triangles) and 40 μ M ruthenium red (light green square). The channel activity over 10 s was taken from \sim 30 s intervals of activity at +40 and -40 mV. For each condition, there is a mean (continuous line) \pm SEM (discontinuous line) of the scatter plot. *Significantly different from prior condition, determined by unpaired Student's *t*-test, $p < 0.05$. **D**) Average relative P_o ($\log_{10} \text{rel } P_o$) was calculated in the same way as in Figure 4.4. P_o was measured from \sim 90 s traces of RyR1 activity, $n = 5-13$ channel traces. Error bars indicate + or - SEM. Control P_o values in Tables 4.1 and 4.4a. The mean \pm SEM $\log_{10} \text{rel } P_o$ values for peptide buffer (water) additions are shown as continuous pink line and discontinuous pink line, respectively. The data for V490-M524 peptides is a re-plot of the data shown in Fig. 4.4D. *Significantly different from control activity set at zero, determined using a paired Student's *t*-test, $p < 0.05$. #Significantly different from β_{1a} V490-M524. †Significantly different from β_{1a} V490-M524 LLW/A peptide. *†Significance determined by ANOVA, $p < 0.05$. Note that some of the channel experiments were undertaken by Dr. Yamuna A. Karunasekara (Muscle Research Group, John Curtin School of Medical Research, Australian National University, Canberra, Australia).

Table 4. 4a Mean control parameters for channels used in analysis of β_{1a} V490-M524 LLW/A, β_{1a} V490-M524 L496A, β_{1a} V490-M524 L500A and β_{1a} V490-M524 W503A peptides.

Open probability (P_o) and mean open time (T_o) mean \pm SEM and number (n) of observations for the data presented in Figure 4.15 and Figure 4.16

Channel parameter	Control for <i>cis</i> β_{1a} peptide	[peptide] (nM)	Voltage (mV)	Mean parameter	\pm SEM	n
P_o	V490-M524 LLW/A	10	+40	0.057	0.012	10
			-40	0.139	0.040	10
		100	+40	0.054	0.017	7
			-40	0.141	0.068	7
	V490-M524 L496A	10	+40	0.141	0.025	12
			-40	0.116	0.032	12
		100	+40	0.218	0.110	8
			-40	0.127	0.024	8
	V490-M524 500A	10	+40	0.060	0.016	13
			-40	0.124	0.026	10
		100	+40	0.050	0.015	9
			-40	0.109	0.026	6
	V490-M524 503A	10	+40	0.055	0.018	10
			-40	0.157	0.071	5
		100	+40	0.042	0.020	6
			-40	0.193	0.068	6
T_o (ms)	V490-M524 LLW/A	10	+40	2.846	0.338	8
			-40	3.487	0.958	11
		100	+40	2.317	0.435	7
			-40	3.301	1.413	7
	V490-M524 L496A	10	+40	4.407	0.642	10
			-40	2.286	0.497	12
		100	+40	3.271	0.523	7
			-40	1.960	0.308	8
	V490-M524 500A	10	+40	2.844	0.428	12
			-40	2.424	0.316	9
		100	+40	2.625	0.663	8
			-40	2.107	0.378	6
	V490-M524 503A	10	+40	2.502	0.396	11
			-40	3.415	1.710	6
		100	+40	1.820	0.378	5
			-40	3.675	1.660	6

Table 4.4b. Mean control parameters for channels used in analysis of β_{1a} V490-M524 LLW/A, β_{1a} V490-M524 L496A, β_{1a} V490-M524 L500A and β_{1a} V490-M524 W503A peptides.

Control mean closed time (T_c) and open frequency (F_o) mean \pm SEM and number (n) of observations for the data presented in Figure 4.16.

Channel parameter	Control for cis β_{1a} peptide	[peptide] (nM)	Voltage (mV)	Mean parameter	\pm SEM	n
T_c (ms)	V490-M524 LLW/A	10	+40	141.4	75.26	10
			-40	41.26	15.75	10
		100	+40	179.3	106.3	7
			-40	51.27	21.79	7
	V490-M524 L496A	10	+40	104.6	33.66	10
			-40	32.80	11.28	12
		100	+40	90.67	43.49	8
			-40	13.87	3.312	7
	V490-M524 500A	10	+40	115.1	48.30	11
			-40	11.70	2.650	9
		100	+40	57.49	18.87	7
			-40	20.61	3.665	6
V490-M524 503A	10	+40	90.27	25.44	10	
		-40	31.07	13.42	6	
	100	+40	85.46	28.88	5	
		-40	31.72	14.49	6	
F_o (s^{-1})	V490-M524 LLW/A	10	+40	17.37	3.470	8
			-40	54.91	10.96	9
		100	+40	25.34	7.807	5
			-40	68.26	22.94	4
	V490-M524 L496A	10	+40	34.41	14.30	8
			-40	50.54	7.827	11
		100	+40	17.18	11.36	6
			-40	66.91	17.49	4
	V490-M524 500A	10	+40	29.84	8.549	12
			-40	66.37	11.72	8
		100	+40	25.92	9.401	9
			-40	46.83	12.48	6
	V490-M524 503A	10	+40	27.81	9.859	9
			-40	43.84	23.18	3
		100	+40	20.32	11.78	4
			-40	52.30	21.83	4

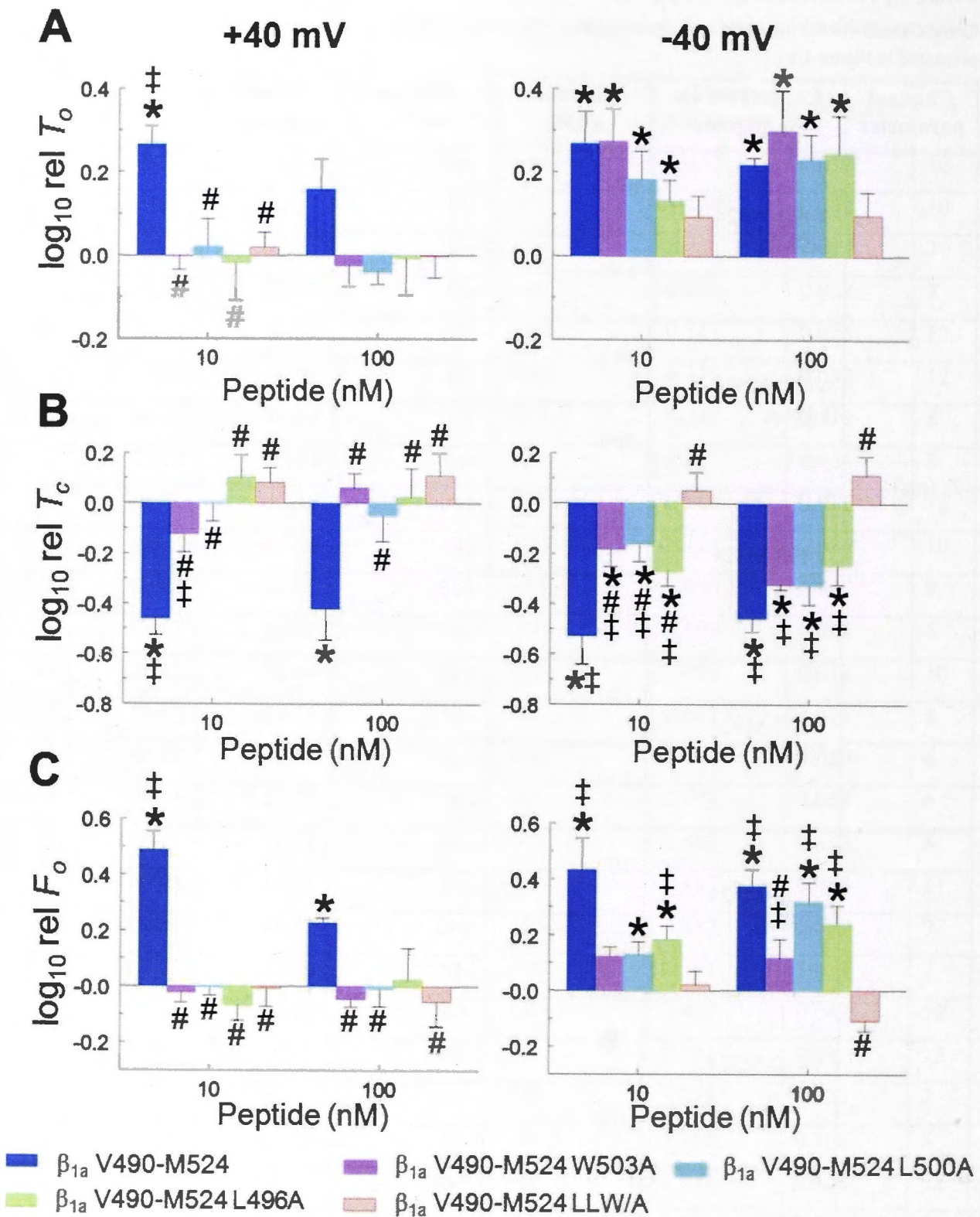


Figure 4. 16 The effect of β_{1a} V490-M524 hydrophobic surface repeat peptides on single channel gating parameters in lipid bilayers.

The average mean open time (\log_{10} rel T_o ; **A**), mean closed time (\log_{10} rel T_c ; **B**) and open frequency (\log_{10} rel F_o ; **C**) was calculated in the same way as the \log_{10} rel P_o (Figure 4.4) from ~ 90 s of single channel activity at either +40 mV (left) or -40 mV (right). Error bars indicate + or - SEM. Control values shown in Table 4.1 and Table 4.4, $n = 3-12$ channel traces. The data for V490-M524 peptides is a re-plot of the data shown in Fig. 4.5. *Significantly different from control activity set at zero, determined using a paired Student's t-test, $p < 0.05$. #Significantly different from β_{1a} V490-M524 peptide. ‡Significantly different from β_{1a} V490-M524 LLW/A. ##Significance determined by ANOVA, $p < 0.05$.

Additionally, the individual mutants also significantly ($p = 0.001-0.039$) decreased the relative T_c (**Figure 4.16B**). Although relative T_c was reduced in all cases, the effects of 10 nM individual mutants on relative T_c values were significantly lower than the action of 10 nM β_{1a} V490-M524 peptide ($p = 0.003-0.024$) (**Figure 4.16B**). In terms of the effect on F_o , all individual β_{1a} V490-M524 mutants significantly ($p = 0.003-0.042$) increased the relative F_o , with the exception of 10 nM β_{1a} V490-M524 W503A, (**Figure 4.16C**).

It is interesting to note that the actions of the individual mutants on channel gating properties were very similar, regardless of peptide concentration or which residue was mutated. Overall, the results indicate that collectively, the hydrophobic surface residues are essential for RyR1 activation by β_{1a} V490-M524 peptide. Individually, these residues are essential at +40 mV, but only slightly alter activation by the β_{1a} V490-M524 peptide on single channel gating properties at -40 mV.

4.3.7 The zebrafish β_{1a} C-terminal residues modulate RyR1 activity

To examine the influence of the zebrafish C-terminal region on RyR1 activity, the effect of a peptide (β_{1a} V490-L520 zf; containing the zebrafish β_{1a} region V490-L520 that is equivalent to the mouse β_{1a} V490-M524 region), was tested on RyR1 in lipid bilayers. The experiments were carried out by adding 10 and 100 nM to the *cis* chamber and recording channel activity at both +40 and -40 mV. As shown in single channel traces, addition of 100 nM β_{1a} V490-L520 zf peptide increases RyR1 activity at both voltages (**Figure 4.17, A and B**). This increase in activity was typically observed within the first minute of addition, as shown in **Figure 4.17C**. Although the activity following addition was quite variable as usual, the average activity in the time period following addition of β_{1a} V490-L520 zf peptide was higher ($p < 0.001$) than control (**Figure 4.17C**). Note that increasing the concentration of β_{1a} V490-L520 zf peptide from 10 to 100 nM did not alter ($p = 0.393$) channel activity further over time (**Figure 4.17C**). As the effect of β_{1a} V490-L520 zf did not significantly ($p = 0.228-0.968$) differ between +40 and -40 mV (e.g. Log_{10} rel P_o of 10 nM β_{1a} V490-L520 zf was 0.21 ± 0.02 and 0.23 ± 0.06 , respectively), these values were combined. Both 10 and 100 nM β_{1a} V490-L520 zf peptide increased ($p \leq 0.002$) channel activity by 1.6- and 1.8-fold, respectively (**Figure 4.17D**). However, there was a significant 39% ($p = 0.001$) reduction in the activation produced by 10 nM β_{1a} V490-L520 zf peptide when compared with the effect of 10 nM β_{1a} V490-M524 peptide (**Figure 4.17D**). Therefore, the efficacy of the β_{1a} V490-L520 zf peptide as a mammalian RyR1 modulator is slightly lower than β_{1a} V490-M524 peptide. As with β_{1a} V490-M524 peptide, the β_{1a} V490-L520 zf peptide significantly increased relative T_o , decreased relative T_c and increased relative F_o (**Figure 4.18**). Therefore the β_{1a} V490-L520 zf peptide increases the average duration and frequency of channel openings and decreases duration between channel openings. Notably, the effect of 10 nM β_{1a} V490-L520 zf peptide was slightly lower ($p = 0.003-0.015$) than the effect

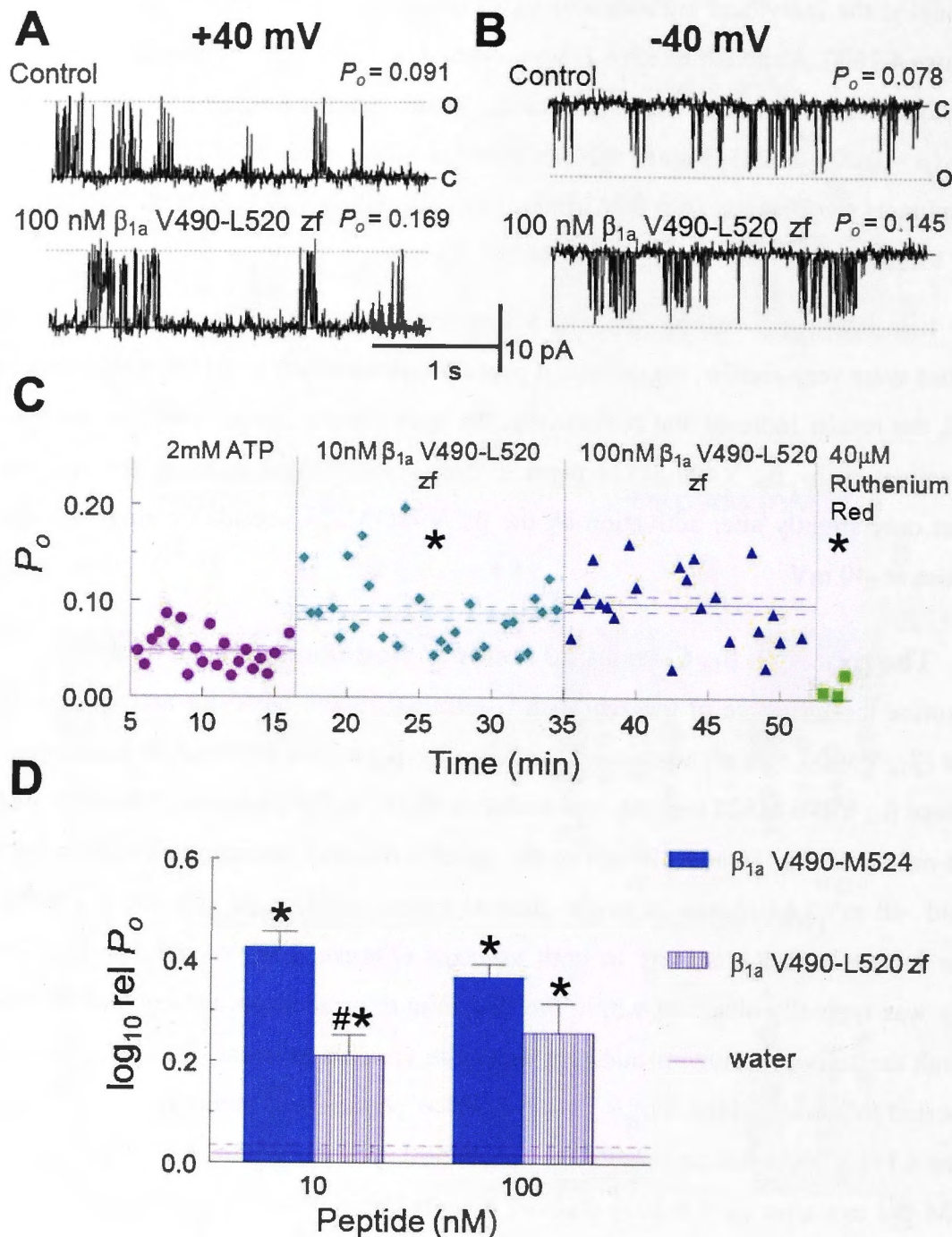


Figure 4.17 The similar modulatory effect of mouse and zebrafish β_{1a} C-tail peptides on RyR1 activity in lipid bilayers.

A and B) Three second records of single channel activity at +40 mV (**A**) or -40 mV (**B**) that display representative channel activity before (top traces: control) and after (bottom traces) *cis* addition of 100 nM β_{1a} V490-L520 zf peptide. Open probability (P_o) is shown in the right top corner. **C**) A timeline of channel activity following sequential *cis* addition of 2 mM ATP (pink circle), 10 nM β_{1a} V490-L520 zf peptide (green diamonds), 100 nM β_{1a} V490-L520 zf peptide (blue triangles) and 40 μ M ruthenium red (light green square). The channel activity over 10 s was taken from \sim 30 s intervals of activity at +40 and -40 mV. For each condition, there is a mean (continuous line) \pm SEM (discontinuous line) of the scatter plot. *Significantly different from prior condition, determined by unpaired Student's t-test, $p < 0.05$. **D**) Average relative P_o ($\log_{10} \text{rel } P_o$) was calculated in the same way as in Figure 4.4. P_o was measured from \sim 90 s traces of RyR1 activity, $n = 6-12$ channel traces. Error bars indicate \pm SEM. Control P_o values in Tables 4.1 and 4.5. The mean \pm SEM $\log_{10} \text{rel } P_o$ values for peptide buffer (water) additions are shown as continuous pink line and discontinuous pink line, respectively *Significantly different from control activity set at zero, determined using a paired Student's t-test, $p < 0.05$. #Significantly different from β_{1a} subunit, determined by ANOVA, $p < 0.05$.

Table 4.5 Mean control parameters for channels used in analysis of β_{1a} V490-L520 zf peptide.

Open probability (P_o), mean open time (T_o), mean closed time (T_c) and open frequency (F_o) mean \pm SEM and number (n) of observations for data presented in Fig 4.17 and Fig 4.18

Channel parameter	[peptide] (nM)	Mean parameter	\pm SEM	n
P_o	10	0.079	0.021	10
	100	0.084	0.023	9
T_o (ms)	10	4.181	1.518	7
	100	4.181	1.518	7
T_c (ms)	10	49.71	15.88	8
	100	51.53	18.22	7
F_o (s^{-1})	10	37.23	13.45	8
	100	25.45	8.031	6

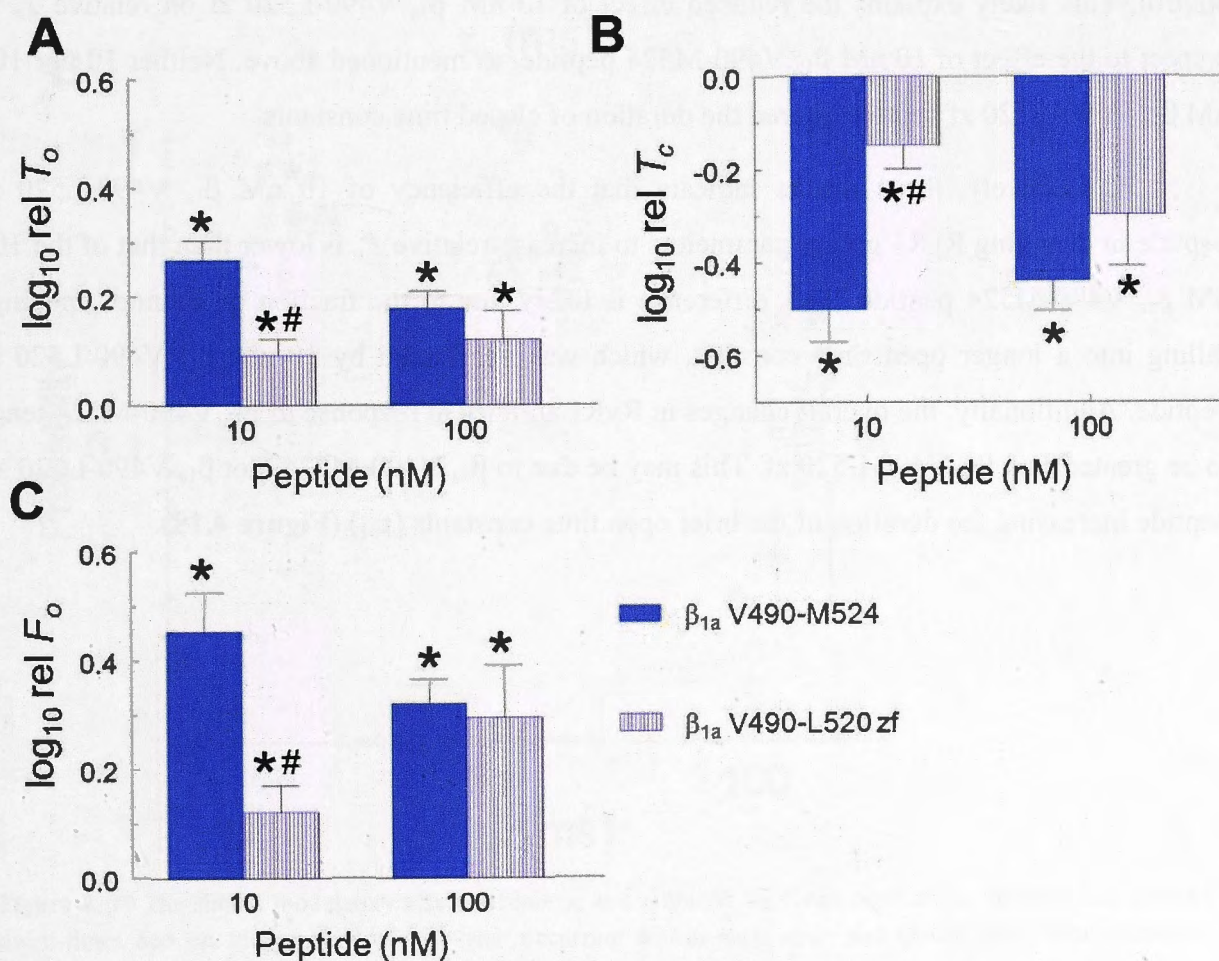


Figure 4.18 The effect of mouse and zebrafish β_{1a} C-tail peptides on single channel gating parameters in lipid bilayers:

The average mean open time (\log_{10} rel T_o ; **A**), mean closed time (\log_{10} rel T_c ; **B**) and open frequency (\log_{10} rel F_o ; **C**) was calculated in the same way as the \log_{10} rel P_o (Figure 4.4) from ~ 90 s of single channel activity. Error bars indicate + or - SEM. Control values in Table 4.5, $n = 3-12$ channel traces. *Significantly different from control activity set at zero, determined using a paired Student's t-test, $p < 0.05$. #Significantly different from β_{1a} V490-M524 peptide, determined by ANOVA, $p < 0.05$.

of 10 nM β_{1a} V490-M524 peptide (**Figure 4.18**), but still the increase was never-the-less significant ($p = 0.022-0.042$).

Delving deeper into the effect of these peptides on single channel kinetics, β_{1a} V490-L520 zf peptide altered dwell-time distributions in a similar fashion as β_{1a} V490-M524 peptide. The 10 and 100 nM β_{1a} V490-L520 zf peptide shifted a fraction of events from the τ_{o1} to the τ_{o2} by $12.6 \pm 5.6\%$ ($p = 0.013$) and $13.4 \pm 6.1\%$ ($p = 0.009$), respectively (**Figure 4.19A**). However, the β_{1a} V490-L520 zf peptide did not significantly ($p = 0.280$ and 0.100) increase the duration of the τ_{o1} values, whereas β_{1a} V490-M524 peptide did. This difference may contribute the reduced efficiency of β_{1a} V490-L520 zf in increasing relative T_o when compared to β_{1a} V490-M524 peptide (**Figure 4.18A**). In terms of closed time distributions, 100 nM β_{1a} V490-L520 zf peptide significantly shifted a fraction of events from the τ_{c3} to the τ_{c1} by $11.0 \pm 6.0\%$ ($p = 0.020$) (**Figure 4.19B**). Although 10 nM β_{1a} V490-L520 zf peptide increased a fraction of events ($p = 0.027$) of the τ_{c1} , the fraction of events falling into the τ_{c3} was not altered ($p = 0.344$) relative to control. This likely explains the reduced effect of 10 nM β_{1a} V490-L520 zf on relative T_c in respect to the effect of 10 nM β_{1a} V490-M524 peptide, as mentioned above. Neither 10 nor 100 nM β_{1a} V490-L520 zf peptide altered the duration of closed time constants.

Collectively, these results indicate that the efficiency of 10 nM β_{1a} V490-L520 zf peptide in changing RyR1 gating parameters to increase relative P_o is lower than that of the 100 nM β_{1a} V490-M524 peptide. This difference is likely due to the fraction of channel openings falling into a longer open time constant, which was unaffected by 10 nM β_{1a} V490-L520 zf peptide. Additionally, the overall changes in RyR1 activity in response to β_{1a} V490-M524 tends to be greater than β_{1a} V490-L520 zf. This may be due to β_{1a} V490-M524, not β_{1a} V490-L520 zf, peptide increasing the duration of the brief open time constants (τ_{o1}) (**Figure 4.19**).

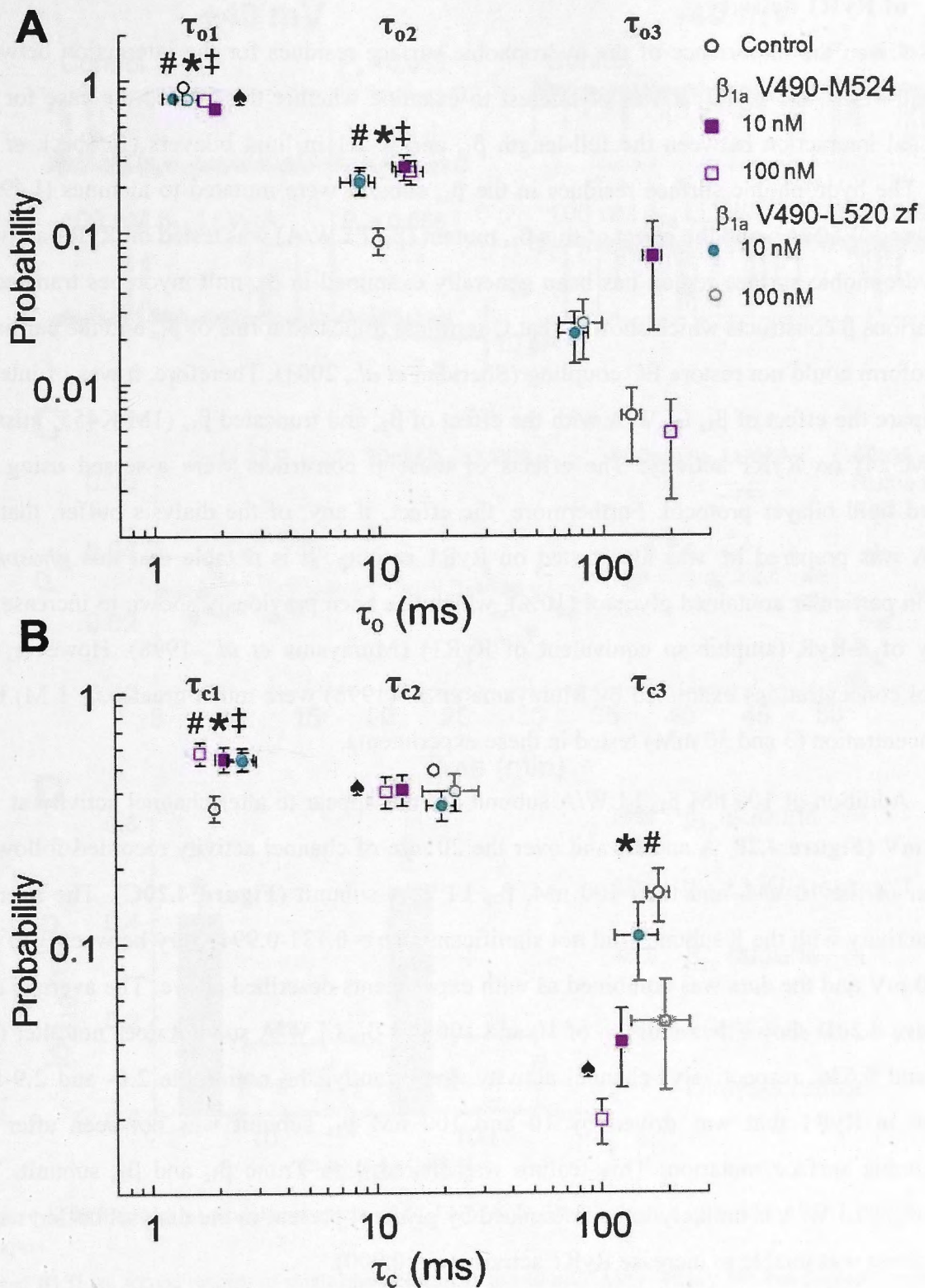


Figure 4.19 The similar modulatory effects of mouse and zebrafish β_{1a} C-tail peptides on the open and closed dwell-times and on the probability of events occurring within each open and closed dwell-time constant components.

The open (τ_o , **A**) and closed (τ_c , **B**) time constants and the probability of events in each time constant component were calculated from ~ 90 s of single channel activity. $n = 5$ -23 channel records. The individual open time constants (τ_{o1} , τ_{o2} and τ_{o3}) and individual closed time constants (τ_{c1} , τ_{c2} and τ_{c3}) are indicated on the graphs in **A** and **B**, respectively. Error bars indicate \pm SEM. *Significant difference between the probability of events in each time constant in control with 10 and 100 nM β_{1a} V490-M524 peptide. †Significant difference between the probability of events in each time constant in control with 10 nM β_{1a} V490-L520 zf peptide. # Significant difference between the probability of events in each time constant in control with 100 nM β_{1a} V490-L520 zf peptide. *Significant difference between the dwell time constant under control conditions with of 10 or 100 nM β_{1a} V490-M524. *†#*Significance determined by ANOVA, $p < 0.05$.

4.3.8 The hydrophobic surface residues are important for β_{1a} subunit modulation of RyR1 activity

Given the importance of the hydrophobic surface residues for the interaction between β_{1a} V490-M524 and RyR1, it was of interest to examine whether this is also the case for the functional interaction between the full-length β_{1a} and RyR1 in lipid bilayers (Rebbeck *et al.*, 2011). The hydrophobic surface residues in the β_{1a} subunit were mutated to alanines (L496A, L500A and W503A), and the effect of this β_{1a} mutant (β_{1a} LLW/A) was tested on RyR1 activity. The hydrophobic surface region has been generally examined in β_{1a} -null myotubes transfected with various β constructs which showed that C-terminal truncated forms of β_{1a} and the cardiac β (β_{2a}) isoform could not restore EC coupling (Sheridan *et al.*, 2003). Therefore, it was of interest to compare the effect of β_{1a} LLW/A with the effect of β_{2a} and truncated β_{1a} (1M-K455; missing A456-M524) on RyR1 activity. The effects of these β constructs were assessed using the standard lipid bilayer protocol. Furthermore, the effect, if any, of the dialysis buffer, that β_{1a} LLW/A was prepared in, was also tested on RyR1 activity. It is notable that this *phosphate* buffer in particular contained glycerol (10%), which has been previously shown to increase the activity of α -RyR (amphibian equivalent of RyR1) (Murayama *et al.*, 1998). However, the glycerol concentrations examined by Murayama *et al.* (1998) were much greater (≥ 1 M) than the concentration (3 and 30 mM) tested in these experiments.

Addition of 100 nM β_{1a} LLW/A subunit did not appear to alter channel activity at +40 or -40 mV (**Figure 4.20, A and B**) and over the 20 min of channel activity recorded following addition of the 10 nM, and then 100 nM, β_{1a} LLW/A subunit (**Figure 4.20C**). The average RyR1 activity with the β subunits did not significantly ($p = 0.131-0.994$) vary between +40 mV and -40 mV and the data was combined as with experiments described above. The average data in **Figure 4.20D** shows that addition of 10 and 100 nM β_{1a} LLW/A subunit does not alter ($p = 0.928$ and 0.626 , respectively) channel activity. Importantly, the noticeable 2.6- and 2.9-fold increase in RyR1 that was driven by 10 and 100 nM β_{1a} subunit was not seen after the hydrophobic surface mutation. This feature was shared with Trunc β_{1a} and β_{2a} subunit. The effect of β_{1a} LLW/A is unlikely to be influenced by glycerol present in the dialysis buffer, as the buffer alone was unable to increase RyR1 activity ($p = 0.900$).

The effects of the β proteins on relative P_o were appropriately reflected by the effects of these proteins on single channel gating parameters. Only the full-length β_{1a} subunit significantly ($p \leq 0.005$) increased relative T_o and relative F_o , as well as decreasing the relative T_c (**Figure 4.21**). All of these changes were ~ 2 -fold, as was also seen with the effect of the β_{1a} V490-M524 peptide and a previous report of β_{1a} subunit in the same conditions (Rebbeck *et al.*, 2011). Note that the gating parameters with β_{1a} LLW/A were not significantly ($p = 0.120-0.591$) different from control, and importantly, were significantly ($p \leq 0.001$) different from the effect of the β_{1a} subunit (**Figure 4.21**).

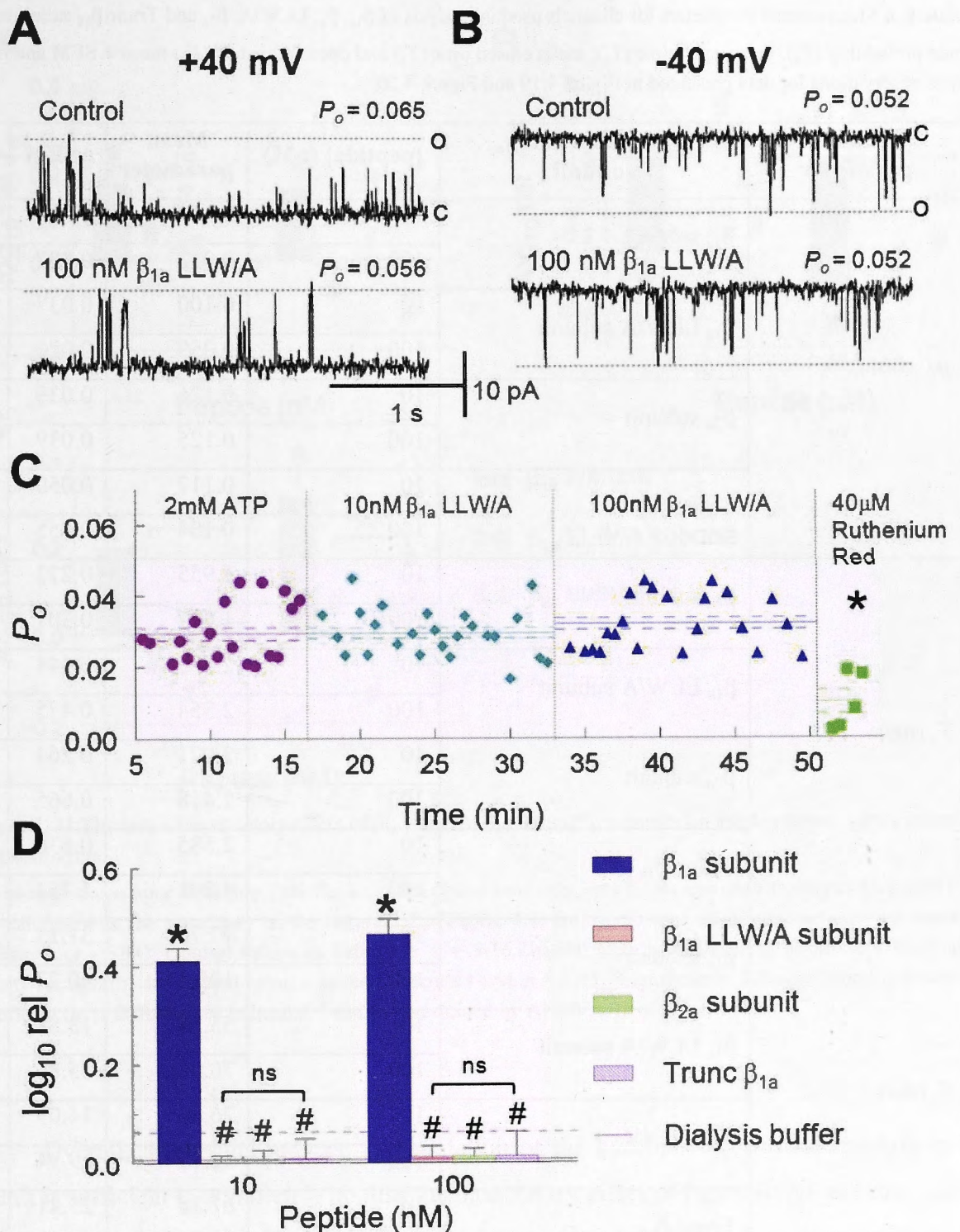


Figure 4.20 The lack of modulatory effect of β_{1a} LLW/A, β_{2a} , and Trunc β_{1a} subunits on RyR1 activity in lipid bilayers.

A and B) Three second records of single channel activity at +40 mV (**A**) or -40 mV (**B**) that display representative channel activity before (top records: control) and after (bottom records) *cis* addition of 100 nM β_{1a} LLW/A subunit. Open probability (P_o) is shown in the right top corner. **C**) A timeline of channel activity following sequential *cis* addition of 2 mM ATP (pink circle), 10 nM β_{1a} LLW/A (green diamonds), 100 nM β_{1a} LLW/A (blue triangles) and 40 μ M ruthenium red (light green square). The channel activity over 10 s was taken from ~30 s intervals of activity at +40 and -40 mV. For each condition, there is a mean (continuous line) \pm SEM (discontinuous line) of the scatter plot. *Significantly different from prior condition, determined by unpaired Student's t-test, $p < 0.05$. **D**) Average relative P_o ($\log_{10} \text{rel } P_o$) was calculated in the same way as in Figure 4.4. Error bars indicate \pm SEM. P_o was measured from ~90 s records of RyR1 activity, $n = 7-16$ channel records. Control P_o values in Tables 4.6. The mean \pm SEM $\log_{10} \text{rel } P_o$ values for subunit dialysis buffer additions are shown as continuous pink line and discontinuous pink line, respectively *Significantly different from control activity set at zero, determined using a paired Student's t-test, $p < 0.05$. #Significantly different from β_{1a} subunit, determined by ANOVA, $p < 0.05$. Note that experiments using β_{2a} subunit were undertaken by Courtney Segovis (Muscle Research Group, John Curtin School of Medical Research, Australian National University, Canberra, Australia).

Table 4. 6 Mean control parameters for channels used in analysis of β_{1a} , β_{1a} LLW/A, β_{2a} and Trunc β_{1a} subunits. Open probability (P_o), mean open time (T_o), mean closed time (T_c) and open frequency (F_o) mean \pm SEM and number (n) of observations for data presented in Figure 4.19 and Figure 4.20

Channel parameter	Control for <i>cis</i> β_{1a} subunit	[peptide] (nM)	Mean parameter	\pm SEM	n
P_o	β_{1a} subunit	10	0.048	0.014	15
		100	0.032	0.007	12
	β_{1a} LLW/A subunit	10	0.100	0.037	16
		100	0.059	0.020	15
	β_{2a} subunit	10	0.126	0.039	14
		100	0.125	0.039	10
	Trunc β_{1a}	10	0.117	0.050	8
		100	0.104	0.055	7
T_o (ms)	β_{1a} subunit	10	1.955	0.273	13
		100	1.677	0.301	10
	β_{1a} LLW/A subunit	10	2.583	0.444	16
		100	2.354	0.475	14
	β_{2a} subunit	10	2.021	0.261	7
		100	2.418	0.665	6
	Trunc β_{1a}	10	2.585	0.636	6
		100	4.293	1.751	6
T_c (ms)	β_{1a} subunit	10	97.76	31.15	13
		100	105.15	40.23	9
	β_{1a} LLW/A subunit	10	55.58	13.88	16
		100	70.08	15.86	14
	β_{2a} subunit	10	26.46	14.09	7
		100	42.19	19.94	7
	Trunc β_{1a}	10	61.38	25.41	5
		100	76.13	23.78	5
F_o (s^{-1})	β_{1a} subunit	10	24.30	5.631	13
		100	24.22	6.287	6
	β_{1a} LLW/A subunit	10	43.64	10.74	16
		100	38.21	10.66	15
	β_{2a} subunit	10	68.60	18.77	12
		100	78.82	26.47	7
	Trunc β_{1a}	10	28.21	9.935	5
		100	21.65	9.630	5

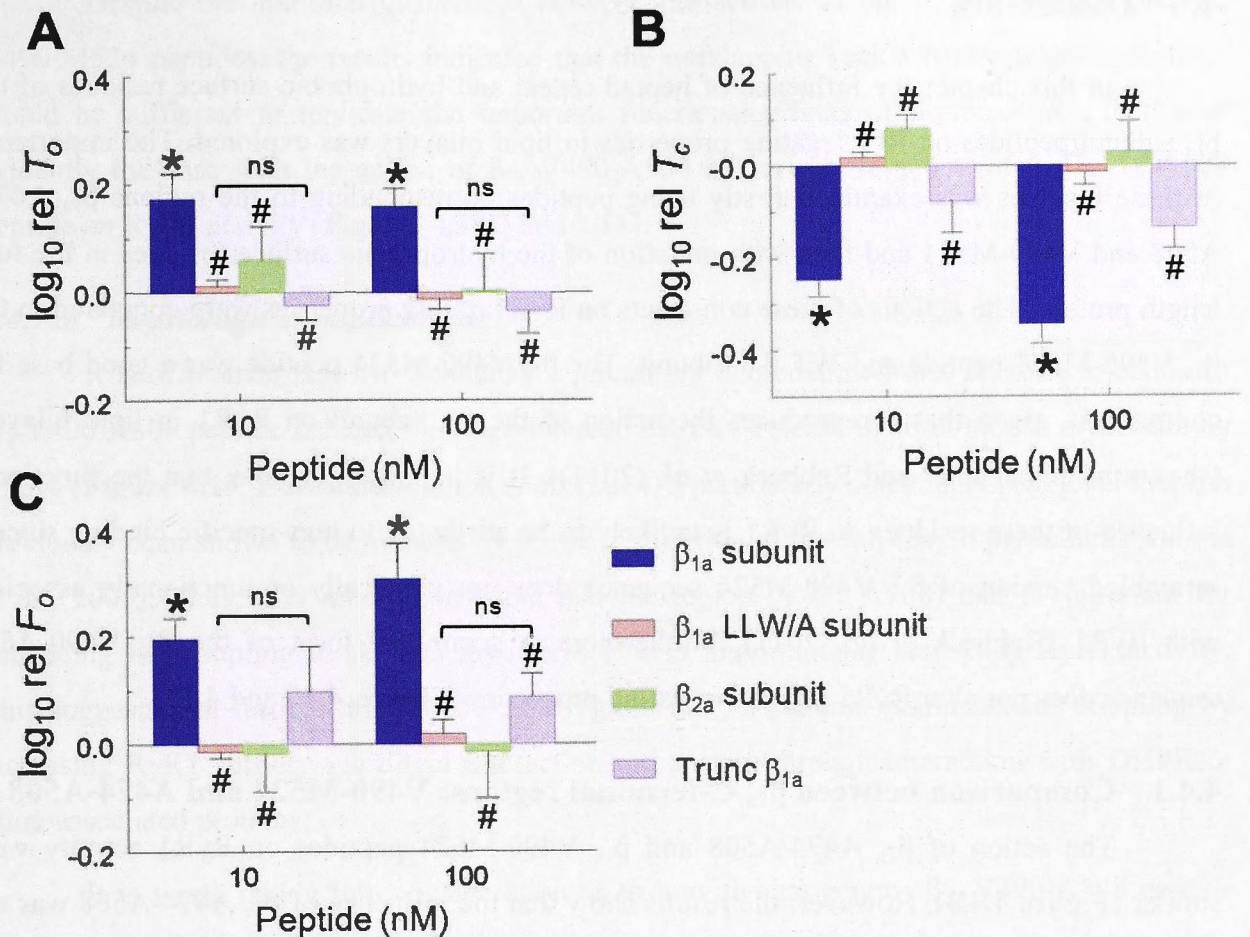


Figure 4.21 The lack of modulatory effect of β_{1a} LLW/A, β_{2a} , Trunc β_{1a} subunits on single channel gating parameters in lipid bilayers.

The average mean open time ($\log_{10} \text{ rel } T_o$; **A**), mean closed time ($\log_{10} \text{ rel } T_c$; **B**) and open frequency ($\log_{10} \text{ rel } F_o$; **C**) was calculated in the same way as the $\log_{10} \text{ rel } P_o$ (Figure 4.4) from ~ 90 s of single channel activity. Error bars indicate + or - SEM. Control values in Table 4.6, $n = 5-16$ channel records. *Significantly different from control activity set at zero, determined using a paired Student's t-test, $p < 0.05$. #Significantly different from β_{1a} subunit. No significant (ns) difference is indicated. # and ns determined by ANOVA, $p < 0.05$.

Overall, the results indicate that mutation of the hydrophobic surface residues in β_{1a} subunit is sufficient to completely abolish the modulatory effect of β_{1a} on RyR1 activity. This is impressive, given that the effect of mutating three residues on relative P_o is comparable to the consequence of removing the majority of the C-terminal residues and a subunit that shares only 28% C-terminal sequence similarity (**Figure 4.1B**) with the β_{1a} subunit.

4.4 Discussion

In this chapter the influence of heptad repeat and hydrophobic surface residues of the β_{1a} subunit/peptides on RyR1 gating properties in lipid bilayers was explored. The importance of these residues was examined firstly using peptides corresponding to the regions β_{1a} A474-A508 and V490-M524 and then with mutation of the hydrophobic surface residues in the full-length protein. The actions of these constructs on RyR1 gating properties were compared to the β_{1a} V490-M524 peptide and WT β_{1a} subunit. The β_{1a} V490-M524 peptide was a good base for comparison, given that it reproduces the action of the β_{1a} subunit on RyR1 in lipid bilayers (shown in this chapter and Rebbeck *et al.* (2011)). It is important to note, that the functional influence of these residues on RyR1 is unlikely to be attributed to non-specific binding since a scrambled version of β_{1a} V490-M524 sequence does not physically or functionally associate with RyR1 (Rebbeck *et al.*, 2011). Furthermore, a scrambled form of the β_{1a} V490-A508 sequence does not alter RyR1 activity or gating properties (**Figure, 4.10** and **4.11**).

4.4.1 Comparison between β_{1a} C-terminal regions: V490-M524 and A474-A508

The action of β_{1a} A474-A508 and β_{1a} V490-M524 peptides on RyR1 activity were similar (**Figure 4.4D**). However, the results show that the influence of β_{1a} A474-A508 was not as stable over time and did not increase the overall duration of channel openings to the level observed by β_{1a} V490-M524 peptide (**Figure, 4.4C** and **4.5A**). This suggests that the stability of the interaction between β_{1a} A474-A508 and RyR1 may be slightly lower than the interaction between β_{1a} V490-M524 and RyR1. A difference in the stability of the interaction could have been established by assessing the ability of these peptides to retain RyR1 in affinity chromatography assays. Unfortunately, the biotinylated form of β_{1a} A474-A508 is hydrophobic and visible peptide aggregation during the assay meant that accurate assessment was not feasible.

There are two factors that could account for the observed difference in function between β_{1a} A474-A508 and β_{1a} V490-M524 peptides. These are 1) a lack of the extreme 16 C-tail residues and/or 2) addition of β_{1a} A474-V490 residues. Given that the β_{1a} V490-A508 peptide displayed the same modulatory effects as β_{1a} A474-A508 on RyR1 gating parameters, it is likely that the addition of β_{1a} A474-V490 residues is not a factor. However, the mean open times at -40 mV increased following addition of β_{1a} A474-A508 LVV/A, not β_{1a} A474-A508, suggesting that the presence of the heptad repeat residues within the β_{1a} A474-V490 region may contribute to the lack of β_{1a} A474-A508 effect on average mean open times at -40 mV (**Figure 4.8A**). Granted, this does not account for the lack of action on the duration of channel openings when channels were exposed to the β_{1a} A474-A508 peptide. Consequently, it is plausible that the extreme 16 C-tail residues contribute to the C-terminal interaction with RyR1 in lipid bilayers.

Despite the marginal differences between the actions of the β_{1a} A474-A508 and β_{1a} V490-M524 peptides, the results indicated that the overlapping region between these peptides would be sufficient to replicate the important functional effects of β_{1a} on RyR1. This was evidently the case with the action of β_{1a} V490-A508 mirroring the action of β_{1a} A474-A508 peptide on RyR1 activity (**Figure, 4.10D and 4.11**).

4.4.1.1 Physiological implications

It is of interest that MF Schneider's laboratory demonstrated that pressure injection of β_{1a} V490-A508 peptide enhances voltage-induced SR Ca^{2+} release in adult mouse myofibres by ~50% (**Figure 4.13**; Hernández-Ochoa *et al.* (2014)), particularly since this is the level that has previously been shown to be induced by pressure injection of the full-length β_{1a} subunit (Garcia *et al.*, 2005). Thus, it is nicely consistent that the region (V490-A508) that is important for enhancing EC coupling in skeletal myofibres is also important for increasing RyR1 activity. This suggests that through the V490-A508 region, the β_{1a} subunit modulates EC coupling by increasing RyR1 activity via direct interaction rather than through interaction with DHPR or other associated proteins.

It is worth taking into consideration as to how the exogenous β_{1a} V490-A508 peptide enhances voltage-induced SR Ca^{2+} release in adult mouse myofibres when presumably healthy levels of endogenous β_{1a} subunit would be also present in the myofibres. Given that the β_{1a} V490-A508 peptide has the same effect as exogenous β_{1a} subunit, the action is unlikely to be through displacing endogenous β_{1a} subunit, but rather by binding to an unoccupied β_{1a} -binding site on RyR1. This quite possible, particularly as only every second RyR1 is coupled to DHPR (Block, 1988, Paolini *et al.*, 2004b).

As mentioned above, the extreme 16 β_{1a} C-tail residues may slightly enhance the interaction between β_{1a} C-terminal residues and RyR1 in lipid bilayer experiments. However, it is unlikely that these C-tail residues influence skeletal EC coupling because truncation of 21 β_{1a} C-terminal residues did not alter restoration of EC coupling by exogenous expression of β_{1a} in β_{1a} -null myotubes (Sheridan *et al.*, 2003). Furthermore, microinjection with β_{1a} V490-A508 region is sufficient to replicate the full-effect of full-length β_{1a} on SR Ca^{2+} release in fibres (**Figure 4.13**; Garcia *et al.* (2005)) and consequently the 16 C-tail residues are not necessary for the effect of β_{1a} subunit in SR Ca^{2+} release.

4.4.2 The irrelevance of heptad repeat residues in modulating RyR1 activity

Given that the β_{1a} V490-M524 region, containing only one of the three heptad repeat residues, is sufficient to communicate the functional effect of the β_{1a} subunit on RyR1 in lipid bilayers, it is unlikely that all heptad repeat residues influence the interaction between β_{1a} and RyR1. Furthermore, the results demonstrate that the three heptad repeat residues together do not enhance this interaction. This is underlined by the finding that mutation of all three residues did

not reduce the action of β_{1a} A474-A508 peptide on RyR1 activity (**Figure 4.7**). Intriguingly, this mutant partially restored the increase in single channel mean open times (**Figure 4.8**) that was seen with β_{1a} V490-M524 peptide, but not β_{1a} A474-A508 peptide. Since the overall action of β_{1a} A474-A508 LVV/A peptide on RyR1 activity did not significantly differ from the action of β_{1a} A474-A508 peptide, further exploration if this restoration was not justified.

4.4.2.1 Physiological implications

The expression of the β_{1a} subunit with the heptad repeat residue mutated to alanines drastically altered restoration of skeletal EC coupling mouse β_{1a} -null myotubes (Sheridan *et al.*, 2004), but not zebrafish β_{1a} myotubes (Dayal *et al.*, 2010). The results from the present study are similar to the zebrafish study and suggest that the heptad repeat residues do not influence skeletal EC coupling in mouse myotubes by facilitating the interaction between β_{1a} C-terminal residues and RyR1.

4.4.3 Importance of hydrophobic surface residue in modulating RyR1 activity

All of the results presented in this chapter support the importance of the hydrophobic surface residues for the interaction between β_{1a} and RyR1, particularly given that mutation of all three residues abolishes the action of β_{1a} V490-M524 peptide and β_{1a} subunit on RyR1 activity. In addition, the action of β_{1a} on RyR1 activity is largely mirrored by peptides that contain the identical sequence (such as β_{1a} A474-A508, β_{1a} A474-A508 LVV/A and β_{1a} V490-A508) or a similar aligned sequence (such as β_{1a} V490-L520 zf). Furthermore, the β_{2a} subunit and Trunc β_{1a} , that do not contain a comparable hydrophobic surface region, do not modulate RyR1 activity (**Figure 4.19**).

4.4.3.1 The action of the hydrophobic surface residues

The present results indicate that the hydrophobic surface residues are responsible for the modulatory action of β_{1a} subunit on RyR1 activity. In addition, results from affinity chromatography demonstrate that these residues are largely responsible for the physical interaction between β_{1a} V490-M524 peptide and RyR1. There was residual binding when the residues were neutralised, which is likely specific, given that a scrambled form of the β_{1a} V490-M524 peptide did not associate at all with RyR1 from skeletal SR vesicles (Rebbeck *et al.*, 2011). Together, the bilayer and affinity chromatography results indicate that these residues are responsible for the functional interaction between β_{1a} and RyR1 and mostly responsible for the physical interaction between β_{1a} and RyR1. Given that NMR analysis has shown that this mutation does not alter the propensity of residues within L493-G504 region to adopt an α -helical structure, it is likely that the hydrophobic surface residues are important in the direct interaction with RyR1 rather than maintaining structural integrity of β_{1a} C-terminus.

The residual RyR1 retained by the β_{1a} V490-M524 LLW/A peptide in affinity chromatography assay suggests that other residues within V490-M524 facilitate the physical interaction between β_{1a} and RyR1. The facilitating residue(s) may be situated within the extreme 16 residue C-tail, which would explain the reduced stability of peptides lacking this region. An alternative possibility is that the alanine mutation does not completely abolish the hydrophobic surface.

4.4.3.2 The role of the individual proteins

The role of the individual hydrophobic surface residues is complicated by the voltage-dependence of their actions. Individual mutation of the hydrophobic surface residues abolished the action β_{1a} V490-M524 peptide at +40 mV, but not at -40 mV. The reason for this voltage-dependent effect is not clear. There have been multiple reports of peptides inducing voltage-dependent effects on RyR gating. This effect has typically been accredited to a positive net charge in the peptide and the peptide binding to a region near the pore that is influenced by the membrane field (e.g. Dulhunty *et al.* (2004), Gibbs *et al.* (2006), Diaz-Sylvester and Copello (2009)). This is unlikely to be the case with the peptides used in this study since β_{1a} V490-M524 and the individual mutant peptides do not have a net charge. An alternative possibility is that the conformation of the β_{1a} binding site on RyR1 is altered by the change in voltage in such a way that at +40 mV, two hydrophobic surface residues are insufficient for functional interaction, whereas at -40 mV, two residues are sufficient. Although RyR1 is not generally known to be modulated by membrane potential, a few studies have reported a voltage-dependent inhibition of RyR channels at positive bilayer potentials (Percival *et al.*, 1994, Laver *et al.*, 1995, Laver & Lamb, 1998, Abdellatif *et al.*, 2007). Of particular interest, Laver and Lamb (1998) and Abdellatif *et al.* (2007) reported a voltage-dependent inhibition of high activity channels when the voltage was shifted from -40 mV to +40 mV. Indeed, average control P_o values in this study showed a trend, though infrequently significant, to be higher at -40 mV than at +40 mV within individual channels. Given that the range of membrane potentials used in this study has been demonstrated to alter gating characteristics (Laver & Lamb, 1998, Abdellatif *et al.*, 2007), it is feasible that the RyR1 conformation may differ between voltages. However, a link between RyR1 conformation in lipid bilayers and membrane potential has not, to the author's knowledge, been experimentally demonstrated.

4.4.3.3 Physiological implications

There is emerging evidence that four hydrophobic C-terminal residues of β_{1a} (namely L488, L493, L496 and L500) are important for DHPR tetrad formation and depolarisation-induced Ca^{2+} release in β_{1a} -null mouse myotubes expressing a truncated form of the β_{1a} subunit (14 amino acid C-tail truncation; β_{1a} -14) (Perez *et al.*, 2013). Perez and colleagues (2013) presented findings that although expression of β_{1a} -14 fully restores tetrad formation and

depolarisation-induced SR Ca^{2+} release in β_{1a} -null myotubes, mutation of several hydrophobic residues (L488A, L493A, L496A and L500A) abolishes restoration of tetrad formation and greatly reduced restoration of Ca^{2+} release. Thus, two of the three hydrophobic surface residues have been shown to potentially facilitate mouse EC coupling. Given that the affinity chromatography results presented in this chapter demonstrate that the hydrophobic surface residues have a large role in physical interaction with RyR1, it is possible that tetrad formation and consequently EC coupling may be facilitated through direct interaction between RyR1 and β_{1a} subunit. Arguably, without individual mutation of these hydrophobic residues in β_{1a} constructs introduced into in β_{1a} -null myotubes, it is difficult to ascertain whether the hydrophobic surface residues actually facilitate tetrad formation and EC coupling. As yet, the possibility that only residues L488 and L493 facilitate EC coupling due to facilitating tetrad formation alone cannot be excluded.

4.4.4 Comparison between the effectiveness of zebrafish and mouse β_{1a} C-tail residues in RyR1 modulation

The results indicate that the β_{1a} V490-L520 zf peptide modulates RyR1 activity in a similar fashion as β_{1a} V490-M524, although with a marginally reduced effect at 10 nM peptide (**Figure 4.17**). Additionally, the response of RyR1 activity to 100 nM β_{1a} V490-L520 zf peptide was more variable than the response to 100 nM β_{1a} V490-M524 peptide, suggesting that the interaction may be less stable. A reduction in interaction stability may have also contributed to the observation that the β_{1a} V490-M524 peptide, not β_{1a} V490-L520 zf peptide, increased the duration of the medium open time constant (**Figure 4.19**).

The small reduction in β_{1a} V490-L520 zf peptide's effect on RyR1 is unlikely to be attributed to a difference in β_{1a} V490-L520 zf peptide structure, as the structure of the zebrafish β_{1a} V490-L520 region is predicted to adopt the same surface alignment of hydrophobic residues along one side of an α -helical region (Karunasekara *et al.*, 2012). Consequently, the difference in peptide actions is likely attributed to one or more of the sequence differences between the peptides, which include two of the three comparable hydrophobic surface residues. This discrepancy is minor given that the residues, zebrafish M500 and L503 *versus* mouse L500 and W503, can both engage in hydrophobic interactions. However, this difference may be sufficient to reduce the stability of the interaction between 10 nM peptide with RyR1. Other notable sequence variations include: absence of G513-V516 that is present in the mouse β_{1a} V490-M524 region, and replacement of S501 and G504 in the mouse β_{1a} with aspartate and glutamate residues, respectively, in the zebrafish β_{1a} . Without knowledge of the β_{1a} binding site in RyR1, it is difficult to picture which sequence variation may contribute to the reduction in stability. The influence of each of these regions on interaction with RyR1 could be examined in future by testing the individual substitution of these residues/regions in the mouse β_{1a} V490-M524 peptide.

4.4.4.1 *Physiological implications*

A previous report demonstrated that the role of β_{1a} subunit in zebrafish skeletal EC coupling is species independent, particularly as exogenous expression of rabbit β_{1a} restores EC coupling in β_{1a} -null myotubes to the same extent as expression of zebrafish β_{1a} (Schredelseker *et al.*, 2009). However, the reported importance of the heptad repeat motif largely differs between mouse and zebrafish skeletal EC coupling (Sheridan *et al.*, 2004, Dayal *et al.*, 2013). Given that the results in this study demonstrate that the heptad repeat residues do not influence the direct interaction between mammalian forms of β_{1a} subunit and RyR1 and that the β_{1a} V490-L520 zf peptide modulates RyR1, it is likely that the zebrafish β_{1a} C-terminal residues participate in EC coupling by virtue of RyR1 interaction.

4.5 Conclusion

The results presented and discussed in this chapter clearly demonstrate that the hydrophobic surface residues, not the heptad repeat residues, are important for physical and functional interaction between β_{1a} and RyR1 in *in vitro* studies. The physiological implications are that this hydrophobic region may facilitate mammalian and zebrafish EC coupling through directly increasing RyR1 activity.

CHAPTER FIVE – REGIONS OF THE RYR RESPONSIBLE FOR THE BETA1A SUBUNIT INTERACTION

5.1 Introduction

Studies showing that the skeletal DHPR and RyR1 isoforms are critical for skeletal-type EC coupling (Tanabe *et al.*, 1990b, Nakai *et al.*, 1997, Beurg *et al.*, 1999b, Fessenden *et al.*, 2000, Protasi *et al.*, 2000), suggest that these proteins contain isoform specific regions which enable their unique interaction in skeletal muscle. Certainly, several studies have attempted to identify the DHPR binding site(s) on RyR1 by investigating the ability of RyR1 regions in RyR2 or RyR3 backgrounds to restore skeletal EC coupling in *dyspedic* myotubes (as discussed in detail in section 1.4.2). It is possible that one/some of these RyR1 regions that are not conserved with RyR2 or RyR3 may be responsible for binding the skeletal β_{1a} isoform. However, it is difficult to test for a potential lack of interaction between RyR2/3 and β_{1a} in *dyspedic* myotubes as RyR1 is also required for tetrad formation (Protasi *et al.*, 2000, Protasi *et al.*, 2002), which is vital for the transfer of the EC coupling signal from DHPR to RyR1. Using the lipid bilayer technique, the potential for interaction between β_{1a} and RyR2 can be measured without the complication from loss of DHPR tetrad formation.

In considering the physical interaction between β_{1a} subunit and RyR1, the binding site has been suggested to be in a RyR1 region between residues 3201 and 3661, based on results of pull down assays (Cheng *et al.*, 2005). Within this region, Cheng and colleagues (2005) found a polybasic K3495-R3502 motif that, when mostly deleted (Δ K3495-R3499) or mutated to glutamine residues (KtoQ), greatly reduced association between the RyR1 fragment and β_{1a} subunit. Expression of either mutation in full-length RyR1 significantly reduced restoration of Ca^{2+} transients in *dyspedic* mouse myotubes (Cheng *et al.*, 2005). The authors concluded that the polybasic region influences the docking of β_{1a} subunit to RyR1 and transmission of EC coupling signal from DHPR β_{1a} subunit to RyR1. However, whether this region is important for the functional interaction between RyR1 and β_{1a} subunit was unknown and can only be specifically examined in the isolated bilayer system.

5.1.1 Aim

There were two objectives explored in this chapter: to 1) examine the effect of β_{1a} subunit on RyR2 activity and 2) examine whether the KtoQ mutant in full-length RyR1 effects the modulatory action of β_{1a} subunit on RyR1. Investigating whether the β_{1a} interaction is conserved between RyR1 and RyR2 may provide clues to the RyR1 regions that contribute to interaction with β_{1a} subunit. The response of these RyRs to β_{1a} subunit was assessed using lipid bilayer experiments.

5.2 Materials and Methods

5.2.1 Materials

5.2.1.1 Reagents and chemicals

Gibco F15 MEM powder was purchased from Life Technologies (Carlsbad, CA, USA). Complete protease inhibitor cocktail was obtained from Roche Diagnostics (Mannheim, Germany). The other reagents and chemicals were purchased as specified in section 2.1.1.

5.2.1.2 Plasmid constructs

The β_{1a} subunit was obtained as discussed in section 2.1.3. The rabbit wild type (WT) RyR1 (NCBI reference sequence NM_001101718.1) and RyR1 KtoQ mutant cDNA in pCIneo vector (*MluI* at the 5' and *XbaI* at the 3') were obtained from Prof. Robert T. Dirksen and Dr. Linda Groom (Department of Pharmacology and Physiology, University of Rochester Medical Center, Rochester, NY, USA). The pCIneo vector was chosen on the basis that successful expression of WT RyR1 in a human embryonic kidney cell line (HEK293)-based system has been established using this vector (Kimura *et al.*, 2005, Goonasekera *et al.*, 2007, Kimura *et al.*, 2007).

5.2.2 Methods

5.2.3 Expression and purification of β_{1a} subunit

The WT β_{1a} subunit was expressed and purified using the protocols described in section 2.2.3.

5.2.4 Preparation of skeletal SR vesicles

The skeletal SR vesicles were prepared by Mrs. Suzy Pace and Mrs. Joan Stivala (Muscle Research Group, John Curtin School of Medical Research, Australian National University, Canberra, Australia) as described in section 2.2.2.

5.2.5 Preparation of cardiac SR vesicles

This method was used only for results described in this chapter and was not addressed in the general methods in Chapter Two. The experimental procedure for cardiac SR vesicle preparation was undertaken by Mrs. Suzy Pace and Mrs. Joan Stivala (Muscle Research Group, John Curtin School of Medical Research, Australian National University, Canberra, Australia) in accordance with Laver *et al.* (1995). Cardiac SR vesicles were collected from sheep hearts that underwent homogenisation and isolation through a series of centrifugation steps that were developed by Chamberlain and Fleischer (1988).

Immediately following euthanasia of a sheep (IV delivery of 3.25mg/ml of sodium pentobarbitone per 2 kg of body weight), the heart was excised and trimmed of fat, blood

vessels and atrial tissue. The remaining heart ventricle was then sequentially diced and homogenised using a Waring blender (Waring Products Division; Connecticut, USA) in 10 s bursts three times in 500 ml of *homogenising* buffer consisting of: 290 mM sucrose, 10 mM imidazole, 0.05 mM DTT and 3 mM NaN₃, pH adjusted to 6.9 with 6 M HCl. The homogenate was centrifuged at 12 295.8 x g using a Sorvall SLA-1500 rotor in a Sorvall RC-5B high-speed centrifuge (Dupont; Norwalk, USA) for 20 min at 4 °C. The supernatant was filtered through four levels of cotton gauze to remove excess fat. The filtrate was then centrifuged at 104 350.1 x g using a Ti-45 rotor in a Beckman L8-70 centrifuge (Beckman Instruments; Gladesville, Australia) for 2 h at 4 °C. The resulting supernatant was discarded and the insoluble membrane that formed the pellet was resuspended in a solution of 649 mM KCl in *homogenising* buffer (pH adjusted to 6.7 with 6 M HCl) using a Potter homogeniser. The homogenised solution was incubated on ice for 30 min and then centrifuged at 6 084.1 x g using Sorval SLA 3000 Super lite rotor in a Sorvall RC-5B high speed centrifuge (Dupont: Norwalk, USA) for 10 min at 4 °C. The resulting supernatant was then further centrifuged at 256 630.8 x g using a Ti-70 rotor in a Beckman L8-70 centrifuge for 90 min at 4 °C. The subsequent supernatant was discarded and the pellet was resuspended in 15 ml of solution with 649 mM KCl in *homogenising* buffer (pH 6.7) and then homogenised using a Potter homogeniser. The SR vesicle preparation was separated into 20 µl aliquots and frozen at -70 °C. The final protein concentration was determined using DC Protein Assay kit (section 2.2.7.3).

5.2.6 Expression of recombinant WT RyR1 and RyR1 KtoQ mutant and isolation of micro vesicles

The two RyR1 constructs were expressed using calcium precipitation-induced transfection of HEK293 cells, and the HEK293 membrane vesicles were isolated using a series centrifugation steps as described in Kimura *et al.* (2005). Studies have shown that HEK293 cells endogenously express functional RyR1 and RyR2 (Querfurth *et al.*, 1998, Luo *et al.*, 2005). However, the level of protein expression drastically reduces following multiple passage (P) numbers above P25 (Luo *et al.*, 2005). To avoid mixture of our recombinant RyR1 samples with endogenous WT RyR1, HEK293 cells with passage numbers above P30 were typically transfected with the RyR1 constructs. Markedly, only adherent HEK293 cells that displayed morphology typical of healthy HEK293 cells, as viewed under the 20 x objective of a light microscope, were transfected. In addition, HEK293 cells were mock-transfected using deionised water in place of cDNA as a negative control.

5.2.6.1 Expression of recombinant WT RyR1 and RyR1 KtoQ mutant

HEK293 cells were cultured on 175 cm² nucleon delta treated flask (Thermo Scientific: Rockford, USA) in minimum essential medium (MEM) F15 media (consisting of 26.2 mM NaHCO₃, 9.61 g/L of F15 MEM powder) in Heracell 240i CO₂ Incubator (Thermo Scientific:

Rockford, USA) at 37 °C with constant 5% CO₂. The media was refreshed when the adherent cells had grown to 50-60% confluency.

The calcium precipitate transfectant mixture was prepared by slowly adding 1.3125 ml of DNA solution (80 µg DNA and 285.7 mM CaCl₂) to 1.6875 ml of *phosphate* buffer solution (1.24 mM NaH₂PO₄, 250 mM NaCl, 45 mM 4-(2-hydroxyethyl)-1-piperazineethanesulfonic acid and 0.13 mM Na₂HPO₄, pH adjusted to 7.2 with 4 M NaOH) that was simultaneously being aerated by pipette aspiration. This was incubated at ~21 °C for 45 min and then dripped over the cells 3 h following media refreshment. The transfected cells were incubated for 24 h at 37 °C and then the media was refreshed. Following further 24 h incubation, the cells were removed from the plate using a cell scraper. The cells were spun down at 155 x g using an Universal 16 centrifuge (Andreas Hettich GmbH & Co.: Tuttlingen, Germany) for 5 min and supernatant was removed. Then the cells were resuspended in 2 ml of *resuspension* buffer (0.5 mM EDTA in PBS) and further spun down at 1 387 x g for 20 min. The cell pellet was stored at -70 °C.

5.2.6.2 Isolation of micro vesicles

The frozen cells were resuspended in 1.5 ml of *homogenising* buffer (300 mM sucrose, 5 mM imidazole and 1 x Complete protease inhibitor cocktail, pH 7.4). Using an IKA®T10 Basic Homogenizer (IKA®Works: Selangor, Malaysia), the cell mixture was homogenised twice in 5 s bursts. The cell membrane components were spun down at 11 600 x g using an Eppendorf centrifuge 5415 (Hamburg, Germany) for 20 min at 4 °C. The cell pellet was resuspended in 1.2 ml of sucrose-imidazole buffer and re-homogenised using the IKA®T10 Basic Homogenizer three times in 5 s bursts. Then, the insoluble cellular components were spun down at 91 943 x g using a Beckman TLA120.2 rotor in a Beckman Optima MAX ultracentrifuge (Beckman Instruments; Gladesville, Australia) for 2 h at 4 °C. The pellet was resuspended in 300 µl of *homogenising* buffer, and homogenised for 5 min using a Potter homogeniser. The preparation was further homogenised by sonication using a Branson Ultrasonics Sonifier 250 (Danbury, CT) twice in 2 s bursts. The preparation was separated into 15 µl aliquots and stored at -70 °C. All preparations were tested for RyR1 using western blot after SDS-PAGE, as described in sections 2.2.6 and 2.2.4, respectively. Notably, mock-transfected HEK293 cells did not contain RyR, at least not to amounts that were visible by immuno-detection.

5.2.7 Planar bilayer recordings of RyR

The planar bilayer experiments were carried out as described in section 2.2.9. Following channel incorporation, the initial *cis* and *trans* chamber solutions were identical, consisting of 20 mM CsCl, 230 mM CsCH₃O₃S, 10 mM TES and 1 mM CaCl₂, pH 7.4. The typical full-length experiment proceeded with *cis* addition of 1 mM BAPTA (quantity determined by Ca²⁺ electrode) to reduce ~1 mM [Ca²⁺] to 10 µM. Then, 2 mM ATP was added to the *cis* chamber

and control channel activity was recorded for at least 10 min, alternating between +40 and -40 mV every 30 s.

5.3 Results

5.3.1 β_{1a} subunit modulates RyR2 activity

In order to identify potential sites for β_{1a} interaction, it was of interest to investigate whether the modulatory effect of β_{1a} is conserved between RyR1 and RyR2 in lipid bilayers. The effect of β_{1a} subunit on native RyR2 was assessed using the same experimental design used to assess the effects of peptides on RyR1 activity (described in section 4.3.1), with exception that pig cardiac SR vesicles were incorporated into the lipid bilayer. It was also important to confirm channel identity (as RyR2) and orientation in the lipid bilayer. This was achieved by observing gating, conductance and response to cytoplasmic RyR1 regulators, such as ATP, $[Ca^{2+}]$ and ruthenium red.

5.3.1.1 Characteristics of RyR2 in lipid bilayers

The gating characteristics of RyR2 were similar to those of RyR1, which were extensively described in Chapter Three. The average single RyR2 channels displayed maximal conductance of 261.2 ± 33.2 pS ($n = 4$) and 284.8 ± 8.2 pS ($n = 3$) at +40 and -40 mV, respectively, calculated using Equation 2.11. This is similar to the Cs^+ conductance of RyR1, and agrees with previous observations by Williams (1992). Another similar feature was that most openings were to the maximal amplitude for single channel openings rather than sub-state openings (see “control” in Figure 5.1A).

5.3.1.2 Response of RyR2 to cytosolic modulators

Following incorporation of cardiac SR vesicles into lipid bilayers, channel activity was recorded for 2 min prior to and after reduction of *cis* free $[Ca^{2+}]$ from 1 mM to 10 μ M. The decrease in free *cis* $[Ca^{2+}]$ from 1 mM to 10 μ M did not typically alter channel activity at +40 or -40 mV, which averaged to $\text{Log}_{10} \text{rel } P_o$ of 0.06 ± 0.06 ($n = 15$, $p = 0.33$). This lack of response agrees with earlier reports that show average RyR2 activity does not differ with *cis* $[Ca^{2+}]$ 0.01 and 1 mM, both of which are on the plateau of the curve relating RyR2 P_o to cytoplasmic $[Ca^{2+}]$ over a range of 100 nM to 1M $[Ca^{2+}]_{cis}$ (Laver *et al.*, 1995, Laver, 2007).

To further confirm the channel identity and orientation in the bilayer, channel activity was assessed following *cis* addition of 2 mM ATP. This addition increased RyR2 activity by 2.1-fold ($\text{Log}_{10} \text{rel } P_o$ of 0.32 ± 0.06 , $n = 10$, $p < 0.001$). A similar increase in channel activity has been reported in other studies that characterised the action of ATP on RyR2 activity and used 2 mM ATP and activating *cis* $[Ca^{2+}]$ to confirm identity of RyR2 (e.g. Rousseau *et al.* (1986), Williams and Ashley (1989), Laver *et al.* (1995), Laver *et al.* (1997b)).

Addition of 40 μM ruthenium red near the end of a channel recording typically reduced or abolished RyR2 activity (**Figure 5.1C**). This agrees with the response of RyR2 to ruthenium red reported in other studies that have tested a range of concentrations between 10-30 μM (e.g. Rousseau *et al.* (1986), Sitsapesan and Williams (1990), Laver *et al.* (1995), Dulhunty *et al.* (2005)).

The combined response of channels from cardiac SR vesicle preparations to RyR modulators confirmed the identity of the channels as RyR2. Any channels that did not respond in the appropriate manner to changes in *cis* $[\text{Ca}^{2+}]$ and ATP were discontinued. Additionally, any channel that did not respond to addition of ruthenium red was not analysed.

5.3.1.3 β_{1a} subunit increases RyR2 activity

The actions of β_{1a} subunit on RyR2 were assessed by examining the effect *cis* addition of 10 and 100 nM β_{1a} on RyR2 gating properties using the same experimental design that was used to assess the functional effect of the β_{1a} subunit on RyR1 activity (section 4.3.7). Addition of 10 nM β_{1a} subunit increased RyR2 activity at both +40 and -40 mV, an effect that was enhanced following addition of 100 nM β_{1a} subunit (**Figure 5.1, A and B**). Despite the intrinsic activity fluctuations over time, the average channel activity was increased significantly by 2-fold ($p \leq 0.001$) following addition of 10 nM β_{1a} subunit. The modulatory effect of the β_{1a} subunit was marginally enhanced by 1.4-fold ($p = 0.011$) after increasing its concentration to 100 nM (**Figure 5.1C**). The effect of β_{1a} on RyR activity did not significantly differ ($p = 0.387-0.939$) between +40 and -40 mV (e.g. for RyR2, Log_{10} rel P_o of 10 nM β_{1a} was 0.30 ± 0.05 and 0.32 ± 0.08 , respectively), therefore these values were combined. On average, addition of 10 and 100 nM β_{1a} subunit to RyR2 increased relative P_o 1.8- and 2.6-fold ($p \leq 0.001$), respectively. Markedly, the action of 10 nM β_{1a} subunit on relative RyR2 P_o was significantly lower ($p \leq 0.001$) than the action of 100 nM β_{1a} on both RyR1 and RyR2, and significantly lower than the effect of 10 nM β_{1a} on RyR1 (**Figure 5.1D**). This reduced efficacy at 10 nM indicates that the effective concentration of β_{1a} for the activation of RyR2 by β_{1a} is higher than that between β_{1a} and RyR1.

The action of β_{1a} on single channel gating parameters mostly reflected the average relative P_o results (**Figure, 5.1D and 5.2**). On Average, 10 and 100 nM β_{1a} subunit increased relative T_o values by 1.6- to 1.9-fold, decreased relative T_c values by 1.7- to 1.9-fold and increased relative F_o values by 1.6- to 2.1-fold, respectively (**Figure 5.2**). There appears to be a general trend for the action of 100 nM β_{1a} on single RyR2 channel gating parameters to be higher than the action of 10 nM (**Figure 5.2**). Overall, the results clearly show that β_{1a} increases the average duration and frequency of RyR1 and RyR2 single channel openings, and decreases the average duration between channel openings.

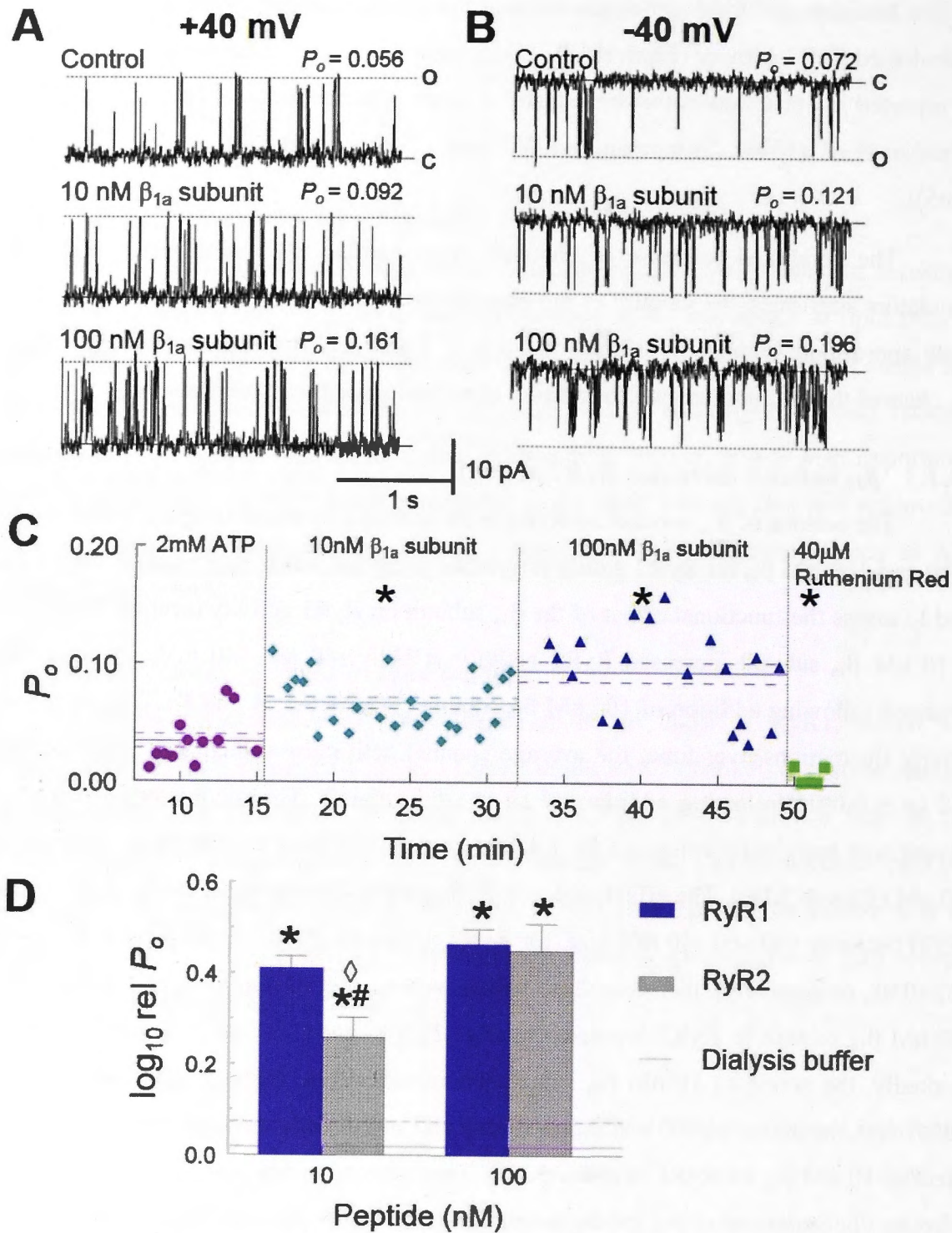


Figure 5. 1 The effect of β_{1a} subunit on RyR1 and RyR2 activity in lipid bilayers.

A and B) Three second records of single channel activity at +40 mV (**A**) or -40 mV (**B**) that display representative native RyR2 activity before (top records: control) and after *cis* addition of 10 nM β_{1a} subunit (middle record) and 100 nM β_{1a} subunit (bottom record). Open probability (P_o) is shown in the right top corner. **C**) A timeline of RyR2 activity following sequential *cis* addition of 2 mM ATP (pink circle), 10 nM β_{1a} (green diamonds), 100 nM β_{1a} (blue triangles) and 40 μ M ruthenium red (light green square). The channel activity over 10 s was taken from \sim 30 s intervals of activity at +40 and -40 mV. For each condition, there is a mean (continuous line) \pm SEM (discontinuous line) of the scatter plot. *Significantly different from prior condition, determined using a paired Student's t-test, $p < 0.05$. **D**) Average relative P_o ($\log_{10} \text{rel } P_o$) was calculated in the same way as Figure 4.4. P_o was measured from \sim 90 s records of RyR1 activity, $n = 8$ -15 channel records. Error bars indicate \pm SEM. Control P_o values in Tables 4.6 and 5.1. The mean \pm SEM $\log_{10} \text{rel } P_o$ values for dialysis buffer additions are shown as continuous pink line and discontinuous pink line, respectively. The data for 'RyR1' is a re-plot of the ' β_{1a} ' data shown in Fig. 4.20D. *Significantly different from control activity set at zero, determined using a paired Student's t-test, $p < 0.05$. #Significantly different from 10 nM β_{1a} on RyR1. \diamond Significantly different from 100 nM β_{1a} on RyR2 activity. $\#^{\diamond}$ Significance determined by ANOVA, $p < 0.05$.

Table 5. 1 Mean control parameters for channels used in analysis of β_{1a} subunit on RyR2.

Open probability (P_o), mean open time (T_o), mean closed time (T_c) and open frequency (F_o) mean \pm SEM and number (n) of observations for data presented in Figure 5.1 and Figure 5.2

Channel parameter	[subunit] (nM)	Mean Parameter	\pm SEM	n
P_o	10	0.119	0.029	13
	100	0.079	0.027	8
T_o (ms)	10	6.423	1.465	9
	100	6.448	2.074	9
T_c (ms)	10	63.662	20.61	13
	100	67.701	13.93	11
F_o (s^{-1})	10	24.865	6.157	11
	100	17.857	3.632	7

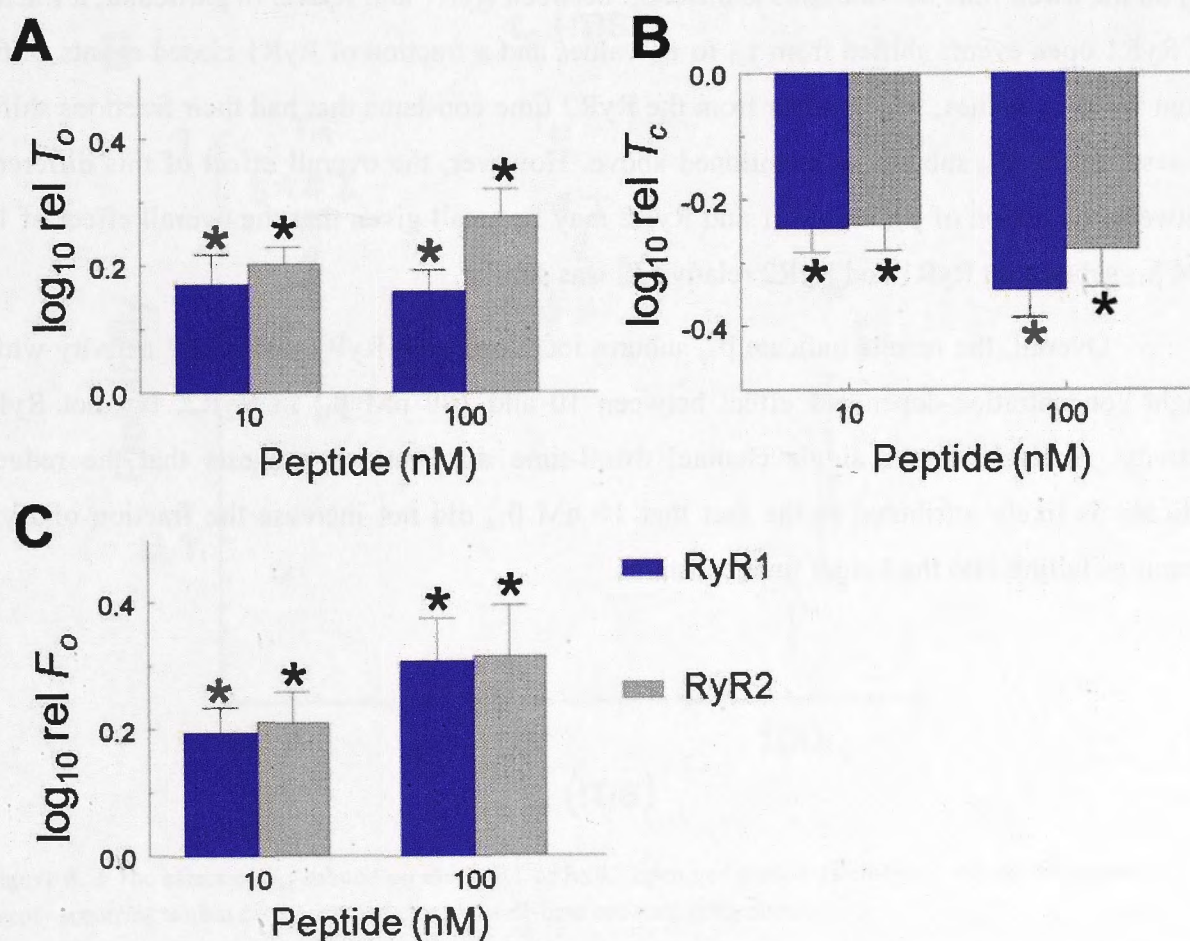


Figure 5. 2 The similar modulatory effect of β_{1a} subunit on RyR1 and RyR2 single channel gating parameters in lipid bilayers.

The average mean open time ($\log_{10} \text{ rel } T_o$; **A**), mean closed time ($\log_{10} \text{ rel } T_c$; **B**) and open frequency ($\log_{10} \text{ rel } F_o$; **C**) was calculated in the same way as the $\log_{10} \text{ rel } P_o$ (Figure 4.4) from ~ 90 s of single channel activity, $n = 6-13$ channel records. Error bars indicate \pm SEM. The data for 'RyR1' is a re-plot of the ' β_{1a} ' data shown in Fig. 4.21.

*Significantly different from control activity set at zero, determined using a paired Student's t-test, $p < 0.05$.

Not all dwell-time distributions were equivalent in control RyR1 and RyR2, in the absence of β_{1a} subunit. In particular, the fraction of RyR2 events at the τ_{o2} were greater ($p < 0.001$), events in the τ_{o1} were lower ($p < 0.001$) and events in the τ_{c1} were greater ($p = 0.047$) relative to the fractions of events falling into respective RyR1 dwell-time constant components (**Figure 5.3**). Both, 10 and 100 nM β_{1a} subunit decreased the fraction of RyR2 open events falling in the τ_{o1} by $18.7 \pm 1.8\%$ ($p = 0.003$) and $16.3 \pm 2.0\%$ ($p = 0.012$), respectively, relative to control. However, only 100 nM β_{1a} subunit significantly ($p = 0.012$) increased the fraction of RyR2 open events falling in the τ_{o3} value, which likely contributes to the reduced action of 10 nM β_{1a} subunit on RyR2 relative P_o in respect to 100 nM. In contrast to the open dwell-time distributions, there is no significant difference between the effect of 10 and 100 nM β_{1a} subunit on RyR2 closed dwell-time distributions relative to control. Both, 10 and 100 nM β_{1a} subunit shifted a fraction of RyR2 closed events from the τ_{c2} to τ_{c1} values by $14.9 \pm 3.1\%$ ($p = 0.002$) and $13.8 \pm 4.7\%$ ($p = 0.024$), respectively, relative to control. It is noteworthy that the effect of β_{1a} on the dwell time distributions is different between RyR1 and RyR2. In particular, a fraction of RyR1 open events shifted from τ_{o1} to τ_{o2} values and a fraction of RyR1 closed events shifted from τ_{c3} to τ_{c1} values, which differ from the RyR2 time constants that had their fractions shifted in response to β_{1a} subunit, as mentioned above. However, the overall effect of this difference between the action of β_{1a} on RyR1 and RyR2 may be small given that the overall effect of 100 nM β_{1a} subunit on RyR1 and RyR2 relative P_o was similar.

Overall, the results indicate β_{1a} subunit increases both RyR1 and RyR2 activity with a slight concentration-dependent effect between 10 and 100 nM β_{1a} in RyR2, but not RyR1, activity. Analysis of the single channel dwell-time distributions suggests that the reduced efficacy is likely attributed to the fact that 10 nM β_{1a} did not increase the fraction of RyR2 openings falling into the longer time constants.

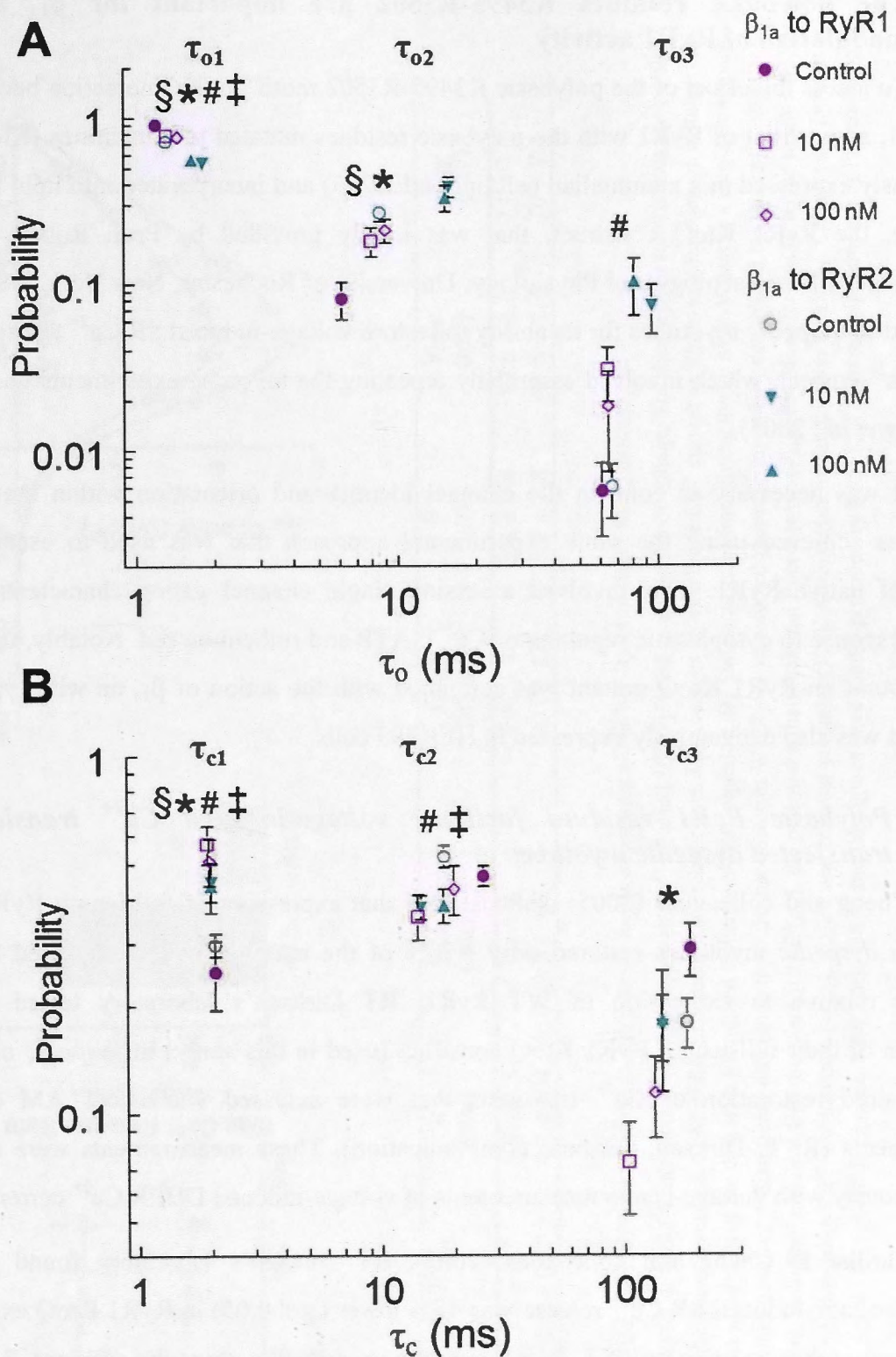


Figure 5.3 The effect of β_{1a} subunit on the RyR1 or RyR2 open and closed dwell-times and on the probability of events occurring within each open and closed dwell-time constant components.

The open (τ_o , **A**) and closed (τ_c , **B**) time constants and the probability of events in each time constant component were calculated from ~ 90 s of single channel activity, $n = 6-12$ channel records. The individual open time constants (τ_{o1} , τ_{o2} and τ_{o3}) and individual closed time constants (τ_{c1} , τ_{c2} and τ_{c3}) are indicated on the graphs in **A** and **B**, respectively. Error bars indicate \pm SEM. §Significant difference between the probability of events in each time constant in control RyR1 and RyR2, determined by Student's t-test, $p < 0.05$. *Significant difference between the probability of events in each time constant group under control conditions and with 10 or 100 nM β_{1a} subunit on RyR1. †Significant difference between the probability of events in each time constant in control and with 10 nM β_{1a} subunit on RyR2. #Significant difference between the probability of events in each time constant in control and with 100 nM β_{1a} subunit on RyR2. *#Significance determined by ANOVA, $p < 0.05$.

5.3.2 The polybasic residues K3495-R3502 are important for β_{1a} subunit modulation of RyR1 activity

To assess the effect of the polybasic K3495-R3502 motif on the interaction between β_{1a} and RyR1, a construct of RyR1 with the polybasic residues mutated to glutamines (KtoQ) was exogenously expressed in a mammalian cell line (HEK293) and incorporated into lipid bilayers. Markedly, the RyR1 KtoQ construct, that was kindly provided by Prof. Robert Dirksen (Department of Pharmacology and Physiology, University of Rochester, New York, USA), was also tested in *dyspedic* myotubes for its ability to restore voltage-induced SR Ca^{2+} transients and DHPR Ca^{2+} current, which involved essentially repeating the myotube experiments undertaken by (Cheng *et al.*, 2005).

It was necessary to confirm the channel identity and orientation within the bilayer, which was achieved using the same experimental approach that was used to establish the identity of native RyR1. This involved assessing single channel gating characteristics and activity response to cytoplasmic regulators: $[\text{Ca}^{2+}]$, ATP and ruthenium red. Notably, the action of β_{1a} subunit on RyR1 KtoQ mutant was compared with the action of β_{1a} on wild type (WT) RyR1 that was also exogenously expressed in HEK293 cells.

5.3.2.1 Polybasic RyR1 residues facilitate voltage-induced Ca^{2+} transients in transfected *dyspedic* myotubes

Cheng and colleagues (2005) demonstrated that expression of full-length RyR1 KtoQ mutant in *dyspedic* myotubes restored only ~50% of the maximal voltage-induced SR Ca^{2+} transients relative to expression of WT RyR1. RT Dirksen's laboratory tested whether expression of their full-length RyR1 KtoQ construct (used in this study) in *dyspedic* myotubes also impaired restoration of Ca^{2+} transients that were assessed via Indo-1 AM confocal measurements (R. T. Dirksen, personal communication). These measurements were obtained simultaneously with voltage-clamp measurements of voltage-induced DHPR Ca^{2+} current.

Similar to Cheng and colleagues (2005), RT Dirksen's laboratory found that the maximal voltage-induced SR Ca^{2+} release was 47% lower ($p < 0.05$) in RyR1 KtoQ expressing *dyspedic* myotubes relative to WT RyR1 expressing *dyspedic* myotube (**Figure 5.4A**). In addition, the maximal Ca^{2+} release rate was significantly reduced ($p < 0.05$) (**Figure 5.4B**), but the midpoint potential (V_{half}) remained the same in RyR1 KtoQ expressing *dyspedic* myotubes (**Figure 4.5Ci**). These findings indicate that RyR1 KtoQ mutant reduces restoration of voltage-induced SR Ca^{2+} release, but not voltage activation of DHPR.

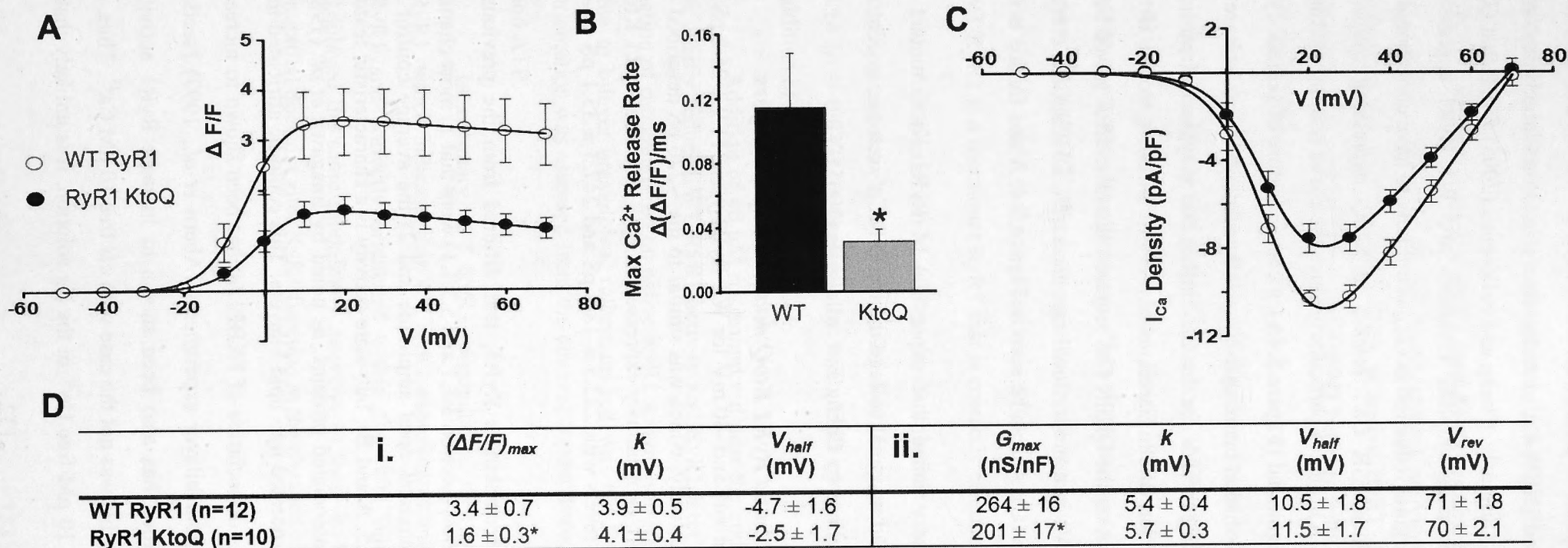


Figure 5. 4 The voltage-induced maximal SR Ca²⁺ release and DHPR Ca²⁺ current in *dyspedic* myotubes expressing either WT RyR1 or RyR1 KtoQ mutant.

Dyspedic myotubes were transfected with either WT RyR1 or RyR1 KtoQ mutant. **A**) Average peak Ca²⁺ release ($\Delta F/F$) plotted as a function of voltage. The data was fit (continuous line) with a Boltzmann function. Error bars indicate \pm SEM. **B**) The average mean \pm SEM of the maximum Ca²⁺ release rate. **C**) Averages of membrane Ca²⁺ current in fibres as a function of voltage. The continuous line between data points represents the least squares fit of the data with a modified Boltzmann-Ohm equation. **D**) The parameters from fitting the i), $\Delta F/F$ -V data to a single Boltzmann function, and ii), I-V data to a modified Boltzmann-Ohm function. * Significant difference from the parameter in WT RyR1 transfected *dyspedic* myotubes, determined by Student's t-test, $p < 0.05$. i) The mean \pm SEM for the Boltzmann parameters, including: maximal Ca²⁺ transient [$(\Delta F/F)_{max}$], the potential at half maximal fluorescence (V_{half}) and slope factor (k). ii) the mean \pm SEM for the modified Boltzmann-Ohm parameters, including: maximum Ca²⁺ conductance (G_{max}), V_{half} , k and reversal potential (V_{rev}). All experiments undertaken by Dr. L. Groom (RT Dirksen's Laboratory, Department of Pharmacology and Physiology, University of Rochester, New York, USA) and the figures were kindly provided by Prof. R. T. Dirksen (Department of Pharmacology and Physiology, University of Rochester, New York, USA)

As shown in **Figure 5.4C**, the density voltage-induced DHPR Ca^{2+} current was largely restored in RyR1 KtoQ expressing *dyspedic* myotubes to levels seen in WT RyR1 expressing myotubes. The maximal voltage-induced DHPR Ca^{2+} conductance (G_{max}) was largely restored, with a slight 24% reduction ($p < 0.05$). Curiously, Cheng and colleagues (2005) found that G_{max} was fully restored in both KtoQ expressing *dyspedic* myotubes and WT RyR1 expressing *dyspedic* myotubes. Regardless, the marginal reduction in G_{max} is unlikely to have contributed to the substantially reduced voltage-induced SR Ca^{2+} release in KtoQ expressing *dyspedic* myotubes (mentioned above; **Figure 5.4A**). This is particularly since the curve relating maximal Ca^{2+} release to voltage (I-V curve) is sigmoidal (**Figure 5.4A**), a classic feature of skeletal-type EC coupling. This is opposed to a bell-shaped curve that classically relates SR Ca^{2+} release to Ca^{2+} influx through the DHPR, following the I-V for the Ca^{2+} influx that is typical of cardiac-type EC coupling (Beuckelmann & Wier, 1988, Garcia *et al.*, 1994). In other words, if the maximal SR Ca^{2+} release was dependent on the DHPR Ca^{2+} current, then the $\Delta F/F$ would have decreased at higher voltages (> 20 mV) in a proportional manner as the DHPR Ca^{2+} current does at these higher voltages (**Figure 5.4C**). As can be seen in **Figure 5.4, A and C**, this is not the case.

Overall, RT Dirksen's laboratory found that expression of RyR1 KtoQ mutant in *dyspedic* myotubes only partially restored maximal voltage-induced SR Ca^{2+} release, in contrast to WT RyR1, which is similar to the findings by Cheng and colleagues (2005).

5.3.2.2 Characteristics of WT RyR1 and RyR1 KtoQ mutant in lipid bilayers

In this study, the conductance at +40 and -40 mV for WT RyR1 was 311.9 ± 25.2 pS ($n = 4$) and 236.5 ± 12.5 pS ($n = 3$), respectively, which was similar to the ~ 220 pS described by Goonasekera *et al.* (2007) for WT RyR1 exogenously expressed in HEK293. The RyR1 KtoQ mutants displayed similar conductance levels with 222.3 ± 18.5 pS and 247.3 ± 33.1 pS at -40 and +40 mV, respectively.

Two notable features of the recombinant RyR1, that differed from the previously characterised native RyR gating properties, (section 3.3.1 and 5.3.1.1) were that 1) most channel openings were to a sub-state of the maximal open amplitude and 2) the average control P_o values were ~ 2 -fold greater (**Figure 5.5, A and B**). Sub-state activity is a characteristic feature of isolated RyR1 that lack the native associated proteins, as noted by Imagawa *et al.* (1987) when RyR1 was first purified and incorporated into lipid bilayers. This could be attributed to a lack of FKBP12.0-RyR1 association, as dissociation of FKBP12.0 has been shown to increase the incidence of sub-state activity in lipid bilayer experiments (Ahern *et al.*, 1997) (section 1.4.3.5). Although FKBP12.0 dissociation has also been shown to increase RyR1 activity, Ahern and colleagues (1997) found that this was not the case with *cis* free $10 \mu\text{M}$ Ca^{2+} . Thus, as experiments here were performed with $10 \mu\text{M}$ free Ca^{2+} in the *cis* solution, it is unlikely that a

lack of associated FKBP12.0 also contributes to the increase in average control P_o values. Given that native RyR have an array of endogenous modulators (section 1.4.3), it is not possible to attribute these features to a particular factor, without further extensive investigations.

5.3.2.3 Response of WT RyR1 and KtoQ mutant to cytoplasmic regulators

WT RyR1 and RyR1 KtoQ mutant activity was modulated by $[Ca^{2+}]$, ATP and ruthenium red in a similar fashion as native RyR1. Indeed, the modulatory effect of these regulators was similar ($p = 0.356-0.894$) between +40 and -40 mV, and consequently the data was combined.

The decrease in *cis* free $[Ca^{2+}]$ from 1 mM to 10 μ M increased WT RyR1 and RyR1 KtoQ relative P_o by 1.7- and 1.6-fold (Log_{10} rel P_o of 0.22 ± 0.06 [$p = 0.013$] and 0.20 ± 0.09 [$p = 0.048$], respectively, $n = 7$). This change in channel activity is similar to that in recombinant WT RyR1 activity in lipid bilayer and [3 H]ryanodine binding experiments (Goonasekera *et al.*, 2007). Furthermore, this is also similar to the increase in native RyR1 activity upon reducing *cis* $[Ca^{2+}]$ from 1 mM to 10 μ M (section 3.3.3.1; Laver *et al.* (1995)). These results suggest that the WT RyR1 is a functional RyR1 that is correctly orientated within the lipid bilayer.

Addition of 2 mM ATP to the *cis* chamber solution increased both WT RyR1 and RyR1 KtoQ mutant activity by 2.2- and 2.5-fold (Log_{10} rel P_o of 0.34 ± 0.12 [$p = 0.032$] and 0.40 ± 0.14 [$p = 0.037$], respectively, $n = 7$). This agrees with the response of native RyR1 to *cis* addition of ATP (section 3.3.3.2).

Addition of 40 μ M ruthenium red near the end of a full experiment typically abolished or greatly reduced WT RyR1 activity and RyR1 KtoQ mutant activity, which agreed with the action of ruthenium red on native RyR1 activity (above). When experiments ended prematurely due to bilayer breakdown, ruthenium red was not tested. In these cases, RyR1 identity and orientation was assessed from the channel conductance and response of P_o to cytoplasmic $[Ca^{2+}]$ and ATP.

In summary, WT RyR1 responded to RyR regulators in the same fashion as native RyR1, which indicates that WT RyR1 experiments analysed in this study were fully functional RyR1 and correctly orientated within the lipid bilayer. Given that RyR1 KtoQ mutants displayed the same modulatory response to these RyR modulators, it is likely that the KtoQ mutation does not alter RyR1 function in the absence of β_{1a} subunit.

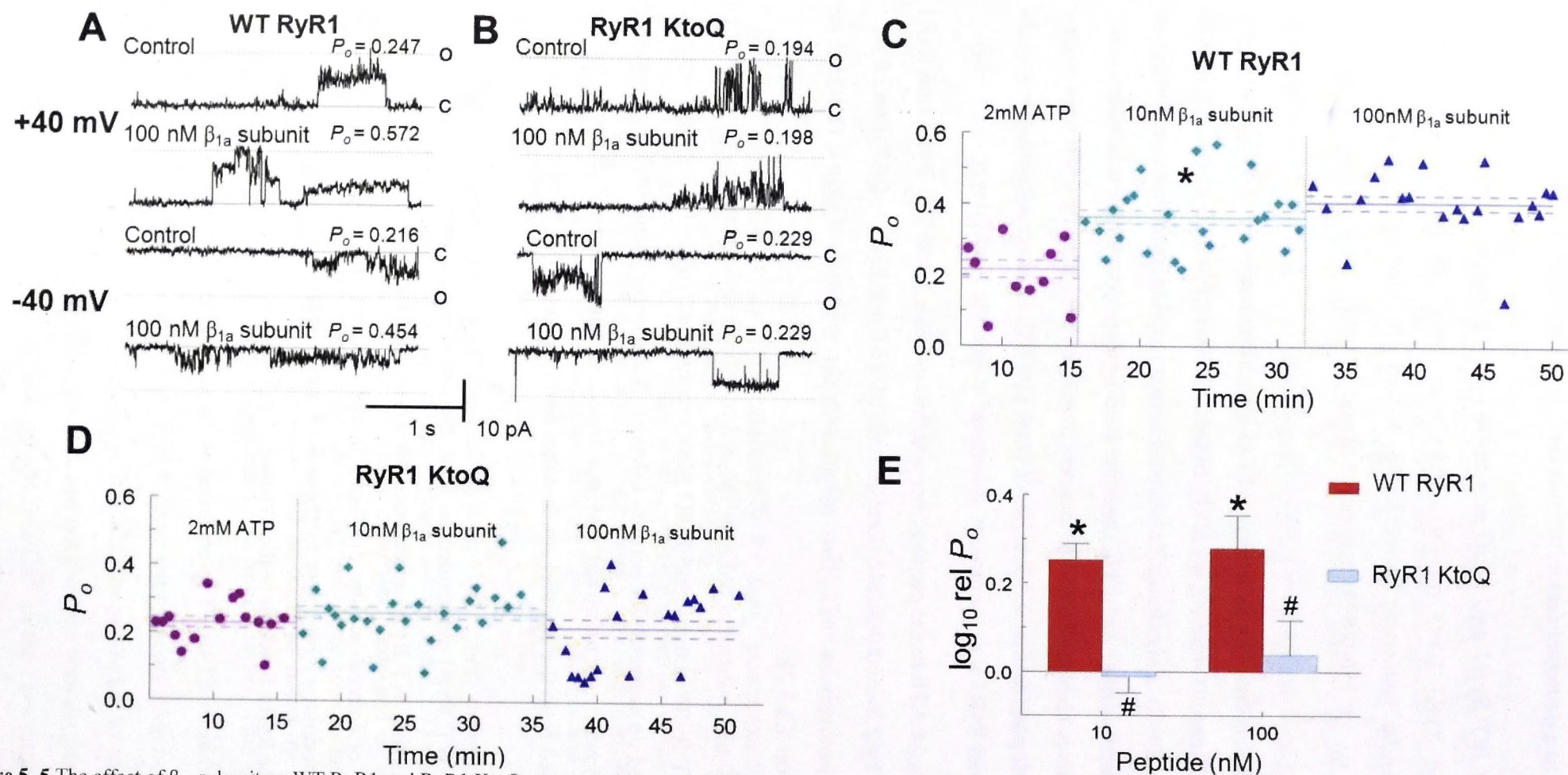


Figure 5.5 The effect of β_{1a} subunit on WT RyR1 and RyR1 KtoQ mutant activity in lipid bilayers.

A and **B**) Three second records of single channel activity at +40 mV (upper) or -40 mV (lower) that display representative channel activity before (top records: control) and after (bottom records) *cis* addition of 100 nM β_{1a} subunit on WT RyR1 (**A**) and RyR1 KtoQ (**B**). Open probability (P_o) is shown in the right top corner. **C**) A timeline of channel activity following sequential *cis* addition of 2 mM ATP (pink circle), 10 nM β_{1a} (green diamonds), 100 nM β_{1a} (blue triangles) and 40 μ M ruthenium red (light green square). The channel activity over 10 s was taken from ~30 s intervals of activity at +40 and -40 mV. For each condition, there is a mean (continuous line) \pm SEM (discontinuous line) of the scatter plot. * Significantly different from prior condition, determined by Student's t-test, $p < 0.05$. **D**) Average relative P_o ($\log_{10} \text{rel } P_o$) was calculated in the same way as Figure 4.4. P_o was measured from ~90 s traces of RyR1 activity, $n = 6$ -14 channel traces. Control P_o values in Tables 5.2. *Significantly different from control activity set at zero, determined using a paired Student's t-test, $p < 0.05$. #Significantly different from $[\beta_{1a}]$ on WT RyR1, determined by ANOVA, $p < 0.05$.

Table 5. 2 Mean control parameters for channels used in analysis of β_{1a} on Wt RyR1 and RyR1 KtoQ.

Open probability (P_o), mean open time (T_o), mean closed time (T_c) and open frequency (F_o) mean \pm SEM and number (n) of observations for data presented in Figure 5.5 and Figure 5.6.

Channel parameter	Control for <i>cis</i> β_{1a} subunit	[subunit] (nM)	Mean Parameter	\pm SEM	<i>n</i>
P_o	WT RyR1	10	0.265	0.041	14
		100	0.255	0.057	9
	RyR1 KtoQ	10	0.197	0.067	11
		100	0.249	0.114	6
T_o (ms)	WT RyR1	10	7.524	1.787	10
		100	11.74	6.050	7
	RyR1 KtoQ	10	16.65	11.79	9
		100	2.935	0.541	6
T_c (ms)	WT RyR1	10	38.43	14.96	11
		100	56.37	25.60	6
	RyR1 KtoQ	10	117.8	38.03	9
		100	78.37	48.84	6
F_o (s^{-1})	WT RyR1	10	33.51	9.295	6
		100	19.20	9.107	4
	RyR1 KtoQ	10	50.99	25.39	9
		100	72.77	35.31	6

5.3.2.4 The RyR1 polybasic K3495-R3502 motif residues are important for β_{1a} subunit modulation of RyR1 activity

Since the WT RyR1 displayed the same regulatory and conductance properties as native RyR1, it was predicted that the action of 10 and 100 nM β_{1a} subunit on WT RyR1 would be similar to that on native RyR1. Therefore, these concentrations were tested. Addition of 100 nM β_{1a} subunit to the *cis* chamber solution typically increased WT RyR1 activity at both voltages (**Figure 5.5, A and B**) within the first 2 minutes of peptide addition. Despite intrinsic variability channel activity over time, the channel activity typically remained activated over the 15-20 min time course following addition of the peptide. This response was not mirrored by RyR1 KtoQ mutants, which was unaffected by addition of 100 nM β_{1a} subunit (**Figure 5.5B**). Over the time course of each experiment, addition of 10 nM β_{1a} subunit increased WT RyR1, not RyR1 KtoQ, activity (**Figure 5.5, C and D**), and this action was not enhanced by addition of 100 nM β_{1a} subunit to WT RyR1 or RyR1 KtoQ (**Figure 5.5C and D**).

The effect of β_{1a} subunit on WT or RyR1 KtoQ did not differ ($p = 0.677-0.991$) between +40 and -40 mV and as a result these values were combined as usual. On average, 10 and 100 nM β_{1a} subunit significantly increased WT RyR1 relative P_o by 1.8- and 1.9-fold ($p \leq 0.006$),

respectively (**Figure 5.5D**). Whereas, RyR1 KtoQ relative P_o was not altered ($p = 0.80$ and 0.21 , respective to 10 and 100 nM) after addition of β_{1a} subunit (**Figure 5.5D**). Thus, the modulatory effect of β_{1a} subunit was lost when the polybasic residues within the K4395-R3502 region were neutralised.

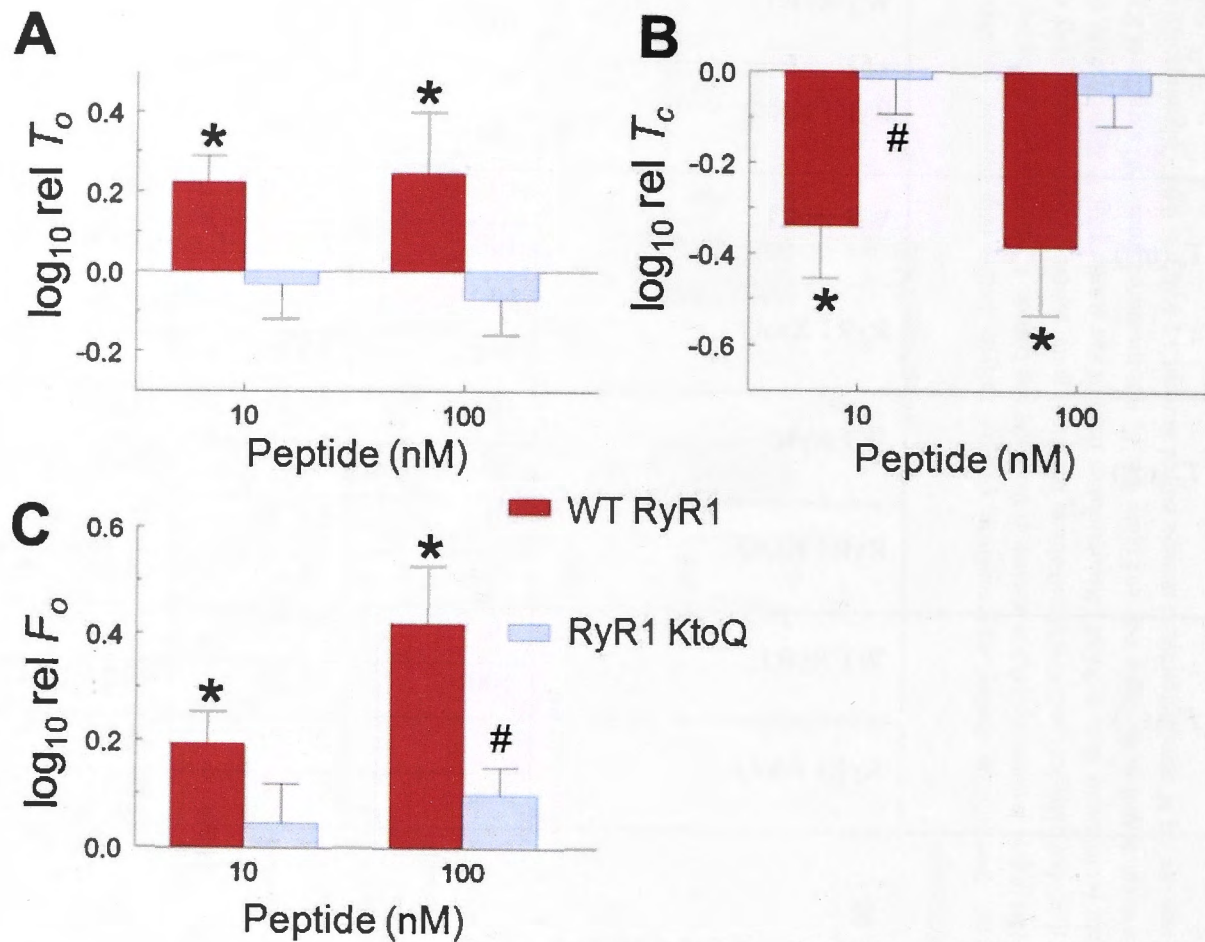


Figure 5. 6 The effect of β_{1a} subunit on WT RyR1 and RyR1 KtoQ single channel gating parameters in lipid bilayers.

The average mean open time (\log_{10} rel T_o ; **A**), mean closed time (\log_{10} rel T_c ; **B**) and open frequency (\log_{10} rel F_o ; **C**) was calculated in the same way as the \log_{10} rel P_o (Figure 4.4) from ~ 90 s of single channel activity, $n = 3-12$ channel traces. Error bars indicate + or SEM. *Significantly different from control activity set at zero, determined using a paired Student's t-test, $p < 0.05$. # Significantly different from the same $[\beta_{1a}]$ on WT RyR1, determined by ANOVA, $p < 0.05$

The response of average single channel gating characteristics reflected the action of the β_{1a} subunit on relative P_o values. Addition of 10 and 100 nM β_{1a} subunit increased single WT RyR1 channel relative T_o and relative F_o values and decreased relative T_c , whereas RyR1 KtoQ channel parameters did not differ from control (**Figure 5.6**). This indicates that the action of β_{1a} subunit in increasing the duration and frequency of channel openings and decreasing the duration between channel openings is lost upon neutralisation of the polybasic residues.

Overall, the action of β_{1a} subunit on WT RyR1 gating is abolished when the polybasic residues are neutralised. Consequently, this indicates that the polybasic residues support the functional effect of the β_{1a} subunit on RyR1 activity.

5.4 Discussion

The focus of the experiments presented in this chapter was to establish whether the functional action of β_{1a} subunit was conserved between RyR1 and RyR2, and to examine the role of the RyR1 polybasic motif in the functional interaction between β_{1a} subunit and RyR1. The effect of the β_{1a} subunit on recombinant RyR1 constructs and native RyR2 was examined in lipid bilayers.

5.4.1 The action of β_{1a} subunit is conserved between RyR1 and RyR2

The results demonstrate that the functional effect of 100 nM β_{1a} subunit was conserved between RyR1 and RyR2 (**Figure 5.1**), however, the modulatory effect of 10 nM β_{1a} was lower in RyR2 activity than RyR1 (**Figure 5.1**). This difference in effect on RyR isoforms is likely due to the binding affinity of 10 nM β_{1a} subunit for RyR2 being lower than its affinity for RyR1. This is opposed to a difference in ability to maximally modulate RyR activity, although this was not specifically tested by increasing β_{1a} to concentrations higher than 100 nM. However, 100 nM β_{1a} imposes the same functional effect on RyR1 and RyR2 gating properties (**Figure 5.1**) and the dwell-time distributions indicated that 10 nM β_{1a} does not increase the fraction of events in the longer open time constant group in RyR2, whereas 100 nM β_{1a} does (**Figure 5.3**).

The implications of these results are that the β_{1a} binding site is likely conserved between RyR1 and RyR2, but with difference in either the binding site or the surrounding region that contributes to a minor reduction in β_{1a} affinity for RyR2 relative to RyR1. It is difficult to extrapolate as to which sequences could account for the affinity difference of β_{1a} , particularly since there is 13.2% complete sequence disparity between RyR1 and RyR2 isoforms, as determined using CLUSTALW multiple alignment (Combet *et al.*, 2000) of rabbit RyR1 (Swiss-Prot: P11716.1) and RyR2 (Swiss-Prot: P30957.3). Markedly, there is emerging evidence that the first of two alternatively spliced regions (ASI(-) lacks residues 3481-3485; section 1.4.2) in RyR1 is modulated by 10 nM β_{1a} in the same manner as RyR2 (Ms. H. Willemse, personal communication). Specifically, the modulatory effect of 10 nM β_{1a} subunit is lower on ASI (-) than ASI (+). This is noteworthy since rabbit (and predicted pig) RyR2 sequence lacks four of the five ASI residues when aligned with rabbit RyR1. It is also noteworthy that the ASI region is nine residues upstream of the RyR1 polybasic motif that has been shown to influence EC coupling and β_{1a} modulation of RyR1 (section 5.3.2; Cheng *et al.* (2005)). Thus, it may be that the altered effect between 10 and 100 nM of β_{1a} subunit on RyR2 is attributed to the lack of ASI region.

5.4.1.1 Physiological relevance and implications

At first glance, conservation of the modulatory effect of β_{1a} subunit on RyR1 and RyR2 does not reflect the *in vivo* situation, particularly as several studies have shown that RyR2 is

unable to replace RyR1 in skeletal EC coupling (Nakai *et al.*, 1997, Protasi *et al.*, 2002). However, as DHPR tetrads are not formed in RyR2 expressing dyspedic myotubes (Protasi *et al.*, 2002), it is likely that with β_{1a} anchored to α_{1S} it would not be in a position to interact with RyR2.

5.4.2 Action of the β_{1a} subunit on WT RyR1

It is notable that the effect of the β_{1a} subunit on WT recombinant RyR1 was ~30% lower than its effect on native RyR1 isolated from muscle (Figures 4.19D, 5.1D and 5.5). Given that WT RyR1 gating properties and channel response to RyR modulators were similar to those observed by native RyR1 (sections 3.3.3 and 5.3.1.2), it is unlikely that the difference in β_{1a} modulation would be attributed to a difference in RyR1 structural integrity. Instead, the difference in β_{1a} modulation could be due to native RyR1 associated proteins, such that one or more associated proteins facilitate the interaction between β_{1a} and RyR1. However, it is more likely that the 2-fold larger control P_o contributed to the discrepancy in effect on WT RyR1 and native RyR1, which likely reduced the level of possible activation before reaching the maximal P_o intrinsic to each channel. Evidence for this being the case is that β_{1a} subunit increases recombinant WT RyR1 activity by 3- to 4-fold ($p < 0.05$, $n = 5$ channels), when ATP is not present and the control P_o is ~0.1 (H. Willemse, personal correspondence). Certainly, this level of control activity is more similar to control activity exhibited by native RyR1, than WT RyR1, used in this study. Therefore, it is likely that the β_{1a} -driven modulation of RyR1 activity is independent of RyR1 associated proteins and consequently the interaction between β_{1a} subunit and RyR1 is through a direct interaction between the two proteins.

5.4.3 The importance of the RyR1 polybasic motif for interaction with β_{1a} subunit

The role of the RyR1 polybasic motif for the interaction with β_{1a} subunit was assessed by recording the response of recombinant RyR1 KtoQ activity following addition of β_{1a} subunit. The response of RyR1 KtoQ to cytoplasmic modulators was similar to WT RyR1 (section 5.3.2.2), indicating that the channels were fully functional. This also indicated that neutralisation of the polybasic motif in RyR1 K3495-R3502 abolished the action of β_{1a} subunit on WT RyR1 activity and gating parameters, rather than being a by-product of altered RyR1 integrity. Given that Cheng and colleagues (2005) demonstrated that the polybasic region is important for pull down of β_{1a} subunit by a RyR1 fragment, the results suggest that the action of β_{1a} subunit on RyR1 KtoQ can be attributed to a lack of binding. The importance of the polybasic region is likely through maintaining RyR1 conformation for β_{1a} access to the binding site, rather than forming the direct binding site, particularly because it is unlikely that of the polybasic motif would interact directly with the β_{1a} hydrophobic surface residues.

Given that the effect of β_{1a} on RyR1 and RyR2 activity is similar, it is important to note that the polybasic motif is also largely conserved between RyR isoforms (RyR1 K3495KKRR_R3502; RyR2 K3452MKRK_R3459). This further supports the importance of the polybasic region for the β_{1a} -RyR interaction, which will be discussed further in Section 6.3.

It is of interest that the RyR1 polybasic motif has been implicated in the process of ASI-mediated inter-domain inhibition of RyR1 activity (section 1.4.2) (Kimura *et al.*, 2007, Kimura *et al.*, 2009). Indeed, Kimura and colleagues (2009) found that the propensity of the polybasic motif region to form an α -helix within a peptide corresponding to RyR1 T3471-G3500, was not altered by substituting three of the six basic residues with alanines. Hence, neutralisation of the polybasic motif is more likely to disrupt an inter-domain interaction rather than intrinsic structure of the ASI-polybasic region. It is important to note that both recombinant RyR1, WT RyR1 and RyR1 KtoQ, respond similarly to cytoplasmic $[Ca^{2+}]$ and ATP (section 5.3.2.2). Also, since control activity was quite similar (**Table 5.2**), there were no signs that RyR1 activity was different between WT RyR1 and RyR1 KtoQ constructs without β_{1a} subunit. Thus, the results here differ from the previously suggested involvement of the polybasic motif residues in the intrinsic gating properties of RyR1 by Kimura and colleagues (2005, 2007 and 2009). However, it should be noted that the results in this study do not necessarily disagree with Kimura and colleagues' findings, particularly since Kimura and colleagues (2005, 2007 and 2009) used conditions with cytoplasmic free Ca^{2+} of 100 μ M, whereas 0.01 and 1 mM $[Ca^{2+}]_{cyto}$ were tested here. Nevertheless, the disruption of RyR1 polybasic motif mediated inter-domain interactions may alter β_{1a} access to the binding site on RyR1.

Overall, the RyR1 polybasic motif appears to be essential for the functional interaction between RyR1 and β_{1a} subunit. However, the role of these residues for interaction between β_{1a} and RyR1 is not clear, but may become more apparent with future understanding of the RyR1 structure.

5.4.3.1 Physiological implications

Given that the RyR1 polybasic motif is essential for the functional interaction between RyR1 and β_{1a} subunit, it can be inferred that the influence of the polybasic motif on EC coupling would directly equate to the role of β_{1a} subunit in directly transmitting the EC coupling signal from DHPR to RyR1. Since Cheng and colleagues (2005) and the RT Dirksen's laboratory (as shown in **Figure 5.4**) found neutralisation of the polybasic motif reduced restoration of voltage-induced maximal Ca^{2+} transients by ~50% in *dyspedic* myotubes, this suggests that β_{1a} subunit contribute to 50% of the EC coupling signal transmission.

5.5 Conclusion

The results presented in this chapter indicate the β_{1a} binding site is conserved between RyR1 and RyR2 and that this region is greatly influenced by the polybasic motif in the RyRs. A physiological implication is that the isoform specificity for RyR1, not RyR2, of skeletal EC coupling is unlikely to be attributed to a specific interaction between β_{1a} subunit and RyR1. Furthermore, the influence of the RyR1 polybasic residues on skeletal EC coupling is likely due to enabling the direct activation of RyR1 activity by β_{1a} subunit. In addition, the results, in combination with the literature, support the theory that the interaction between DHPR and RyR1 is multifaceted with more than β_{1a} subunit directly transmitting the EC coupling signal from DHPR to RyR1 during EC coupling.

CHAPTER SIX – GENERAL DISCUSSION

6.1 Introduction

EC coupling in skeletal muscle fibres requires a physical interaction between DHPR and RyR1, although many of the physical components of this interaction are unknown. Both the α_{1S} subunit and β_{1a} subunit of the DHPR are essential for EC coupling, but whether these subunits are directly involved in transmitting the EC coupling signal to RyR1 is somewhat contentious. Though the region of α_{1S} that is important for skeletal EC coupling has been localised to a “critical” region in the II-III loop (Nakai *et al.*, 1998b, Wilkens *et al.*, 2001, Takekura *et al.*, 2004), the corresponding binding site on RyR1 has yet to be discovered. Consequently, whether the II-III loop is directly involved in the interaction or whether this region supports β_{1a} subunit or another associated DHPR protein for the purposes of direct interaction with RyR1 is disputed. In contrast, regions of β_{1a} subunit (V490-M524) and RyR1 (polybasic K3495-R3502 motif) that are important for β_{1a} /RyR1 binding in *in vitro* studies have also been found to strongly influence EC coupling (Beurg *et al.*, 1999a, Cheng *et al.*, 2005, Rebbeck *et al.*, 2011). Furthermore, a peptide corresponding to the β_{1a} subunit 35 residue extreme C-terminus can enhance RyR1 activity in lipid bilayers in a similar fashion as the full length β_{1a} subunit (Rebbeck *et al.*, 2011). Together, these findings highlight the β_{1a} subunit C-terminus as a potential candidate for directly activating RyR1 during EC coupling. However, the degree to which β_{1a} subunit contributes to the DHPR-RyR1 interaction is uncertain, particularly as the β_{1a} subunit has additional roles in α_{1S} membrane expression and DHPR tetrad formation that are both essential for EC coupling (sections 1.3.4.3.1 and 1.3.4.3.3). Thus, distinguishing between the contributions of the β_{1a} to EC coupling has been very difficult in *in vivo* models. It is noteworthy that a heptad repeat motif in the β_{1a} C-terminus has been shown to strongly influence skeletal EC coupling (Sheridan *et al.*, 2004). It is questionable whether the β_{1a} heptad repeat motif and the RyR1 polybasic motif are involved in the modulatory effect of β_{1a} subunit on RyR1. Thus, the focus of this study was to distinguish between the influence of residues and regions of β_{1a} subunit and RyR1 that may be important for the modulatory effect of β_{1a} subunit on RyR1 activity. In investigating the β_{1a} C-terminal residues that are involved in physically binding to RyR1 and modulating channel activity, the novel findings are as follows:

1. Heptad repeat residues do not impact the activating effect of β_{1a} C-terminal residues on RyR1 activity. Alanine substitution of β_{1a} heptad repeat residues (L478, V485 and V492) did not alter the overall activating effect of the β_{1a} A474-A508 peptide on RyR1 activity. This suggests that these residues may not influence EC coupling through facilitating the functional interaction between β_{1a} C-terminal residues and RyR1, but by another mechanism that is not conserved between mammalian and zebrafish EC coupling.

2. The β_{1a} V490-A508 region is sufficient to replicate the modulatory action of β_{1a} subunit on native RyR1 activity. A peptide corresponding to this region activated RyR1 to similar levels observed by the full-length β_{1a} subunit. Hence, the functional effect of the subunit is governed by residues within the V490-A508 region. It is notable that this agrees with *in vivo* studies that show cytoplasmic addition of β_{1a} V490-A508 peptide into adult myofibres enhances maximal Ca^{2+} transients to the same level exhibited by addition of full length β_{1a} subunit (presented in section 4.3.4; Garcia *et al.* (2005), Hernández-Ochoa *et al.* (2014)). Combined, these observations imply that the β_{1a} subunit is involved in EC coupling through interaction with residues within the β_{1a} V490-A508 region.
3. Hydrophobic surface residues are important for direct physical interaction of the β_{1a} C-terminal residues with RyR1. Alanine substitution of all β_{1a} hydrophobic surface residues (L496, L500 and W503) strongly diminished the level of RyR1 pulled down by β_{1a} V490-M524 peptide.
4. Hydrophobic surface residues are essential for functional interaction between β_{1a} and RyR1. Despite residual binding in affinity chromatography, alanine substitution of all β_{1a} hydrophobic surface residues abolished the activation of native RyR1 by the β_{1a} subunit. Curiously, individual alanine substitutions only abolished activation by the β_{1a} V490-M524 peptide at positive, not negative, potentials. Given that the individual and combined alanine substitutions do not alter secondary structure, the role of these residues is likely through their binding to RyR1, not to maintaining structure. The implication of the results is that all three hydrophobic surface residues cooperatively form a hydrophobic binding pocket for binding for RyR1.
5. Activation of RyR by the β_{1a} C-terminal residues is largely conserved between the zebrafish and mouse β_{1a} sequence. The β_{1a} V490-M524 peptide and a peptide of the equivalent zebrafish β_{1a} (V490-L520) sequence both activated native RyR1 to a similar degree, although the effect on native RyR1 activity was slightly lower with 10 nM β_{1a} V490-L520 zf peptide relative to 10 nM β_{1a} V490-M524 peptide. The physiological implications of this finding is that involvement of the β_{1a} C-terminus in EC coupling through directly binding to RyR1 and increasing its activity may be conserved between zebrafish and mice.

In investigating the RyR1 regions that are involved in physically binding to β_{1a} subunit and modulating channel activity, the novel findings are as follows:

1. The modulatory effect of β_{1a} subunit is conserved between RyR1 and RyR2, but with potentially higher affinity for RyR1 than RyR2. It then follows that the β_{1a} binding site is likely to be conserved between RyR1 and RyR2. Given that RyR2 cannot replace

RyR1 for skeletal EC coupling in myotubes, it follows that the improper alignment of DHPR to RyRs when RyR2 is expressed in dyspedic myotubes limits the functional effect of the β_{1a} on RyR2 activity.

2. The RyR1 polybasic motif is important for the modulatory effect of β_{1a} subunit on RyR1 activity. Glutamine mutation of the RyR1 polybasic motif in full-length RyR1 abolished activation of recombinant RyR1 by the β_{1a} subunit. Neutralisation of the polybasic residues with this substitution has been previously shown to largely reduce restoration of skeletal EC coupling in *dyspedic* myotubes and this has been confirmed in RT Dirksen's laboratory with the construct used here (section 5.3.2.1). Consequently, it appears that these residues are important for the full activation of RyR1 by the β_{1a} subunit during EC coupling. This result supports the model that the DHPR transmits the EC coupling signal through multiple pathways, because neutralisation of the residues does not completely abolish skeletal EC coupling.

6.2 Possible mechanism of interaction between RyR1 and β_{1a}

The β_{1a} subunit/peptides likely increase RyR1 activity through ligand binding. There are two results that primarily justify this statement. Firstly, the β_{1a} peptides/subunits increase channel activity within the first 2 min after their addition, which is typical of ligand binding rather than promotion of a post-translational modification. Secondly, the recombinant RyR1 and native RyR1 can be similarly activated by β_{1a} subunit, so that it is unlikely that the action is due to allosteric modification of the RyR1 interaction with, or directly displacing, an endogenous RyR inhibitor.

It should be noted that an effective method to test whether regulation involves ligand binding rather than post-translational modification is to examine whether the effect is reversible following ligand wash out. Washout reversal has been previously tested by replacing the *cis* chamber solution by perfusion after addition of 10 nM β_{1a} V490-M524 peptide with 10 ml of control solution. Although the solution exchange was effectively diluting the peptide concentration to < 10 pM and these concentrations have been shown to not alter RyR1 activity, the increase in channel activity was only reversed to control levels in 50% of channels analysed (Rebbeck *et al.*, 2011). However, this is likely to be due to the time required to reverse the high affinity binding, rather than an irreversible chemical modification or irreversible dissociation of a RyR inhibitor. These possibilities were not pursued further in the present study.

The activation of native RyR1 by β_{1a} V490-M524 is influenced by cytoplasmic $[Ca^{2+}]$, Mg^{2+} and ATP, though this is not straightforward. In the presence of inhibitory levels (≥ 1 mM) of cytosolic Ca^{2+} and Mg^{2+} , RyR1 activation by the peptide is abolished. Furthermore, the presence of ATP is necessary for the activation when *cis* Ca^{2+} is 100 nM (Rebbeck *et al.*, 2011). There are two implications of these results. Firstly, β_{1a} subunit is unable to reverse RyR1

inhibition by $[Ca^{2+}]$ and $[Mg^{2+}]$. This discounts the possibility that the β_{1a} subunit may initiate EC coupling by relieving Mg^{2+} -mediated RyR1 inhibition as suggested by the Mg^{2+} de-repression hypothesis (section 1.4.3.2). Secondly, the channel must be partially activated, by either removal of $[Mg^{2+}]$ inhibition or by ATP-mediated RyR1 activation or $[Ca^{2+}]$ -mediated RyR1 activation, for activation of RyR1 by β_{1a} (Rebbeck *et al.*, 2011).

Overall, the results indicate that β_{1a} binds to the cytoplasmic face of RyR1 and that this interaction induces a conformation change in RyR1 that regulates channel gating. Notably, either the physical or functional interaction of β_{1a} with RyR1 relies on RyR1 being partially activated.

6.3 Possible β_{1a} subunit binding sites on RyR1 and RyR2

Given that the RyR1 binding site on β_{1a} has been localised to the hydrophobic surface residues on β_{1a} , it is logical that the β_{1a} binding partner on RyR2 will also be a hydrophobic site. The results from this study and other studies highlight several regions of RyR1 that are important for its interaction with the β_{1a} subunit. The results in section 5.3.1 demonstrate that RyR activation by the β_{1a} subunit is largely conserved between native RyR1 and RyR2. It is likely that the minor variation between the effect on RyR1 and RyR2 is due to the lack of four-fifths of the ASI region, as discussed in section 5.4.1. Therefore, the binding site is likely conserved between RyR1 and RyR2, and the RyR conformational change resulting from cytosolic binding to the open channel would likely also be the same in the two isoforms. This is somewhat supported by the similarity of the RyR polybasic motif in the isoforms, particularly because the polybasic motif is important for RyR1 activation by β_{1a} , as shown in this study (section 5.3.2).

Another factor to take into consideration when contemplating the β_{1a} binding site is that Cheng and colleagues (2005) identified the β_{1a} binding site in an RyR1 fragment containing residues 3201 and 3661. This RyR1 fragment contains a CaM binding site (within RyR1 region 3614-3643 (Rodney *et al.*, 2001)), which has been localised to a cleft between RyR1 globular domains 3 and 8 (Wagenknecht *et al.*, 1997, Moore *et al.*, 1999, Samso & Wagenknecht, 2002, Cornea *et al.*, 2009), as shown in **Figure 6.1**. Hence, it is likely that the β_{1a} binding site is also localised, or close, to these globular RyR1 domains.

In summary, the results presented in this thesis suggest that the β_{1a} binding site on RyR1 is a hydrophobic pocket that is conserved in RyR1 and RyR2, and is likely influenced by the RyR1 polybasic motif and ASI region. In addition, the β_{1a} binding site is localised to the 3201-3661 residues, which places it approximately at the cleft between globular domains 3 and 8, as shown in **Figure 6.1**.

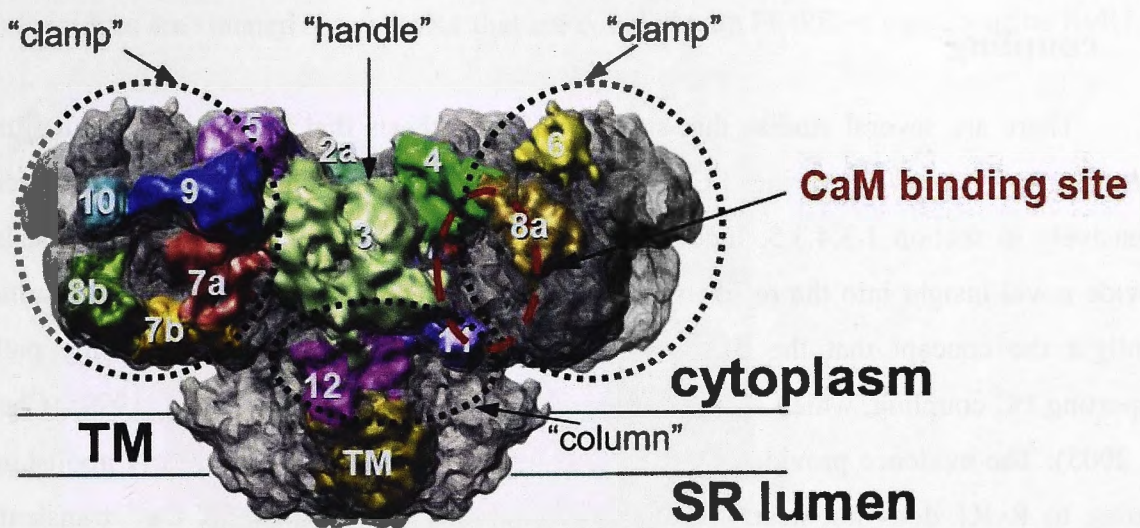


Figure 6. 1 The possible location of β_{1a} binding site on RyR1, as based on CaM binding site.

Suggested localisation of the Ca^{2+} -calmodulin (CaM) binding site (Cornea *et al.*, 2009) on a 9.6Å reconstruction of the RyR1 from single particle analysis of cryo-EM images (Ludtke *et al.*, 2005) that was slightly adapted by Serysheva *et al.* (2008) to include highlighted globular domains of one monomer and RyR1 regions circled. The CaM binding site resides within the sequence of a RyR1 fragment that binds with β_{1a} subunit (Rodney *et al.*, 2001, Cheng *et al.*, 2005). Thus the β_{1a} binding site may also be localised to this general site of the cleft between domains 3 and 8.

6.4 Limitations

The most obvious limitation of this study is that the lipid bilayer conditions do not reflect the entirety of physiological conditions. However, most of the experiments were carried out using native preparations of SR vesicles that included SR membrane embedded proteins and other proteins tightly associated with RyR1. Furthermore, the *cis* $[\text{Ca}^{2+}]$ replicated $[\text{Ca}^{2+}]_{\text{cyto}}$ of a muscle fibre during contraction. On the other hand, the setup does not include many physiological factors that are known to modulate RyR1 activity. This includes Mg^{2+} , factors that maintain chemical modification levels (reducing and oxidising agents, ROS, kinases and phosphatases), DHPR and proteins associated with DHPR. The possibility that these factors could influence the functional interaction between RyR1 and β_{1a} during EC coupling cannot be excluded.

A potential limitation of using peptides is that they may engage in interactions that would not normally occur in physiological conditions, i.e. peptides may provide a binding site that is not accessible under physiological conditions. However, control measures were undertaken to minimise the possibility of a false positive result, which included the use of scrambled peptides, which did not alter RyR1 activity (this study; Rebbeck *et al.* (2011)). Furthermore, there is evidence that the β_{1a} C-terminal peptides enhance RyR1 activity and voltage-induced SR Ca^{2+} transients in adult myofibres to the same level as the full length β_{1a} subunit (this study; Garcia *et al.* (2005), Rebbeck *et al.* (2011), Hernández-Ochoa *et al.* (2014)).

6.5 Proposed role of β_{1a} subunit and RyR1 interaction in skeletal EC coupling

There are several studies that support the hypothesis that the β_{1a} C-terminus directly increases RyR1 activity during EC coupling through its binding to RyR1, as discussed extensively in section 1.3.4.3.5. Indeed, the results in this thesis support this hypothesis and provide novel insight into the residues/regions responsible for the interaction. The results also highlight the concept that the β_{1a} subunit C-terminal interaction is not the only pathway supporting EC coupling, which agrees with several other studies (Beurg *et al.*, 1999a, Cheng *et al.*, 2005). The evidence provided by the other studies demonstrates that nearly abolishing β_{1a} binding to RyR1 does not nearly abolish EC coupling, as maximal SR Ca^{2+} transients are restored to 50% of the WT RyR1 level when the RyR1 KtoQ mutant is expressed in *dyspedic* myotubes (Cheng *et al.*, 2005). Given that neutralisation of the polybasic motif in full-length RyR1 abolishes the functional interaction between β_{1a} subunit and RyR1 (this study), the failure of the mutant to abolish EC coupling suggests that the direct interaction between RyR1 and the β_{1a} subunit may contribute to only 50% of the maximal Ca^{2+} transient during EC coupling.

Several studies and the results presented here support the prospect of β_{1a} subunit directly enhancing RyR1 activity during EC coupling (discussed above), but structural studies in the current literature do not clearly indicate whether the β_{1a} subunit is localised in a position where it can interact with the cleft between globular domains 3 and 8 that is likely to contain the β_{1a} C-terminal binding site (discussed above in section 6.3). Indeed, there is little knowledge of the structure of the N- and C- termini, although known that the extreme tails are sufficiently close (<5 nm) for biomolecular fluorescence complementation (Sheridan *et al.*, 2012). In addition, the termini are suspected to be mostly intrinsically disordered, and in β_{2a} and β_3 are subject to rapid proteolysis in contrast to the highly structured SH3 and GK domains (Opatowsky *et al.*, 2003). However, there is no current evidence to negate the possibility of *in vivo* interaction between β_{1a} subunit and RyR1 globular domains 3 and 8. The current understandings are that the DHPR tetrad is likely localised above globular domains 4 and 6 (Paolini *et al.*, 2004b) and that the β_{1a} N- and C-termini are mostly intrinsically disordered and situated away from the middle of the tetrad (Opatowsky *et al.*, 2003, Sheridan *et al.*, 2012). A model produced by Sheridan and colleagues (2012) has the N- and C-termini directed towards the clamp region of each RyR1 that neighbours the RyR1 aligned with the DHPR tetrad, which is shown in **Figure 6.2B**. Interestingly, there is no experimental evidence that the β_{1a} subunit cannot interact with neighbouring DHPR-uncoupled RyR1. Indeed these arguments raise the possibility that β_{1a} may facilitate activation of the uncoupled RyR1 during EC coupling. Given the uncertainties in the structure of the C-terminus in full length β_{1a} and the regions of RyR1

that align with DHPR during muscle contraction, it is not currently possible to postulate whether the β_{1a} residues are situated above RyR1 that are coupled with DHPR or neighbouring RyR1.

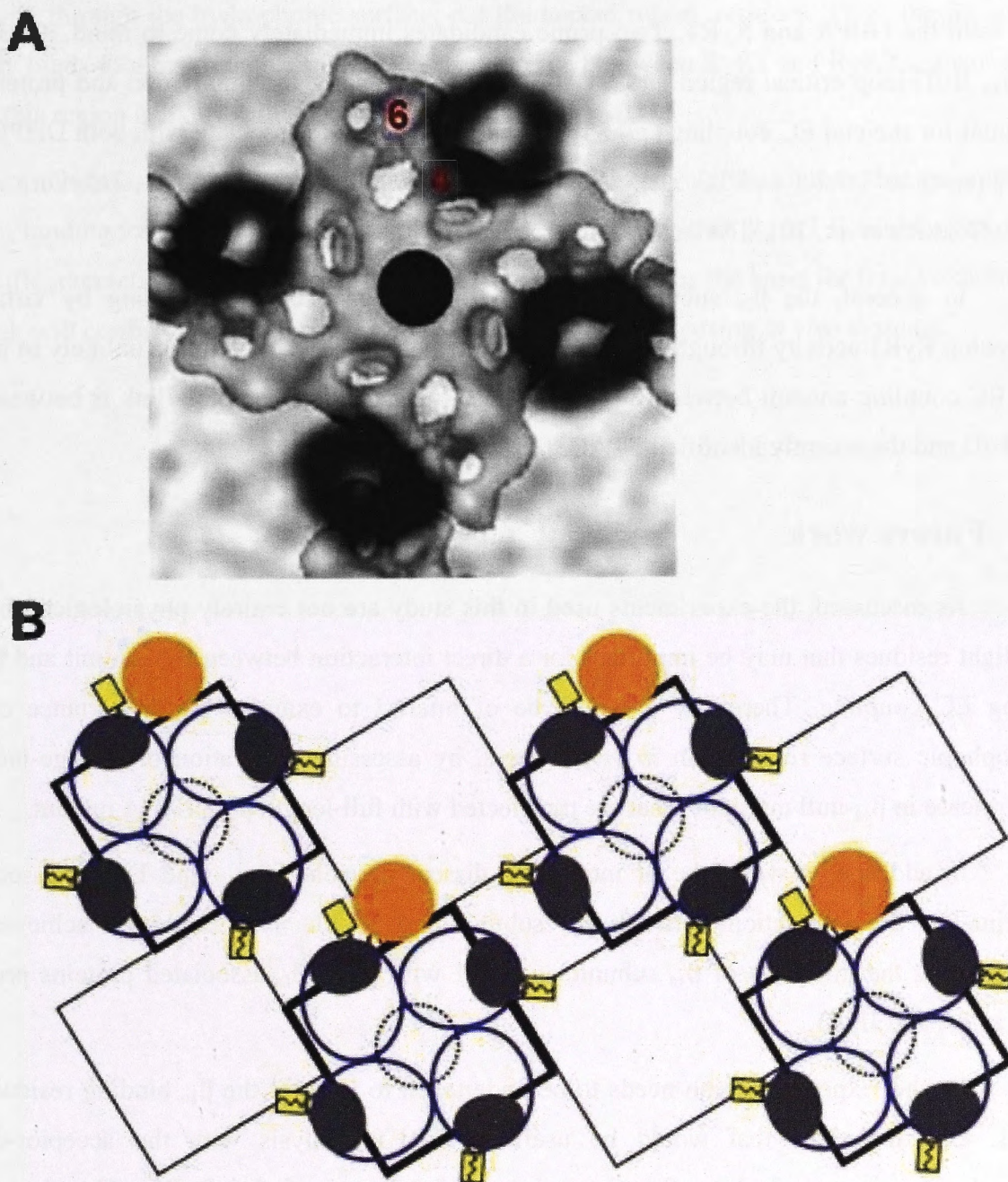


Figure 6. 2 The DHPR tetrad arrangement and possible β_{1a} subunit positioning in relation to RyR1.

A) A scaled superimposition of a DHPR tetrad (black) above a 3-dimensional reconstruction of RyR1 globular domains 4 and 6 in skeletal muscle. Image slightly adapted from Paolini *et al.* (2004b). **B)** A possible model for the arrangement of β_{1a} subunit in DHPR tetrads that juxtapose every second RyR1 (indicated by black squares). The β_{1a} positioning is based on biomolecular fluorescence complementation of the N- and C-termini and gold-streptavidin binding (Sheridan *et al.*, 2012). Each DHPR complex is represented as blue ovals, with the β_{1a} represented as dark grey ovals and protruding grey lines that represent the N and C-termini. The ends of each terminus are sufficiently close for complementation of the yellow fluorescent tag components (yellow rectangle in combined form) attached to each terminus. An orange circle represents the binding of gold streptavidin bound to either terminus. The black squares reflect the RyR1 that are coupled (bold) and uncoupled (thin line) from a DHPR tetrad. Image from Sheridan *et al.* (2012). Notably, Sheridan and colleagues (2012) based this model the DHPR-RyR1 complex model proposed by Wolf *et al.* (2003), but have previously stated that their model takes into account the DHPR tetrad localisation to RyR1 model produced by Paolini and colleagues (2004b) (Leuranguer *et al.*, 2006).

The question arises as to which other junctional proteins transmit the EC coupling signal from DHPR to RyR1. As charge movement within α_{1S} subunit triggers RyR1 activation, the signal transmitter is likely to be a component of the DHPR or a protein that is associated with both the DHPR and RyR1. Two prime candidates immediately come to mind. These are the α_{1S} II-III loop critical region and STAC3, particularly since the this region and protein are essential for skeletal EC coupling and STAC3 has been found to associate with both DHPR and RyR1 (sections 1.3.1.1 and 1.3.5.2)(Nakai *et al.*, 1998b, Wilkens *et al.*, 2001, Takekura *et al.*, 2004, Horstick *et al.*, 2013, Nelson *et al.*, 2013).

In general, the β_{1a} subunit appears to directly enhance EC coupling by virtue of increasing RyR1 activity through a hydrophobic interaction, but β_{1a} subunit is unlikely to be the sole EC coupling conduit between the DHPR and RyR1. Another possible link is between the α_{1S} II-III and the recently identified STAC3.

6.6 Future work

As discussed, the experiments used in this study are not entirely physiological, but do highlight residues that may be important for a direct interaction between β_{1a} subunit and RyR1 during EC coupling. Therefore, it would be of interest to examine the importance of the hydrophobic surface residues an *in vivo* system, by assessing restoration of voltage-induced Ca^{2+} release in β_{1a} -null myotubes that are transfected with full-length β_{1a} LLW/A mutant.

In addition, it would be of interest to dissect the role of α_{1S} and DHPR associated proteins on the interaction between β_{1a} subunit and RyR1. This could be achieved by investigating the influence of β_{1a} subunit on RyR1 with other β_{1a} -associated proteins present, such as α_{1S} and JP-45.

Further experimentation needs to be undertaken to identify the β_{1a} binding residues on RyR1. One technique that would be useful is FRET analysis with the acceptor-donor fluorophore pairs attached to β_{1a} C-terminus and regions of the RyR1. This has been successfully employed to identify the binding location of FKBP12.6 on RyR1 (Girgenrath *et al.*, 2013), and may be applicable for identifying the β_{1a} binding region on RyR1. An alternative approach would be to undertake pull-down assays using smaller fragments of a β_{1a} binding RyR1 fragment (3201-3661) that was identified by Cheng and colleagues (2005). A different approach would be to use a proteolysis digest and identify the regions that bound the β_{1a} subunit/peptide using mass spectrometry.

6.7 Conclusion

The results presented in this thesis highlight that the β_{1a} C-terminus modulates RyR1 activity through the hydrophobic surface, not the heptad repeat, residues. Thus, the β_{1a} subunit likely binds to a hydrophobic pocket that is conserved between RyR1 and RyR2 sequences and that this region is likely influenced by the polybasic motif.

Overall, the importance of the work is that by identifying the regions that are important in β_{1a} binding to RyR1, we further substantiate the potential role of β_{1a} in EC coupling through a specific interaction with RyR1. Furthermore, this work provides the basis for future experiments which will confirm the role these residues have in EC coupling using *in vivo* systems.

REFERENCES

- Abdellatif, Y., D. Liu, E.M. Gallant, P.W. Gage, P.G. Board & A.F. Dulhunty, (2007) The Mu class glutathione transferase is abundant in striated muscle and is an isoform-specific regulator of ryanodine receptor calcium channels. *Cell calcium* **41**: 429-440.
- Adams, B.A. & K.G. Beam, (1989) A novel calcium current in dysgenic skeletal muscle. *The Journal of general physiology* **94**: 429-444.
- Adams, B.A., T. Tanabe, A. Mikami, S. Numa & K.G. Beam, (1990) Intramembrane charge movement restored in dysgenic skeletal muscle by injection of dihydropyridine receptor cDNAs. *Nature* **346**: 569-572.
- Adams, B.A. & K.G. Beam, (1991) Contractions of dysgenic skeletal muscle triggered by a potentiated, endogenous calcium current. *The Journal of general physiology* **97**: 687-696.
- Ahern, C.A., D. Bhattacharya, L. Mortenson & R. Coronado, (2001a) A component of excitation-contraction coupling triggered in the absence of the T671-L690 and L720-Q765 regions of the II-III loop of the dihydropyridine receptor alpha(1s) pore subunit. *Biophysical journal* **81**: 3294-3307.
- Ahern, C.A., P.A. Powers, G.H. Biddlecome, L. Roethe, P. Vallejo, L. Mortenson, C. Strube, K.P. Campbell, R. Coronado & R.G. Gregg, (2001b) Modulation of L-type Ca²⁺ current but not activation of Ca²⁺ release by the gamma subunit of the dihydropyridine receptor of skeletal muscle. *BMC physiology* **1**: 8.
- Ahern, C.A., D.C. Sheridan, W. Cheng, L. Mortenson, P. Nataraj, P. Allen, M. De Waard & R. Coronado, (2003) Ca²⁺ current and charge movements in skeletal myotubes promoted by the beta-subunit of the dihydropyridine receptor in the absence of ryanodine receptor type 1. *Biophysical journal* **84**: 942-959.
- Ahern, G.P., P.R. Junankar & A.F. Dulhunty, (1994) Single channel activity of the ryanodine receptor calcium release channel is modulated by FK-506. *FEBS letters* **352**: 369-374.
- Ahern, G.P., P.R. Junankar & A.F. Dulhunty, (1997) Subconductance states in single-channel activity of skeletal muscle ryanodine receptors after removal of FKBP12. *Biophysical journal* **72**: 146-162.
- Almagor, L., O. Chomsky-Hecht, A. Ben-Mocha, D. Hendin-Barak, N. Dascal & J.A. Hirsch, (2012) The role of a voltage-dependent Ca²⁺ channel intracellular linker: a structure-function analysis. *The Journal of neuroscience : the official journal of the Society for Neuroscience* **32**: 7602-7613.
- Altier, C., A. Garcia-Caballero, B. Simms, H. You, L. Chen, J. Walcher, H.W. Tedford, T. Hermosilla & G.W. Zamponi, (2011) The Cavbeta subunit prevents RFP2-mediated ubiquitination and proteasomal degradation of L-type channels. *Nature neuroscience* **14**: 173-180.
- Anderson, A.A., S. Treves, D. Biral, R. Betto, D. Sandona, M. Ronjat & F. Zorzato, (2003) The novel skeletal muscle sarcoplasmic reticulum JP-45 protein. Molecular cloning, tissue distribution, developmental expression, and interaction with alpha 1.1 subunit of the voltage-gated calcium channel. *The Journal of biological chemistry* **278**: 39987-39992.
- Anderson, A.A., X. Altafaj, Z. Zheng, Z.M. Wang, O. Delbono, M. Ronjat, S. Treves & F. Zorzato, (2006) The junctional SR protein JP-45 affects the functional expression of the voltage-dependent Ca²⁺ channel Cav1.1. *Journal of cell science* **119**: 2145-2155.
- Andersson, D.C., M.J. Betzenhauser, S. Reiken, A. Umanskaya, T. Shiomi & A.R. Marks, (2012) Stress-induced increase in skeletal muscle force requires protein kinase A phosphorylation of the ryanodine receptor. *The Journal of physiology* **590**: 6381-6387.
- Angelotti, T. & F. Hofmann, (1996) Tissue-specific expression of splice variants of the mouse voltage-gated calcium channel alpha2/delta subunit. *FEBS letters* **397**: 331-337.

- Aracena, P., G. Sanchez, P. Donoso, S.L. Hamilton & C. Hidalgo, (2003) S-glutathionylation decreases Mg²⁺ inhibition and S-nitrosylation enhances Ca²⁺ activation of RyR1 channels. *The Journal of biological chemistry* **278**: 42927-42935.
- Aracena, P., W. Tang, S.L. Hamilton & C. Hidalgo, (2005) Effects of S-glutathionylation and S-nitrosylation on calmodulin binding to triads and FKBP12 binding to type 1 calcium release channels. *Antioxidants & redox signaling* **7**: 870-881.
- Araya, R., J.L. Liberona, J.C. Cardenas, N. Riveros, M. Estrada, J.A. Powell, M.A. Carrasco & E. Jaimovich, (2003) Dihydropyridine receptors as voltage sensors for a depolarization-evoked, IP3R-mediated, slow calcium signal in skeletal muscle cells. *The Journal of general physiology* **121**: 3-16.
- Arias, J.M., J. Murbartian, I. Vitko, J.H. Lee & E. Perez-Reyes, (2005) Transfer of beta subunit regulation from high to low voltage-gated Ca²⁺ channels. *FEBS letters* **579**: 3907-3912.
- Arikkath, J., C.C. Chen, C. Ahern, V. Allamand, J.D. Flanagan, R. Coronado, R.G. Gregg & K.P. Campbell, (2003) Gamma 1 subunit interactions within the skeletal muscle L-type voltage-gated calcium channels. *The Journal of biological chemistry* **278**: 1212-1219.
- Armstrong, C.M., F.M. Bezanilla & P. Horowicz, (1972) Twitches in the presence of ethylene glycol bis(-aminoethyl ether)-N,N'-tetracetic acid. *Biochimica et biophysica acta* **267**: 605-608.
- Ashley, R.H. & A.J. Williams, (1990) Divalent cation activation and inhibition of single calcium release channels from sheep cardiac sarcoplasmic reticulum. *The Journal of general physiology* **95**: 981-1005.
- Avila, G. & R.T. Dirksen, (2000) Functional impact of the ryanodine receptor on the skeletal muscle L-type Ca(2+) channel. *The Journal of general physiology* **115**: 467-480.
- Avila, G., K.M. O'Connell, L.A. Groom & R.T. Dirksen, (2001) Ca²⁺ release through ryanodine receptors regulates skeletal muscle L-type Ca²⁺ channel expression. *The Journal of biological chemistry* **276**: 17732-17738.
- Avila, G., E.H. Lee, C.F. Perez, P.D. Allen & R.T. Dirksen, (2003) FKBP12 binding to RyR1 modulates excitation-contraction coupling in mouse skeletal myotubes. *The Journal of biological chemistry* **278**: 22600-22608.
- Ball, S.L., M.W. McEnery, A.M. Yunker, H.S. Shin & R.G. Gregg, (2011) Distribution of voltage gated calcium channel beta subunits in the mouse retina. *Brain research* **1412**: 1-8.
- Balog, E.M. & E.M. Gallant, (1999) Modulation of the sarcolemmal L-type current by alteration in SR Ca²⁺ release. *The American journal of physiology* **276**: C128-135.
- Balog, E.M., B.R. Fruen, N.H. Shomer & C.F. Louis, (2001) Divergent effects of the malignant hyperthermia-susceptible Arg(615)-->Cys mutation on the Ca(2+) and Mg(2+) dependence of the RyR1. *Biophysical journal* **81**: 2050-2058.
- Bannister, R.A., M. Grabner & K.G. Beam, (2008) The alpha(1S) III-IV loop influences 1,4-dihydropyridine receptor gating but is not directly involved in excitation-contraction coupling interactions with the type 1 ryanodine receptor. *The Journal of biological chemistry* **283**: 23217-23223.
- Bannister, R.A. & K.G. Beam, (2009) Ryanodine modification of RyR1 retrogradely affects L-type Ca(2+) channel gating in skeletal muscle. *Journal of muscle research and cell motility* **30**: 217-223.
- Bannister, R.A., S. Papadopoulos, C.S. Haarmann & K.G. Beam, (2009) Effects of inserting fluorescent proteins into the alpha1S II-III loop: insights into excitation-contraction coupling. *The Journal of general physiology* **134**: 35-51.
- Beam, K.G., C.M. Knudson & J.A. Powell, (1986) A lethal mutation in mice eliminates the slow calcium current in skeletal muscle cells. *Nature* **320**: 168-170.

- Beard, N.A., M.M. Sakowska, A.F. Dulhunty & D.R. Laver, (2002) Calsequestrin is an inhibitor of skeletal muscle ryanodine receptor calcium release channels. *Biophysical journal* **82**: 310-320.
- Beard, N.A., L. Wei, S.N. Cheung, T. Kimura, M. Varsanyi & A.F. Dulhunty, (2008) Phosphorylation of skeletal muscle calsequestrin enhances its Ca²⁺ binding capacity and promotes its association with junctin. *Cell calcium* **44**: 363-373.
- Bers, D.M., (2002) Cardiac excitation-contraction coupling. *Nature* **415**: 198-205.
- Bertocchini, F., C.E. Ovitt, A. Conti, V. Barone, H.R. Scholer, R. Bottinelli, C. Reggiani & V. Sorrentino, (1997) Requirement for the ryanodine receptor type 3 for efficient contraction in neonatal skeletal muscles. *The EMBO journal* **16**: 6956-6963.
- Beuckelmann, D.J. & W.G. Wier, (1988) Mechanism of release of calcium from sarcoplasmic reticulum of guinea-pig cardiac cells. *The Journal of physiology* **405**: 233-255.
- Beurg, M., M. Sukhareva, C. Strube, P.A. Powers, R.G. Gregg & R. Coronado, (1997) Recovery of Ca²⁺ current, charge movements, and Ca²⁺ transients in myotubes deficient in dihydropyridine receptor beta 1 subunit transfected with beta 1 cDNA. *Biophysical journal* **73**: 807-818.
- Beurg, M., C.A. Ahern, P. Vallejo, M.W. Conklin, P.A. Powers, R.G. Gregg & R. Coronado, (1999a) Involvement of the carboxy-terminus region of the dihydropyridine receptor beta1a subunit in excitation-contraction coupling of skeletal muscle. *Biophysical journal* **77**: 2953-2967.
- Beurg, M., M. Sukhareva, C.A. Ahern, M.W. Conklin, E. Perez-Reyes, P.A. Powers, R.G. Gregg & R. Coronado, (1999b) Differential regulation of skeletal muscle L-type Ca²⁺ current and excitation-contraction coupling by the dihydropyridine receptor beta subunit. *Biophysical journal* **76**: 1744-1756.
- Bhat, M.B., J. Zhao, H. Takeshima & J. Ma, (1997) Functional calcium release channel formed by the carboxyl-terminal portion of ryanodine receptor. *Biophysical journal* **73**: 1329-1336.
- Bichet, D., V. Cornet, S. Geib, E. Carlier, S. Volsen, T. Hoshi, Y. Mori & M. De Waard, (2000) The I-II loop of the Ca²⁺ channel alpha1 subunit contains an endoplasmic reticulum retention signal antagonized by the beta subunit. *Neuron* **25**: 177-190.
- Blaustein, M., Kao, J., Matteson, D., (2004) *Cellular Physiology*. Elsevier, Philadelphia, Pennsylvania.
- Block, B.A., Imagawa T., Campbell K. P. and Franzini-Armstrong C., (1988) Structural Evidence for Direct Interaction between the Molecular Components of the Transverse Tubule/Sarcoplasmic Reticulum Junction in Skeletal Muscle. *The Journal of cell biology* **107**: 2587-2600.
- Boncompagni, S., M. Thomas, J.R. Lopez, P.D. Allen, Q. Yuan, E.G. Kranias, C. Franzini-Armstrong & C.F. Perez, (2012) Triadin/Junctin double null mouse reveals a differential role for Triadin and Junctin in anchoring CASQ to the jSR and regulating Ca(2+) homeostasis. *PloS one* **7**: e39962.
- Bower, N.I., D.G. de la Serrana, N.J. Cole, G.E. Hollway, H.T. Lee, S. Assinder & I.A. Johnston, (2012) Stac3 is required for myotube formation and myogenic differentiation in vertebrate skeletal muscle. *The Journal of biological chemistry* **287**: 43936-43949.
- Brillantes, A.B., K. Ondrias, A. Scott, E. Kobrinsky, E. Ondriasova, M.C. Moschella, T. Jayaraman, M. Landers, B.E. Ehrlich & A.R. Marks, (1994) Stabilization of calcium release channel (ryanodine receptor) function by FK506-binding protein. *Cell* **77**: 513-523.
- Buraei, Z. & J. Yang, (2010) The ss subunit of voltage-gated Ca²⁺ channels. *Physiological reviews* **90**: 1461-1506.

- Buraei, Z. & J. Yang, (2013) Structure and function of the beta subunit of voltage-gated Ca₂(+ channels. *Biochimica et biophysica acta* **1828**: 1530-1540.
- Burgess, D.L., L.A. Gefrides, P.J. Foreman & J.L. Noebels, (2001) A cluster of three novel Ca₂⁺ channel gamma subunit genes on chromosome 19q13.4: evolution and expression profile of the gamma subunit gene family. *Genomics* **71**: 339-350.
- Campiglio, M., V. Di Biase, P. Tuluc & B.E. Flucher, (2013) Stable incorporation versus dynamic exchange of beta subunits in a native Ca₂⁺ channel complex. *Journal of cell science* **126**: 2092-2101.
- Canato, M., M. Scorzeto, M. Giacomello, F. Protasi, C. Reggiani & G.J. Stienen, (2010) Massive alterations of sarcoplasmic reticulum free calcium in skeletal muscle fibers lacking calsequestrin revealed by a genetically encoded probe. *Proceedings of the National Academy of Sciences of the United States of America* **107**: 22326-22331.
- Carbonneau, L., D. Bhattacharya, D.C. Sheridan & R. Coronado, (2005) Multiple loops of the dihydropyridine receptor pore subunit are required for full-scale excitation-contraction coupling in skeletal muscle. *Biophysical journal* **89**: 243-255.
- Castellano, A., X. Wei, L. Birnbaumer & E. Perez-Reyes, (1993a) Cloning and expression of a neuronal calcium channel beta subunit. *The Journal of biological chemistry* **268**: 12359-12366.
- Castellano, A., X. Wei, L. Birnbaumer & E. Perez-Reyes, (1993b) Cloning and expression of a third calcium channel beta subunit. *The Journal of biological chemistry* **268**: 3450-3455.
- Caswell, A.H., H.K. Motoike, H. Fan & N.R. Brandt, (1999) Location of ryanodine receptor binding site on skeletal muscle triadin. *Biochemistry* **38**: 90-97.
- Catanzariti, A.M., T.A. Soboleva, D.A. Jans, P.G. Board & R.T. Baker, (2004) An efficient system for high-level expression and easy purification of authentic recombinant proteins. *Protein science : a publication of the Protein Society* **13**: 1331-1339.
- Chamberlain, B.K. & S. Fleischer, (1988) Isolation of canine cardiac sarcoplasmic reticulum. *Methods in enzymology* **157**: 91-99.
- Chen, F., Y. Liu, Y. Sugiura, P.D. Allen, R.G. Gregg & W. Lin, (2011) Neuromuscular synaptic patterning requires the function of skeletal muscle dihydropyridine receptors. *Nature neuroscience* **14**: 570-577.
- Chen, Y.H., M.H. Li, Y. Zhang, L.L. He, Y. Yamada, A. Fitzmaurice, Y. Shen, H. Zhang, L. Tong & J. Yang, (2004) Structural basis of the alpha1-beta subunit interaction of voltage-gated Ca₂⁺ channels. *Nature* **429**: 675-680.
- Chen, Y.H., L.L. He, D.R. Buchanan, Y. Zhang, A. Fitzmaurice & J. Yang, (2009) Functional dissection of the intramolecular Src homology 3-guanylate kinase domain coupling in voltage-gated Ca₂⁺ channel beta-subunits. *FEBS letters* **583**: 1969-1975.
- Cheng, W., X. Altafaj, M. Ronjat & R. Coronado, (2005) Interaction between the dihydropyridine receptor Ca₂⁺ channel beta-subunit and ryanodine receptor type 1 strengthens excitation-contraction coupling. *Proceedings of the National Academy of Sciences of the United States of America* **102**: 19225-19230.
- Chu, P.J., J.K. Larsen, C.C. Chen & P.M. Best, (2004) Distribution and relative expression levels of calcium channel beta subunits within the chambers of the rat heart. *Journal of molecular and cellular cardiology* **36**: 423-434.
- Cohen, R.M., J.D. Foell, R.C. Balijepalli, V. Shah, J.W. Hell & T.J. Kamp, (2005) Unique modulation of L-type Ca₂⁺ channels by short auxiliary beta1d subunit present in cardiac muscle. *American journal of physiology. Heart and circulatory physiology* **288**: H2363-2374.

- Collins, J.H., (1991) Sequence analysis of the ryanodine receptor: possible association with a 12K, FK506-binding immunophilin/protein kinase C inhibitor. *Biochemical and biophysical research communications* **178**: 1288-1290.
- Combet, C., C. Blanchet, C. Geourjon & G. Deleage, (2000) NPS@: network protein sequence analysis. *Trends in biochemical sciences* **25**: 147-150.
- Conti, A., L. Gorza & V. Sorrentino, (1996) Differential distribution of ryanodine receptor type 3 (RyR3) gene product in mammalian skeletal muscles. *The Biochemical journal* **316** (Pt 1): 19-23.
- Copello, J.A., S. Barg, H. Onoue & S. Fleischer, (1997) Heterogeneity of Ca²⁺ gating of skeletal muscle and cardiac ryanodine receptors. *Biophysical journal* **73**: 141-156.
- Cornea, R.L., F. Nitu, S. Gruber, K. Kohler, M. Satzer, D.D. Thomas & B.R. Fruen, (2009) FRET-based mapping of calmodulin bound to the RyR1 Ca²⁺ release channel. *Proceedings of the National Academy of Sciences of the United States of America* **106**: 6128-6133.
- Cornea, R.L., F.R. Nitu, M. Samsó, D.D. Thomas & B.R. Fruen, (2010) Mapping the ryanodine receptor FK506-binding protein subunit using fluorescence resonance energy transfer. *The Journal of biological chemistry* **285**: 19219-19226.
- Cui, Y., H.S. Tae, N.C. Norris, Y. Karunasekara, P. Pouliquin, P.G. Board, A.F. Dulhunty & M.G. Casarotto, (2009) A dihydropyridine receptor alpha1s loop region critical for skeletal muscle contraction is intrinsically unstructured and binds to a SPRY domain of the type 1 ryanodine receptor. *Int J Biochem Cell Biol* **41**: 677-686.
- Curtis, B.M.a.C.W.A., (1984) Purification of the Calcium Antagonist Receptor of the Voltage-Sensitive Calcium Channel from Skeletal Muscle Transverse Tubules. *Biochemistry* **23**: 2113-2118.
- Dainese, M., M. Quarta, A.D. Lyfenko, C. Paolini, M. Canato, C. Reggiani, R.T. Dirksen & F. Protasi, (2009) Anesthetic- and heat-induced sudden death in calsequestrin-1-knockout mice. *FASEB journal : official publication of the Federation of American Societies for Experimental Biology* **23**: 1710-1720.
- Damiani, E., P. Volpe & A. Margreth, (1990) Coexpression of two isoforms of calsequestrin in rabbit slow-twitch muscle. *Journal of muscle research and cell motility* **11**: 522-530.
- Dayal, A., J. Schredelseker, C. Franzini-Armstrong & M. Grabner, (2010) Skeletal muscle excitation-contraction coupling is independent of a conserved heptad repeat motif in the C-terminus of the DHPRbeta(1a) subunit. *Cell calcium* **47**: 500-506.
- Dayal, A., V. Bhat, C. Franzini-Armstrong & M. Grabner, (2013) Domain cooperativity in the beta1a subunit is essential for dihydropyridine receptor voltage sensing in skeletal muscle. *Proceedings of the National Academy of Sciences of the United States of America* **110**: 7488-7493.
- De Crescenzo, V., K.E. Fogarty, J.J. Lefkowitz, K.D. Bellve, E. Zvaritch, D.H. MacLennan & J.V. Walsh, Jr., (2012) Type 1 ryanodine receptor knock-in mutation causing central core disease of skeletal muscle also displays a neuronal phenotype. *Proceedings of the National Academy of Sciences of the United States of America* **109**: 610-615.
- De Waard, M., M. Pragnell & K.P. Campbell, (1994) Ca²⁺ channel regulation by a conserved beta subunit domain. *Neuron* **13**: 495-503.
- De Waard, M., D.R. Witcher, M. Pragnell, H. Liu & K.P. Campbell, (1995) Properties of the alpha 1-beta anchoring site in voltage-dependent Ca²⁺ channels. *The Journal of biological chemistry* **270**: 12056-12064.
- Delbono, O., J. Xia, S. Treves, Z.M. Wang, R. Jimenez-Moreno, A.M. Payne, M.L. Messi, A. Brigue, F. Schaerer, M. Nishi, H. Takeshima & F. Zorzato, (2007) Loss of skeletal muscle strength by ablation of the sarcoplasmic reticulum protein JP45. *Proceedings of the National Academy of Sciences of the United States of America* **104**: 20108-20113.

- Di Biase, V. & C. Franzini-Armstrong, (2005) Evolution of skeletal type e-c coupling: a novel means of controlling calcium delivery. *The Journal of cell biology* **171**: 695-704.
- Diaz-Sylvester, P.L. & J.A. Copello, (2009) Voltage-dependent modulation of cardiac ryanodine receptors (RyR2) by protamine. *PloS one* **4**: e8315.
- Dirksen, R.T. & K.G. Beam, (1999) Role of calcium permeation in dihydropyridine receptor function. Insights into channel gating and excitation-contraction coupling. *The Journal of general physiology* **114**: 393-403.
- Du, G.G., B. Sandhu, V.K. Khanna, X.H. Guo & D.H. MacLennan, (2002) Topology of the Ca²⁺ release channel of skeletal muscle sarcoplasmic reticulum (RyR1). *Proceedings of the National Academy of Sciences of the United States of America* **99**: 16725-16730.
- Du, G.G., G. Avila, P. Sharma, V.K. Khanna, R.T. Dirksen & D.H. MacLennan, (2004) Role of the sequence surrounding predicted transmembrane helix M4 in membrane association and function of the Ca(2+) release channel of skeletal muscle sarcoplasmic reticulum (ryanodine receptor isoform 1). *The Journal of biological chemistry* **279**: 37566-37574.
- Dulhunty, A.F. & P.W. Gage, (1983) Asymmetrical charge movement in slow- and fast-twitch mammalian muscle fibres in normal and paraplegic rats. *The Journal of physiology* **341**: 213-231.
- Dulhunty, A.F., D. Laver, S.M. Curtis, S. Pace, C. Haarmann & E.M. Gallant, (2001) Characteristics of irreversible ATP activation suggest that native skeletal ryanodine receptors can be phosphorylated via an endogenous CaMKII. *Biophysical journal* **81**: 3240-3252.
- Dulhunty, A.F., C.S. Haarmann, D. Green, D.R. Laver, P.G. Board & M.G. Casarotto, (2002) Interactions between dihydropyridine receptors and ryanodine receptors in striated muscle. *Prog Biophys Mol Biol* **79**: 45-75.
- Dulhunty, A.F., S.M. Curtis, L. Cengia, M. Sakowska & M.G. Casarotto, (2004) Peptide fragments of the dihydropyridine receptor can modulate cardiac ryanodine receptor channel activity and sarcoplasmic reticulum Ca²⁺ release. *The Biochemical journal* **379**: 161-172.
- Dulhunty, A.F., P. Pouliquin, M. Coggan, P.W. Gage & P.G. Board, (2005) A recently identified member of the glutathione transferase structural family modifies cardiac RyR2 substate activity, coupled gating and activation by Ca²⁺ and ATP. *The Biochemical journal* **390**: 333-343.
- El-Hayek, R., B. Antoniu, J. Wang, S.L. Hamilton & N. Ikemoto, (1995) Identification of calcium release-triggering and blocking regions of the II-III loop of the skeletal muscle dihydropyridine receptor. *The Journal of biological chemistry* **270**: 22116-22118.
- El-Hayek, R. & N. Ikemoto, (1998) Identification of the minimum essential region in the II-III loop of the dihydropyridine receptor alpha 1 subunit required for activation of skeletal muscle-type excitation-contraction coupling. *Biochemistry* **37**: 7015-7020.
- Eltit, J.M., W. Feng, J.R. Lopez, I.T. Padilla, I.N. Pessah, T.F. Molinski, B.R. Fruen, P.D. Allen & C.F. Perez, (2010) Ablation of skeletal muscle triadin impairs FKBP12/RyR1 channel interactions essential for maintaining resting cytoplasmic Ca²⁺. *The Journal of biological chemistry* **285**: 38453-38462.
- Eltit, J.M., H. Li, C.W. Ward, T. Molinski, I.N. Pessah, P.D. Allen & J.R. Lopez, (2011) Orthograde dihydropyridine receptor signal regulates ryanodine receptor passive leak. *Proceedings of the National Academy of Sciences of the United States of America* **108**: 7046-7051.
- Eltit, J.M., R.A. Bannister, O. Moua, F. Altamirano, P.M. Hopkins, I.N. Pessah, T.F. Molinski, J.R. Lopez, K.G. Beam & P.D. Allen, (2012) Malignant hyperthermia susceptibility arising from altered resting coupling between the skeletal muscle L-type Ca²⁺ channel

- and the type 1 ryanodine receptor. *Proceedings of the National Academy of Sciences of the United States of America* **109**: 7923-7928.
- Ertel, E.A., K.P. Campbell, M.M. Harpold, F. Hofmann, Y. Mori, E. Perez-Reyes, A. Schwartz, T.P. Snutch, T. Tanabe, L. Birnbaumer, R.W. Tsien & W.A. Catterall, (2000) Nomenclature of voltage-gated calcium channels. *Neuron* **25**: 533-535.
- Fang, K. & H.M. Colecraft, (2011) Mechanism of auxiliary beta-subunit-mediated membrane targeting of L-type (Ca_v1.2) channels. *The Journal of physiology* **589**: 4437-4455.
- Fessenden, J.D., Y. Wang, R.A. Moore, S.R. Chen, P.D. Allen & I.N. Pessah, (2000) Divergent functional properties of ryanodine receptor types 1 and 3 expressed in a myogenic cell line. *Biophysical journal* **79**: 2509-2525.
- Fessenden, J.D. & M. Mahalingam, (2013) Site-specific labeling of the type 1 ryanodine receptor using biarsenical fluorophores targeted to engineered tetracysteine motifs. *PloS one* **8**: e64686.
- Findeisen, F. & D.L. Minor, Jr., (2009) Disruption of the IS6-AID linker affects voltage-gated calcium channel inactivation and facilitation. *The Journal of general physiology* **133**: 327-343.
- Fleischer, S., E.M. Ogunbunmi, M.C. Dixon & E.A. Fleer, (1985) Localization of Ca²⁺ release channels with ryanodine in junctional terminal cisternae of sarcoplasmic reticulum of fast skeletal muscle. *Proceedings of the National Academy of Sciences of the United States of America* **82**: 7256-7259.
- Flucher, B.E., R.G. Weiss & M. Grabner, (2002) Cooperation of two-domain Ca²⁺ channel fragments in triad targeting and restoration of excitation-contraction coupling in skeletal muscle. *Proceedings of the National Academy of Sciences of the United States of America* **99**: 10167-10172.
- Foell, J.D., R.C. Balijepalli, B.P. Delisle, A.M. Yunker, S.L. Robia, J.W. Walker, M.W. McEnery, C.T. January & T.J. Kamp, (2004) Molecular heterogeneity of calcium channel beta-subunits in canine and human heart: evidence for differential subcellular localization. *Physiological genomics* **17**: 183-200.
- Franzini-Armstrong, C. & K.R. Porter, (1964) Sarcolemmal Invaginations Constituting the T System in Fish Muscle Fibers. *The Journal of cell biology* **22**: 675-696.
- Franzini-Armstrong, C., (1972) Studies of the triad. 3. Structure of the junction in fast twitch fibers. *Tissue Cell* **4**: 469-478.
- Franzini-Armstrong, C., (1973) Studies of the triad. IV. Structure of the junction in frog slow fibers. *The Journal of cell biology* **56**: 120-128.
- Franzini-Armstrong, C., F. Protasi & V. Ramesh, (1998) Comparative ultrastructure of Ca²⁺ release units in skeletal and cardiac muscle. *Annals of the New York Academy of Sciences* **853**: 20-30.
- Freise, D., B. Held, U. Wissenbach, A. Pfeifer, C. Trost, N. Himmerkus, U. Schweig, M. Freichel, M. Biel, F. Hofmann, M. Hoth & V. Flockerzi, (2000) Absence of the gamma subunit of the skeletal muscle dihydropyridine receptor increases L-type Ca²⁺ currents and alters channel inactivation properties. *The Journal of biological chemistry* **275**: 14476-14481.
- Froemming, G.R., B.E. Murray, S. Harmon, D. Pette & K. Ohlendieck, (2000) Comparative analysis of the isoform expression pattern of Ca²⁺-regulatory membrane proteins in fast-twitch, slow-twitch, cardiac, neonatal and chronic low-frequency stimulated muscle fibers. *Biochimica et biophysica acta* **1466**: 151-168.
- Fruen, B.R., E.M. Balog, J. Schafer, F.R. Nitu, D.D. Thomas & R.L. Cornea, (2005) Direct detection of calmodulin tuning by ryanodine receptor channel targets using a Ca²⁺-sensitive acrylodan-labeled calmodulin. *Biochemistry* **44**: 278-284.

- Gach, M.P., G. Cherednichenko, C. Haarmann, J.R. Lopez, K.G. Beam, I.N. Pessah, C. Franzini-Armstrong & P.D. Allen, (2008) Alpha2delta1 dihydropyridine receptor subunit is a critical element for excitation-coupled calcium entry but not for formation of tetrads in skeletal myotubes. *Biophysical journal* **94**: 3023-3034.
- Garcia, J., T. Tanabe & K.G. Beam, (1994) Relationship of calcium transients to calcium currents and charge movements in myotubes expressing skeletal and cardiac dihydropyridine receptors. *The Journal of general physiology* **103**: 125-147.
- Garcia, M.C., E. Carrillo, J.M. Galindo, A. Hernandez, J.A. Copello, M. Fill & J.A. Sanchez, (2005) Short-term regulation of excitation-contraction coupling by the beta1a subunit in adult mouse skeletal muscle. *Biophysical journal* **89**: 3976-3984.
- Garcia, R., E. Carrillo, S. Rebolledo, M.C. Garcia & J.A. Sanchez, (2002) The beta1a subunit regulates the functional properties of adult frog and mouse L-type Ca²⁺ channels of skeletal muscle. *The Journal of physiology* **545**: 407-419.
- Gibbs, G.M., M.J. Scanlon, J. Swarbrick, S. Curtis, E. Gallant, A.F. Dulhunty & M.K. O'Bryan, (2006) The cysteine-rich secretory protein domain of Tpx-1 is related to ion channel toxins and regulates ryanodine receptor Ca²⁺ signaling. *The Journal of biological chemistry* **281**: 4156-4163.
- Girgenrath, T., M. Mahalingam, B. Svensson, F.R. Nitu, R.L. Cornea & J.D. Fessenden, (2013) N-terminal and central segments of the type 1 ryanodine receptor mediate its interaction with FK506-binding proteins. *The Journal of biological chemistry* **288**: 16073-16084.
- Glover, L., K. Culligan, S. Cala, C. Mulvey & K. Ohlendieck, (2001) Calsequestrin binds to monomeric and complexed forms of key calcium-handling proteins in native sarcoplasmic reticulum membranes from rabbit skeletal muscle. *Biochimica et biophysica acta* **1515**: 120-132.
- Golini, L., C. Chouabe, C. Berthier, V. Cusimano, M. Fornaro, R. Bonvallet, L. Formoso, E. Giacomello, V. Jacquemond & V. Sorrentino, (2011) Junctophilin 1 and 2 proteins interact with the L-type Ca²⁺ channel dihydropyridine receptors (DHPRs) in skeletal muscle. *The Journal of biological chemistry* **286**: 43717-43725.
- Goonasekera, S.A., N.A. Beard, L. Groom, T. Kimura, A.D. Lyfenko, A. Rosenfeld, I. Marty, A.F. Dulhunty & R.T. Dirksen, (2007) Triadin binding to the C-terminal luminal loop of the ryanodine receptor is important for skeletal muscle excitation contraction coupling. *The Journal of general physiology* **130**: 365-378.
- Gordon, A.M., E. Homsher & M. Regnier, (2000) Regulation of contraction in striated muscle. *Physiological reviews* **80**: 853-924.
- Gregg, R.G., A. Messing, C. Strube, M. Beurg, R. Moss, M. Behan, M. Sukhareva, S. Haynes, J.A. Powell, R. Coronado & P.A. Powers, (1996) Absence of the beta subunit (cchb1) of the skeletal muscle dihydropyridine receptor alters expression of the alpha 1 subunit and eliminates excitation-contraction coupling. *Proceedings of the National Academy of Sciences of the United States of America* **93**: 13961-13966.
- Groh, S., I. Marty, M. Ottolia, G. Prestipino, A. Chapel, M. Villaz & M. Ronjat, (1999) Functional interaction of the cytoplasmic domain of triadin with the skeletal ryanodine receptor. *The Journal of biological chemistry* **274**: 12278-12283.
- Guo, W. & K.P. Campbell, (1995) Association of triadin with the ryanodine receptor and calsequestrin in the lumen of the sarcoplasmic reticulum. *The Journal of biological chemistry* **270**: 9027-9030.
- Haase, H., A. Kresse, A. Hohaus, H.D. Schulte, M. Maier, K.J. Osterziel, P.E. Lange & I. Morano, (1996) Expression of calcium channel subunits in the normal and diseased human myocardium. *Journal of molecular medicine* **74**: 99-104.

- Hain, J., S. Nath, M. Mayrleitner, S. Fleischer & H. Schindler, (1994) Phosphorylation modulates the function of the calcium release channel of sarcoplasmic reticulum from skeletal muscle. *Biophysical journal* **67**: 1823-1833.
- Hakamata, Y., J. Nakai, H. Takeshima & K. Imoto, (1992) Primary structure and distribution of a novel ryanodine receptor/calcium release channel from rabbit brain. *FEBS letters* **312**: 229-235.
- Hanlon, M.R., N.S. Berrow, A.C. Dolphin & B.A. Wallace, (1999) Modelling of a voltage-dependent Ca²⁺ channel beta subunit as a basis for understanding its functional properties. *FEBS letters* **445**: 366-370.
- Harris, A.J., M.J. Duxson, J.E. Butler, P.W. Hodges, J.L. Taylor & S.C. Gandevia, (2005) Muscle fiber and motor unit behavior in the longest human skeletal muscle. *The Journal of neuroscience : the official journal of the Society for Neuroscience* **25**: 8528-8533.
- Helton, T.D., D.J. Kojetin, J. Cavanagh & W.A. Horne, (2002) Alternative splicing of a beta4 subunit proline-rich motif regulates voltage-dependent gating and toxin block of Cav2.1 Ca²⁺ channels. *The Journal of neuroscience : the official journal of the Society for Neuroscience* **22**: 9331-9339.
- Hernández-Ochoa, Erick O., Rotimi O. Olojo, Robyn T. Rebbeck, Angela F. Dulhunty & Martin F. Schneider, (2014) β 1a490–508, a 19-Residue Peptide from C-Terminal Tail of Cav1.1 β 1a Subunit, Potentiates Voltage-Dependent Calcium Release in Adult Skeletal Muscle Fibers. *Biophysical journal* **106**: 535-547.
- Herrmann, A., M.J. Clague & R. Blumenthal, (1993) Enhancement of viral fusion by nonadsorbing polymers. *Biophysical journal* **65**: 528-534.
- Herzig, S., I.F. Khan, D. Grundemann, J. Matthes, A. Ludwig, G. Michels, U.C. Hoppe, D. Chaudhuri, A. Schwartz, D.T. Yue & R. Hullin, (2007) Mechanism of Ca(v)1.2 channel modulation by the amino terminus of cardiac beta2-subunits. *FASEB journal : official publication of the Federation of American Societies for Experimental Biology* **21**: 1527-1538.
- Hill, J. & E.N. Olson, (2012) Muscle: Fundamental Biology and Mechanisms of Disease. In. Amsterdam: Elsevier Science, pp.
- Hille, B., (2001) *Ion Channels of Excitable Membranes (3rd edn)*. Sinauer Associates, Sunderland, Massachusetts, U.S.A.
- Hochuli, E., H. Dobeli & A. Schacher, (1987) New metal chelate adsorbent selective for proteins and peptides containing neighbouring histidine residues. *Journal of chromatography* **411**: 177-184.
- Hodgkin, A.L. & P. Horowicz, (1960) Potassium contractures in single muscle fibres. *The Journal of physiology* **153**: 386-403.
- Horstick, E.J., J.W. Linsley, J.J. Dowling, M.A. Hauser, K.K. McDonald, A. Ashley-Koch, L. Saint-Amant, A. Satish, W.W. Cui, W. Zhou, S.M. Sprague, D.S. Stamm, C.M. Powell, M.C. Speer, C. Franzini-Armstrong, H. Hirata & J.Y. Kuwada, (2013) Stac3 is a component of the excitation-contraction coupling machinery and mutated in Native American myopathy. *Nature communications* **4**: 1952.
- Hullin, R., D. Singer-Lahat, M. Freichel, M. Biel, N. Dascal, F. Hofmann & V. Flockerzi, (1992) Calcium channel beta subunit heterogeneity: functional expression of cloned cDNA from heart, aorta and brain. *The EMBO journal* **11**: 885-890.
- Hullin, R., I.F. Khan, S. Wirtz, P. Mohacsi, G. Varadi, A. Schwartz & S. Herzig, (2003) Cardiac L-type calcium channel beta-subunits expressed in human heart have differential effects on single channel characteristics. *The Journal of biological chemistry* **278**: 21623-21630.
- Huxley, A.F. & R. Niedergerke, (1954) Structural changes in muscle during contraction; interference microscopy of living muscle fibres. *Nature* **173**: 971-973.

- Huxley, A.F. & R.E. Taylor, (1958) Local activation of striated muscle fibres. *The Journal of physiology* **144**: 426-441.
- Huxley, H. & J. Hanson, (1954) Changes in the cross-striations of muscle during contraction and stretch and their structural interpretation. *Nature* **173**: 973-976.
- Imagawa, T., J.S. Smith, R. Coronado & K.P. Campbell, (1987) Purified ryanodine receptor from skeletal muscle sarcoplasmic reticulum is the Ca²⁺-permeable pore of the calcium release channel. *The Journal of biological chemistry* **262**: 16636-16643.
- Inesi, G. & L. de Meis, (1989) Regulation of steady state filling in sarcoplasmic reticulum. Roles of back-inhibition, leakage, and slippage of the calcium pump. *The Journal of biological chemistry* **264**: 5929-5936.
- Jayaraman, T., A.M. Brillantes, A.P. Timerman, S. Fleischer, H. Erdjument-Bromage, P. Tempst & A.R. Marks, (1992) FK506 binding protein associated with the calcium release channel (ryanodine receptor). *The Journal of biological chemistry* **267**: 9474-9477.
- Jeyakumar, L.H., J.A. Copello, A.M. O'Malley, G.M. Wu, R. Grassucci, T. Wagenknecht & S. Fleischer, (1998) Purification and characterization of ryanodine receptor 3 from mammalian tissue. *The Journal of biological chemistry* **273**: 16011-16020.
- Jeyakumar, L.H., L. Ballester, D.S. Cheng, J.O. McIntyre, P. Chang, H.E. Olivey, L. Rollins-Smith, J.V. Barnett, K. Murray, H.B. Xin & S. Fleischer, (2001) FKBP binding characteristics of cardiac microsomes from diverse vertebrates. *Biochemical and biophysical research communications* **281**: 979-986.
- Jones, L.R., L. Zhang, K. Sanborn, A.O. Jorgensen & J. Kelley, (1995) Purification, primary structure, and immunological characterization of the 26-kDa calsequestrin binding protein (junctin) from cardiac junctional sarcoplasmic reticulum. *The Journal of biological chemistry* **270**: 30787-30796.
- Jorgensen, A.O., A.C. Shen, W. Arnold, A.T. Leung & K.P. Campbell, (1989) Subcellular distribution of the 1,4-dihydropyridine receptor in rabbit skeletal muscle in situ: an immunofluorescence and immunocolloidal gold-labeling study. *The Journal of cell biology* **109**: 135-147.
- Jorquera, G., F. Altamirano, A. Contreras-Ferrat, G. Almarza, S. Buvinic, V. Jacquemond, E. Jaimovich & M. Casas, (2013) Cav1.1 controls frequency-dependent events regulating adult skeletal muscle plasticity. *Journal of cell science* **126**: 1189-1198.
- Kakizawa, S., T. Yamazawa, Y. Chen, A. Ito, T. Murayama, H. Oyamada, N. Kurebayashi, O. Sato, M. Watanabe, N. Mori, K. Oguchi, T. Sakurai, H. Takeshima, N. Saito & M. Iino, (2012) Nitric oxide-induced calcium release via ryanodine receptors regulates neuronal function. *The EMBO journal* **31**: 417-428.
- Kakizawa, S., T. Yamazawa & M. Iino, (2013) Nitric oxide-induced calcium release: activation of type 1 ryanodine receptor by endogenous nitric oxide. *Channels* **7**: 1-5.
- Kandel, E.R., J.H. Schwartz & T.M. Jessell, (2000) Principles of Neural Science. In. U.S.A.: McGraw-Hill, pp.
- Kargacin, G.J., R. Aschar-Sobbi & M.E. Kargacin, (2005) Inhibition of SERCA2 Ca(2+)-ATPases by Cs(+). *Pflugers Arch* **449**: 356-363.
- Karunasekara, Y., R.T. Rebbeck, L.M. Weaver, P.G. Board, A.F. Dulhunty & M.G. Casarotto, (2012) An alpha-helical C-terminal tail segment of the skeletal L-type Ca²⁺ channel beta1a subunit activates ryanodine receptor type 1 via a hydrophobic surface. *FASEB journal : official publication of the Federation of American Societies for Experimental Biology* **26**: 5049-5059.
- Kimlicka, L., K. Lau, C.C. Tung & F. Van Petegem, (2013) Disease mutations in the ryanodine receptor N-terminal region couple to a mobile intersubunit interface. *Nature communications* **4**: 1506.

- Kimura, T., M. Nakamori, J.D. Lueck, P. Pouliquin, F. Aoike, H. Fujimura, R.T. Dirksen, M.P. Takahashi, A.F. Dulhunty & S. Sakoda, (2005) Altered mRNA splicing of the skeletal muscle ryanodine receptor and sarcoplasmic/endoplasmic reticulum Ca²⁺-ATPase in myotonic dystrophy type 1. *Hum Mol Genet* **14**: 2189-2200.
- Kimura, T., S.M. Pace, L. Wei, N.A. Beard, R.T. Dirksen & A.F. Dulhunty, (2007) A variably spliced region in the type 1 ryanodine receptor may participate in an inter-domain interaction. *The Biochemical journal* **401**: 317-324.
- Kimura, T., J.D. Lueck, P.J. Harvey, S.M. Pace, N. Ikemoto, M.G. Casarotto, R.T. Dirksen & A.F. Dulhunty, (2009) Alternative splicing of RyR1 alters the efficacy of skeletal EC coupling. *Cell calcium* **45**: 264-274.
- Kistner, U., C.C. Garner & M. Linial, (1995) Nucleotide binding by the synapse associated protein SAP90. *FEBS letters* **359**: 159-163.
- Knudson, C.M., K.K. Stang, C.R. Moomaw, C.A. Slaughter & K.P. Campbell, (1993) Primary structure and topological analysis of a skeletal muscle-specific junctional sarcoplasmic reticulum glycoprotein (triadin). *The Journal of biological chemistry* **268**: 12646-12654.
- Kugler, G., R.G. Weiss, B.E. Flucher & M. Grabner, (2004) Structural requirements of the dihydropyridine receptor alpha1S II-III loop for skeletal-type excitation-contraction coupling. *The Journal of biological chemistry* **279**: 4721-4728.
- Kupzig, S., D. Bouyoucef, G.E. Cozier & P.J. Cullen, (2006) Studying the spatial and temporal regulation of Ras GTPase-activating proteins. *Methods in enzymology* **407**: 64-82.
- Lai, F.A., H.P. Erickson, E. Rousseau, Q.Y. Liu & G. Meissner, (1988) Purification and reconstitution of the calcium release channel from skeletal muscle. *Nature* **331**: 315-319.
- Lai, F.A., Q.Y. Liu, L. Xu, A. el-Hashem, N.R. Kramarcy, R. Sealock & G. Meissner, (1992) Amphibian ryanodine receptor isoforms are related to those of mammalian skeletal or cardiac muscle. *The American journal of physiology* **263**: C365-372.
- Lamb, G.D. & T. Walsh, (1987) Calcium currents, charge movement and dihydropyridine binding in fast- and slow-twitch muscles of rat and rabbit. *The Journal of physiology* **393**: 595-617.
- Lamb, G.D. & D.G. Stephenson, (1990) Control of calcium release and the effect of ryanodine in skinned muscle fibres of the toad. *The Journal of physiology* **423**: 519-542.
- Lamb, G.D. & D.G. Stephenson, (1991) Excitation-contraction coupling in skeletal muscle fibres of rat and toad in the presence of GTP gamma S. *The Journal of physiology* **444**: 65-84.
- Lamb, G.D. & D.G. Stephenson, (1992) Importance of Mg²⁺ in Excitation-Contraction Coupling in Skeletal Muscle. *News in physiological sciences* **7**: 270-274.
- Lamb, G.D. & D.G. Stephenson, (1994) Effects of intracellular pH and [Mg²⁺] on excitation-contraction coupling in skeletal muscle fibres of the rat. *The Journal of physiology* **478** (Pt 2): 331-339.
- Lanner, J.T., D.K. Georgiou, A.D. Joshi & S.L. Hamilton, (2010) Ryanodine receptors: structure, expression, molecular details, and function in calcium release. *Cold Spring Harbor perspectives in biology* **2**: a003996.
- Laver, D., (2001) The power of single channel recording and analysis: its application to ryanodine receptors in lipid bilayers. *Clin Exp Pharmacol Physiol* **28**: 675-686.
- Laver, D.R., L.D. Roden, G.P. Ahern, K.R. Eager, P.R. Junankar & A.F. Dulhunty, (1995) Cytoplasmic Ca²⁺ inhibits the ryanodine receptor from cardiac muscle. *The Journal of membrane biology* **147**: 7-22.

- Laver, D.R., T.M. Baynes & A.F. Dulhunty, (1997a) Magnesium inhibition of ryanodine-receptor calcium channels: evidence for two independent mechanisms. *The Journal of membrane biology* **156**: 213-229.
- Laver, D.R., V.J. Owen, P.R. Junankar, N.L. Taske, A.F. Dulhunty & G.D. Lamb, (1997b) Reduced inhibitory effect of Mg²⁺ on ryanodine receptor-Ca²⁺ release channels in malignant hyperthermia. *Biophysical journal* **73**: 1913-1924.
- Laver, D.R. & G.D. Lamb, (1998) Inactivation of Ca²⁺ release channels (ryanodine receptors RyR1 and RyR2) with rapid steps in [Ca²⁺] and voltage. *Biophysical journal* **74**: 2352-2364.
- Laver, D.R., K.R. Eager, L. Taoube & G.D. Lamb, (2000) Effects of cytoplasmic and luminal pH on Ca(2+) release channels from rabbit skeletal muscle. *Biophysical journal* **78**: 1835-1851.
- Laver, D.R., G.K. Lenz & G.D. Lamb, (2001) Regulation of the calcium release channel from rabbit skeletal muscle by the nucleotides ATP, AMP, IMP and adenosine. *The Journal of physiology* **537**: 763-778.
- Laver, D.R., E.R. O'Neill & G.D. Lamb, (2004) Luminal Ca²⁺-regulated Mg²⁺ inhibition of skeletal RyRs reconstituted as isolated channels or coupled clusters. *The Journal of general physiology* **124**: 741-758.
- Laver, D.R., (2006) Regulation of ryanodine receptors from skeletal and cardiac muscle during rest and excitation. *Clin Exp Pharmacol Physiol* **33**: 1107-1113.
- Laver, D.R., (2007) Ca²⁺ stores regulate ryanodine receptor Ca²⁺ release channels via luminal and cytosolic Ca²⁺ sites. *Biophysical journal* **92**: 3541-3555.
- Laver, D.R., T. Hamada, J.D. Fessenden & N. Ikemoto, (2007) The ryanodine receptor pore blocker neomycin also inhibits channel activity via a previously undescribed high-affinity Ca(2+) binding site. *The Journal of membrane biology* **220**: 11-20.
- Laver, D.R. & D.F. van Helden, (2011) Three independent mechanisms contribute to tetracaine inhibition of cardiac calcium release channels. *Journal of molecular and cellular cardiology* **51**: 357-369.
- Lee, E.H., J.R. Lopez, J. Li, F. Protasi, I.N. Pessah, D.H. Kim & P.D. Allen, (2004) Conformational coupling of DHPR and RyR1 in skeletal myotubes is influenced by long-range allostereism: evidence for a negative regulatory module. *American journal of physiology. Cell physiology* **286**: C179-189.
- Lee, K.J., J.S. Woo, J.H. Hwang, C. Hyun, C.H. Cho, H. Kim do & E.H. Lee, (2013) STIM1 negatively regulates Ca²⁺ release from the sarcoplasmic reticulum in skeletal myotubes. *The Biochemical journal* **453**: 187-200.
- Leong, P. & D.H. MacLennan, (1998) The cytoplasmic loops between domains II and III and domains III and IV in the skeletal muscle dihydropyridine receptor bind to a contiguous site in the skeletal muscle ryanodine receptor. *The Journal of biological chemistry* **273**: 29958-29964.
- Leuranguer, V., S. Papadopoulos & K.G. Beam, (2006) Organization of calcium channel beta1a subunits in triad junctions in skeletal muscle. *The Journal of biological chemistry* **281**: 3521-3527.
- Liu, Y., S.L. Carroll, M.G. Klein & M.F. Schneider, (1997) Calcium transients and calcium homeostasis in adult mouse fast-twitch skeletal muscle fibers in culture. *The American journal of physiology* **272**: C1919-1927.
- Lorenzon, N.M., C.S. Haarmann, E.E. Norris, S. Papadopoulos & K.G. Beam, (2004) Metabolic biotinylation as a probe of supramolecular structure of the triad junction in skeletal muscle. *The Journal of biological chemistry* **279**: 44057-44064.

- Lorenzon, N.M. & K.G. Beam, (2007) Accessibility of targeted DHPR sites to streptavidin and functional effects of binding on EC coupling. *The Journal of general physiology* **130**: 379-388.
- Ludtke, S.J., Serysheva, II, S.L. Hamilton & W. Chiu, (2005) The pore structure of the closed RyR1 channel. *Structure* **13**: 1203-1211.
- Ludwig, A., V. Flockerzi & F. Hofmann, (1997) Regional expression and cellular localization of the alpha1 and beta subunit of high voltage-activated calcium channels in rat brain. *The Journal of neuroscience : the official journal of the Society for Neuroscience* **17**: 1339-1349.
- Luo, D., H. Sun, R.P. Xiao & Q. Han, (2005) Caffeine induced Ca²⁺ release and capacitative Ca²⁺ entry in human embryonic kidney (HEK293) cells. *European journal of pharmacology* **509**: 109-115.
- Ma, J., M. Fill, C.M. Knudson, K.P. Campbell & R. Coronado, (1988) Ryanodine receptor of skeletal muscle is a gap junction-type channel. *Science* **242**: 99-102.
- Ma, J., (1993) Block by ruthenium red of the ryanodine-activated calcium release channel of skeletal muscle. *The Journal of general physiology* **102**: 1031-1056.
- Ma, J., (1995) Desensitization of the skeletal muscle ryanodine receptor: evidence for heterogeneity of calcium release channels. *Biophysical journal* **68**: 893-899.
- Maier, L.S. & D.M. Bers, (2002) Calcium, calmodulin, and calcium-calmodulin kinase II: heartbeat to heartbeat and beyond. *Journal of molecular and cellular cardiology* **34**: 919-939.
- Maltez, J.M., D.A. Nunziato, J. Kim & G.S. Pitt, (2005) Essential Ca(V)beta modulatory properties are AID-independent. *Nature structural & molecular biology* **12**: 372-377.
- Marieb, E. & K. Hoehn, (2010) *Human anatomy and physiology*. Benjamin Cummings, San Francisco.
- Marty, I., M. Robert, M. Ronjat, I. Bally, G. Arlaud & M. Villaz, (1995) Localization of the N-terminal and C-terminal ends of triadin with respect to the sarcoplasmic reticulum membrane of rabbit skeletal muscle. *The Biochemical journal* **307 (Pt 3)**: 769-774.
- Marty, I., D. Thevenon, C. Scotto, S. Groh, S. Sainnier, M. Robert, D. Grunwald & M. Villaz, (2000) Cloning and characterization of a new isoform of skeletal muscle triadin. *The Journal of biological chemistry* **275**: 8206-8212.
- Meissner, G., (1984) Adenine nucleotide stimulation of Ca²⁺-induced Ca²⁺ release in sarcoplasmic reticulum. *The Journal of biological chemistry* **259**: 2365-2374.
- Meissner, G., (1986) Ryanodine activation and inhibition of the Ca²⁺ release channel of sarcoplasmic reticulum. *The Journal of biological chemistry* **261**: 6300-6306.
- Miledi, R., I. Parker & P.H. Zhu, (1984) Extracellular ions and excitation-contraction coupling in frog twitch muscle fibres. *The Journal of physiology* **351**: 687-710.
- Miller, C. & E. Racker, (1976) Ca⁺⁺-induced fusion of fragmented sarcoplasmic reticulum with artificial planar bilayers. *The Journal of membrane biology* **30**: 283-300.
- Moore, C.P., G. Rodney, J.Z. Zhang, L. Santacruz-Tolozza, G. Strasburg & S.L. Hamilton, (1999) Apocalmodulin and Ca²⁺ calmodulin bind to the same region on the skeletal muscle Ca²⁺ release channel. *Biochemistry* **38**: 8532-8537.
- Most, P., A. Remppis, C. Weber, J. Bernotat, P. Ehlermann, S.T. Pleger, W. Kirsch, M. Weber, D. Uttenweiler, G.L. Smith, H.A. Katus & R.H. Fink, (2003) The C terminus (amino acids 75-94) and the linker region (amino acids 42-54) of the Ca²⁺-binding protein S100A1 differentially enhance sarcoplasmic Ca²⁺ release in murine skinned skeletal muscle fibers. *The Journal of biological chemistry* **278**: 26356-26364.

- Muik, M., R. Schindl, M. Fahrner & C. Romanin, (2012) Ca(2+) release-activated Ca(2+) (CRAC) current, structure, and function. *Cellular and molecular life sciences : CMLS* **69**: 4163-4176.
- Murayama, T., N. Kurebayashi & Y. Ogawa, (1998) Stimulation by polyols of the two ryanodine receptor isoforms of frog skeletal muscle. *Journal of muscle research and cell motility* **19**: 15-24.
- Murphy, R.M., T.L. Dutka, D. Horvath, J.R. Bell, L.M. Delbridge & G.D. Lamb, (2013) Ca²⁺-dependent proteolysis of junctophilin-1 and junctophilin-2 in skeletal and cardiac muscle. *The Journal of physiology* **591**: 719-729.
- Nabhani, T., T. Shah & J. Garcia, (2005) Skeletal muscle cells express different isoforms of the calcium channel alpha2/delta subunit. *Cell biochemistry and biophysics* **42**: 13-20.
- Nakai, J., T. Imagawa, Y. Hakamat, M. Shigekawa, H. Takeshima & S. Numa, (1990) Primary structure and functional expression from cDNA of the cardiac ryanodine receptor/calcium release channel. *FEBS letters* **271**: 169-177.
- Nakai, J., R.T. Dirksen, H.T. Nguyen, I.N. Pessah, K.G. Beam & P.D. Allen, (1996) Enhanced dihydropyridine receptor channel activity in the presence of ryanodine receptor. *Nature* **380**: 72-75.
- Nakai, J., T. Ogura, F. Protasi, C. Franzini-Armstrong, P.D. Allen & K.G. Beam, (1997) Functional nonequivalency of the cardiac and skeletal ryanodine receptors. *Proceedings of the National Academy of Sciences of the United States of America* **94**: 1019-1022.
- Nakai, J., N. Sekiguchi, T.A. Rando, P.D. Allen & K.G. Beam, (1998a) Two regions of the ryanodine receptor involved in coupling with L-type Ca²⁺ channels. *The Journal of biological chemistry* **273**: 13403-13406.
- Nakai, J., T. Tanabe, T. Konno, B. Adams & K.G. Beam, (1998b) Localization in the II-III loop of the dihydropyridine receptor of a sequence critical for excitation-contraction coupling. *The Journal of biological chemistry* **273**: 24983-24986.
- Narita, A., T. Yasunaga, T. Ishikawa, K. Mayanagi & T. Wakabayashi, (2001) Ca(2+)-induced switching of troponin and tropomyosin on actin filaments as revealed by electron cryo-microscopy. *Journal of molecular biology* **308**: 241-261.
- Nelson, B.R., F. Wu, Y. Liu, D.M. Anderson, J. McAnally, W. Lin, S.C. Cannon, R. Bassel-Duby & E.N. Olson, (2013) Skeletal muscle-specific T-tubule protein STAC3 mediates voltage-induced Ca²⁺ release and contractility. *Proceedings of the National Academy of Sciences of the United States of America* **110**: 11881-11886.
- Neuhuber, B., U. Gerster, F. Doring, H. Glossmann, T. Tanabe & B.E. Flucher, (1998a) Association of calcium channel alpha1S and beta1a subunits is required for the targeting of beta1a but not of alpha1S into skeletal muscle triads. *Proceedings of the National Academy of Sciences of the United States of America* **95**: 5015-5020.
- Neuhuber, B., U. Gerster, J. Mitterdorfer, H. Glossmann & B.E. Flucher, (1998b) Differential effects of Ca²⁺ channel beta1a and beta2a subunits on complex formation with alpha1S and on current expression in tsA201 cells. *The Journal of biological chemistry* **273**: 9110-9118.
- Nishi, M., A. Mizushima, K. Nakagawara & H. Takeshima, (2000) Characterization of human junctophilin subtype genes. *Biochemical and biophysical research communications* **273**: 920-927.
- O'Brien, J.J., W. Feng, P.D. Allen, S.R. Chen, I.N. Pessah & K.G. Beam, (2002) Ca²⁺ activation of RyR1 is not necessary for the initiation of skeletal-type excitation-contraction coupling. *Biophysical journal* **82**: 2428-2435.
- Obermair, G.J., G. Kugler, S. Baumgartner, P. Tuluc, M. Grabner & B.E. Flucher, (2005) The Ca²⁺ channel alpha2delta-1 subunit determines Ca²⁺ current kinetics in skeletal muscle

- but not targeting of $\alpha 1S$ or excitation-contraction coupling. *The Journal of biological chemistry* **280**: 2229-2237.
- Ohashi, R., S. Sakata, A. Naito, N. Hirashima & M. Tanaka, (2014) Dendritic differentiation of cerebellar Purkinje cells is promoted by ryanodine receptors expressed by Purkinje and granule cells. *Developmental neurobiology* **74**: 467-480.
- Ohkura, M., K. Furukawa, H. Fujimori, A. Kuruma, S. Kawano, M. Hiraoka, A. Kuniyasu, H. Nakayama & Y. Ohizumi, (1998) Dual regulation of the skeletal muscle ryanodine receptor by triadin and calsequestrin. *Biochemistry* **37**: 12987-12993.
- Olojo, R.O., E.O. Hernandez-Ochoa, N. Ikemoto & M.F. Schneider, (2011) Effects of conformational peptide probe DP4 on bidirectional signaling between DHPR and RyR1 calcium channels in voltage-clamped skeletal muscle fibers. *Biophysical journal* **100**: 2367-2377.
- Ono, F., S. Higashijima, A. Shcherbatko, J.R. Fetcho & P. Brehm, (2001) Paralytic zebrafish lacking acetylcholine receptors fail to localize rapsyn clusters to the synapse. *The Journal of neuroscience : the official journal of the Society for Neuroscience* **21**: 5439-5448.
- Opatowsky, Y., O. Chomsky-Hecht, M.G. Kang, K.P. Campbell & J.A. Hirsch, (2003) The voltage-dependent calcium channel beta subunit contains two stable interacting domains. *The Journal of biological chemistry* **278**: 52323-52332.
- Opatowsky, Y., C.C. Chen, K.P. Campbell & J.A. Hirsch, (2004a) Structural analysis of the voltage-dependent calcium channel beta subunit functional core and its complex with the alpha 1 interaction domain. *Neuron* **42**: 387-399.
- Opatowsky, Y., O. Chomsky-Hecht & J.A. Hirsch, (2004b) Expression, purification and crystallization of a functional core of the voltage-dependent calcium channel beta subunit. *Acta Crystallogr D Biol Crystallogr* **60**: 1301-1303.
- Otsu, K., H.F. Willard, V.K. Khanna, F. Zorzato, N.M. Green & D.H. MacLennan, (1990) Molecular cloning of cDNA encoding the Ca^{2+} release channel (ryanodine receptor) of rabbit cardiac muscle sarcoplasmic reticulum. *The Journal of biological chemistry* **265**: 13472-13483.
- Paolini, C., J.D. Fessenden, I.N. Pessah & C. Franzini-Armstrong, (2004a) Evidence for conformational coupling between two calcium channels. *Proceedings of the National Academy of Sciences of the United States of America* **101**: 12748-12752.
- Paolini, C., F. Protasi & C. Franzini-Armstrong, (2004b) The relative position of RyR feet and DHPR tetrads in skeletal muscle. *Journal of molecular biology* **342**: 145-153.
- Paolini, C., M. Quarta, A. Nori, S. Boncompagni, M. Canato, P. Volpe, P.D. Allen, C. Reggiani & F. Protasi, (2007) Reorganized stores and impaired calcium handling in skeletal muscle of mice lacking calsequestrin-1. *The Journal of physiology* **583**: 767-784.
- Papadopoulos, S., V. Leuranguer, R.A. Bannister & K.G. Beam, (2004) Mapping sites of potential proximity between the dihydropyridine receptor and RyR1 in muscle using a cyan fluorescent protein-yellow fluorescent protein tandem as a fluorescence resonance energy transfer probe. *The Journal of biological chemistry* **279**: 44046-44056.
- Peralvarez-Marin, A., H. Tae, P.G. Board, M.G. Casarotto, A.F. Dulhunty & M. Samsó, (2011) 3D Mapping of the SPRY2 domain of ryanodine receptor 1 by single-particle cryo-EM. *PloS one* **6**: e25813.
- Percival, A.L., A.J. Williams, J.L. Kenyon, M.M. Grinsell, J.A. Airey & J.L. Sutko, (1994) Chicken skeletal muscle ryanodine receptor isoforms: ion channel properties. *Biophysical journal* **67**: 1834-1850.
- Pereon, Y., C. Dettbarn, Y. Lu, K.N. Westlund, J.T. Zhang & P. Palade, (1998) Dihydropyridine receptor isoform expression in adult rat skeletal muscle. *Pflugers Archiv : European journal of physiology* **436**: 309-314.

- Perez-Reyes, E., A. Castellano, H.S. Kim, P. Bertrand, E. Baggstrom, A.E. Lacerda, X.Y. Wei & L. Birnbaumer, (1992) Cloning and expression of a cardiac/brain beta subunit of the L-type calcium channel. *The Journal of biological chemistry* **267**: 1792-1797.
- Perez, C.F., S. Mukherjee & P.D. Allen, (2003) Amino acids 1-1,680 of ryanodine receptor type 1 hold critical determinants of skeletal type for excitation-contraction coupling. Role of divergence domain D2. *The Journal of biological chemistry* **278**: 39644-39652.
- Perez, C.F., M. Thomas & C. Franzini-Armstrong, (2013) Carboxyl-Terminal Domain of DHPR β 1A is Essential for DHPR Tetrad Formation. *Biophysical journal* **104**: 104a-105a.
- Pichler, M., T.N. Cassidy, D. Reimer, H. Haase, R. Kraus, D. Ostler & J. Striessnig, (1997) Beta subunit heterogeneity in neuronal L-type Ca^{2+} channels. *The Journal of biological chemistry* **272**: 13877-13882.
- Pietri-Rouxel, F., C. Gentil, S. Vassilopoulos, D. Baas, E. Mouisel, A. Ferry, A. Vignaud, C. Hourde, I. Marty, L. Schaeffer, T. Voit & L. Garcia, (2010) DHPR alpha1S subunit controls skeletal muscle mass and morphogenesis. *The EMBO journal* **29**: 643-654.
- Polster, A., J.D. Ohrtman, K.G. Beam & S. Papadopoulos, (2012) Fluorescence resonance energy transfer (FRET) indicates that association with the type I ryanodine receptor (RyR1) causes reorientation of multiple cytoplasmic domains of the dihydropyridine receptor (DHPR) alpha(1S) subunit. *The Journal of biological chemistry* **287**: 41560-41568.
- Popova, O.B., M.R. Baker, T.P. Tran, T. Le & Serysheva, II, (2012) Identification of ATP-binding regions in the RyR1 $\text{Ca}(2)(+)$ release channel. *PloS one* **7**: e48725.
- Porter, K.R. & G.E. Palade, (1957) Studies on the endoplasmic reticulum. III. Its form and distribution in striated muscle cells. *J Biophys Biochem Cytol* **3**: 269-300.
- Powell, J.A., F. Rieger, B. Blondet, P. Dreyfus & M. Pincon-Raymond, (1984) Distribution and quantification of ACh receptors and innervation in diaphragm muscle of normal and mdg mouse embryos. *Dev Biol* **101**: 168-180.
- Powers, P.A., S. Liu, K. Hogan & R.G. Gregg, (1992) Skeletal muscle and brain isoforms of a beta-subunit of human voltage-dependent calcium channels are encoded by a single gene. *The Journal of biological chemistry* **267**: 22967-22972.
- Pragnell, M., M. De Waard, Y. Mori, T. Tanabe, T.P. Snutch & K.P. Campbell, (1994) Calcium channel beta-subunit binds to a conserved motif in the I-II cytoplasmic linker of the alpha 1-subunit. *Nature* **368**: 67-70.
- Proenza, C., C.M. Wilkens & K.G. Beam, (2000) Excitation-contraction coupling is not affected by scrambled sequence in residues 681-690 of the dihydropyridine receptor II-III loop. *The Journal of biological chemistry* **275**: 29935-29937.
- Proenza, C., J. O'Brien, J. Nakai, S. Mukherjee, P.D. Allen & K.G. Beam, (2002) Identification of a region of RyR1 that participates in allosteric coupling with the alpha(1S) (Ca(V)1.1) II-III loop. *The Journal of biological chemistry* **277**: 6530-6535.
- Prosser, B.L., N.T. Wright, E.O. Hernandez-Ochoa, K.M. Varney, Y. Liu, R.O. Olojo, D.B. Zimmer, D.J. Weber & M.F. Schneider, (2008) S100A1 binds to the calmodulin-binding site of ryanodine receptor and modulates skeletal muscle excitation-contraction coupling. *The Journal of biological chemistry* **283**: 5046-5057.
- Prosser, B.L., E.O. Hernandez-Ochoa, D.B. Zimmer & M.F. Schneider, (2009) Simultaneous recording of intramembrane charge movement components and calcium release in wild-type and S100A1 $^{-/-}$ muscle fibres. *The Journal of physiology* **587**: 4543-4559.
- Protasi, F., X.H. Sun & C. Franzini-Armstrong, (1996) Formation and maturation of the calcium release apparatus in developing and adult avian myocardium. *Dev Biol* **173**: 265-278.
- Protasi, F., C. Franzini-Armstrong & P.D. Allen, (1998) Role of ryanodine receptors in the assembly of calcium release units in skeletal muscle. *The Journal of cell biology* **140**: 831-842.

- Protasi, F., H. Takekura, Y. Wang, S.R. Chen, G. Meissner, P.D. Allen & C. Franzini-Armstrong, (2000) RYR1 and RYR3 have different roles in the assembly of calcium release units of skeletal muscle. *Biophysical journal* **79**: 2494-2508.
- Protasi, F., C. Paolini, J. Nakai, K.G. Beam, C. Franzini-Armstrong & P.D. Allen, (2002) Multiple regions of RyR1 mediate functional and structural interactions with alpha(1S)-dihydropyridine receptors in skeletal muscle. *Biophysical journal* **83**: 3230-3244.
- Protasi, F., C. Paolini, M. Canato, C. Reggiani & M. Quarta, (2011) Lessons from calsequestrin-1 ablation in vivo: much more than a Ca(2+) buffer after all. *Journal of muscle research and cell motility* **32**: 257-270.
- Querfurth, H.W., N.J. Haughey, S.C. Greenway, P.W. Yacono, D.E. Golan & J.D. Geiger, (1998) Expression of ryanodine receptors in human embryonic kidney (HEK293) cells. *The Biochemical journal* **334 (Pt 1)**: 79-86.
- Ramachandran, S., A. Chakraborty, L. Xu, Y. Mei, M. Samsó, N.V. Dokholyan & G. Meissner, (2013) Structural determinants of skeletal muscle ryanodine receptor gating. *The Journal of biological chemistry* **288**: 6154-6165.
- Rebeck, R.T., Y. Karunasekara, E.M. Gallant, P.G. Board, N.A. Beard, M.G. Casarotto & A.F. Dulhunty, (2011) The beta(1a) subunit of the skeletal DHPR binds to skeletal RyR1 and activates the channel via its 35-residue C-terminal tail. *Biophysical journal* **100**: 922-930.
- Reiken, S., A. Lacampagne, H. Zhou, A. Kherani, S.E. Lehnart, C. Ward, F. Huang, M. Gaburjakova, J. Gaburjakova, N. Rosemlit, M.S. Warren, K.L. He, G.H. Yi, J. Wang, D. Burkhoff, G. Vassort & A.R. Marks, (2003) PKA phosphorylation activates the calcium release channel (ryanodine receptor) in skeletal muscle: defective regulation in heart failure. *The Journal of cell biology* **160**: 919-928.
- Reinholt, B.M., X. Ge, X. Cong, D.E. Gerrard & H. Jiang, (2013) Stac3 is a novel regulator of skeletal muscle development in mice. *PLoS one* **8**: e62760.
- Rezgui, S.S., S. Vassilopoulos, J. Brocard, J.C. Platel, A. Bouron, C. Arnoult, S. Oddoux, L. Garcia, M. De Waard & I. Marty, (2005) Triadin (Trisk 95) overexpression blocks excitation-contraction coupling in rat skeletal myotubes. *The Journal of biological chemistry* **280**: 39302-39308.
- Rios, E. & G. Brum, (1987) Involvement of dihydropyridine receptors in excitation-contraction coupling in skeletal muscle. *Nature* **325**: 717-720.
- Robin, G. & B. Allard, (2012) Dihydropyridine receptors actively control gating of ryanodine receptors in resting mouse skeletal muscle fibres. *The Journal of physiology* **590**: 6027-6036.
- Rodney, G.G., C.P. Moore, B.Y. Williams, J.Z. Zhang, J. Krol, S.E. Pedersen & S.L. Hamilton, (2001) Calcium binding to calmodulin leads to an N-terminal shift in its binding site on the ryanodine Receptor. *The Journal of biological chemistry* **276**: 2069-2074.
- Rousseau, E., J.S. Smith, J.S. Henderson & G. Meissner, (1986) Single channel and $^{45}\text{Ca}^{2+}$ flux measurements of the cardiac sarcoplasmic reticulum calcium channel. *Biophysical journal* **50**: 1009-1014.
- Royer, L., M. Sztretye, C. Manno, S. Pouvreau, J. Zhou, B.C. Knollmann, F. Protasi, P.D. Allen & E. Rios, (2010) Paradoxical buffering of calcium by calsequestrin demonstrated for the calcium store of skeletal muscle. *The Journal of general physiology* **136**: 325-338.
- Rullman, E., D.C. Andersson, M. Melin, S. Reiken, D.M. Mancini, A.R. Marks, L.H. Lund & T. Gustafsson, (2013) Modifications of skeletal muscle ryanodine receptor type 1 and exercise intolerance in heart failure. *The Journal of Heart and Lung Transplantation* **32**: 925-929.

- Ruth, P., A. Rohrkasten, M. Biel, E. Bosse, S. Regulla, H.E. Meyer, V. Flockerzi & F. Hofmann, (1989) Primary structure of the beta subunit of the DHP-sensitive calcium channel from skeletal muscle. *Science* **245**: 1115-1118.
- Saito, A., S. Seiler, A. Chu & S. Fleischer, (1984) Preparation and morphology of sarcoplasmic reticulum terminal cisternae from rabbit skeletal muscle. *The Journal of cell biology* **99**: 875-885.
- Samso, M. & T. Wagenknecht, (2002) Apocalmodulin and Ca²⁺-calmodulin bind to neighboring locations on the ryanodine receptor. *The Journal of biological chemistry* **277**: 1349-1353.
- Samso, M., T. Wagenknecht & P.D. Allen, (2005) Internal structure and visualization of transmembrane domains of the RyR1 calcium release channel by cryo-EM. *Nature structural & molecular biology* **12**: 539-544.
- Samso, M., X. Shen & P.D. Allen, (2006) Structural characterization of the RyR1-FKBP12 interaction. *Journal of molecular biology* **356**: 917-927.
- Samso, M., W. Feng, I.N. Pessah & P.D. Allen, (2009) Coordinated movement of cytoplasmic and transmembrane domains of RyR1 upon gating. *PLoS biology* **7**: e85.
- Sawada, K., E. Hosoi, M. Bando, H. Sakata-Haga, N.S. Lee, Y.G. Jeong & Y. Fukui, (2008) Differential alterations in expressions of ryanodine receptor subtypes in cerebellar cortical neurons of an ataxic mutant, rolling mouse Nagoya. *Neuroscience* **152**: 609-617.
- Schneider, M.F. & W.K. Chandler, (1973) Voltage dependent charge movement of skeletal muscle: a possible step in excitation-contraction coupling. *Nature* **242**: 244-246.
- Schredelseker, J., V. Di Biase, G.J. Obermair, E.T. Felder, B.E. Flucher, C. Franzini-Armstrong & M. Grabner, (2005) The beta 1a subunit is essential for the assembly of dihydropyridine-receptor arrays in skeletal muscle. *Proceedings of the National Academy of Sciences of the United States of America* **102**: 17219-17224.
- Schredelseker, J., A. Dayal, T. Schwerte, C. Franzini-Armstrong & M. Grabner, (2009) Proper restoration of excitation-contraction coupling in the dihydropyridine receptor beta1-null zebrafish relaxed is an exclusive function of the beta1a subunit. *The Journal of biological chemistry* **284**: 1242-1251.
- Schredelseker, J., M. Shrivastav, A. Dayal & M. Grabner, (2010) Non-Ca²⁺-conducting Ca²⁺ channels in fish skeletal muscle excitation-contraction coupling. *Proceedings of the National Academy of Sciences of the United States of America* **107**: 5658-5663.
- Scott, V.E., M. De Waard, H. Liu, C.A. Gurnett, D.P. Venzke, V.A. Lennon & K.P. Campbell, (1996) Beta subunit heterogeneity in N-type Ca²⁺ channels. *The Journal of biological chemistry* **271**: 3207-3212.
- Seok, J.H., L. Xu, N.R. Kramarcy, R. Sealock & G. Meissner, (1992) The 30 S lobster skeletal muscle Ca²⁺ release channel (ryanodine receptor) has functional properties distinct from the mammalian channel proteins. *The Journal of biological chemistry* **267**: 15893-15901.
- Serysheva, II, S.L. Hamilton, W. Chiu & S.J. Ludtke, (2005) Structure of Ca²⁺ release channel at 14 Å resolution. *Journal of molecular biology* **345**: 427-431.
- Serysheva, II, S.J. Ludtke, M.L. Baker, Y. Cong, M. Topf, D. Eramian, A. Sali, S.L. Hamilton & W. Chiu, (2008) Subnanometer-resolution electron cryomicroscopy-based domain models for the cytoplasmic region of skeletal muscle RyR channel. *Proceedings of the National Academy of Sciences of the United States of America* **105**: 9610-9615.
- Shao, Y., K.J. Czymmek, P.A. Jones, V.P. Fomin, K. Akanbi, R.L. Duncan & M.C. Farach-Carson, (2009) Dynamic interactions between L-type voltage-sensitive calcium channel Cav1.2 subunits and ahnak in osteoblastic cells. *American journal of physiology. Cell physiology* **296**: C1067-1078.

- Shen, X., C. Franzini-Armstrong, J.R. Lopez, L.R. Jones, Y.M. Kobayashi, Y. Wang, W.G. Kerrick, A.H. Caswell, J.D. Potter, T. Miller, P.D. Allen & C.F. Perez, (2007) Triadins modulate intracellular Ca(2+) homeostasis but are not essential for excitation-contraction coupling in skeletal muscle. *The Journal of biological chemistry* **282**: 37864-37874.
- Sheridan, D.C., W. Cheng, C.A. Ahern, L. Mortenson, D. Alsammarae, P. Vallejo & R. Coronado, (2003) Truncation of the carboxyl terminus of the dihydropyridine receptor beta1a subunit promotes Ca2+ dependent excitation-contraction coupling in skeletal myotubes. *Biophysical journal* **84**: 220-237.
- Sheridan, D.C., W. Cheng, L. Carbonneau, C.A. Ahern & R. Coronado, (2004) Involvement of a heptad repeat in the carboxyl terminus of the dihydropyridine receptor beta1a subunit in the mechanism of excitation-contraction coupling in skeletal muscle. *Biophysical journal* **87**: 929-942.
- Sheridan, D.C., H. Takekura, C. Franzini-Armstrong, K.G. Beam, P.D. Allen & C.F. Perez, (2006) Bidirectional signaling between calcium channels of skeletal muscle requires multiple direct and indirect interactions. *Proceedings of the National Academy of Sciences of the United States of America* **103**: 19760-19765.
- Sheridan, D.C., O. Moua, N.M. Lorenzon & K.G. Beam, (2012) Bimolecular fluorescence complementation and targeted biotinylation provide insight into the topology of the skeletal muscle Ca (2+) channel beta1a subunit. *Channels* **6**: 26-40.
- Shin, D.W., J. Ma & D.H. Kim, (2000) The asp-rich region at the carboxyl-terminus of calsequestrin binds to Ca(2+) and interacts with triadin. *FEBS letters* **486**: 178-182.
- Siekierka, J.J., M.J. Staruch, S.H. Hung & N.H. Sigal, (1989) FK-506, a potent novel immunosuppressive agent, binds to a cytosolic protein which is distinct from the cyclosporin A-binding protein, cyclophilin. *J Immunol* **143**: 1580-1583.
- Sigworth, F.J. & S.M. Sine, (1987) Data transformations for improved display and fitting of single-channel dwell time histograms. *Biophysical journal* **52**: 1047-1054.
- Simms, B.A. & G.W. Zamponi, (2012) Trafficking and stability of voltage-gated calcium channels. *Cellular and molecular life sciences : CMLS* **69**: 843-856.
- Sitsapesan, R. & A.J. Williams, (1990) Mechanisms of caffeine activation of single calcium-release channels of sheep cardiac sarcoplasmic reticulum. *The Journal of physiology* **423**: 425-439.
- Sitsapesan, R. & A.J. Williams, (1994) Gating of the native and purified cardiac SR Ca(2+)-release channel with monovalent cations as permeant species. *Biophysical journal* **67**: 1484-1494.
- Smith, J.S., R. Coronado & G. Meissner, (1986) Single channel measurements of the calcium release channel from skeletal muscle sarcoplasmic reticulum. Activation by Ca2+ and ATP and modulation by Mg2+. *The Journal of general physiology* **88**: 573-588.
- Smith, J.S., T. Imagawa, J. Ma, M. Fill, K.P. Campbell & R. Coronado, (1988) Purified ryanodine receptor from rabbit skeletal muscle is the calcium-release channel of sarcoplasmic reticulum. *The Journal of general physiology* **92**: 1-26.
- Sonnleitner, A., S. Fleischer & H. Schindler, (1997) Gating of the skeletal calcium release channel by ATP is inhibited by protein phosphatase 1 but not by Mg2+. *Cell calcium* **21**: 283-290.
- Stokes, L., J. Gordon & G. Grafton, (2004) Non-voltage-gated L-type Ca2+ channels in human T cells: pharmacology and molecular characterization of the major alpha pore-forming and auxiliary beta-subunits. *The Journal of biological chemistry* **279**: 19566-19573.
- Strube, C., M. Beurg, P.A. Powers, R.G. Gregg & R. Coronado, (1996) Reduced Ca2+ current, charge movement, and absence of Ca2+ transients in skeletal muscle deficient in dihydropyridine receptor beta 1 subunit. *Biophysical journal* **71**: 2531-2543.

- Strube, C., M. Beurg, M. Sukhareva, C.A. Ahern, J.A. Powell, P.A. Powers, R.G. Gregg & R. Coronado, (1998) Molecular origin of the L-type Ca²⁺ current of skeletal muscle myotubes selectively deficient in dihydropyridine receptor beta1a subunit. *Biophysical journal* **75**: 207-217.
- Sun, Q.A., D.T. Hess, L. Nogueira, S. Yong, D.E. Bowles, J. Eu, K.R. Laurita, G. Meissner & J.S. Stamler, (2011) Oxygen-coupled redox regulation of the skeletal muscle ryanodine receptor-Ca²⁺ release channel by NADPH oxidase 4. *Proceedings of the National Academy of Sciences of the United States of America* **108**: 16098-16103.
- Sun, Q.A., B. Wang, M. Miyagi, D.T. Hess & J.S. Stamler, (2013) Oxygen-coupled Redox Regulation of the Skeletal Muscle Ryanodine Receptor/Ca²⁺ Release Channel (RyR1): SITES AND NATURE OF OXIDATIVE MODIFICATION. *The Journal of biological chemistry* **288**: 22961-22971.
- Szegedi, C., S. Sarkozi, A. Herzog, I. Jona & M. Varsanyi, (1999) Calsequestrin: more than 'only' a luminal Ca²⁺ buffer inside the sarcoplasmic reticulum. *The Biochemical journal* **337 (Pt 1)**: 19-22.
- Szent-Gyorgyi, A.G., (1975) Calcium regulation of muscle contraction. *Biophysical journal* **15**: 707-723.
- Szpyt, J., N. Lorenzon, C.F. Perez, E. Norris, P.D. Allen, K.G. Beam & M. Samsó, (2012) Three-dimensional localization of the alpha and beta subunits and of the II-III loop in the skeletal muscle L-type Ca²⁺ channel. *The Journal of biological chemistry* **287**: 43853-43861.
- Tae, H.S., N.C. Norris, Y. Cui, Y. Karunasekara, P.G. Board, A.F. Dulhunty & M.G. Casarotto, (2009) Molecular recognition of the disordered dihydropyridine receptor II-III loop by a conserved spry domain of the type 1 ryanodine receptor. *Clin Exp Pharmacol Physiol* **36**: 346-349.
- Tae, H.S., Y. Cui, Y. Karunasekara, P.G. Board, A.F. Dulhunty & M.G. Casarotto, (2011) Cyclization of the intrinsically disordered alpha1S dihydropyridine receptor II-III loop enhances secondary structure and in vitro function. *The Journal of biological chemistry* **286**: 22589-22599.
- Takahashi, M., M.J. Seagar, J.F. Jones, B.F.X. Reber & W.A. Catterall, (1987) Subunit Structure of Dihydropyridine-Sensitive Calcium Channels from Skeletal Muscle. *PNAS* **84**: 5478-5482.
- Takekura, H., C. Paolini, C. Franzini-Armstrong, G. Kugler, M. Grabner & B.E. Flucher, (2004) Differential contribution of skeletal and cardiac II-III loop sequences to the assembly of dihydropyridine-receptor arrays in skeletal muscle. *Mol Biol Cell* **15**: 5408-5419.
- Takekura, H., S. Nishimura, T. Matsumoto, H. Ishida, K. Kangawa, N. Minamino, H. Matsuo, M. Ueda, M. Hanaoka, T. Hirose & et al., (1989) Primary structure and expression from complementary DNA of skeletal muscle ryanodine receptor. *Nature* **339**: 439-445.
- Takekura, H., M. Iino, H. Takekura, M. Nishi, J. Kuno, O. Minowa, H. Takano & T. Noda, (1994) Excitation-contraction uncoupling and muscular degeneration in mice lacking functional skeletal muscle ryanodine-receptor gene. *Nature* **369**: 556-559.
- Takekura, H., S. Komazaki, M. Nishi, M. Iino & K. Kangawa, (2000) Junctophilins: a novel family of junctional membrane complex proteins. *Molecular cell* **6**: 11-22.
- Tal, M., A. Silberstein & E. Nusser, (1985) Why does Coomassie Brilliant Blue R interact differently with different proteins? A partial answer. *The Journal of biological chemistry* **260**: 9976-9980.
- Tanabe, T., H. Takekura, A. Mikami, V. Flockerzi, H. Takahashi, K. Kangawa, M. Kojima, H. Matsuo, T. Hirose & S. Numa, (1987) Primary structure of the receptor for calcium channel blockers from skeletal muscle. *Nature* **328**: 313-318.

- Tanabe, T., K.G. Beam, J.A. Powell & S. Numa, (1988) Restoration of excitation-contraction coupling and slow calcium current in dysgenic muscle by dihydropyridine receptor complementary DNA. *Nature* **336**: 134-139.
- Tanabe, T., K.G. Beam, B.A. Adams, T. Niidome & S. Numa, (1990a) Regions of the skeletal muscle dihydropyridine receptor critical for excitation-contraction coupling. *Nature* **346**: 567-569.
- Tanabe, T., A. Mikami, S. Numa & K.G. Beam, (1990b) Cardiac-type excitation-contraction coupling in dysgenic skeletal muscle injected with cardiac dihydropyridine receptor cDNA. *Nature* **344**: 451-453.
- Tanaka, O., H. Sakagami & H. Kondo, (1995) Localization of mRNAs of voltage-dependent Ca(2+)-channels: four subtypes of alpha 1- and beta-subunits in developing and mature rat brain. *Brain research. Molecular brain research* **30**: 1-16.
- Tang, W., C.P. Ingalls, W.J. Durham, J. Snider, M.B. Reid, G. Wu, M.M. Matzuk & S.L. Hamilton, (2004) Altered excitation-contraction coupling with skeletal muscle specific FKBP12 deficiency. *FASEB journal : official publication of the Federation of American Societies for Experimental Biology* **18**: 1597-1599.
- Timerman, A.P., E. Ogunbumni, E. Freund, G. Wiederrecht, A.R. Marks & S. Fleischer, (1993) The calcium release channel of sarcoplasmic reticulum is modulated by FK-506-binding protein. Dissociation and reconstitution of FKBP-12 to the calcium release channel of skeletal muscle sarcoplasmic reticulum. *The Journal of biological chemistry* **268**: 22992-22999.
- Timerman, A.P., G. Wiederrecht, A. Marcy & S. Fleischer, (1995) Characterization of an exchange reaction between soluble FKBP-12 and the FKBP.ryanodine receptor complex. Modulation by FKBP mutants deficient in peptidyl-prolyl isomerase activity. *The Journal of biological chemistry* **270**: 2451-2459.
- Timerman, A.P., H. Onoue, H.B. Xin, S. Barg, J. Copello, G. Wiederrecht & S. Fleischer, (1996) Selective binding of FKBP12.6 by the cardiac ryanodine receptor. *The Journal of biological chemistry* **271**: 20385-20391.
- Treves, S., E. Scutari, M. Robert, S. Groh, M. Ottolia, G. Prestipino, M. Ronjat & F. Zorzato, (1997) Interaction of S100A1 with the Ca²⁺ release channel (ryanodine receptor) of skeletal muscle. *Biochemistry* **36**: 11496-11503.
- Tripathy, A., L. Xu, G. Mann & G. Meissner, (1995) Calmodulin activation and inhibition of skeletal muscle Ca²⁺ release channel (ryanodine receptor). *Biophysical journal* **69**: 106-119.
- Tripathy, A. & G. Meissner, (1996) Sarcoplasmic reticulum lumenal Ca²⁺ has access to cytosolic activation and inactivation sites of skeletal muscle Ca²⁺ release channel. *Biophysical journal* **70**: 2600-2615.
- Ursu, D., S. Seville, B. Dietze, D. Freise, V. Flockerzi & W. Melzer, (2001) Excitation-contraction coupling in skeletal muscle of a mouse lacking the dihydropyridine receptor subunit gamma1. *The Journal of physiology* **533**: 367-377.
- Van Petegem, F., K.A. Clark, F.C. Chatelain & D.L. Minor, Jr., (2004) Structure of a complex between a voltage-gated calcium channel beta-subunit and an alpha-subunit domain. *Nature* **429**: 671-675.
- Van Petegem, F., K.E. Duderstadt, K.A. Clark, M. Wang & D.L. Minor, Jr., (2008) Alanine-scanning mutagenesis defines a conserved energetic hotspot in the CaValpha1 AID-CaVbeta interaction site that is critical for channel modulation. *Structure* **16**: 280-294.
- Vance, C.L., C.M. Begg, W.L. Lee, H. Haase, T.D. Copeland & M.W. McEnery, (1998) Differential expression and association of calcium channel alpha1B and beta subunits during rat brain ontogeny. *The Journal of biological chemistry* **273**: 14495-14502.

- Vassilopoulos, S., D. Thevenon, S.S. Rezgui, J. Brocard, A. Chapel, A. Lacampagne, J. Lunardi, M. Dewaard & I. Marty, (2005) Triadins are not triad-specific proteins: two new skeletal muscle triadins possibly involved in the architecture of sarcoplasmic reticulum. *The Journal of biological chemistry* **280**: 28601-28609.
- Vendel, A.C., M.D. Terry, A.R. Striegel, N.M. Iverson, V. Leuranguer, C.D. Rithner, B.A. Lyons, G.E. Pickard, S.A. Tobet & W.A. Horne, (2006) Alternative splicing of the voltage-gated Ca²⁺ channel beta4 subunit creates a uniquely folded N-terminal protein binding domain with cell-specific expression in the cerebellar cortex. *The Journal of neuroscience : the official journal of the Society for Neuroscience* **26**: 2635-2644.
- Volsen, S.G., N.C. Day, A.L. McCormack, W. Smith, P.J. Craig, R.E. Beattie, D. Smith, P.G. Ince, P.J. Shaw, S.B. Ellis, N. Mayne, J.P. Burnett, A. Gillespie & M.M. Harpold, (1997) The expression of voltage-dependent calcium channel beta subunits in human cerebellum. *Neuroscience* **80**: 161-174.
- Vukcevic, M., F. Zorzato, S. Keck, D.A. Tsakiris, J. Keiser, R.M. Maizels & S. Treves, (2013) Gain of function in the immune system caused by a ryanodine receptor 1 mutation. *Journal of cell science* **126**: 3485-3492.
- Wagenknecht, T., M. Radermacher, R. Grassucci, J. Berkowitz, H.B. Xin & S. Fleischer, (1997) Locations of calmodulin and FK506-binding protein on the three-dimensional architecture of the skeletal muscle ryanodine receptor. *The Journal of biological chemistry* **272**: 32463-32471.
- Waithe, D., L. Ferron, K.M. Page, K. Chaggar & A.C. Dolphin, (2011) Beta-subunits promote the expression of Ca(V)_{2.2} channels by reducing their proteasomal degradation. *The Journal of biological chemistry* **286**: 9598-9611.
- Wang, J. & P.M. Best, (1992) Inactivation of the sarcoplasmic reticulum calcium channel by protein kinase. *Nature* **359**: 739-741.
- Wang, Y., X. Li, H. Duan, T.R. Fulton, J.P. Eu & G. Meissner, (2009) Altered stored calcium release in skeletal myotubes deficient of triadin and junctin. *Cell calcium* **45**: 29-37.
- Wang, Y., X. Deng, S. Mancarella, E. Hendron, S. Eguchi, J. Soboloff, X.D. Tang & D.L. Gill, (2010) The calcium store sensor, STIM1, reciprocally controls Orai and CaV1.2 channels. *Science* **330**: 105-109.
- Ward, C.W., S. Reiken, A.R. Marks, I. Marty, G. Vassort & A. Lacampagne, (2003) Defects in ryanodine receptor calcium release in skeletal muscle from post-myocardial infarct rats. *FASEB journal : official publication of the Federation of American Societies for Experimental Biology* **17**: 1517-1519.
- Wei, L., E.M. Gallant, A.F. Dulhunty & N.A. Beard, (2009) Junctin and triadin each activate skeletal ryanodine receptors but junctin alone mediates functional interactions with calsequestrin. *Int J Biochem Cell Biol.*
- Wiechelman, K.J., R.D. Braun & J.D. Fitzpatrick, (1988) Investigation of the bicinchoninic acid protein assay: identification of the groups responsible for color formation. *Analytical biochemistry* **175**: 231-237.
- Wilkens, C.M., N. Kasielke, B.E. Flucher, K.G. Beam & M. Grabner, (2001) Excitation-contraction coupling is unaffected by drastic alteration of the sequence surrounding residues L720-L764 of the alpha 1S II-III loop. *Proceedings of the National Academy of Sciences of the United States of America* **98**: 5892-5897.
- Wilkens, C.M. & K.G. Beam, (2003) Insertion of alpha1S II-III loop and C terminal sequences into alpha1H fails to restore excitation-contraction coupling in dysgenic myotubes. *Journal of muscle research and cell motility* **24**: 99-109.
- Williams, A.J. & R.H. Ashley, (1989) Reconstitution of cardiac sarcoplasmic reticulum calcium channels. *Annals of the New York Academy of Sciences* **560**: 163-173.

- Williams, A.J., (1992) Ion conduction and discrimination in the sarcoplasmic reticulum ryanodine receptor/calcium-release channel. *Journal of muscle research and cell motility* **13**: 7-26.
- Williams, A.J., (1995) *The measurement of the function of ion channels reconstituted into artificial membranes*. Oxford University Press, New York.
- Witcher, D.R., M. De Waard, H. Liu, M. Pragnell & K.P. Campbell, (1995) Association of native Ca²⁺ channel beta subunits with the alpha 1 subunit interaction domain. *The Journal of biological chemistry* **270**: 18088-18093.
- Wium, E., A.F. Dulhunty & N.A. Beard, (2012) A skeletal muscle ryanodine receptor interaction domain in triadin. *PloS one* **7**: e43817.
- Wolf, M., A. Eberhart, H. Glossmann, J. Striessnig & N. Grigorieff, (2003) Visualization of the domain structure of an L-type Ca²⁺ channel using electron cryo-microscopy. *Journal of molecular biology* **332**: 171-182.
- Wright, N.T., K.M. Varney, K.C. Ellis, J. Markowitz, R.K. Gitti, D.B. Zimmer & D.J. Weber, (2005) The three-dimensional solution structure of Ca(2+)-bound S100A1 as determined by NMR spectroscopy. *Journal of molecular biology* **353**: 410-426.
- Wright, N.T., B.L. Prosser, K.M. Varney, D.B. Zimmer, M.F. Schneider & D.J. Weber, (2008) S100A1 and calmodulin compete for the same binding site on ryanodine receptor. *The Journal of biological chemistry* **283**: 26676-26683.
- Xu, X., Y.J. Lee, J.B. Holm, M.D. Terry, R.E. Oswald & W.A. Horne, (2011) The Ca²⁺ channel beta4c subunit interacts with heterochromatin protein 1 via a PXVXL binding motif. *The Journal of biological chemistry* **286**: 9677-9687.
- Yamaguchi, N., C. Xin & G. Meissner, (2001) Identification of apocalmodulin and Ca²⁺-calmodulin regulatory domain in skeletal muscle Ca²⁺ release channel, ryanodine receptor. *The Journal of biological chemistry* **276**: 22579-22585.
- Yamaguchi, N., B.L. Prosser, F. Ghassemi, L. Xu, D.A. Pasek, J.P. Eu, E.O. Hernandez-Ochoa, B.R. Cannon, P.T. Wilder, R.M. Lovering, D. Weber, W. Melzer, M.F. Schneider & G. Meissner, (2011) Modulation of sarcoplasmic reticulum Ca²⁺ release in skeletal muscle expressing ryanodine receptor impaired in regulation by calmodulin and S100A1. *American journal of physiology. Cell physiology* **300**: C998-C1012.
- Yamazawa, T., H. Takeshima, M. Shimuta & M. Iino, (1997) A region of the ryanodine receptor critical for excitation-contraction coupling in skeletal muscle. *The Journal of biological chemistry* **272**: 8161-8164.
- Yang, T., E. Esteve, I.N. Pessah, T.F. Molinski, P.D. Allen & J.R. Lopez, (2007) Elevated resting [Ca(2+)](i) in myotubes expressing malignant hyperthermia RyR1 cDNAs is partially restored by modulation of passive calcium leak from the SR. *American journal of physiology. Cell physiology* **292**: C1591-1598.
- Zhou, W., L. Saint-Amant, H. Hirata, W.W. Cui, S.M. Sprague & J.Y. Kuwada, (2006) Non-sense mutations in the dihydropyridine receptor beta1 gene, CACNB1, paralyze zebrafish relaxed mutants. *Cell calcium* **39**: 227-236.
- Zhu, L., X. Zhong, S.R. Chen, N. Banavali & Z. Liu, (2013) Modeling a ryanodine receptor N-terminal domain connecting the central vestibule and the corner clamp region. *The Journal of biological chemistry* **288**: 903-914.
- Zissimopoulos, S. & F.A. Lai, (2007) Ryanodine receptor structure, function and pathophysiology. In: *New Comprehensive Biochemistry*. K. Joachim & M. Marek (eds). Elsevier, pp. 287-342.
- Zorzato, F., J. Fujii, K. Otsu, M. Phillips, N.M. Green, F.A. Lai, G. Meissner & D.H. MacLennan, (1990) Molecular cloning of cDNA encoding human and rabbit forms of the Ca²⁺ release channel (ryanodine receptor) of skeletal muscle sarcoplasmic reticulum. *The Journal of biological chemistry* **265**: 2244-2256.

Zorzato, F., A.A. Anderson, K. Ohlendieck, G. Froemming, R. Guerrini & S. Treves, (2000)
Identification of a novel 45 kDa protein (JP-45) from rabbit sarcoplasmic-reticulum
junctional-face membrane. *The Biochemical journal* **351 Pt 2**: 537-543.